MONASH University

Investigations of Novel Treatment Strategies in Atherosclerosis and Thrombosis

Alex Lin-i Huang
BHB, MBChB

A thesis submitted for the degree of Doctor of Philosophy at
Monash University in 2018
In affiliation with Baker Heart and Diabetes Institute

Copyright notice

Abstract

Atherosclerosis is a chronic inflammatory disease affecting medium and large arteries. The pivotal event that transitions atherosclerosis from a subclinical disease to the devastating manifestations of stroke or heart attack is atherosclerotic plaque rupture and ensuing thrombotic complications. Thus, these are two areas where effective therapeutic interventions could translate to substantial clinical benefit.

The first part of this PhD project investigated novel strategies in preventing arterial thrombosis. Emerging evidence has implicated a role of neutrophils in thrombosis, mediated by neutrophil extracellular traps (NETs), a lattice of deoxyribonucleic acid (DNA), histones and proteases. High Mobility Group Box 1 (HMGB1), an alarmin, is a recognised inducer of NETs. The first aim of this thesis was to investigate the feasibility of preventing thrombosis through antibody-mediated HMGB1 neutralisation and inhibition of NET formation. It was found that pre-treatment with HMGB1 neutralising monoclonal antibody (α-HMGB1 mAb) in male C57Bl6 mice, compared to isotype control, was highly effective in preventing arterial thrombosis, as evidenced by preserved carotid arterial flow and improved carotid artery patency time following ferric chloride-induced vascular injury. Similarly, pre-treatment of α-HMGB1 mAb in mice saw a reduction in the size of laser-induced mesenteric thrombi. Importantly, the improved patency time due to HMGB1 neutralisation observed in the ferric chloride-induced carotid thrombosis mouse model, was abolished upon the depletion of neutrophils or the prevention of NET formation. The antithrombotic effects of HMGB1 neutralisation was independent of platelets or monocytes. Further, HMGB1 did not affect haemostatic function. The efficacy of HMGB1 neutralisation, in relation to its safety profile, compared favourably to clinical antithrombotics.

Proprotein convertase subtilisin kexin type 9 (PCSK9) is a protein that regulates cholesterol metabolism by promoting the degradation of the low-density lipoprotein receptor (LDLR). Recently, two large-scale clinical trials have confirmed that inhibition of PCSK9 significantly reduces cardiovascular risk. In addition to cholesterol-lowering, it was hypothesised that PCSK9 may also stabilise atherosclerotic plaque development and stability. Therefore, using a mouse model of diet-induced atherosclerosis, female apoE*3-Leiden.CTEP (E3LC) mice aged 13-17 weeks were fed high fat diet for 6 weeks, prior to commencing on weekly injections of

a monoclonal antibody against mouse PCSK9 (α-PCSK9 mAb) or matching isotype control. Mice received weekly injections and were maintained on high fat diet for a further 13 weeks. It was found that PCSK9 inhibition significantly lowered plasma cholesterol concentrations ($p<0.05$) and significantly reduced the size of atherosclerotic plaques in the aortic sinus (by 56%, $p<0.01$). PCSK9 inhibition also changed plaque composition, as indicated by lower lipid content and macrophage infiltration within atherosclerotic plaques, and an abundance of vascular smooth muscle cells. PCSK9 inhibition also increased splenic and lymph node B cell populations.

In conclusion, HMGB1 neutralisation, through inhibition of NET formation, safely and effectively prevented arterial thrombosis. In addition, PCSK9 inhibition reduced atherosclerotic plaque size and promoted a stable phenotype, providing a mechanistic explanation to the clinical observations that α-PCSK9 mAb improves patient outcomes.

Declaration

This thesis contains no material which has been accepted for the award of any other degree or diploma at any university or equivalent institution and that, to the best of my knowledge and belief, this thesis contains no material previously published or written by another person, except where due reference is made in the text of the thesis.

Signature: ……

Print Name: Alex Lin-i Huang

Date: July 24, 2018

Publications During Enrolment

1. **Huang AL**, Bosco JJ and Peter K. Mast Cell: An Unexpected Villain in Venous Thromboembolism? *Circ Res*. 2017;121:899-901.

2. Htun NM, Chen YC, Lim B, Schiller T, Maghzal GJ, **Huang AL**, Elgass KD, Rivera J, Schneider HG, Wood BR, Stocker R and Peter K. Near-infrared autofluorescence induced by intraplaque hemorrhage and heme degradation as marker for high-risk atherosclerotic plaques. *Nat Commun*. 2017;8:75.

3. Lim B, Yao Y, **Huang AL**, Yap ML, Flierl U, Palasubramaniam J, Zaldivia MTK, Wang X and Peter K. A Unique Recombinant Fluoroprobe Targeting Activated Platelets Allows In Vivo Detection of Arterial Thrombosis and Pulmonary Embolism Using a Novel Three-Dimensional Fluorescence Emission Computed Tomography (FLECT) Technology. *Theranostics*. 2017;7:1047-1061.

4. Chen YC, **Huang AL**, Kyaw TS, Bobik A and Peter K. Atherosclerotic Plaque Rupture: Identifying the Straw That Breaks the Camel's Back. *Arterioscler Thromb Vasc Biol*. 2016;36:e63-72.

<u>Manuscripts under preparation</u>

Huang AL, Chen YC, Lim B, Yao Y, Zaldivia K, Bobik A and Peter K. Therapeutic Targeting of the Alarmin, HMGB1, Safely and Effectively Prevents Arterial Thrombosis Through Inhibition of NET Formation.

Huang AL, Chen YC, Ying YL, Yu E, Lim B, Yao Y, Zaldivia K, Bobik A and Peter K. PCSK9 Inhibition Reduces and Stabilises Atherosclerotic Plaques in a Mouse Model of Diet-Induced Atherosclerosis.

Acknowledgements

I would like to thank my principal supervisor Prof. Karlheinz Peter, who accepted me as a PhD student and gave me the opportunity to start a career in science. You have been kind and supportive. Despite your busy schedule, you have always been generous with your time and patience, and kindly accommodated many of my last-minute requests. I also want to thank you for giving me the freedom to try my ideas, and never declined my ordering request – I know it's a luxury few PhD students have!

I would like to thank my co-supervisor Prof. Alex Bobik. Thank you for your insightful advice on the project and your feedback on my thesis, they have really helped moving forward.

I would like to thank National Heart Foundation for their support through a National Heart Foundation Postgraduate Scholarship.

I would like to thank everyone in Atherothrombosis Lab, who helped and supported me through this very long journey, teaching me so much about science and beyond. In particular, I would like to thank Ben who kindly taught me so many invaluable animal techniques and assisted me on whatever project I was working on. I would also like to thank Bock for the intellectual discussion, technical guidance and teaching me the rigor of science. To Joy, you always gave me your time no matter how busy you were and sheltered me when I really needed it. Alice, a big thanks to you, I don't think many PhD students would have a fellow student voluntarily stayed until 11pm on a Friday night to help out, so yes, you are right, I have been lucky! Thank you Eefang, for being the supportive and helpful little sister in the lab, you make it feel like family. Thank you Kris, thank you for generously sharing your insights on how to survive PhD. Also to Tin and Prof. Rebecca Ritchie, thank you for extending your support when I most needed it, I appreciate it! I am very grateful to have met all of you, you have changed my life forever.

I would like to thank my family, who gave me courage when I felt tired, brought me up when I was down. Also, the sage words from you, the life wisdom really helped me getting through the tough times.

Most importantly, I want to thank my wife Natalie. Thank you for being a superb mentor and life coach who guided and directed me through this long and winding road. I am so grateful for your support and allowing me to pursue my dream and embark on this difficult journey. Thank you for being more than accommodating, putting me first and supporting me all the way through. I still remember the dinners you brought to me at Baker when I was pulling all-nighters, the nicest food I ever had. You always said we are a team, but secretly I know I have got more than my fair share. I couldn't have done it without you.

Table of Contents

Abbreviations

α-SMA	smooth muscle actin-α
ACS	acute coronary syndrome
ADP	adenosine diphosphate
AHA	American Heart Association
Akt	protein kinase B
AMREP	Alfred Medical Research and Education Precinct
APC	allophycocyanin
Apo	apolipoprotein
APTT	activated partial thromboplastin time
ATP	adenosine triphosphate
AUC	area-under-the-curve
CCL	chemokine (C-C motif) ligand
CD	cluster of differentiation
CETP	cholesteryl ester transfer protein
CpG	cytosine and guanine separated by one phosphate group
CXCL	chemokine (C-X-C motif) ligand
CXCR	chemokine (C-X-C motif) receptor
Cy5.5	Cyanine 5.5
DAMP	damage-associated molecular pattern
DAPI	4',6-diamidino-2-phenylindole
DNA	deoxyribonucleic acid
DNase	deoxyribonuclease
DVT	deep vein thrombosis
E3LC	apoE*3-Leiden. CETP
EGF-1	epidermal growth factor like-1
FACS	fluorescence-activated cell sorting
FBS	fetal bovine serum
$FeCl_3$	ferric chloride
FITC	fluorescein isothiocyanate
FOURIER	Further Cardiovascular Outcomes Research With PCSK9 Inhibition in Subjects With Elevated Risk

FXR	farnesoid X receptor
GP	glycoprotein
H&E	haematoxylin and eosin
HDL	high-density lipoprotein
HFD	high fat diet
HLA	human leukocyte antigen
HMG-CoA	3-hydroxy-3-methyl-glutaryl-coenzyme A
HMGB1	high mobility group box 1
i.p.	intraperitoneal
i.v.	intravenous
IκB	inhibitor of kappa B kinases
ICAM	intracellular adhesion molecule 1
IDL	intermediate-density lipoprotein
IFN	interferon
IL	interleukin
IVC	inferior vena cava
IVUS	intravascular ultrasound
JAK	janus kinase
LAD	left anterior coronary artery
LDL	low-density lipoprotein
LDLR	low-density lipoprotein receptor
LFA-1	lymphocyte function-associated antigen 1
LPS	lipopolysaccharide
LRP	low-density lipoprotein receptor related protein
mAb	monoclonal antibody
MAP	mitogen-activated protein
MCP1	monocyte chemoattractant protein-1
MMP-9	matrix metallopeptidase 9
MPO	myeloperoxidase
MyD88	myeloid differentiation primary response 88
NADPH	nicotinamide adenine dinucleotide phosphate
NET	neutrophil extracellular trap
NETosis	neutrophil extracellular trap formation
NFκB	nuclear factor kappa-light-chain-enhancer of activated B cells

NLR	nucleotide-binding oligomerisation domain-like receptor
NLRP3	nucleotide-binding oligomerisation domain-like receptor protein 3
NLS	nuclear localisation sequences
NOD	nucleotide-binding oligomerisation domain
NSTEMI	non- ST-segment elevation myocardial infarction
OCT	optic coherence tomography
ODYSSEY	Evaluation of Cardiovascular Outcomes After an Acute Coronary Syndrome During Treatment with Alirocumab
p38-MAPK	p38 mitogen-activated protein kinase
PAD4	protein arginine deiminase 4
PAMP	pathogen-associated molecular patterns
PAR	protease activated receptor
PBS	phosphate buffer solution
PCSK9	proprotein convertase subtilisin/kexin type 9
PE	phycoerythrin
PerCP	peridinin-chlorophyll-protein
PKR	double-stranded RNA-dependent protein kinase
PMA	phorbol 12-myristate 13-acetate
PT	prothrombin time
RAGE	receptor for advanced glycation end product
RNA	ribonucleic acid
RPMI	Roswell Park Memorial Institute medium
s.c.	subcutaneous
SEM	standard error of the mean
SR	scavenger receptor
SRA	scavenger receptor A
SREBP	sterol regulatory element-binding protein
STAT	signal transducer and activator of transcription proteins
STEMI	ST-segment elevation myocardial infarction
TCR	T cell receptor
TF	tissue factor
TLR	toll-like receptor
TNF	tumour necrosis factor
uPA	urokinase plasminogen activator

VLDL	very low-density lipoprotein
vWF	von Willebrand factor

List of Figures

List of Tables

List of Appendices

CHAPTER 1

Introduction and Literature Review

1.1 Overview of atherosclerosis

Atherosclerosis is a chronic inflammatory disease characterised by the deposition of cholesterol, infiltration of immune cells and migration of vascular smooth muscle cells, thus forming an intimal mass in medium and large arteries. In susceptible individuals, the disease process can initiate as early as the foetal period[1]. However, clinical disease typically does not manifest until the 4th or 5th decade of life. This prolonged and largely clinically silent disease process is heterogeneous in both temporal course and spatial distribution. Contemporary studies have demonstrated that atherosclerosis does not progress in an orderly and predictable fashion[2]. Instead, atherosclerotic plaques undergo episodes of rapid expansion with intervening periods of dormancy[3]. Similarly, occurrences of clinical events are often sudden and unexpected with devastating consequences. In the spatial aspect, while atherosclerosis could affect different parts of the arterial vasculature, it has a predilection for carotid, coronary and peripheral circulations[4], where ischemia and infarction are clinically manifested as stroke, myocardial infarction and acute limb ischemia, collectively referred to atherosclerotic vascular disease.

Atherosclerotic vascular disease represents a major unmet medical need for 3 main reasons. Firstly, it is the leading cause of mortality in the world[5]. Secondly, in survivors of atherosclerotic vascular disease, critical end organ damage results in major disability, impairs the quality of life of affected individuals and incurs a significant social and economic cost[6]. Thirdly, due to lifestyle changes, ageing of population and the rising epidemics of obesity and diabetes, the incidence of atherosclerotic vascular disease is projected to rise[7]. Thus, the development of novel therapeutics through a better understanding of the disease is critically important.

About 20 years ago, a classification system was devised by the American Heart Association (AHA) to define the different stages of atherosclerosis[8-10]. In addition to improving precision in these terms thus promoting more effective communication, more importantly, it provides a useful conceptual framework for physicians and researchers. Subsequently, Virmani et al. proposed a different classification system, arguing the AHA classification is difficult to remember and perhaps falsely implicates that atherosclerosis follows a linear course of progression. These two systems are both widely adopted and complement each other. In the

following discussion, I will make reference to both systems, which are schematically represented in Fig. 1-1 and Fig. 1-2.

1.2 Classification of atherosclerotic lesions

1.2.1 Adaptive intimal thickening

Intima refers to the layer of the arterial wall between vascular endothelium on the lumenal side and the internal elastic lamina on the medial side[8]. Normally, it is a thin layer of variable thickness. However, in segments predilected to develop atherosclerosis, typically those with low shear and high tensile stress, intima adaptively thickens to normalise wall shear. Importantly, the microscopic composition of the thickened intima is similar to that of normal arterial intima. These changes are not considered pathological, as they occur in response to mechanical stress, independent of the influence of lipoproteins. However, they may provide a nidus for lesion initiation[11].

1.2.2 Early stage lesions

In the AHA classification system (Fig. 1-1), lesion types I and II are grouped as the initial lesion, and lesion type III is also called intermediate lesion. Lesion type I is characterised by the presence of scattered, isolated groups of foam cells, which are macrophages with intracellular cholesterol droplets. Lesion type II, also known as fatty streaks, are yellow streaks visible on macroscopic examination and stain positive for Sudan red, an orange-red dye that is soluble in fat. Fatty streaks are divided into 2 subgroups, IIa and IIb. IIa fatty steaks tend to progress to more complex lesions, while IIb lesions are resistant to progression. The 2 subgroups differ in location and morphology; where type IIa lesions tend to colocalise with intimal thickening and contain more foam cells and greater lipoprotein content. Both subtypes share the commonality that they generally occur early in life (usually before the third decade) and both can regress. In the classification proposed by Virmani et al, these lesions are classified as “intimal xanthoma”. Type III lesions are characterised as dispersed pools of extracellular lipid that are transitioning to advanced lesions. In the Virmani scheme, this is called “pathological intimal thickening”.

These early lesions are subclinical and remain non-obstructive. However, in response to chronic systemic (e.g., hypertension and hypercholesterolemia) and local (e.g., low shear stress)

stimuli, both vascular and immune cells undergo phenotypic changes that eventuate in the development of atherosclerosis. In this situation, the endothelium becomes proinflammatory, upregulating adhesion molecules, and also prothrombotic, due to a decreased bioavailability of nitric oxide[12]. Macrophages, arising from increased haematopoiesis or local proliferation, ingest modified LDL and become foam cells. They then further amplify inflammatory responses through secretion of cytokines, chemokines and proteases[13]. In addition, vascular smooth muscle cells proliferate and adopt a secretory phenotype[14].

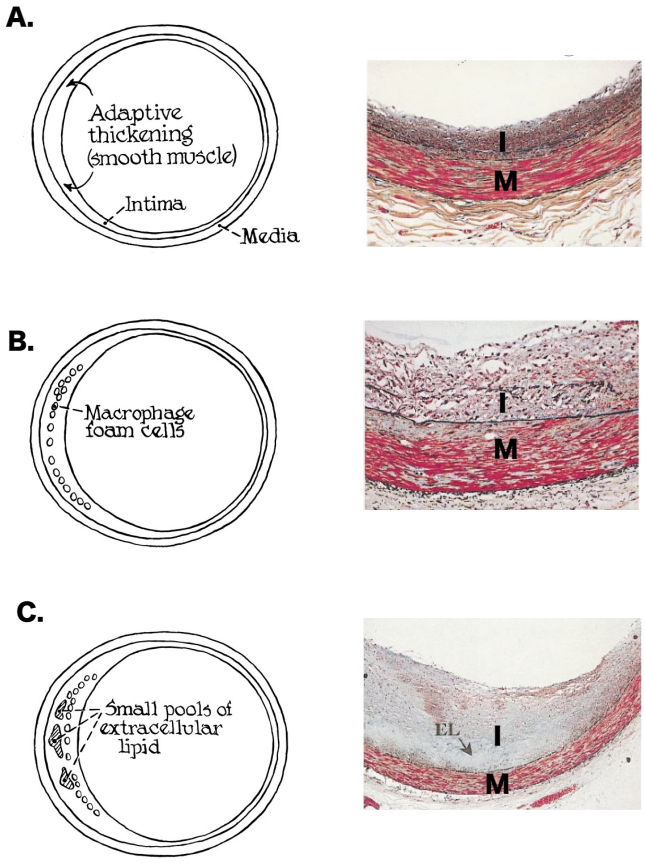

Figure 1-1. Early-stage atherosclerotic lesions. On the left is a schematic representation of the AHA system and on the right, the representative histopathological appearance of different lesions. (A) Adaptive thickening, characterised by a thickened intima made up of vascular smooth muscle cells. (B) Type I/II lesion, initial lesion or intimal xanthoma. This is characterised by the presence of cholesterol-loaded foam cells, which may progress to fatty streaks. (C) Type III lesion, intermediate lesion or pathological intimal thickening. This is characterised by the presence of a dispersed extracellular lipid pool. Figures adapted from Stary et al[10]. and Virmani et al.[15]. Key: I – intima, M – media. EL – extracellular lipid.

1.2.3 Advanced lesions

Atheroma is characterised by a well-defined, coalesced pool of extracellular lipid consisting of cholesterol clefts, free cholesterol and phospholipid, and is classified as type IV lesion under the AHA scheme (Fig. 1-2). When new fibrous tissue develops over the underlying lipid pool, it is referred to as a fibroatheroma, or type V lesion. Here, the AHA system further divides type V lesions based on the histological characteristics of the fibrous cap, where type Va refers to fibrolipid plaques, type Vb refers to calcific lesions and type Vc refers to fibrous lesions where there is little or no lipid core. Both type IV and V lesions can have structural tears or rupture, and both can be complicated by thrombosis, at which point, they are classified as type VI lesion. Type VI lesions are subdivided into type VIa, if they are complicated by disrupted plaque surface, type VIb, if complicated by haematoma or haemorrhage, or type VIc, if complicated by thrombosis.

As Virmani et al. pointed out, there is a considerable overlap in lesions type IV, V and VI[15]. Further, the AHA classification system implies a linear, sequential progression of atherosclerotic plaques, but this is not entirely supported by current evidence. Illustrating this are scenarios where eroded plaques are complicated by thrombosis; whilst eroded plaques often have the morphology of a pathological intimal thickening (AHA type III), they may be complicated by thrombi (AHA type VIc) and precipitate clinical events. Instead, Virmani et al. proposed the term fibrous cap atheroma that encompasses both type IV and V lesions[15].

In both schemes, however, it was emphasised that a fibrous cap atheroma can erode or rupture, which may lead to thrombus formation, vascular occlusion and end organ infarct or ischemia. When this happens, it could manifest clinically as stroke, myocardial infarction or sudden cardiac death. It can also remain subclinical and result in intraplaque haematoma and sudden

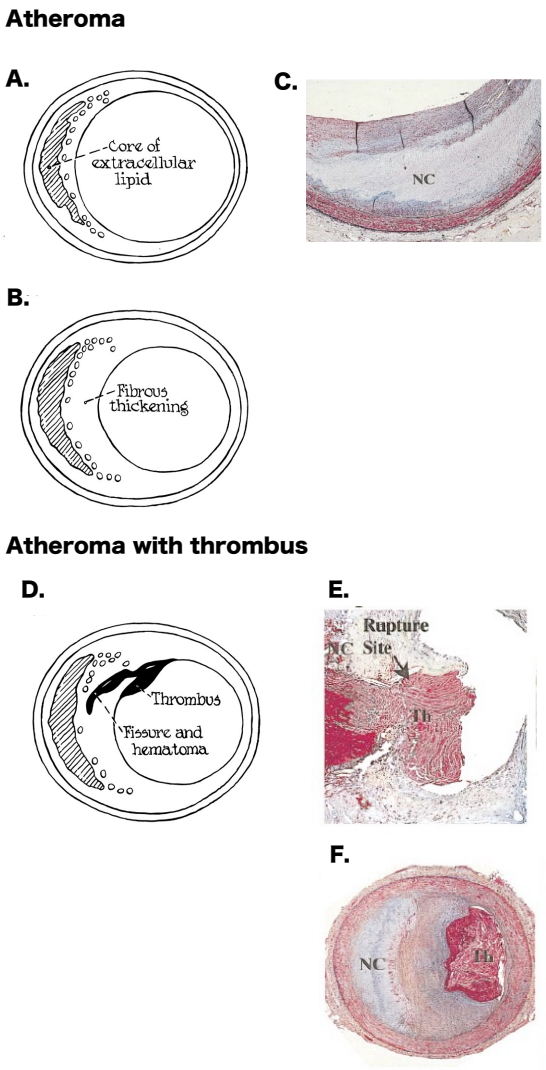

Figure 1-2. Advanced atherosclerotic lesions. In the AHA system, (A) type IV lesions, or atheroma, are characterised by the presence of a lipid pool/necrotic core. (B) Type V lesion, or fibroatheroma, is distinguished from a type IV lesion by the fibrous tissue overlying lipid pool. (C) Virmani et al. did not make this distinction and collectively called these lesions fibrous cap atheroma. Advanced lesions may be complicated by thrombus. (D) Type VI lesion refers to lesions complicated by rupture of fibrous tissue, fissures or haemorrhage. Virmani et al. proposed to use descriptive terms to describe lesions complicated by thrombosis, including (E) plaque rupture, where atherogenic core is exposed or (F) plaque erosion, where there is loss of endothelium. Key: NC – necrotic core, Th – thrombus. Adapted from Stary et al[9]. and Virmani et al[15].

expansion of atherosclerotic plaques. Post-mortem examinations have found three types of lesions were associated with lumenal thrombosis: plaque rupture, plaque erosion and calcific nodules.

1.2.4 Plaque rupture

Plaque rupture is defined as a structural defect in the fibrous cap exposing thrombogenic cores to the lumen, leading to thrombosis[16] (Fig. 1-2). In addition, fibrous caps are often inflamed and have abundant immune cell infiltrates (both macrophages and lymphocytes), but they are scant in vascular smooth muscle cells. The culprit atherosclerotic lesions usually have large necrotic cores rich in lipid and cholesterol clefts. Frequently, ruptured plaques are accompanied by obstructive or occlusive thrombi at the lumenal side. Other histological features of ruptured plaques include intraplaque haemorrhage, adventitial inflammation, spotty calcification, positive remodelling of the vessel and neovascularisation from angiogenesis[17].

In a worldwide survey that included 22 autopsy studies where 1847 fatal coronary thrombi were examined, plaque rupture was the most common cause of coronary thrombosis and accounted for 73% of all cases[18]. Further, irrespective of the clinical presentation (plaque rupture found in 79% of patients who died of myocardial infarction and 65% of patients died of sudden coronary death), age (plaque rupture found in 77% of >60 years and 64% of <60 years), gender (plaque rupture found in 76% of men and 55% of women) and geographic location where the study was conducted (plaque rupture found in 72% in studies performed in Europe, 68% in USA and 81% in Asia), plaque rupture remains the leading cause of coronary thrombosis[18]. As autopsy series are inherently limited by its retrospective nature and selection bias, it is important to corroborate this with clinical studies. Using intracoronary optic coherence tomography (OCT), an imaging technique with superb resolution (10μm) that allows the visualisation of plaque microstructure in patients, Jia et al. have shown that in a series of 126 patients with acute coronary syndrome (ACS), the prevalence of plaque rupture was 43.7%[19].

1.2.5 Plaque erosion

Plaque erosion is defined as a loss or disruption of lumenal endothelial cells, but the fibrous capsule remains intact[16] (Fig. 1-2F). Morphologically, eroded plaques are very different to ruptured plaques. Firstly, eroded plaques retain structural integrity and have intact fibrous caps, internal elastic lamina and external elastic lamina. In contrast, these structures are often disrupted in ruptured plaques[20]. Secondly, the media of eroded plaques are preserved with contractile vascular smooth muscle cells[20], whereas media of ruptured plaques are often atrophied and disorganised. Indeed, the intima of eroded plaques consist mainly of vascular smooth muscle cells and proteoglycan. Thirdly, eroded plaques are less inflamed and have fewer lesional macrophages[21]. Clinically, eroded plaques appear to be associated with stable angina[22].

In an autopsy series, plaque erosion accounted for approximately 40% of thrombotic sudden coronary death[23] and in an OCT study, it is seen in 31.0% of acute coronary syndrome (ACS) patients. [19]. Notably, in women <50 years, plaque erosion accounts for approximately 80% of acute thrombotic coronary death[15]. Some investigators report that eroded plaques are associated with less lumenal obstruction[23], but a conflicting finding has also been reported [22]. Of note, these discrepant results may be related to differences in the age and clinical presentation of the patients studied[22].

It is important to note that, while endothelial erosion is the defining feature of these thrombotic lesions, it is unclear if endothelial erosion is the cause or consequence of acute thrombosis, as erosion often occurs in proximity to fatal, thrombotic ruptured plaques[15]. It has also been suggested that plaque erosion may result from vasospasm, which is in keeping with the observation these lesions often have well-developed media rich in contractile vascular smooth muscle cells[18].

1.2.6 Calcific nodules

Autopsy studies have shown that, while uncommon, thrombosis may occur at sites where dense and calcific nodules protrude outside of the lesion and contribute to thrombosis[15]. However, in a prospective series using intravascular ultrasound (IVUS) with virtual histology, Xu et al. have

shown that calcific nodules are more prevalent than previously thought, present in approximately 30% of ACS patients, especially in older patients with higher plaque volume. Surprisingly, calcific nodules are associated with a lower risk of adverse events[24].

1.3 Animal models of atherosclerosis

To study atherosclerosis directly in humans is inherently difficult as atherogenesis runs a protracted course that is largely subclinical. In addition, direct access to the site of pathology is limited. This restricts the study of human atherosclerosis to either surgically resected samples or post-mortem examinations. Both types of studies suffer selection bias, as the sample studied are in the late-stage of the disease process. Further, as both type of studies can only be conducted at one time point for a specific patient, it precludes longitudinal assessment of atherosclerotic plaque lesions. Because of these reasons, researchers often need to resort to use animal models, in particular, mouse models, to study atherosclerosis. By observing the phenotypic response to genomic manipulation and pharmacological interventions, researchers have gained insight into the disease process, and some studies have led to the development of novel strategies or effective pharmaceuticals[25,26]. As all animal models of atherosclerosis are based on hyperlipidaemia, a brief review of lipoprotein metabolism will first be presented, followed by a discussion on animal models of atherosclerosis and specific models of atherosclerotic plaque rupture.

1.3.1 Cholesterol and lipoproteins

Cholesterol is essential for cell function, as it is a cell membrane constituent, and it is necessary for the production of steroid hormones and bile acid. Because of its critical importance, all cells can synthesise cholesterol *de novo.* However, cholesterol can also be obtained through diet[27].

The body uses lipoproteins to transport cholesterol and triglycerides. Lipoproteins all have similar structures; they are made up of a hydrophobic core that contains cholesterol ester and triglyceride, and a hydrophilic shell that contains apolipoproteins (apo) and phospholipids[28]. Lipoprotein can be classified into different fractions, according to their density, into chylomicron, very-low density lipoprotein (VLDL), low-density lipoprotein (LDL) and high-density lipoprotein (HDL). The difference in density relates to the relative proportion of fat and cholesterol contained. For example, chylomicron is high in triglycerides with little

cholesterol, therefore it has a very low density. On the other hand, HDL is cholesterol-rich and triglyceride-poor[28].

Different lipoprotein fractions serve different purposes. Chylomicron and VLDL primarily transport triglycerides to the periphery, and LDL transports cholesterol from the liver to peripheral tissues such as muscles and adipose tissues. HDL, on the other hand, transports cholesterol from the periphery (e.g., atheroma) back to the liver[29]. LDL is atherogenic, as supported by epidemiology studies, Mendelian randomisation studies and clinical trials showing lowering LDL cholesterol is associated with reduced cardiovascular risk[30]. On the other hand, the role of HDL is less certain. Though it has traditionally been associated with lower cardiovascular risk, insight from Mendelian randomisation studies and negative results obtained from recent clinical trials have prompted researchers to reassess the contribution of HDL to atherosclerosis[31-33].

Apolipoproteins, the protein constituent located on the surface of lipoproteins, are important in maintaining the structural integrity of lipoproteins. They also mediate the uptake of lipoproteins by liver or peripheral tissues, as they act as ligands that bind to specific receptors. Of them, three are most significant from a clinical and atherosclerosis standpoint. ApoB100 is the main apolipoprotein of LDL and VLDL, and it serves as the ligand for the LDL receptor (LDLR) and mediates hepatic LDL uptake[28]. Mutations in apoB100 causes familial hypercholesterolaemia and premature coronary artery disease[34]. ApoE is associated with chylomicrons, VLDL, and subgroups of HDL[28], and it binds with high affinity to LDLR and LDLR-related peptide (LRP)[35]. Mutations in apoE or the apoE2 isoform cause defective binding to its receptors and an accumulation of VLDL in the plasma, clinically known as type III familial hyperlipoproteinaemia[36], and deficiency in apoE in mouse is one of the most widely-used animal model of atherosclerosis[37]. Lastly, apoAI is the apolipoprotein of HDL that activates lecithin: cholesterol acyltransferase (LCAT), an enzyme that esterifies free cholesterol. ApoAI interacts with adenosine triphosphate (ATP)-binding cassette protein A1 (ABCA1), ABCG1, and class B, type I scavenger receptor (SR-B1) and plays important roles in reverse cholesterol transport[28].

Importantly, cholesterol metabolism in humans and mice are different in a number of aspects. Firstly, cholesterol in mice is mainly carried in the HDL fraction, whereas in humans, it is

predominantly carried within the LDL fraction. Secondly, mice do not have cholesterol ester transfer protein, CETP. Lastly, the main apoB in humans in apoB100, which is cleared by LDLR. In mice, the dominant apoB is apoB48, which is cleared through LRP[38].

1.3.2 Ldlr$^{-/-}$ mice

The Ldlr$^{-/-}$ mouse model was designed to mimic human familial hypercholesterolemia, where mutations of *Ldlr* gene lead to defective uptake of LDL cholesterol. In these mice, LDLR is genetically ablated, therefore LDL cannot be taken up by the liver and accumulates in plasma. This in turn leads to the development of atherosclerosis[39]. Plasma cholesterol of Ldlr$^{-/-}$ mice is diet-dependent. When placed on chow diet, these mice have an average plasma cholesterol of approximately 10 mmol/L and very modest lesion development[40]. However, when placed on a prolonged Western type diet (21% fat, 0.20% cholesterol, no cholate), Ldlr$^{-/-}$ mice develop very high levels of plasma cholesterol of approximately 40 mmol/L and widespread, advanced atherosclerotic lesions[40]. Ldlr$^{-/-}$ mice have the advantage that elevated cholesterol is mainly in the LDL fraction, which simulates human pathology more closely.

1.3.3 ApoE$^{-/-}$ mice

ApoE is an apolipoprotein mainly associated with VLDL and mediates hepatic uptake of VLDL and VLDL remnants through two cognate receptors, LDLR and LRP. [35]. Genetic deletion of apoE in mice leads to profound hypercholesterolaemia, mostly in the VLDL fraction [37,41]. When fed a chow diet, apoE$^{-/-}$ mice have an average plasma cholesterol of approximately 15 mmol/L[40]. However, if fed a high fat diet (22% fat, 0.15 cholesterol), plasma cholesterol of apoE$^{-/-}$ mice can be accentuated to 40-50mmol/L[40]. Because of such severe hypercholesterolaemia, they develop extensive and advanced atherosclerosis within short time frames[42]. Compared to Ldlr$^{-/-}$ mice, apoE$^{-/-}$ mice have an accelerated course of atherogenesis. However, in these mice, it is the VLDL lipoprotein fraction that is elevated, which is different to human atherosclerosis, where LDL-cholesterol is elevated. In addition to its function in lipid metabolism, apoE also has diverse immune and inflammatory actions, and exerts its effects on macrophages, T cells and vascular smooth muscle cells[43,44]. These caveats need to be considered when extrapolating experimental findings to humans.

1.3.4 ApoE3*Leiden-CETP (E3LC) mice

ApoE3*Leiden-cholesteryl ester transfer protein (E3LC) transgenic mice fed on high fat diet is another commonly used model of atherosclerosis. E3LC is generated through the transgenesis of two human genes, the first being apoE*3-Leiden (E3L), a variant of the normal apoE3 gene. This was first identified in a Dutch family with type III familial hyperlipoproteinemia and is inherited as a dominant trait[45]. The genetic variation lies in a tandem repeat of residues 121-127, yielding a protein of 306 amino acids. The apolipoprotein E3LC, has defective binding to LDLR. Therefore, mice that carry the E3LC transgene have impaired plasma clearance of chylomicron and VLDL[46]. When fed high fat/cholesterol diet (15% cocoa butter by weight, 1% cholesterol and 0.5% cholate), E3L transgenic mice develop severe hypercholesterolemia (total plasma cholesterol up to 60 mmol/L), mostly in the VLDL/LDL fractions[47,48]. This diet-induced hypercholesterolaemia leads to extensive atherosclerosis, with lesions detected in the proximal coronary arteries, aortic root, aortic arch and its main branch points, thoracic and abdominal aorta, and the renal artery branch points. Some of these lesions are complex and advanced with necrotic core, cholesterol clefts and fibrosis (AHA type IV and V)[48,49]. When the second human transgene, CETP, is expressed in E3L mice, CETP causes a shift in net distribution of cholesterol from HDL to VLDL and LDL, and further aggravates atherosclerotic plaque development, increasing plaque volume by 7-fold[50]. Compared to other genetically modified mice used in atherosclerotic studies, E3LC mice have a more humanised cholesterol profile, with more cholesterol carried in VLDL and LDL rather than HDL. There are three other advantages of E3LC mice. Firstly, E3LC mice have been shown to respond to many hypolipidaemic agents used clinically, including statin[51], niacin[52], fibrate[53], CETP inhibitors[54] and PCSK9 antibodies[55]. Secondly, the degree of hypercholesterolaemia and extent of atherosclerosis can be titrated by changing the composition and duration of high fat/cholesterol diet[48]. Thirdly, E3LC mice can be used to study both the progression and regression of atherosclerosis[56].

1.4 Plaque rupture models

While diet-induced atherosclerosis in apoE$^{-/-}$ and Ldlr$^{-/-}$ mice faithfully recapitulates many features of human atherosclerosis, atherosclerotic plaques do not rupture spontaneously. Over the last 2 decades, much efforts have been directed towards the development of mouse models of atherosclerotic plaque rupture. However, uptake of these models is low for the following

reasons. Firstly, the study period is long, which can take 40-60 weeks [57-59]. Secondly, these models often require complex genetic or surgical manipulations to induce plaque rupture [60,61]. This poses logistical challenges and may not reflect human pathophysiology. Thirdly, the success rate of inducing plaque rupture is low, as features of plaque instability is often seen in <50% of treated mice[62]. Two models will be discussed here, as they require a relatively short study period and have reasonable success rates.

1.4.1 Carotid tandem stenosis model of plaque rupture

In this model, two stenosis in tandem were created in the carotid artery of male apoE$^{-/-}$ mice[63]. In male apoE$^{-/-}$ mice with pre-existing carotid atherosclerotic plaques, this creates an environment with low shear and high tensile stress, which are conducive to the development of spontaneous plaque rupture. This model has a number of advantages; the study duration is relatively short (13 weeks), unstable features are reliably produced (e.g., intra-plaque haemorrhage occurs in 50% of mice), and the surgery required to induce plaque rupture is straightforward. Importantly, the unstable lesions induced are stabilised with statin, thus it can be used as a platform for drug testing.

1.4.2 Elastin fragmentation model

In this model, genetically engineered mice containing a heterozygous mutation (C1039G$^{+/-}$) in the fibrillin-1 (*Fbn1*) gene and deficient in apoE are fed a high fat diet for up to 35 weeks[64]. This model has the advantage that mice develop phenotypes (e.g., 70% mice died suddenly, and 66% showed motor disturbances) that resemble clinical presentation of stroke and myocardial infarction in humans. On histological examination, it was found atherosclerotic lesions of these mice have features of plaque instability including plaque rupture (50% of brachiocephalic arteries and 70% of proximal ascending aorta), intraplaque haemorrhage (90% of mice), enlarged necrotic cores and reduced collagen content. The main drawback of this model is the relatively long study duration (up to 35 weeks). Also, it was not reported if the unstable lesions in this model are amenable to plaque-stabilising medications such as statins.

1.5 Proprotein convertase subtilisin/kexin type 9

Proprotein convertase subtilisin/kexin type 9 (PCSK9) is protein that mediates LDLR degradation. Since the first report linking this protein to cholesterol metabolism[65], it has been extensively studied and the mechanism through which PCSK9 regulates LDLR has been elucidated. Based on this, many therapeutics against PCSK9 have been developed and two large-scale clinical trials completed, all within 15 years of its discovery[66,67]. Here is a review of the key aspects of PCSK9 biology.

1.5.1 Structure and processing of PCSK9 (Fig. 1-3)

PCSK9 is first produced as a 75 kDa soluble zymogen that is made up of 692 amino acids[68]. The primary structure of this precursor protein can be divided into 4 domains. From the N-terminus, first is the signal sequence (residues 1-30), next the prodomain (residues 30-152), then the catalytic domain (residues 152-449) and finally the C-terminal domain (residues 449-692)[69] (Fig. 1-3A). At the endoplasmic reticulum, two proteolytic reactions take place. Firstly, the signal sequence is cleaved off, changing the precursor into a proprotein[68]. Secondly, and importantly, PCSK9 undergoes an intramolecular autocatalytic reaction, where the catalytic domain cleaves the prodomain at the sequence Val-Phe-Ala-Gln_{152}↓Ser-Ilie-Pro (SVFAQ152↓SIP)[68]. After being cleaved, the prodomain remains associated with the active site of the catalytic domain, blocking access to the catalytic site. Thus, PCSK9 has only 1 recognised substrate, which is itself. This reaction is essential for PCSK9 to exit the endoplasmic reticulum[68]. PCSK9 also undergoes a number of post-translational modifications including glycosylation[68], phosophorylation[70] and tyrosine sulfation[71], though the biological significance of these modifications remains unclear. After mature PCSK9 protein is secreted into the circulation as a 60kDa protein, it can undergo another proteolytic reaction, where it is cleaved at residue 218 (motif RFHR) by proprotein convertase C5/6A and furin. This produces a smaller protein of 55kDa, which has lower affinity to LDLR[71], and thus is considered a less active form[72].

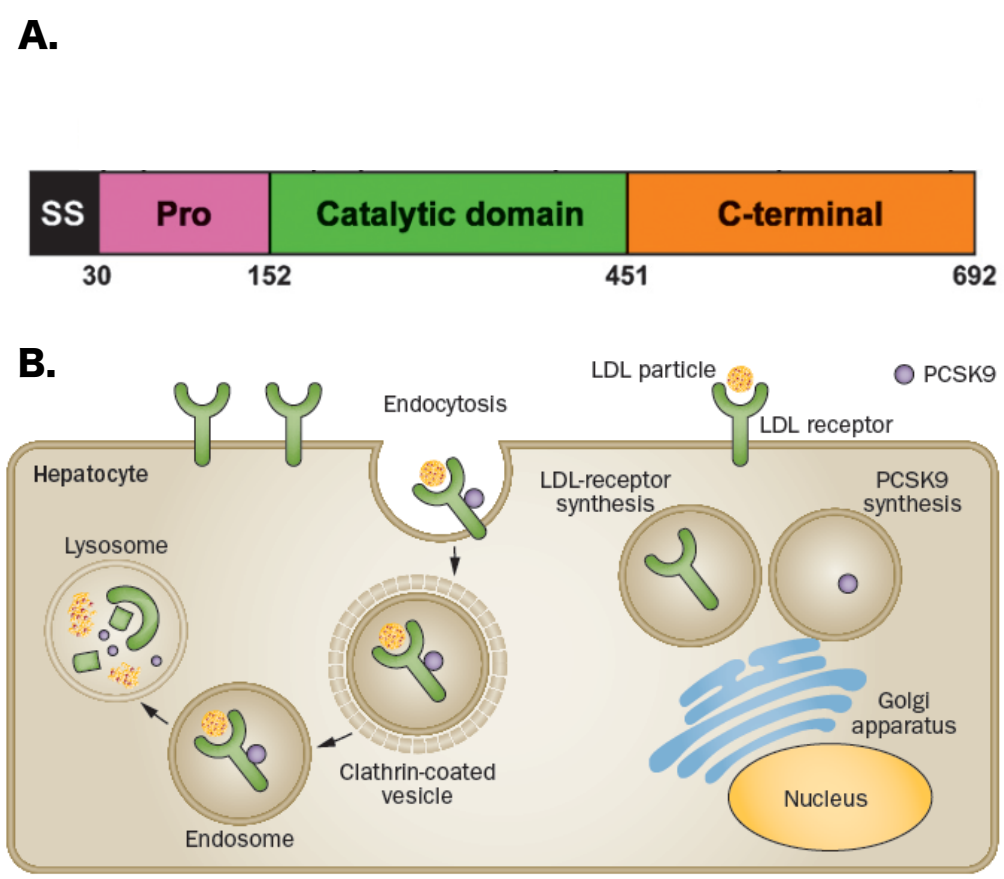

Figure 1-3. Structure and function of PCSK9. (A) Precursor PCSK9 is a protein of 692 amino acids consisting of a signal sequence (SS), a prodomain (Pro), a catalytic domain and the C-terminal. The signal sequence and prodomain are both cleaved off at the endoplasmic reticulum, but the prodomain remains associated with the catalytic domain. PCSK9 is secreted as a 60 kDa protein. (B) PCSK9 binds to LDLR on cell surface of hepatocytes and the complex is internalised through endocytosis as a clathrin-coated vehicle. PCSK9 keeps LDLR in an open conformation and chaperones LDLR to lysosome, where LDLR is degraded. Adapted from Horton et al[73]. and Dadu et al[74].

1.5.2 Functions of PCSK9 (Fig. 1-3B)

PCSK9 was initially thought to be involved in hepatic regeneration and the development of the central nervous system[68]. The first clue of its importance in cholesterol metabolism came from genetic studies, where PCSK9 mutation was shown to be the cause of familial hypercholesterolemia[65]. Following this, a series of experiments revealed that PCSK9 mediates its actions primarily through LDLR[75,76]. Usually, uptake of LDL cholesterol is mediated through LDLR clustered in the clathrin-coated pits. As LDL binds LDLR, this complex is internalised through endocytosis, and descends as endosomes down the pH gradient into lysosomes[77]. In lysosomes, LDL is processed, and the cholesterol and triglycerides are de-esterified to be used by cells, whereas LDLR is channelled back to the cell surface to be recycled[77]. PSCK9 regulates LDLR metabolism as it binds to the epidermal growth factor-1 (EGF-1) like domain of LDLR, keeping it in an open conformation and acts as a chaperone towards lysosomes[78]. In lysosomes, PCSK9-bound LDLR is degraded by lysosomal enzymes. Essentially, PCSK9 enhances LDLR degradation thus reduces LDLR availability (Fig. 1-3B). This means less hepatic uptake of LDL from the plasma (due to fewer LDLR), consequently, higher plasma LDL-cholesterol. In addition to LDLR, PCSK9 binds to the EGF-1 domain of VLDL receptor and apoE receptor 2[79]. It can also bind to LRP, another cognate receptor of apoE[80], however, this may not be biologically significant[81]. Interestingly, LDLR and PCSK9 are both regulated through the transcription factor, sterol regulatory element-binding proteins, SREBP[82]. This means that at times of cholesterol depletion (e.g., in patients who are taking statins), SREBP will be activated which leads to the transcription of genes involved in cholesterol uptake (e.g., LDLR and PCSK9) and cholesterol biosynthesis[82]. Indeed, PCSK9 is upregulated by use of statins[83,84], which provides a potential mechanism of statin resistance.

In addition to lipoprotein metabolism, PCSK9 is implicated in other pathologies. In experimental settings, PSCK9 had been shown to defer steatosis and impair hepatic regeneration after partial liver resection[85]. In addition to LDLR, PCSK9 also down-regulates CD81[86]. Given LDLR and CD81 are both entry receptors for hepatitis C virus, PCSK9 inhibition may adversely affect viral control in patients with hepatitis C. Further, mice deficient of PCSK9 have impaired glucose tolerance[87]. As statins also increase the risk of diabetes[88], this observation may be a secondary effect of lipid-lowering, rather than a direct consequence of PCSK9 inhibition.

1.5.3 PCSK9 and atherosclerosis

After PCSK9 was established as an important regulator of LDL, researchers started to explore its potential as a therapeutic target. In the laboratory, investigators carried out animal studies to assess the impact of PCSK9 manipulation on experimental atherosclerosis. Clinically, researchers conducted epidemiology studies, using genetic variants of PCSK9 genes, to assess the relationships between PCSK9 expression and cardiovascular risk.

From an experimental perspective, Denis et al. first demonstrated that in both C57Bl6 mice and apoE$^{-/-}$ mice, transgenesis of PCSK9 resulted in increased accumulation of cholesterol ester in the mouse aorta, and genetic ablation of PCSK9 was associated with decreased aortic cholesterol ester[89]. Manipulation of PCSK9 gene expression in Ldlr$^{-/-}$ mice however, did not significantly change the amount of cholesterol ester deposited in mouse aorta, highlighting that PCSK9 exerts its effects principally through LDLR[89]. Ason et al. and Kuhnast et al. have both shown that in an E3LC mouse model of atherosclerosis, antibody-mediated inhibition of PCSK9 was associated with smaller atherosclerotic plaques[55,90]. Recently, Landlinger et al. took a different approach, where the investigators used a vaccine to induce immune responses against PCSK9 in E3LC mice. They showed that immunisation with the AT04 vaccine led to lower plasma cholesterol levels and smaller atherosclerotic plaques[91].

On the other hand, genetic epidemiology studies were instrumental in demonstrating the clinical significance and expediting the translation of PCSK9 biology from the bench to bedside. Abifadel et al. recently reviewed 16 studies that examined the relationship between PCSK9 variants and atherosclerotic vascular disease in diverse study populations[92]. These studies have consistently demonstrated the importance of PCSK9 in the regulation of plasma LDL-cholesterol; whereas mutations resulting in gain-of-function of PCSK9 (e.g., S127R and F216L) cause familial hypercholesterolaemia[65], mutations that led to loss-of-function (e.g., Y142X, C679X and K46L) are associated with lower plasma cholesterol[93]. These studies have also found that genetic variation in PCSK9 was associated with the risk of coronary artery disease[93], large-vessel atherosclerotic stroke[94] and peripheral arterial disease[95]. In a cohort of 3363 black and 9524 white Americans, two loss-of-function PCSK9 mutations (Y142X and C679X) found in black Americans were associated with a 28% reduction in LDL cholesterol and a 88% reduction in cardiovascular risk, whereas a genetic variant of PCSK9 found in white Americans (R46L) was associated with a 15% reduction in LDL cholesterol and 47% reduction

in cardiovascular risk[93]. Similar findings were independently reproduced in two other cohorts[96]. Collectively, these studies conclusively demonstrate the association between PCSK9 function, plasma cholesterol and the risk of atherosclerotic vascular disease.

Based on these findings, extensive efforts were made to develop clinical therapeutics against PCSK9. Two monoclonal antibodies against PCSK9, evolocumab and alirocumab, have been evaluated in clinical trials. In the Further Cardiovascular Outcomes Research With PCSK9 Inhibition in Subjects With Elevated Risk (FOURIER) trial, 27,564 patients with stable atherosclerotic vascular disease were treated with evolocumab[66], and in the Evaluation of Cardiovascular Outcomes After an Acute Coronary Syndrome During Treatment with Alirocumab (ODYSSEY) Outcome trial, 18,924 patients were enrolled within 4 weeks of stroke or myocardial infarction and were treated with alirocumab[67]. Despite slightly different patient populations, both antibodies were highly effective in lowering LDL cholesterol, and both achieved approximately 15% relative risk reduction. These two landmark trials demonstrate the efficacy of PCSK9 inhibition and provide the last piece of evidence supporting the role of PCSK9 in cholesterol metabolism and atherosclerosis.

1.6 Atherosclerosis and thrombosis

Under physiological circumstances, it is imperative for the body to maintain fluidity of the circulation. However, when faced with vascular injury, haemostatic function is activated, initiating an orchestrated response to form a clot and stop haemorrhage. This is achieved through a dynamic balance between platelets, coagulation factors and naturally-occurring anticoagulants, as well as the endothelium and leukocytes. Importantly, clot formation can occur inappropriately, a pathological scenario termed thrombosis.

In atherosclerosis, there is a perturbation to haemostasis and patients develop prothrombotic tendencies. Risk factors for atherosclerosis including diabetes modulate platelet responses and promotes a platelet phenotype that aggregates and activates more readily[97]. Oxidative stress induced by hypercholesterolaemia decreases bioavailability of nitric oxide, making the endothelium more pro-thrombotic[98]. Importantly, rupture or erosion of atherosclerotic plaques in late-stage disease causes coronary thrombosis and culminates as the clinical manifestations

of stroke, myocardial infarction or sudden cardiac death[15,99]. As thrombosis is the immediate precipitant of acute clinical events, effective treatment and prevention of arterial thrombosis is the mainstay of current-day ACS management[100,101].

Here, the cellular machinery of haemostasis and thrombosis is reviewed, with an emphasis on neutrophils.

1.6.1 Platelets

Platelets are anucleated cells derived from megakaryocytes in the bone marrow. The cells are discoid in shape and measure 1-3μm in diameter. Platelets contain three types of granules including the dense granule, α-granules and the lysosome. Dense granules have adenosine diphosphate (ADP) and polyphosphate, and α-granules contain adhesion molecules, chemokines, coagulation and fibrinolysis proteins[102]. Lysosomes contain acid hydrolase and cathepsins[102]. On the cell surface there are different types of integrins that mediate platelet interactions with other cells, most notably being glycoprotein (GP) Ib-V-IX, GPVI and GPIIbIIIa.

To achieve haemostasis at times of vascular injury, platelets first need to adhere to the injured vascular surface. This is mediated by circulating von Willebrand factor (vWF) and the integrins on platelet surface. When vascular injury occurs, subendothelial collagen or the core of ruptured atherosclerotic plaques are exposed to the lumen. This allows the binding of circulating vWF to exposed collagen, which results in a conformational change in vWF and enables its binding to platelet GP Ib-V-IX[103]. This collagen-vWF-GP Ib-V-IX binding has a rapid-onset and rapid-offset, thus it is inherently unstable. To reinforce adhesion stability, platelets utilise other integrins to bind to other subendothelial structures. For example, platelet GP VI and integrin $\alpha_2\beta_1$ bind to collagen, and platelet integrin α_5B_1 and laminin $\alpha_6\beta_1$ bind to fibronectin[104]. Once firmly adhered to the injured vascular surface, platelets become activated, which is characterised by the following three features. Firstly, activated platelets degranulate and secrete soluble agonists such as ADP and thrombin. Secondly, when platelets are activated, they undergo morphological changes, and transform from a discoid shape to a speculated, rounded mass. Thirdly, binding of soluble agonists including ADP to the platelet

surface induce conformational changes in integrin GP IIbIIIa, and this allows GPIIbIIIa to bind with high affinity to fibrinogen, fibronectin and vWF.

1.6.2 Coagulation protease factors (Fig. 1-4)

In order to form a stable thrombus, an insoluble mesh network of fibrin atop platelets is required. To do this, the body uses a series of proteases called coagulation factors. Traditionally, this system is divided into 3 parts. These 3 cascades are, the extrinsic cascade, which is initiated by tissue factors released into the circulation upon tissue injury; the intrinsic cascade, which is initiated by activation of circulating factor XII, and the common pathway where the extrinsic and intrinsic pathway converge to form fibrin. Much of this framework was built upon *in vitro* studies. However, more contemporary *in vivo* work has informed us that the intrinsic and extrinsic pathways do not work in parallel but interact with each other. This was recently reviewed by Versteeg et al.[105] and briefly summarised below.

When vascular injury occurs, subendothelial tissue, atherosclerotic plaques or circulating monocytes and neutrophils release tissue factor (TF), which forms a complex with factor VIIa. The TF-VIIa complexes cleave factor X to form factor Xa. Factor Xa reacts with factor Va to form the prothrombinase complex, which serves to convert prothrombin (factor II) into thrombin (IIa) (Fig. 1-4A). Essentially, the intrinsic pathway functions to initiate thrombus formation, and this reaction occurs on the surface of TF-expressing cells.

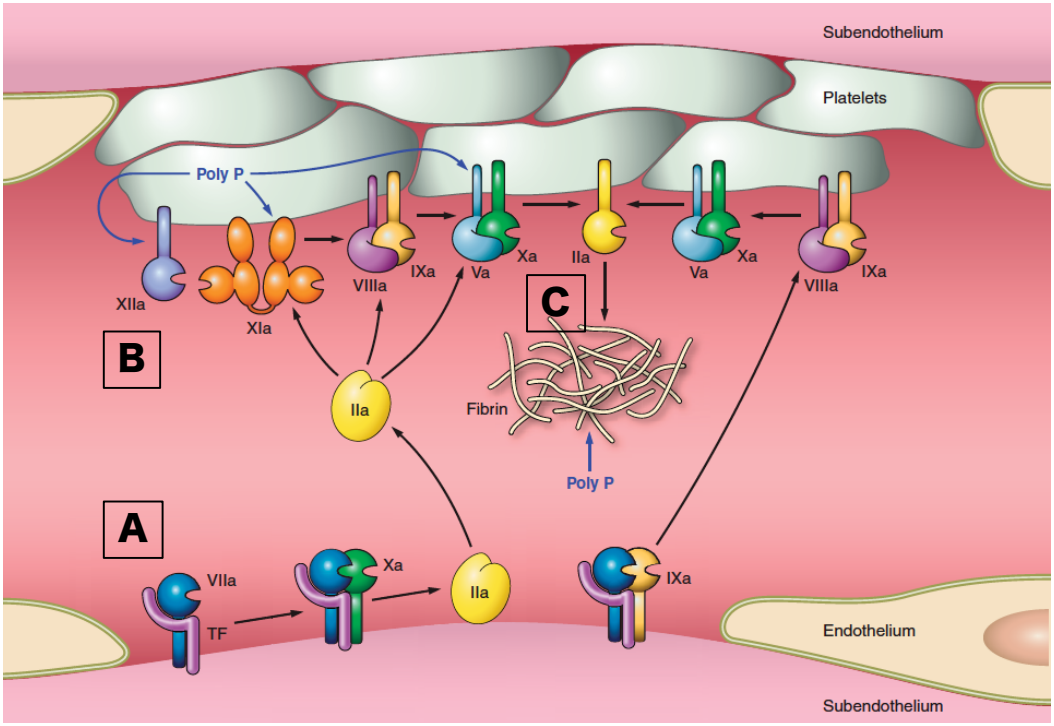

Figure 1-4. Coagulation protease cascade. (A) The coagulation process starts with tissue factor (TF) forming a heterocomplex with factor VIIa, which results in the formation of thrombin (IIa). (B) Thrombin interacts with factor XIa, VIIIa and Va and generates large amounts of thrombin. (C) Thrombin then cleaves fibrinogen to form fibrin, which then gets crosslinked to form the insoluble meshwork. Activated platelets also secrete polyphosphate (Poly P) that stimulates factors XII, XI and V, promoting fibrin formation. Adapted from Versteeg et al[105].

Thrombus amplification occurs on platelets that adhered to injured vascular surface or platelet aggregates, and thrombin generated from the first phase plays a key role in this reaction. As thrombin accumulates, it activates platelets and cleaves factor XI to generate factor XIa. In addition, thrombin converts factor V to Va, which accentuates prothrombinase activity. Thrombin also activates factor VIII, which serves as a cofactor to factor IXa (Fig. 1-4B).

In the third phase, nascent thrombus propagates on phospholipid-containing surfaces, primarily activated platelets. Here, factor XIa converts factor IX to IXa, which in turn reacts with thrombin-activated VIIIa to form tenase. Tenase convert factor X to Xa on phosphatidylserine-exposing cell membrane. Factor Xa forms a heterocomplex with cofactor Va, and this Xa-Va complex generates thrombin in high volumes, which in turn converts fibrinogen to fibrin in abundance. Thrombin also activates factor XIII, which polymerises fibrin by covalent crosslinking. The coagulation cascade is also regulated by platelet-derived polyphosphate, which interacts with factors XII, XI and V and promotes fibrin formation[106].

1.6.3 Neutrophils (Fig. 1-5)

Conventionally, haemostasis and thrombosis are thought to be the result of an interplay between the vascular endothelium, platelets and coagulation factors, as conceptualised by Rudolph Virchow in "Virchow's triad" that underpinned deep vein thrombosis (DVT). Over the recent years, leukocytes, predominantly neutrophils and monocytes, and to a lesser extent, mast cells, basophils and eosinophils have also been implicated in thrombosis.

Neutrophils are the most abundant leukocyte subpopulation and account for approximately 40-70% of all leukocytes in the circulation. Of a myeloid lineage, neutrophils are primarily recognised for their function in innate immunity, phagocytosing and killing micro-organisms through the release of reactive oxygen species. Neutrophils, along with platelets, are the first cells recruited to the site of vascular injury, where they accumulate through interactions between the integrins lymphocyte function-associated antigen 1 (LFA-1) and intracellular adhesion molecule 1 (ICAM-1)[107]. Importantly, TF is found in both human and mouse neutrophils, and it is the main source of TF in a mouse model of laser-induced injury[107,108].

About 15 years ago, it was discovered that upon stimulation by phorbol ester (phorbol 12-myristate 13-acetate, PMA) or lipopolysaccharide (LPS), neutrophils undergo a special form

of cell death where they extrude neutrophil extracellular traps, or NET, a lattice of deoxyribonucleic acid (DNA) coated with histones and neutrophil proteases including elastase, cathepsin G and myeloperoxidase (MPO)[109]. This process requires the enzyme nicotinamide adenine dinucleotide phosphate (NADPH) oxidase, which generates reactive oxygen species[110], the nuclear translocation of neutrophil elastase[111], and another enzyme, peptidylarginine deiminase 4 PAD4), which mediates histone hypercitrullination and chromatin decondensation[112]. NET serves as a scaffold where platelets, coagulation factors and erythrocytes can interact with each other[113]. Extracellular histones, a constituent of NET formation (NETosis), has a number of antithrombotic actions. Histones can cause platelet activation, aggregation and thrombin generation, through toll-like receptor (TLR) 2 and TLR4 signalling[114]. It can promote thrombin formation by inhibiting activation of the anticoagulant protein C[115]. In addition, extracellular histone can promote exposure of phosphatidylserine on erythrocytes[116] and cause endothelial injury[117]. Proteases within NET also exert pro-thrombotic actions. Proteases such as elastase and cathepsin G can activate coagulation factors V[118] and VIII[119], and they can also inhibit anticoagulants such as TF pathway inhibitor[120] or antithrombin[121]. In short, mechanistically, NET has diverse prothrombotic actions.

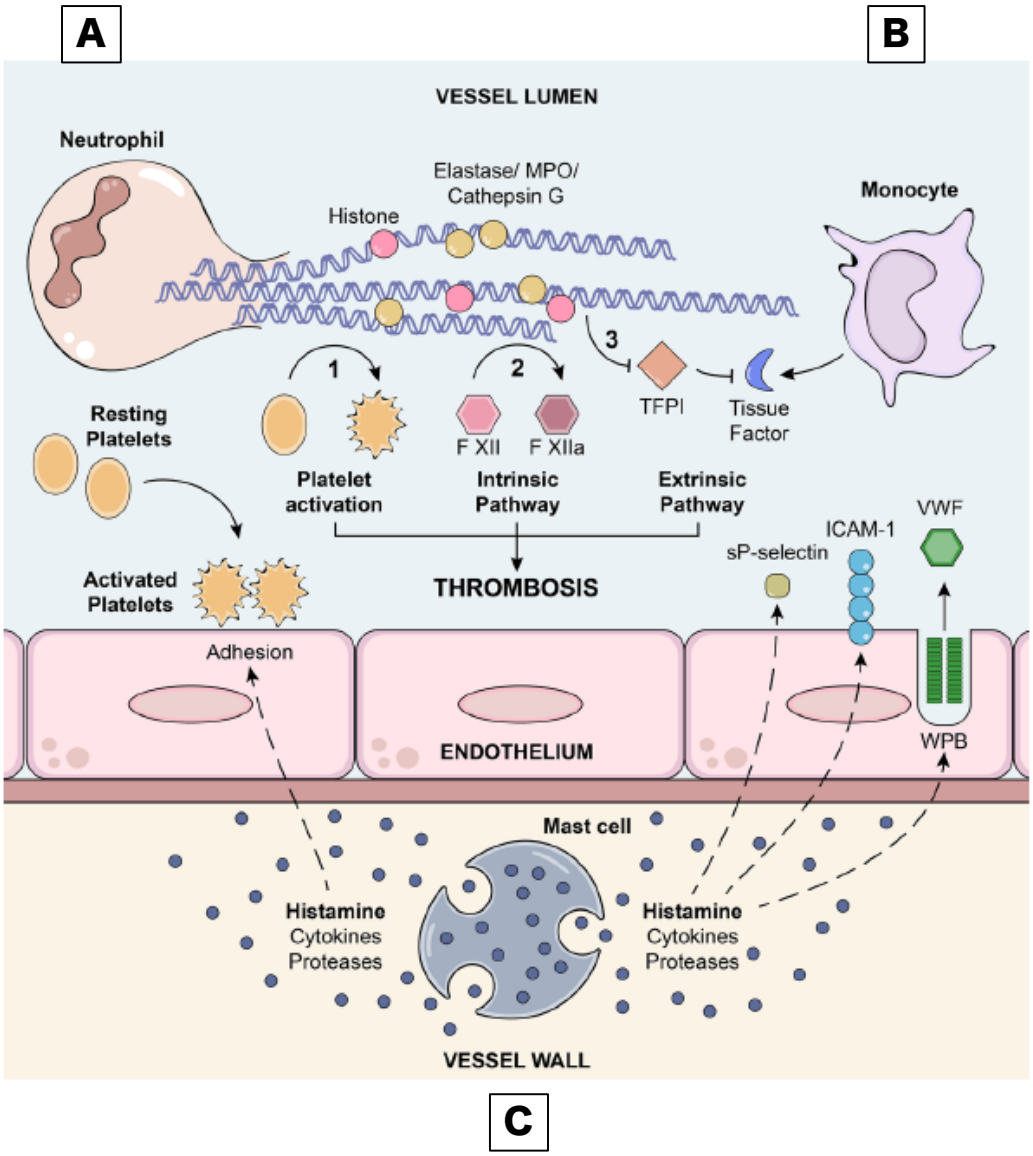

Figure 1-5. Leukocytes contribute to thrombosis. (A) Neutrophils release NETs that activate platelets, intrinsic and extrinsic pathways. (B) Monocytes activate the extrinsic pathway through release of TF. (C) Mast cells may contribute to thrombosis through the release of histamine which activates platelets and stimulates the secretion of soluble P-selectin, vWF and it also causes ICAM-1 expression. Adapted from Huang et al[122].

NETosis plays a significant role in arterial thrombosis. Massberg et al. have demonstrated that genetic ablation of neutrophil serine protease (elastase and cathepsin G) leads to impaired fibrin formation and smaller thrombi in a mouse model of thrombosis[120]. Knight et al. have shown that pharmacological inhibition of NETosis effectively inhibits thrombosis in a mouse model of photochemical injury-induced carotid thrombosis[123]. Further, clinical investigations have validated the clinical relevance of these preclinical studies. NETs have been detected in coronary thrombi in a number of studies[108,124-126]. In a series of 111 ST-segment elevation myocardial infarction (STEMI) patients, the amount of NETosis positively correlated with infarct size and inversely associated with the resolution of the ST-segment on electrocardiogram, a marker of successful restoration of coronary flow[124]. Interestingly, use of DNase augments the lytic power of tissue plasminogen activator, a fibrinolytic agent used in STEMI[124]. Riegger et al. examined 253 coronary thrombi retrieved from patients diagnosed with in-stent thrombosis, and they found that NET was present in 23% of samples. This low frequency was attributed to the use of heparin, an anticoagulant known to dismantle NETosis[125].

On the venous side, NETosis also significantly contributes to thrombosis. In a mouse model of DVT where thrombosis was induced by restricted flow at the inferior vena cava (IVC), investigators showed that thrombus propagation is NET-dependent. Inhibition of NETosis, either through the use of DNase or genetic deletion of PAD4, attenuates thrombotic responses and results in bigger thrombi[127]. Clinical studies have also extended these observations to the bedside. NET have been found in the organising phase of DVT thrombi[128], and markers of NETosis including plasma DNA, nucleosome and elastase–α1-antitrypsin complex levels were increased in DVT patients[129]. In one study, even after adjusting for potential confounders, markers of NETosis were still elevated in patients with DVT, suggesting a potential utility as a biomarker[130]. However, it is important to point out that the impact of NETosis in DVT has yet to be confirmed in other mouse models of DVT. Neutrophil depletion has no effect on thrombus size in a mouse model where DVT was induced by complete flow stasis, [131], and it does not change thrombus size in another mouse model where DVT was induced by ribonucleic acid (RNA) knockdown of anticoagulants protein C and antithrombin [132]. Similarly, in a mouse model of DVT where thrombosis was induced by electrolytic endothelial injury, deficiency of PAD4, an enzyme critical in NETosis, had no influence on thrombus size either[133]. These conflicting findings are somehow difficult to reconciliate, and probably means the contribution of NETosis in DVT is variable, depending on the inciting stimuli and the context of DVT.

1.6.4 Monocytes and mast cells

Monocytes are a major source of TF in the circulation[134]. Upon stimulation, for example, by high mobility group box 1 (HMGB1)[135] and LPS[136], monocytes can increase the expression, release or activity of TF[137]. Mast cells have also been implicated in DVT through degranulation and release of histamine, which in turn trigger the secretion of soluble p-selectin and vWF[138], both are known to promote thrombosis.

1.7 High Mobility Group Box 1 (HMGB1) – Overview

HMGB1 is a 25kDa protein consisting of 215 amino acid residues. It is highly conserved, with a 99% homology between mammalian species. As a non-histone nuclear protein, it was initially recognised as a DNA chaperone that bends DNA and exposes its binding sites for transcription factors so to regulate transcription, recombination, and DNA replication[139,140]. Subsequently, HMGB1 was found to be a damage-associated molecular pattern (DAMP), also known as alarmin, that signals tissue death or damage[141]. It contributes to a wide range of biological processes including recruitment and activation of immune cells, angiogenesis, tissue repair and regeneration[141-143].

1.7.1. Structure of HMGB1 (Fig. 1-6)

Structurally, HMGB1 consists of two DNA-binding domains and a C-terminal tail that contains 30 continuous residues of glutamic and aspartic acid. The Box A domain (amino acid 9-74) has anti-inflammatory properties and acts as a competitive antagonist of full length HMGB1[144,145]. The Box B domain (amino acids 89-162), on the other hand, is pro-inflammatory and induces macrophage cytokine secretion[146]. In addition, HMGB1 has 2 nuclear localisation sequences (NLS, residues 28-44 and 179-85) that enable HMGB1 to translocate into the nuclei.

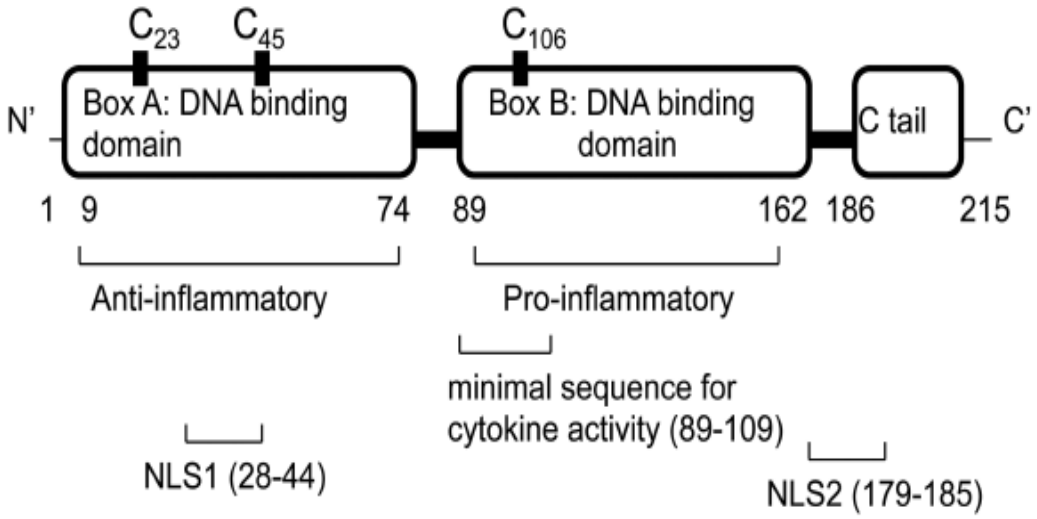

Figure 1-6. Structure of HMGB1. HMGB1 is a protein of 215 amino acid residues that is made up of 2 DNA binding domains named Box A and B, and a glutamate- and aspartate-rich C-terminal tail. The Box A domain (residues 9-74) is anti-inflammatory whereas Box B (residues 89-162) is pro-inflammatory, containing a cytokine-inducing sequence (89-109). It also contains two NLS. Adapted from Yang et al[147].

1.7.2 Mode of release and post-translational modification of HMGB1 (Fig. 1-7)

HMGB1 is subjected to post-translational modifications, which determines its function, subcellular localisation and molecular binding partners. Five post-translational modification to HMGB1 had been described. Of which, the redox modification of the cysteine residues, located at positions 23, 45 and 106 of HMGB1, are best characterised. In the setting of necrosis, HMGB1 is passively and rapidly released in a fully reduced form where all 3 residues exist as thiols (-SH). It forms a complex with chemokine (C-X-C motif) ligand-12 (CXCL12) and signals through chemokine (C-X-C motif) receptor type 4 (CXCR4) [148]. This initiates chemotaxis and leads to cell proliferation and differentiation[149]. HMGB1 can also exist in a partially reduced state where C106 is reduced, and C23 and C45 are connected with an intramolecular disulphide bond[150]. In this state, HMGB1 stimulates macrophages through TLR4 signalling, in a MD-2 dependent manner and leads to subsequent cytokine secretion[145,151,152]. When all three cysteines are oxidised (all take up SO_3H form), as happens during apoptosis where reactive oxygen species are abundantly produced, HMGB1 becomes immunotolerant and exerts no immunological actions[149,153].

In addition, HMGB1 can be modified through acetylation. At quiescent state, HMGB1 freely shuttles between the nucleus and cytoplasm. In order for macrophages to secrete HMGB1, HMGB1 must be prevented from shuttling back to the nucleus. This occurs in sepsis, where bacterial endotoxin LPS binds to TLR4, which upregulates type I-interferon (IFN), activates the janus kinase-signal transducer and activator transcription proteins (JAK/STAT1) pathway,

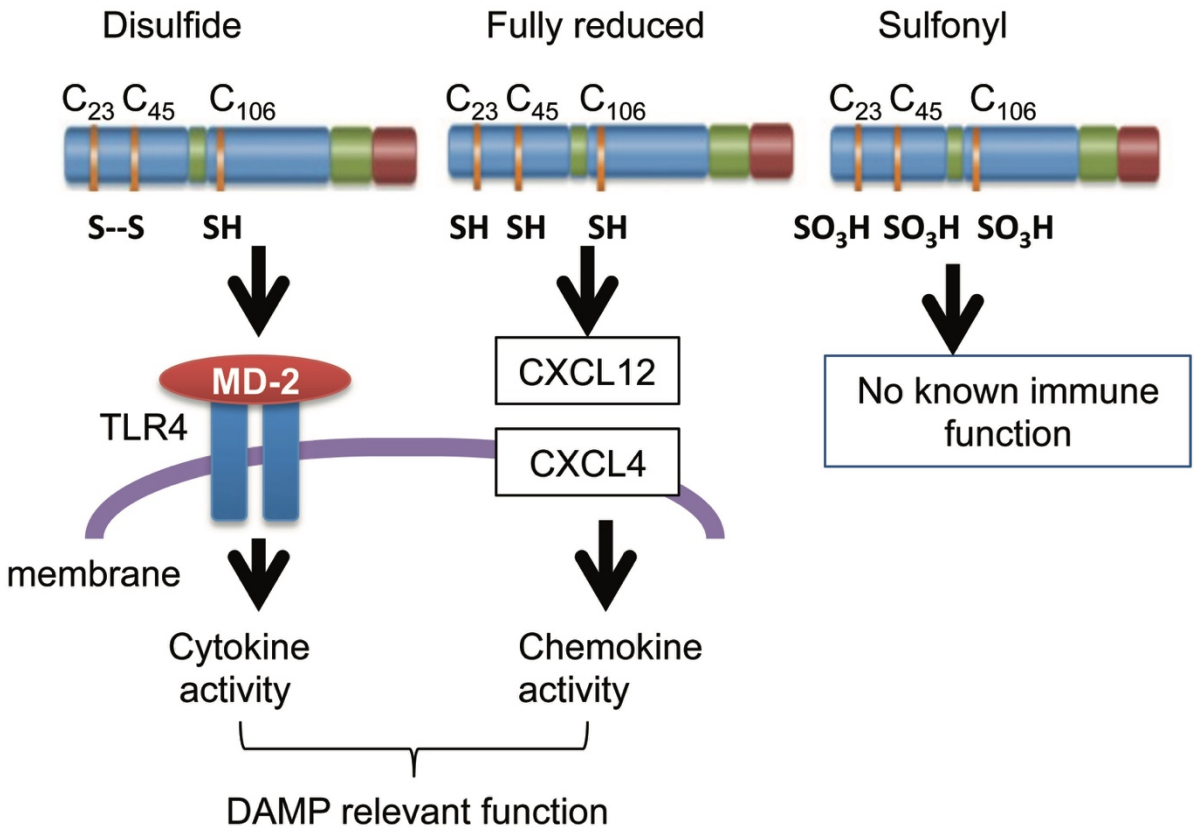

Figure 1-7. Redox status of HMGB1 dictates its molecular partner and downstream activity. When HMGB1 is partially reduced, where C106 is in a thiol form and C23 and C45 are connected by a disulphide bond, HMGB1 binds to TLR4 and stimulates cytokine secretion. When all 3 cysteines are reduced, HMGB1 forms a heterocomplex with CXCL12 which signals through CXCL4 and initiates chemokinesis. When all three cysteines are oxidised, HMGB1 becomes immunotolerant. Adapted from Yang et al[147].

and leads to acetylation of HMGB1[154,155] and its retention in the cytoplasm[156]. A different process occurs in pyroptosis, a form of programmed cell death in the setting of infection. In this process, the activated inflammasome induces autophosphorylation of double-stranded RNA-dependent protein kinase (PKR), which associates with various components of the inflammasome including nucleotide-binding oligomerisation domain (NOD)-like receptors (NLR) proteins, NLRP3 and NLRP1. This allows HMGB1 to be released in a non-classical, lysosome-mediated secretion of HMGB1[157,158]. Further, HMGB1 can undergo phosphorylation and methylation, but they have no known functional significance.

1.7.3 Receptor usage and biological actions

HMGB1 does not have specific or dedicated receptors. Instead, HMBG1 binds to pattern recognition receptors that associate with DAMP and pathogen-associated molecular patterns (PAMP). So far, more than 13 receptors have been shown to associate with HMGB1. Of which, receptor for advanced glycation end product (RAGE) and TLR4 are most well-studied. RAGE was the first HMGB1-interacting receptor identified, and initially was found to be important to neurite formation[159]. The HMGB1-RAGE axis is involved in chemotaxis of immune cells, differentiation of mesenchymal stem cells[160], upregulation of surface proteins (e.g., cluster of differentiation [CD] 80, CD83, CD86, and human leukocyte antigen, [HLA]-A,B,C on dendritic cells)[161], migration of dendritic cells[162], and maturation of dendritic[163] and T cells[163]. Cells may use HMGB1-RAGE to traffic DAMPs or PAMPs into the cytoplasm to access proinflammatory receptors. In addition, HMGB1 can form a heterocomplex with other DAMPs, and these heterocomplexes then bind to RAGE and are endocytosed by macrophages. Once endocytosed into macrophages, HMGB1-DAMP heterocomplexes are translocated to lysosomes, where HMGB1 permeabilises lysosomes to allow HMGB1-bound DAMPs to be released into the cytoplasm for these DAMPs to interact with other cytosolic receptors[164].

TLR4 is another important receptor through which HMGB1 exerts its actions. In monocytes, disulphide HMGB1 binds to TLR4 in a MD2-dependent manner[152], and activates IκB kinases (inhibitors of kappa B kinases). This induces translocation and activation of nuclear factor kappa-light-chain-enhancer of activated B cells (NFκB) and phosphorylation of protein kinase B (Akt) and p38 mitogen-activated protein kinase (p38-MAPK)[165]. This in turn leads to secretion of cytokines including tumour necrosis factor (TNF), interleukin (IL) -1α, IL-1β, IL-

1RA, IL-6, IL-8 but not IL-10 or IL-12[166,167]. Importantly, TLR4 engagement is obligatory for cytokine secretion[146]. In neutrophils, HMGB1 binds to TLR4, activates NADPH oxidase[168] and results in induction of NETosis[169]. Further, HMGB1 can activate dendritic cells through TLR4 signalling, thus improves the efficiency of antigen presentation and enables cytotoxic T cells ($CD8^+$ T cells) to kill or clear tumour cells[170].

HMGB1 can also associate with the receptor CD26-Siglec-10. When HMGB1 binds to CD26-Siglec-10, in contrast to its usual stimulatory actions, this interaction inhibits NFκB and thus limits tissue damage. Interestingly, when LPS signals through CD26-Siglec-10, NFκB is activated and results in an inflammatory response and tissue injury[171]. This explains how cells can distinguish between damage and infection and adjust their inflammatory responses accordingly.

In addition to surface receptors, HMGB1 also interacts with nucleic acid and DNA-containing immune complexes including CpG (cytosine and guanine separated by only one phosphate group)-containing oligonucleotides. This association signals through TLR9-myeloid differentiation primary response 88 (MyD88) in a RAGE-dependent manner, leads to activation of dendritic cells and secretion of cytokines including IFN-α[172,173]. Yanai et al. have extended these findings and demonstrated that in addition to DNA, HMGB proteins (including HMGB1, 2 and 3) also interact with immunogenic RNA and induce type 1 IFN[174]. Given the promiscuity of the binding between HMGB1 and immunogenic nucleic acids, it is speculated that HMGB1 is the universal sensor of viral infection, which then co-ordinates with specific pattern recognition receptors downstream to mount innate responses to thee pathogens[174,175]. It is worth noting, however, in one study carried out in human plasmacytoid dendritic cells, HMGB1 was shown to suppress TLR9-mediated cytokine secretion[176]. The reason for these discrepant observations is unclear, and it could be related to inter-species differences. As aforementioned studies[174,176] were based on *in vitro* experiments, *in vivo* validation would better elucidate the role of HMGB1 in the innate defence against viral infection.

1.7.4 HMGB1 in atherosclerosis and acute coronary syndrome

Atherosclerosis is a disease of chronic sterile inflammation, with complex pathogenesis involving different immune cells, and in particular, monocytes. The role of HMGB1 in

atherosclerosis was first implicated in a study by Kalinina et al., who showed an increased expression of $CD68^+$ monocyte-derived HMGB1 in human aortic atheroma[177]. Two subsequent studies lend further support to the notion that HMGB1 may be an active participant than innocent bystander in atherosclerosis. In a clinical study, serum HMGB1 levels positively correlated the atherosclerotic burden, measured by angiographic Gensini score, a point system that takes into account the location and severity of coronary stenosis[178]. More definitively, using a mouse model of atherosclerosis, Kanellakis et al. demonstrated that HMBG1 neutralisation through inhibition of monocyte recruitment, reduced atherosclerotic plaques by 55% and reduced atheroma retention of immune cells[179]. Collectively, they highlight a pathogenic role of HMGB1 in chronic atherogenesis.

Since HMGB1 functions as a DAMP, mediating both removal of dead tissues and repair of injured cells, its role in acute coronary syndrome and its potential use as a biomarker and therapeutic target have attracted much interest from researchers. In 2006, Goldstein et al. first demonstrated that blood HMGB1 levels are significantly elevated in patients with stroke and myocardial infarction[180]. This finding has been confirmed independently in 7 other studies, summarised in Table 1-1. Plasma HMGB1 levels have been shown to positively correlate with markers of poor prognosis including infarct size and autonomic dysfunction[181,182], and inversely associated with predictors of favourable outcomes such as cardiopulmonary fitness and residual left ventricular function[183]. In a study of 141 STEMI patients, Sorensen et al. showed that plasma HMGB1 levels independently predicted mortality, after adjusting for potential confounders[184]. Similarly, Hashimoto et al. validated the independent predictive value of HMGB1 in a cohort of Non-STEMI (NSTEMI) patients to unstable angina[185]. Taken together, circulating HMGB1 appears to be a valid biomarker. Further, elevated HMGB1 during the course of ACS has deleterious effects and targeting this DAMP may provide clinical benefits.

However, experimental studies that evaluated the impact of HMGB1 inhibition in rodent models of myocardial ischemia and reperfusion (30 minutes and 48 hours respectively) revealed a mixed picture. In a mouse model of ischemia-reperfusion, Andrassy et al. showed that recombinant HMGB1 exacerbated ischemia-reperfusion injury, whereas antagonising HMGB1 using the box A domain reduced infarct size[186]. In this setting, HMGB1 signals

through RAGE, activates mitogen-associated protein (MAP) kinase and increases NFκB binding to DNA. On the other hand, Oozawa et al. injected HMGB1-neutralising antibodies into rats subjected to ischemia-reperfusion injury (30 minutes and 60 minutes respectively) and found this intervention worsened ischemic injuries, as evidenced by a bigger infarct size[187]. In a slightly different setting, where myocardial infarction in mice was induced by permanent left anterior coronary artery (LAD) ligation, mice with HMGB1-overexpressing hearts had a smaller infarct size, enhanced angiogenesis and improved survival[188]. On the other hand, using a similar model of permanent LAD ligation in rats, Kohno et al. showed that HMGB1 blockade resulted in adverse left ventricular remodelling, despite lower macrophage number and reduced expression of inflammatory cytokines TNF-α and IL-1β[189]. These discrepant results probably relate to the difference in species (mouse vs. rats) and experimental conditions (permanent vs. temporary ligation). More importantly, it highlights the complexity of DAMP biology, where each DAMP carries multiple functions, which is dependent on the biological context, and the level and the duration of DAMP elevation and signalling. This is illustrated by a study by Limana et al., who showed that in addition to inflammatory functions, HMGB1 also has a restorative function, as it enhances myocardial regeneration after myocardial infarction by promoting the proliferation and differentiation of c-Kit$^+$ cardiac stem cells[190].

1.7.5 HMGB1 in thrombosis

HMGB1 has been found in human coronary and peripheral arterial thrombi[191-193], and plasma HMGB1 levels are significantly elevated in patients with disseminated intravascular thrombosis[194], implicating a role for HMGB1 in thrombosis. Experimental studies in mice have shown that platelet-derived HMGB1 promotes ferric chloride ($FeCl_3$)-induced carotid thrombosis, a model of arterial thrombosis[195], and it also contributes to venous thrombosis[196]. In microvascular thrombosis such as disseminated intravascular coagulation, HMGB1 seems to play a more ancillary role and enhances thrombin-induced thrombosis[135].

Mechanistically, preclinical investigations have shown that HMGB1 affects all effectors of thrombosis and haemostasis including platelets, coagulation factors, monocytes and neutrophils. Though platelets are anucleate, HMGB1 is abundantly present in the cytoplasm[197]. Upon platelet activation, HMGB1 is exported to the cell surface and released into circulation[197].

HMGB1 can bind to RAGE or TLR4 on activated platelets[191,195]. On its own, HMGB1 does not cause platelet activation or aggregation[191]. However, HMGB1 can amplify platelet responsiveness in the presence of other platelet agonists including collagen-related peptide[195]. Further, platelet-derived HMGB1 induces platelet aggregation, spreading and adhesion, via TLR4-myD88 signalling[195].

Coagulation factors and naturally occurring anticoagulants also interact with HMGB1. *In vitro*, HMGB1 inhibits activation of protein C, a naturally occurring anticoagulant[135]. HMGB1 also interacts with another anticoagulant, thrombomodulin. Thrombomodulin inhibits the inflammatory activity of HMGB1 in two ways. Firstly, the N-terminal lecithin-like domain of thrombomodulin binds to HMGB1, antagonises its engagement with RAGE thus prevents downstream NFκB transcription[198]. Thrombomodulin also enhances thrombin-mediated cleavage of HMGB1, which converts HMGB1 to a degradation product that is less proinflammatory[199]. It remains unclear, however, if HMGB1 modulates thrombin or thrombomodulin during these interactions.

As a DAMP, HMGB1 promotes neutrophil recruitment[200], and importantly, induces NETosis through TLR4 signalling[169], which has been shown to be the dominant mechanism through which HMGB1 promotes DVT[196]. HMGB1 also promotes monocyte recruitment and its expression of TF *in vitro*[135], though the *in vivo* significance of this is unclear.

1.7.6 HMGB1 as a therapeutic target

Since its surprising identification as a DAMP[166], research efforts have been directed to investigate the therapeutic potential of inhibiting HMGB1 in various disease settings[201], summarised in Table 1-2.

A number of strategies have been employed to inhibit HMGB1. Most commonly, monoclonal or polyclonal antibodies that target and neutralise HMGB1 are used. In this thesis, a neutralising antibody that targets the C-terminus of HMBG1 (residues 208-215) and that was

shown effective in reducing the infarct size in a rat model of stroke was used[202]. This particular HMGB1-neutralising antibody had been used in other disease settings, summarised in Table 1-3. Recently, a partially humanised antibody against HMGB1 has been developed, taking this one step closer to the clinic[203,204]. As an alternative, HMGB1 Box A domain works as an antagonist of full-length HMGB1 and represents another strategy of inhibiting HMGB1[143], Efficacy of this approach was validated in mouse models of sepsis [144] and myocardial ischemia-reperfusion injury[186]. However, the precise inhibitory mechanism of HMGB1 Box A remains unknown, posing a barrier to translation. A third strategy was based on the observation that thrombomodulin inactivates HMGB1 by facilitating thrombin cleaving of HMBG1[199], and administration of thrombomodulin improved survival in a mouse model of endotoxemia[205]. However, thrombomodulin and thrombin have significant roles in thrombosis and haemostasis, and in a mouse model of sepsis, infusion of thrombomodulin was associated with elevated thrombin-antithrombin levels[205]. The fourth strategy aimed to block the cognate receptor such as RAGE, and it was shown to confer survival benefits in an animal mode of sepsis[206]. While conceptually this would provide specific targeting of a particular function of HMGB1, it could affect the binding of other ligands and result in off-target toxicity. Finally, a better understanding of the structural biology of HMGB1 has led to the development of a small molecular inhibitor, a tetramer protein with 4 amino acid residues that prevents interactions between HMGB1 and MD-2, an adaptor protein of TLR4. Investigators have demonstrated that in mice, this inhibitor reduced the mortality in sepsis, hepatic ischemia-reperfusion injury and paracetamol toxicity[146]. This is an attractive option as LPS, another TLR4 ligand, does not signal via MD-2. Further, this protein is structurally simple, which may mean a cheap and easy manufacturing process.

HMGB1 had been implicated in diverse pathologies, and there has been particular enthusiasm in developing HMGB1 inhibitors in sepsis. As HMGB1 is a late mediator of infection, it was thought that blocking HMGB1 could ameliorate late inflammatory response in sepsis, for which no specific treatment is currently available. In a mouse caecal ligation and perforation model of sepsis, HMGB1 inhibition with neutralising antibody or the anti-inflammatory HMGB1 Box A domain resulted in improved animal survival, even in the setting of established sepsis[144,166]. The therapeutic potential of HMGB1 inhibition had been evaluated in diverse preclinical models of sterile inflammation including rheumatoid arthritis[145], atherosclerosis[179] and hepatic ischemia-reperfusion injury following paracetamol overdose[200]. These studies

showed that HMGB1 inhibition is a novel and promising strategy to treat diseases of sterile inflammation. Importantly, some of these studies were corroborated with clinical evidence[124], paving the way for clinical translation.

1.8 Concluding summary

Despite the complexity, chronicity and largely subclinical nature of atherosclerosis, posing an almost insurmountable challenge to clinicians and researchers, great strides have been made in atherosclerosis research. It has been recognised that among the many risk factors and pathophysiological processes that contribute to the initiation and development of atherosclerosis, plaque rupture and ensuing thrombosis are the pivotal events that change the course of the disease. In addition to precipitating devastating clinical outcomes such as stroke and myocardial infarction, these events can also cause sudden expansion of atherosclerotic plaques and accelerate disease progression. Therefore, stabilisation of atherosclerotic plaques and prevention of arterial thrombosis are two promising therapeutic strategies that could significantly improve clinical outcomes.

Recently, PCSK9 has emerged as a therapeutic target that, in addition to its effects in LDL metabolism, may also have a role in plaque stability. Epidemiology studies have provided robust evidence that genetic variations in PCSK9 have a substantial impact on lifetime cardiovascular risks, and pharmacological neutralisation of PCSK9 significantly reduces adverse clinical events. Further, a large-scale intravascular imaging study has shown that inhibition of PCSK9 has a modest effect on plaque regression, suggesting PCSK9 inhibition may exert its protective effects by changing plaque composition to a more favourable profile. This thesis used animal models of plaque rupture and atherosclerosis to examine the quantitative and qualitative effects of PCSK9 inhibition in atherosclerosis.

A second focus of this thesis was to investigate the feasibility of a novel approach in preventing arterial thrombosis. Based on accumulating evidence implicating neutrophils, in particular, NETs in thrombosis and haemostasis, it was hypothesised that inhibition of NETosis may be a useful antithrombotic strategy. Specifically, the potential clinical utility of HMGB1 neutralisation was examined. HMGB1 is a protein with diverse functions in immunity and inflammation and a known inducer of NETosis. Experimental studies have also implicated a

role for HMGB1 in the prothrombotic actions of monocytes and platelets, lending further support to its candidacy as a therapeutic target. This thesis aimed to evaluate the translational potential of this novel antithrombotic approach through detailed analysis of its efficacy and safety in animal models of thrombosis.

Table 1-1. Clinical studies that assess the prognostic values of HMGB1

Acute Coronary Syndrome					
Study	**Study Population**	**Control**	**Follow-up Period**	**Findings**	**Multivariate adjustment**
Goldstein et al, 2006[180]	MI (n=9), Stroke (n=7)	Healthy control (n=16)	Cross-sectional	• Blood HMBG1 level was higher in MI and stroke patients (MI vs. control, 2.05 vs. 1.94±2.05 ng/mL, p<0.01; stroke vs. control, 218±18.4 vs. 16.8±10.9 ng/mL, p<0.001)	No
Yamada et al, 2006[207]	ACS with events (n=11)	ACS with no events (n=127)	1 month	• Blood HMGB1 was higher in ACS patients with recurrent events (2.24±0.90 vs. 0.43±0.15μg/L, p<0.0001) • HMGB1 predicts patient outcomes	Not reported
Kohno et al., 2009[189]	STEMI (n=35)	Stable angina patients (n=35)	In-hospital	• Blood HMGB1 was higher in STEMI patients (on admission, stable angina vs. STEMI, 4.5±5.3 vs. 1.0±1.6ng/mL, p=0.0004) • Blood HMGB1 level was higher in patients with complications (pump failure, cardiac rupture, cardiac death)	No
Cirillo et al., 2009[183]	STEMI (n=54)	Age and BMI-matched (n=16)	Cross-sectional	• Blood HMGB1 was higher in MI patients (14.8±6.8 vs. 2.3±1.0 ng/mL, p<0.0001) • HMGB1 inversely correlated to cardiopulmonary fitness (β=-0.276, p=0.01) and echocardiographic findings of LV function (e.g., LVEF, β=-0.312, p=0.02)	None
Giallauria et al., 2010[181]	STEMI (n=67)	None (correlational)	Cross-sectional	• Blood HMGB1 level inversely correlated to autonomic dysfunction (heart rate recovery) in regression analysis (r=-0.387, p<0.001)	Yes
Sorensen et al., 2011[184]	STEMI (n=141)	Healthy control (n=42)	10 months	• Blood HMGB1 level was higher in STEMI patients (2.9 μg/L [range 2.6 to 3.2μg/L] vs. 1.3 μg/L [range 1.1 to 1.5 μg/L], p<0.001) • Blood HMGB1 level was higher in STEMI patients who died (4.8 g/l [range: 3.1 to 7.5 g/l] vs. 2.9 g/l [range: 2.6 to 3.2 g/l], p<0.01) • HMGB1 predicted mortality in STEMI patients, after multivariate adjustment	Yes

Andrassy et al., 2011[182]	STEMI (n = 46) or NSTEMI (n = 49)	Correlational	6 months	• HMGB1 level positively correlated to infarct size (r^2 = 0.81 for STEMI and r^2 = 0.74 for NSTEMI, p < 0.001) • HMGB1 inversely correlated to residual ejection fraction (r^2 = 0.40 for STEMI and r^2 = 0.25 for NSTEMI, P < 0.001) • HMGB1 predicts infarct size and residual ejection fraction after multi-variate adjustment	Yes
Hashimoto et al., Atherosclerosis 2012[185]	NSTEMI/ unstable angina (n=258)	Age and gender-matched healthy control (n=30)	49 months	• Blood HMGB1 was significantly higher in NSTEMI/unstable angina patients (median and interquartile range; 2.4 [1.6-7.1] vs. 0.9 [0.3-0.9] ng/mL, p<0.0001 • In-hospital and cardiovascular mortality were higher in patients with elevated HMGB1 (p=0.0003) • HMGB1 independently predicts cardiovascular mortality after multi-variate adjustment	Yes

Atherosclerosis

Study	**Study Population**	**Control**	**Follow-up Period**	**Findings**	**Multivariate adjustment**
Hu et al., 2009[178]	Stable angina (n=35) unstable angina (n=37)	Control (n=32)	Cross-sectional	• Serum HMGB1 level positively correlated with angiographic Gensini score in patients with stable angina (r=0.786, p<0.05)	Yes

Thrombosis

Study	**Study Population**	**Control**	**Follow-up Period**	**Findings**	**Multivariate adjustment**
Hatada et al., 2005[194]	Suspected disseminated intravascular coagulation (n=201)	Normal		• Plasma HMGB1 was higher in patients with DIC (14.05±12.56 ng/ml vs. non-detectable.) • HMGB1 plasma levels correlated with the DIC score	No

Table 1-2. Strategies to inhibit HMGB1

Strategies	Reference	Species	Disease Model (Disease Inducing Intervention)	Results
Neutralising antibody	Liu et al., 2007[202]	Rat	Stroke (2 Hr MCA occlusion)	• α-HMGB1 mAb reduced infarct size • α-HMGB1 mAb preserved neurological functions • α-HMGB1 mAb reduced TNFα and eNOS
HMGB1 Box A	Yang et al., 2004[144]	Mouse	Sepsis (Caecal ligation and puncture)	• Box A improved mouse survival (Box A vs. control, 68% vs. 28%, $p<0.03$) • Box A improved renal function • Box A reduced TNFα and IL-6 levels
Thrombomodulin	Nagato et al., 2009[205]	Rat	Endotoxinaemia (LPS 4 mg/kg i.v. bolus)	• Thrombomodulin improved rat survival (Thrombomodulin vs. control, 90% vs. 50%, $p<0.03$) • Thrombomodulin improved liver function • Thrombomodulin reduced TNF and IL-1β
RAGE antibody	Lutterloh et al., 2007[206]	Mouse	Sepsis (Caecal ligation and puncture)	• α-RAGE mAb improved mouse survival ($p<0.001$) • α-RAGE mAb deceased lung fluid content
Small molecule to MD-2, P5779 (tetramer peptide)	Yang et al., 2015[152]	Mouse	Ischemia-reperfusion injury (Paracetamol overdose) Sepsis (Caecal ligation and puncture)	Paracetamol overdose model • P5779 improved survival ($p<0.05$) • P5779 reduced hepatic injury • P5779 lowered TNF level Caecal ligation and puncture model • P5779 improved survival ($p<0.05$) • P5779 reduced hepatic injury

Table 1-3. Preclinical models where α-HMGB1 mAb (recognising residues 208-215) was studied

Reference	Disease Model (Inducing Interventions)	Species	Dose	Findings
Liu et al., 2007[202]	Stroke (2Hr MCA Occlusion, followed by reperfusion)	Rat	i.v. α-HMGB1 mAb 200 µg immediately and 6 hours post-reperfusion	• α-HMGB1 mAb reduced infarct size • α-HMGB1 mAb preserved neurological functions • α-HMGB1 mAb reduced TNFα and eNOS
Zhang et al., 2011[208]	Ischemic brain injury (2Hr MCA Occlusion, followed by reperfusion)	Rat	i.v. α-HMGB1 mAb 200 µg immediately and 6 hours post-reperfusion	• α-HMGB1 mAb preserved blood-brain barrier
Oozawa et al., 2008[187]	Myocardial infarction (Left anterior descending artery ligation and reperfusion)	Rat	i.v. α-HMGB1 mAb 0.5mL after 30min occlusion, before reperfusion	• α-HMGB1 mAb increased infarct size and troponin • α-HMGB1 mAb increased noradrenaline and decreases its metabolite
Yang et al., 2011[209]	Retinal ischemia-reperfusion injury (Increase intra-ocular pressure 130mmHg for 45min)	Rat	i.p. α-HMGB1 mAb 200µg 30min before injury; i.v. α-HMGB1 mAb 200µg immediately and 6 hours after reperfusion; topical α-HMGB1 mAb 20µg 30min before ischemia	• α-HMGB1 mAb thinned various layers in the eye, a deleterious outcome. • α-HMGB1 mAb led to lower a- and b- waves in ERG, a deleterious outcome.
Kanellakis et al., 2011[179]	Atherosclerosis (High fat diet for 8 weeks)	Mouse	i.v. α-HMGB1 400µg twice weekly	• α-HMGB1 significantly reduced atherosclerotic plaque volume • α-HMGB1 reduced inflammatory infiltrates • α-HMGB1 reduced cytokines and VCAM expression

CHAPTER 2

Materials and Methods

2.1 Tables

As used in this study, the composition of all buffers and media are listed in Table 2-1 and details of all antibodies for flow cytometry and antibodies for immunohistochemistry are listed in Table 2-2 and 2-3 respectively. Absorbance frequency to determine cholesterol concentration can be found in Table 2-4, for the composition and source of histochemistry stains used, see Table 2-5, and computer software are listed in Table 2-6. Finally, details of all suppliers of equipment or services are in Tables 2-7. These tables are at the end of this chapter.

2.2 Animals

2.2.1 Mice

Unless otherwise stated, all mice used in this study were bred and housed at the AMREP animal facility at The Baker Heart and Diabetes Institute under SPF conditions. Mice could drink water and feed *ad libitum*. All animal experiments were approved by the AMREP animal ethics committee and all additional requirements of the AMREP facility were upheld. To cull mice, animals were first anaesthetised by intraperitoneal (i.p.) injection of 10mg/kg ketamine and 10mg/kg xylazine, followed by cervical dislocation.

2.2.2 Genotyping

Tail clips from all mice were collected and genotyping was undertaken by TransnetYX genotyping service, as per company protocols.

2.2.3 Intraperitoneal injections

Intraperitoneal injections were carried out with a 30-gauge needle (BD Scientific) into the right lower quadrant of the peritoneum of mice. A maximum volume of up to 200µL was injected.

2.2.4 Intravenous injections

Intravenous (i.v.) injections were carried out with a 29-gauge needle (Terumo) into either the tail vein or the jugular vein of mice. A maximum volume of up to 133µL was injected.

2.2.5 Subcutaneous injections

Subcutaneous (s.c.) injections were carried out with a 29-gauge needle (Terumo) into the abdomen of mice. A maximum volume of up to 200µL was injected.

2.2.6 Gavage

Mice were restrained at the scruff of the neck and held to ensure the head is unable to move. Gavage tubes with a 18-22 gauge were inserted into the mouth and over the tongue to the back of the mouth, allowing mice to swallow the needle. Once the needle is in the oesophagus, a maximum volume of up to 200µL was administered.

2.2.7 High fat diet

High fat diet feeding consisted of a diet of 22% fat and 0.15% cholesterol (Diet SF00-219, Specialty Feeds). Diet regimes are outlined in relevant methods below.

2.3 HMGB1 and thrombosis

2.3.1 HMGB1 and thrombosis animal models

2.3.1.1 Mouse Ferric chloride ($FeCl_3$)-induced carotid arterial thrombosis model

Male C57Bl6 mice weighing >15g were anaesthetised as per section 2.2.1 and received an i.v. injection of either 200µg/100µL α-HMGB1 monoclonal antibody (mAb) or 200µg/133µL α-KLH isotype control (both antibodies a generous gift from Dr. Masahiro Nishibori at Okayama University, Japan). To expose the left carotid artery, an incision was made in the neck and the dorsal cervical region was dissected. Within 30 minutes of antibody administration, filter paper soaked with $FeCl_3$ (5% w/v; Sigma-Aldrich) was placed under left carotid artery for 3 minutes. After the $FeCl_3$-soaked filter paper was removed, carotid volume flow was measured using the TS420 Perivascular Flow Module (Transonic), a Doppler flow detector (Nano Doppler flow probe), at baseline and continually for 30 minutes (Figure 2-1).

To compare the relative efficacy of the antithrombotic effects of HMGB1 neutralisation, mice were administered with clinical antithrombotic agents and subjected to $FeCl_3$ thrombosis.

Agents included clopidogrel (Bristol-Myers Squibb) and enoxaparin (Sanofi). Clopidogrel, at a dose of 1 or 3mg/kg, was administered twice via gavage (section 2.2.6); the first gavage was performed approximately 24 hours prior, and the second gavage 2 hours prior to $FeCl_3$-induced thrombosis. Enoxaparin (Sanofi) 10mg i.v. was administered immediately prior to $FeCl_3$-induced thrombosis. Patency time was determined and compared to that of HMGB1 neutralisation. Experiments were performed by Joy Yao with my assistance, and data was analysed using LabChart (ADInstruments) and GraphPad Prism (GraphPad Company).

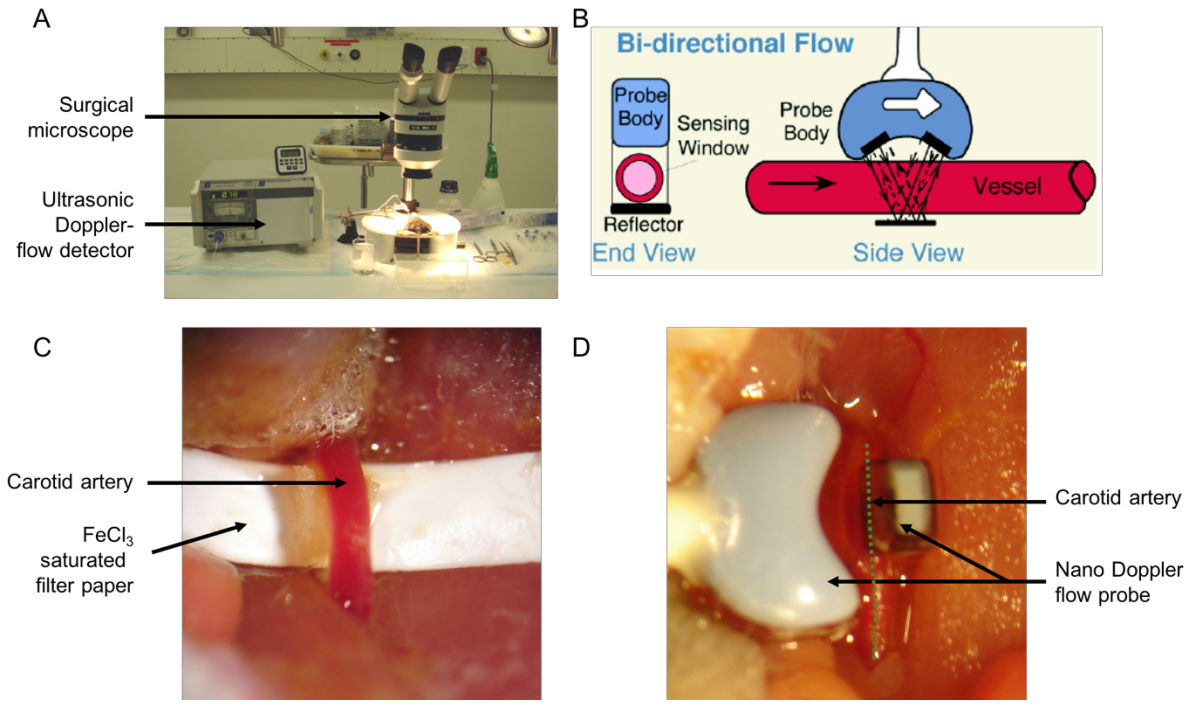

Figure 2-1. Mouse $FeCl_3$-induced carotid arterial thrombosis model. (A) Surgical set-up and equipment. (B) Schematic representation of application of Nano Doppler flow probe (from Chen et al[1].) (C) View from surgical field showing carotid artery exposed to filter paper saturated with ferric chloride (D) View from the surgical field showing Nano Doppler flow probe placed to detect carotid blood flow.

2.3.1.2 Mouse laser-induced mesenteric arterial thrombosis model

Low weight (15-23g) male C57Bl6 mice were used in this series of experiments as they have minimal perivascular fat, which would impair the visualisation of mesenteric arteries. Mice were anaesthetised as per section 2.2.1, and 50-100 µL 0.05% rhodamine (Sigma-Aldrich) was

i.v. injected to fluorescently label all mouse cells. Mice underwent a laparotomy and mesentery vessels were stretched flat and visualised with an Olympus IX81 Inverted Intravital Microscope. The mesenteric artery studied was subjected to a pulse of 440 µm nitrogen dye laser (Andor) to induce localised endothelial injury. A baseline experiment was performed, where thrombosis was induced by pulsed laser in one mesenteric artery before any treatment was given. After baseline measurements were collected, mice were i.v. injected with 200µg/100µL α-HMGB1 mAb or 200µg/133µL α-KLH isotype control, and the laser-induced thrombosis experiment repeated in a different mesenteric artery in the same mouse. Real-time images of the mesentery artery were recorded at 1 frame/ second for 1 minute after laser injury. Captured images were analysed frame-by-frame and thrombus size quantified using Image J computer software (National Institutes of Health).

2.3.1.3 Mouse deep vein thrombosis model

This procedure was described by Diaz et al.[210]. Mice were anaesthetised as per section 2.2.1 and a laparotomy performed. Bowels were exteriorised and rested on a gauze soaked in normal saline. Inferior vena cava (IVC) and abdominal aorta were carefully separated at the level of renal artery. IVC was ligated using a 6-0 suture (Ethilon) and all side and back branches were cauterised or ligated using 7-0 sutures (Ethilon) to induce complete stasis and thrombosis of the IVC flow. Mice received a s.c. injection of 1mg/kg bupivacaine (Pfizer) for local anaesthesia, and a s.c. injection of 5mg/kg carprofen (Pfizer) as an adjunctive analgesia. At the end of surgery, atipamezole (Zoetis) was administered s.c. to reverse the effect of general anaesthesia and mice placed on heat pad for recovery. Mice were culled at 48 hours and IVC thrombus was resected and weighed.

2.3.2 Human blood

Human blood was harvested by personnel with phlebotomy qualifications. All experiments involving the collection of human specimens were approved by the AMREP human research ethics committee and blood was collected, stored and utilised as per the conditions approved.

2.3.3 Neutrophil and NETosis experiments in $FeCl_3$-induced carotid thrombosis

2.3.3.1 Depletion of neutrophils, monocytes and NETs in vivo

This assay has been described in detail elsewhere[211,212]. Briefly, for neutrophil depletion, 500μg α-Ly6G mAb (Bio X Cell) was i.p. injected into >6 week old male C57Bl6 mice 19-20 hours prior to the $FeCl_3$ experiment (section 2.3.1.1). In some experiments, neutrophil-depleted mice also received α-HMGB1 mAb or isotype control prior to $FeCl_3$ experiment. For monocyte depletion, 50mg/kg liposomal clodronate (Clodronate Liposomes) was i.v. injected approximately 19-20 hours prior to the $FeCl_3$ experiment (section 2.3.1.1). Neutrophil and monocyte depletion were verified by flow cytometry (described below). To deplete NETs, mice were anaesthetised (section 2.2.1) and i.v. injected with 1500U DNase (Sigma-Aldrich) immediately prior to the injection of either α-HMGB1 mAb or α-KLH isotype control and surgery.

To assess the efficacy of neutrophil and monocyte depleting strategies, whole blood was collected using heparin as the anticoagulant. Erythrocytes were lysed using BD FACS lysing solution (BD Biosciences). Blood was then centrifuged at 435 × *g* for 10 minutes, the supernatant was then discarded, and the precipitated blood cells resuspended in FACS buffer containing fluorescence-conjugated antibodies specific for neutrophil (CD11b-FITC, Ly6C-V450 and CD45-APC) and monocyte markers (CD11b-FITC and CD45-APC). Blood cells were incubated with these antibodies at RT for 30 minutes then centrifuged again at 435 × *g* for 5 minutes. Precipitated blood cells were resuspended in FACS buffer and placed on ice until flow cytometric examination. Neutrophil were defined as $CD45^{+}Ly6C^{int}CD11b^{hi}$ cells[211]. Monocytes were defined by an intermediate side scatter profile and $CD11b^{+}$ status ($SSC^{Int}CD11b^{Hi}$), a strategy previously validated[212].

2.3.3.2 Human neutrophil isolation

Human neutrophils were isolated using density gradient mediums. Here, 3mL of Histopaque® 1119 (Sigma-Aldrich), 3mL of Histopaque® 1077 (Sigma-Aldrich) and 6mL of whole human blood drawn from volunteers (section 2.3.2) were sequentially layered in a conical centrifuge tube. This preparation was centrifuged at 700 × *g*, at room temperature (RT) for 30 minutes, which separated the preparation into 6 distinct layers. The containing neutrophils was aspirated,

washed and cell purity and concentrations were determined using the Sysmex XS-1000i automated blood cell counter (Sysmex). Cells were then resuspended at a final concentration of $1x10^6$ cells/mL in Roswell Park Memorial Institute 1640 medium (RPMI-1640; Thermo Fisher Scientific). Neutrophil viability was determined by flow cytometry, using 4′,6-diamidino-2-phenylindole (DAPI) as the marker of cell death.

2.3.3.3 Isolation of bone marrow-derived murine neutrophils

Two neutrophil isolation assays were used in this thesis. For each assay, neutrophil purity and viability were determined using flow cytometry. To assess the purity of neutrophils isolated from murine bone marrow, cells were incubated with Peridinin-chlorophyll-protein/Cyanine 5.5 (PerCP/Cy5.5)- or APC/Cyanine 7 (APC/Cy7)-conjugated α-CD11b and phycoerythrin (PE)-conjugated α-Ly6G antibodies at RT for 30 minutes, washed at 435 × *g* for 5 minutes. Neutrophil viability was determined by flow cytometry, using 4′,6-diamidino-2-phenylindole (DAPI) as the marker of cell death. Negative immunomagnetic selection assay yielded the highest purity and this method was used for subsequent *in-vitro* HMGB1- NET induction experiments.

2.3.3.3.1 Isolation of bone marrow-derived murine neutrophils with Histopaque®

This method has been described in detail by Swamydas et al[213]. Briefly, male C57Bl6 mice were culled (section 2.2.1). To harvest bone marrow, mouse hind limbs were dislocated, separated and their overlying skin and muscles removed. Following this, the epiphyses of both ends of femur and tibia were cut off. Bone marrow cells were flushed out with 10mL of RMPI-1640 medium (Thermo Fisher Scientific) using a 25G needle (Terumo). Bone marrow cells from 2 mice were pooled for each isolation experiment. Suspensions were washed in RPMI-1640 medium (Thermo Fisher Scientific) and resuspended in hypotonic saline for 20 seconds to lyse erythrocytes (0.2% sodium chloride; Sigma-Aldrich). Erythrocyte lysis was terminated by adding equal volume of 1.6% sodium chloride (Sigma-Aldrich). Haemolysed bone marrow cells were filtered with a 20μm cell strainer, washed and resuspended in 1mL cold, sterile PBS. A density gradient was then created by sequential layering of 3mL Histopaque® 1119 (Sigma-Aldrich), 3mL Histopaque® 1077 (Sigma-Aldrich), then isolated bone marrow cells. Suspensions were then centrifuged at 872 × *g* at RT for 30 minutes, which separated the preparation into 6 distinct media layers. The layer that contained neutrophils was aspirated,

washed and resuspended at a final concentration of $2x10^6$cells/mL in RPMI-1640 medium (Thermo Fisher Scientific).

2.3.3.3.2 Isolation of bone marrow-derived murine neutrophils using negative immunomagnetic selection

Neutrophils were isolated from a commercially purchased MACS mouse neutrophil isolation kit (Miltenyi Biotec) as per manufacturer's instruction. Briefly, bone marrow cells were harvested as described above (section 2.3.3.3.1) and resuspended at a concentration of $5x10^7$ cells/200µL of MACS buffer (Miltenyi Biotec). Cell suspension was incubated with a cocktail of biotinylated antibody to target the non-neutrophil cells at 4°C for 10 minutes, then washed and resuspended in 400µL of MACS buffer. This suspension was incubated with 100µL of magnetically labelled α-biotin antibodies at 4°C for 15 minutes, washed and resuspended in MACS buffer. Neutrophils were enriched using magnetic negative selection of non-neutrophils. Purified neutrophils were resuspended in RPMI 1640 medium (Thermo Fisher Scientific) at the concentration of $2x10^6$ cells/mL.

2.3.3.4 *In vitro* NET induction of human- and murine-derived neutrophils

Human-derived neutrophils (section 2.3.3.2) suspended in RPMI 1640 medium (Thermo Fisher Scientific) were seeded in a black 96-well plate at a final concentration of $2x10^6$cells/well. Neutrophils were incubated with either (1) PMA 100nM (Sigma-Aldrich) or (2) in RMPI-1640 medium (Thermo Fisher Scientific) at 37°C, 5% CO_2 for 3 hours. Murine-derived neutrophils (section 2.3.3.3.1 and 2.3.3.3.3) suspended in RPMI 1640 medium (Thermo Fisher) were seeded in a black 96-well plate at a final concentration of $1.8x10^6$ cells/well. Neutrophils were incubated at 37°C, 5% CO_2 with (1) PMA at the concentration of 0.1, 1, 10 and 100µM, or (2) RPMI-1640 medium (Thermo Fisher Scientific) for up to 5 hours. In experiments where recombinant HMGB1 (R&D Systems) was used to induce NETosis, murine-derived neutrophils (section 2.3.3.3.3) suspended in RPMI 1640 medium (Thermo Fisher Scientific) were seeded in a black 96-well plate at a final concentration of $1.8x10^6$ cells/well. Neutrophils were incubated with recombinant HMGB1 0.2, 1 or 10µg/mL at 37°C, 5% CO_2 for up to 4 hours.

2.3.3.5 Quantification of NETosis using the SYTOX® Green assay

SYTOX® Green nucleic acid stain (Life Technologies) was used as per manufacturer instruction. At a final concentration of 1μM, SYTOX® Green was added to each well of the 96-well plate where human-or murine- derived neutrophils were incubated with control, PMA (Sigma-Aldrich) or recombinant HMGB1 (R&D Systems) (section 2.3.3.4). Fluorescence was enumerated at specified experimental time points using the Enspire 2300 fluorescence plate reader (Perkin Elma).

2.3.3.6 Visualisation of immunofluorescently-labelled of NETosis

This method was described by Vong et al[214]. Neutrophil suspensions containing $1x10^5$ cells were seeded onto lysine-coated glass coverslips (Neuvitro Corporation) and incubated with 100nM PMA (Sigma-Aldrich) at 37°C, 5% CO_2 for 3 hours. Cells were washed with PBS and incubated in 4% paraformaldehyde (Sigma-Aldrich) at 4°C overnight. Cells were then washed with PBS and permeabilised with ice-cold 100% methanol (Sigma-Aldrich) at -20°C for 10 minutes. To block non-specific binding, cells were washed and incubated with 3% BSA (Sigma-Aldrich) for 1 hour. For human neutrophils, cells were incubated with α-MPO antibody (Agilent Dako) at 37°C for 1 hour, washed with PBS and incubated with Alexa 647-conjugated goat α-rabbit IgG antibody (Thermo Fisher Scientific) at 37°C for 1 hour. For mouse neutrophils, cells were incubated with fluorescein isothiocyanate (FITC)-conjugated α-MPO antibody (Abcam) at 37°C for 1 hour. Cells were washed with PBS, and DNA was stained using Hoechst 33342 or DAPI (Thermo Fisher Scientific) at RT for 10 minutes. They were washed again with PBS, then the glass cover slip adhered with stained neutrophils was mounted to a glass slide using ProLong Diamond antifade mountant (Thermo Fisher Scientific). The immunofluorescently-labelled NETs were examined using the A1R HD Confocal Microscope (Nikon). Details of antibodies used are listed in Table 2-3.

2.3.4 Platelet and haemostasis function assays

2.3.4.1 Platelet-rich plasma and washed platelets

Mice were anaesthetised (section 2.2.1) and whole blood was anticoagulated with citrate (Sigma Aldrich) and collected from IVC using a 25G needle (Terumo). Blood was then centrifuged at 250 × *g* for 5 minutes and the supernatant containing platelet-rich plasma

collected. To maximise the quantity of platelets harvested, remaining whole blood sediments were resuspended in 100µL PBS containing calcium and magnesium, centrifuged at 250 × *g* for 5 minutes and the supernatant was collected. This process was repeated for another 1-2 times and the supernatants collected from each mouse, i.e., platelet-rich plasma, were pooled together.

To purify washed platelets, platelet-rich plasma was then centrifuged at 2000 × *g* for 1 minute, the supernatant was then discarded, and the platelet pellet resuspended in 1mL of platelet wash buffer (PWB). Platelet counts were performed using the Sysmex XS-1000i automated blood cell counter (Sysmex). Suspensions were washed and resuspended at a concentration of 2.0 $\times 10^8$ cells/mL in Tyrode's buffer. Platelets were rested in Tyrode's buffer for 30 minutes prior to platelet activation or aggregation assays.

2.3.4.2 Platelet aggregation

To assess the effects of HMGB1 neutralisation in platelet aggregation, platelet-rich plasma or washed platelets (section 2.3.4.1) were incubated with 100µg/mL α-HMGB1 mAb or α-KLP isotype control for 30 minutes at 37°C. The dose of 100µg/mL was chosen, as this is comparable to the dose given in the *in vivo* experiments (200µg), where the volume of blood of an adult mouse is estimated to be 2mL. Platelet-rich plasma suspensions were incubated with 2µM ADP (Sigma-Aldrich) and stirred at 900 r.p.m. for 10 min at 37°C in the AggRAM™ automated platelet analyser (Helena Laboratories). Washed platelets were incubated with 0.1U/mL thrombin (Siemens) or 2µg/mL collagen (Takeda) and stirred at 600 r.p.m. for 10 min at 37°C in the AggRAM™ automated platelet analyser (Helena Laboratories). Percentage change in optical density as measured by the platelet analyser was proportional to the degree of platelet aggregation.

2.3.4.3 Platelet activation

To assess the effects of HMGB1 neutralisation in platelet activation, washed platelets (section 2.3.4.1) were incubated with α-HMGB1 mAb or α-KLP isotype control at a final concentration of 100µg/mL for 30 minutes at 37°C. They were then incubated with platelet agonists, 20µM ADP (Sigma-Aldrich) or 0.1 U/mL thrombin (Siemens), and allophycocyanin (APC)-conjugated α-CD41 and BV421-conjugated α-CD62P antibodies at RT in the dark for 15 minutes. Platelets activation were examined using flow cytometry.

2.3.4.4 Tail bleeding time

Mice were treated with one of the following; (1) i.v. injection of 200 µg α-HMGB1 mAb; (2) i.v. injection of 200 µg α-KLP isotype control; (3) 2 doses of 1mg/kg clopidogrel (Bristol-Myers Squibb) given via gavage (section 2.2.6) approximately 24 hours apart; (4) gavage administration of 2 doses of 3mg/kg clopidogrel (Bristol-Myers Squibb) approximately 24 hours apart or (5) i.v. injection of 10 mg/kg enoxaparin (Sanofi). Mice were anaesthetised as per section 2.2.1, and mouse tails were transected at 3mm from the tip of the tail. The tail was then immediately immersed in warm saline (37°C). Bleeding time is defined as the duration from transection to the point where blood flow stops for >30 seconds. Bleeding was monitored for up to 30 minutes. If bleeding continued beyond 30 minutes, mice were culled as per section 2.2.1.

2.3.4.5 Platelet count, activated partial thromboplastin time (APTT) and prothrombin time (PT)

Mice were i.v. injected with 200µg α-HMGB1 mAb or 200 µg α-KLP isotype control and culled 30 minutes later as per section 2.2.1. Whole blood was collected from IVC using citrate (Sigma Aldrich) as an anticoagulant. Platelet count was determined using Sysmex XS-1000i automated blood cell counter (Sysmex). Blood was centrifuged at 2000 × *g* for 15 minutes at 4°C. With the assistance of the Alfred Hospital Pathology services, APTT and PT was measured using a commercial kit containing phospholipids, micronized silica and calcium (TriniCLOT™ aPTT S reagent and TriniCLOT™ aPTT S $CaCl_2$ reagent; Stago). This kit was added to plasma and clotting time determined using the STA R Max2 automated haemostasis analyser (Stago). To determine PT, a commercial kit containing thromboplastin, a heparin inhibitor and calcium (Neoplastine® C1; Stago) was added to plasma and clotting time determined using the STAR Max 2 automated haemostasis analyser (Stago).

2.4 Atherosclerosis studies

2.4.1 Induction of atherosclerosis

To induce the formation of atherosclerotic plaques, male apoE$^{-/-}$ mice ≥6 weeks old were fed a high fat diet that consisted of 22% fat and 0.15% cholesterol (Diet SF00-219, Specialty Feeds) for 13 weeks. Female apoE*3-Leiden.CETP (E3LC) mice aged 13-17 weeks were fed the same high fat diet for 19 weeks.

2.4.2 Animal model of atherosclerosis: carotid tandem stenosis model in apoE$^{-/-}$ mice

Male apoE$^{-/-}$ mice on a C57BL/6J background were obtained from the Animal Resource Centre in Western Australia. They were backcrossed at least 10 generations. At 6 weeks-old, apoE$^{-/-}$ mice were placed on a high fat diet, as per section 2.4.1. After 6 weeks of high fat diet, mice were subjected to carotid tandem stenosis surgery, described in detail elsewhere[63] and represented schematically in Figure 2-2. Briefly, mice were anaesthetised as per section 2.2.1 and an incision was made in the neck. The right common carotid artery was dissected and a suture needle with a diameter of 150μm was placed over the right common carotid artery in order to create a non-occluding stenosis. Tandem stenosis was created by placing two narrowing ligature, using 6-0 blue braided polyester fibre sutures (Covidien), at each end of the right common carotid artery. The distal narrowing ligature was located 1mm from the carotid artery bifurcation, and the proximal narrowing suture was placed at 3mm from the distal stenosis. The needle was removed from the suture, the incision closed, and mice were kept on heat pads for recovery. After surgery, mice received weekly i.v. injections of 10mg/kg evolocumab (Amgen), a humanised α-PCSK9 mAb or PBS. Surgery was performed by Dr. Yung-Chih Chen with my assistance. Mice continued on a high fat diet for 7 weeks until the experimental end point. The study design is outlined in Figure 2.2. To establish tandem stenosis model in E3LC mice, eight-week old female E3LC mice purchased from Leiden University Medical Center were placed on a high fat diet for 6 weeks and then subjected to carotid tandem stenosis surgery. After surgery, mice were fed the same high fat diet for a further 13 weeks (Fig 2-3). To assess the effect of PCSK9 inhibition in the development of atherosclerosis, female E3LC received weekly s.c. injections post carotid tandem stenosis surgery of either 10mg/kg α-PCSK9 mAb (Amgen) or 10mg/kg α-AGP3 isotype control (clone 4D2, Amgen) while continued on high fat feeding (Fig 2-4).

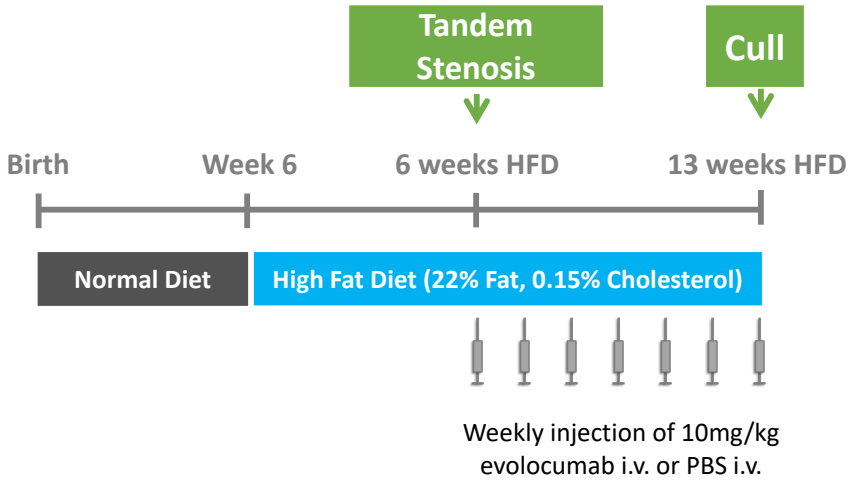

Figure 2-2. Mouse models of atherosclerotic plaque rupture. Male apoE$^{-/-}$ mice aged 6 weeks old were fed a high fat diet (HFD) for 6 weeks and subjected to carotid tandem stenosis surgery. High fat diet was continued for another 7 weeks while mice concomitantly received weekly i.v. injections of either 10m/kg evolocumab or PBS.

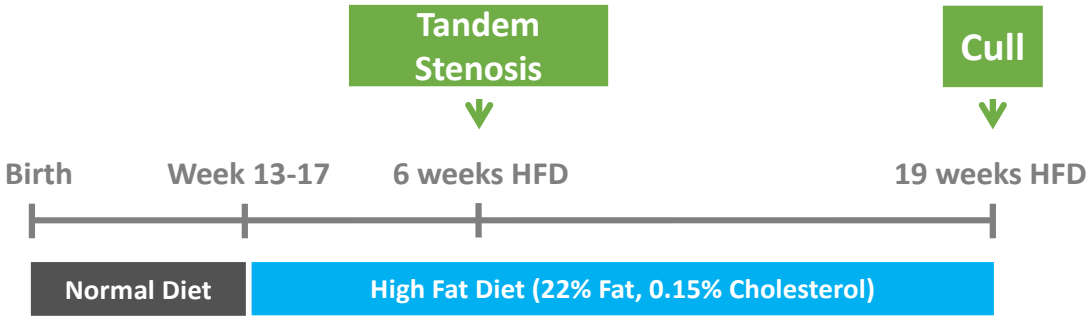

Figure 2-3. Study design - proposed E3LC model of atherosclerotic plaque rupture. Female E3LC mice aged 13-17 weeks were commenced on a high fat diet for 6 weeks before they were subjected to carotid tandem stenosis surgery. High fat diet feeding was continued for a further 13 weeks before mice were culled for analysis.

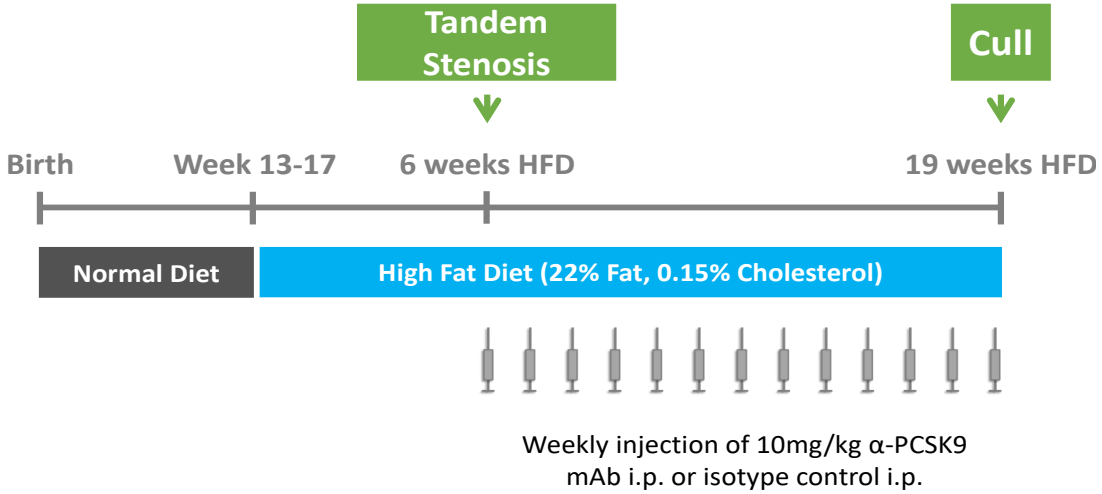

Figure 2-4. Study design - proposed E3LC model of diet-induced atherosclerosis and atherosclerotic plaque rupture, used to evaluate PCSK9 inhibition. Female E3LC mice aged 13-17 weeks were commenced on a high fat diet for 6 weeks before they were subjected to carotid tandem stenosis surgery. High fat diet feeding was continued for further 13 weeks while mice concomitantly received weekly i.p. injections of either 10m/kg α-PCSK9 mAb or isotype control.

2.4.3 Tissue harvest and preparation

Mice were anaesthetised via an i.p. injection of 10mg/kg ketamine and 10mg/kg xylazine and weighed. Mice were next culled (section 2.2.1) and perfused with PBS until liver changed colour. Mouse liver and kidney were resected, weighed and snap frozen using liquid nitrogen. They were stored at -80°C until further processing. Mouse spleen was resected, weighed then homogenised and resuspended in BD FACS lysing solution (BD Biosciences) on ice for 60 minutes. FACS buffer was added to terminate red cell lysis and spleen cell suspension were centrifuged at 300 × *g* for 10 minutes at 4°C and cells resuspended in FACS buffer. Spleen cell suspensions were filtered with a nylon mesh and kept on ice until flow cytometry examination. Axillary and inguinal lymph nodes were removed and placed in FACS buffer on ice. They were homogenised and resuspended in FACS buffer and centrifuged at 300 × *g* at 4°C for 10 minutes. The precipitated cells were resuspended in FACS buffer. Lymph cells suspensions were filtered with a nylon mesh and kept on ice until further flow cytometry experiments. Heart, aorta and right common carotid artery were carefully dissected, isolated and embedded in Tissue-Tek® optimal cutting temperature compound (Sakura Finetek Europe B.V.), and then snap frozen on dry ice. Aorta and carotid samples were sectioned at 6µm intervals, starting from the aortic

cusp. For histochemistry analysis of aortic sinus in apoE$^{-/-}$ mice, 3 sections 60µm apart were taken to represent proximal, mid and distal aortic sinus, and an average of the 3 sections was taken. For histochemistry analysis of aortic sinus in E3LC mice, 3 sections 40µm apart were taken to represent proximal, mid and distal aortic sinus, and an average of the 3 sections was taken. For histochemistry examination of the carotid tandem stenosis plaques, only segment I, defined as the section between the origin of carotid artery and the first stenosing ligature that was analysed. This is because segment I has a phenotype of unstable plaques. In studies where apoE$^{-/-}$ mice were used, a total of 3 slides, taken at proximal, mid and distal carotid segment I, 60µm apart, were stained and analysed. For PCSK9 in E3LC mice studies, there was little regional heterogeneity within segment I, hence only one carotid section was processed for histochemistry examination.

2.4.4 Blood collection, processing and flow cytometric examination

Mice were culled (section 2.2.1) and whole blood collected via cardiac puncture using 25G needle (BD Bioscience) loaded onto a 1mL syringe (BD Biosciences) containing enoxaparin (Sanofi). Blood was centrifuged at 250 × *g* for 5 minutes to harvest platelet-rich plasma. One microliter of platelet-rich plasma was kept for the platelet activation study, and the rest of the blood was centrifuged at 300 × *g* for 10 minutes at 4°C. For the platelet activation study, 1µL of platelet-rich plasma was diluted with 50µL of PBS containing calcium and magnesium. Diluted platelet-rich plasma was incubated with 20µM ADP (Sigma Aldrich) and CD41-APC and CD62P-PerCP antibodies at RT in the dark for 15 minutes. Then 200µL of BD CellFIX fixing buffer (BD Biosciences) was added to diluted platelet-rich plasma. Platelets were placed on ice until flow cytometry examination.

The rest of the plasma-containing supernatant was stored at -80°C until further analysis and erythrocytes and leukocytes were incubated in BD FACS lysing solution (BD Biosciences) for 10 minutes at RT on a roller. Cells were centrifuged at 300 × *g* for 10 minutes at 4°C, and precipitated leukocytes were resuspended in FACS buffer and passed through a nylon mesh filter for flow cytometry examination. Single cell suspension from the blood, spleen and lymph nodes were seeded to 96-well plates, at a density of $2x10^6$ cells/well. They were first incubated with a Fc blocking antibody (α-CD16/CD32,) for 15 minutes at 4°C to remove non-specific binding. To examine monocytes from blood and spleen, single cell suspensions were incubated with the following fluoroprobe conjugated antibodies including CD11b-FITC, CD45-APC and

Ly6C-V450 for 30 minutes at 4°C. To examine lymphocytes from blood, spleen and lymph nodes, single cell suspension from these organs were incubated with TCRβ-FITC, CD4-V450, CD8α-PerCP for 30 minutes at 4°C. After incubation, these cells were then washed at 300 × *g* for 10 minutes at 4°C and resuspended in 150µL FACS buffer and subjected to flow cytometry analysis.

Flow cytometry analysis was performed using flow cytometers BD FACSCanto™ II and BD LSRFortessa™ (BD Biosciences). Flow cytometry experiments were analysed using Flowlogic (Inivai Technologies) or FlowJo (FlowJo, LLC) flow cytometry analysis software.

2.4.5 Plasma cholesterol and glucose analysis

Enzymatic, colorimetric assays were used to determine plasma cholesterol levels. In the study that assessed effects of evolocumab on plaque stability in apoE$^{-/-}$ mice and the investigation that aimed to validate carotid tandem stenosis model in E3LC mice, total plasma cholesterol, triglyceride and HDL cholesterol were determined using Cobra Integra 400 system (Roche). In the study that assessed of PCSK9 inhibition on atherosclerotic plaque development and stability, plasma lipid was analysed using the LX20PRO Analyser (Beckman Coulter; located in Monash University). Both were based on enzymatic colorimetric assay. To measure total plasma cholesterol, cholesterol ester was hydrolysed into free cholesterol and fatty acid. Free cholesterol was then oxidised with cholesterol oxidase, and the hydrogen peroxide produced reacted with 4-aminoantipyrine (4-AAP) and phenol to form a red quinone-imine dye, whose colour intensity was directly proportional to the cholesterol concentration. To determine plasma triglyceride concentration, plasma sample underwent a series of reactions catalysed by lipase, glycerol kinase, glycerophosphate oxidase and horseradish peroxidase. This generated hydrogen peroxide as one of its final products. Hydrogen peroxide then reacted with 4-AAP and 3, 5-dichloro-2-hydroxybenzenesulfonic acid to form a red dyestuff, whose colour intensity is proportional to triglyceride concentration. HDL cholesterol was measured directly using a homogeneous assay. In this assay, HDL cholesterol was first separated from other cholesterol fractions using specific detergents or magnetically response particles that targets apoprotein B or apoprotein CIII. Cholesterol was then released from HDL and subjected to cholesterol esterase and oxidase, which yields hydrogen peroxide that reacts with 4AA and sodium N(-2-hyrdoxy-3sulfopropyl)-3,5-dimethoxyaniline to form blue quinoneimine, the intensity of which was directly proportional to HDL-cholesterol concentration. The absorbance

frequency for each reaction are summarised in the Table 2-4. LDL-cholesterol was determined using the enzymatic colorimetric method. Plasma glucose concentration was determined using the enzymatic reference method. In this method, glucose was phosphorylated to glucose-6-phosphate, G6P, which in turn could be oxidised using G6P dehydrogenase. This reaction would concurrently reduce nicotinamide adenine dinucleotide (NAD^+) into the reduced form (NADH), which causes a change in absorbance at 340/660 nm. The change in absorption is proportional to the concentration of glucose. Glucose measurement was performed using Beckman Coulter LX20PRO Analyser (Brea, CA, USA), located at Monash University.

2.4.6 Histochemistry

2.4.6.1 Haematoxylin and Eosin staining

Frozen sections of aortic sinus and carotid segment I were thawed for 30 minutes and washed in deionised water for 5 minutes before a 15-second immersion in Harris Haematoxylin (Amber Scientific). These sections were then washed in alkaline water (sodium bicarbonate in tap water) for 10 seconds, rinsed in tap water for 5 minutes, then immersed in Eosin 1% alcoholic stain (Amber Scientific) for 2 minutes. Then, these slides were briefly dipped in 95% ethanol (Sigma-Aldrich), followed by dehydration with ethanol (95% ethanol for 5 minutes, then 100% ethanol twice, 5 minutes each) and clearing with xylene (Thermo Fisher Scientific; 100% xylene twice, 5 minutes each). Cover glasses were mounted using DPX (Thermo Fisher Scientific) neutral mounting medium.

2.4.6.2 Oil Red-O staining

Frozen sections of aortic sinus and carotid segment I were first fixed in 10% neutral-buffered formalin (Sigma-Aldrich), followed by a 4-minute wash in PBS and a 30-second wash in 60% isopropanol (Sigma-Aldrich). The slides were then immersed in oil-red-o solution (Sigma-Aldrich) for 1 hour. They were then differentiated in 60% isopropanol, washed in deionised water for 2 minutes before a 2-minute counterstain with Mayers Haematoxylin (Amber Scientific). After sequential wash in tap and deionised water (3 minutes each), cover glass was mounted with Aquatex (Merck).

2.4.6.3 Picrosirius red staining

Frozen section of aortic sinus and carotid segment I were first thawed for 30 minutes, then fixed in 10% neutral-buffered formalin (Sigma-Aldrich). After two 5-minute washes in PBS, slides were immersed in picrosirius red solution for 1 hour (see Table 2-5), followed by 2 minutes differentiation using 0.01M hydrochloric acid (Sigma-Aldrich). Slides were examined under microscope to ensure adequate differentiation. Staining was continued with dehydration with ethanol and clearing with xylene (section 2.4.6.1), before mounting of a cover glass using DPX mounting medium (Thermo Fisher Scientific).

2.4.6.4 Martius scarlet blue staining

Frozen section of carotid segment I were first incubated in a solution containing Weigert's Haematoxylin solution (Amber Scientific) for 3 minutes, then washed under tap water for 5 minutes. These sections were incubated in 96% ethanol (Sigma-Aldrich) for 2 minutes and immersed in Picric acid orange G (EMS) for 10 minutes, followed by wash in deionised water for 10 seconds. Then, these sections were stained with brilliant crystal scarlet (Sigma-Aldrich) for 10 minutes and washed in deionised water for 10 seconds. They were then placed in 1% phosphotungstic acid (EMS) for 5 minutes and washed in deionised water for 10 seconds, followed by staining with Analine Blue solution (Sigma-Aldrich) for 4 minutes. Adequacy of Analine staining was examined under light microscope. They were then washed in deionised water for 10 seconds and placed in acetic acid for 10 seconds before they were blot dry. Staining was finished with dehydration with ethanol (Signa-Aldrich) and clearing with xylene (Sigma-Aldrich), and cover glasses were mounted using DPX mounting medium (Thermo Fisher Scientific).

2.4.7 Immunohistochemistry

Frozen sections of aortic sinus were thawed for 30 minutes before being fixed in acetone (Sigma-Aldrich) at -20°C for 20 minutes. They were washed in PBS twice for 5 minutes each and then immersed in 3% hydrogen peroxidase (Sigma-Aldrich) at RT for 30 minutes then washed twice in PBS containing 0.05% Tween-20 (Sigma-Aldrich). Sections were then incubated in 10% normal serum from the host species where secondary antibody was raised (Vector Laboratories) at RT for 1 hour. Endogenous avidin and biotin were then blocked using commercial Avidin-Biotin blocking kit (Vector Laboratories), as per manufacturer's instructions. After a quick rinse in PBS containing 0.05% Tween-20 (Sigma-Aldrich), frozen

sections were incubated with primary antibodies, washed in PBS containing 0.05% Tween-20 (Sigma-Aldrich), then incubated in corresponding secondary antibodies. Primary antibodies against CD68, α-SMA and MCP1 and matching isotype antibodies were used, (Table 2-3). Following incubation with secondary antibodies, frozen sections of aortic sinus were incubated with streptavidin horseradish peroxidise complex (Vectastain ABC Kit, Vector Laboratories). Antigens were visualised using 3,3-diaminobenzidine (DAB, Vector Laboratories). These sections were then counterstained with Mayer's Haematoxylin (Sigma-Aldrich), washed, dehydrated with ethanol (Sigma-Aldrich) and cleared with xylene (Sigma-Aldrich). Cover glass was mounted using DPX mounting medium (Thermo Fisher Scientific).

2.4.8 Quantification of histochemical and immunohistochemical staining

For the study that assessed the effects of evolocumab in apoE$^{-/-}$ mice, the microscopy system consisted of Leica microscope 5410006 and an automated graphic software, Optimas 6.2 VideoPro-32 (Meyer Instruments) were used. For the two studies where E3LC mice were used (validation of tandem stenosis model in E3LC and effects of PCSK9 inhibition in plaque development and stability), a system consisted of the Olympus BX43 microscope and Fiji imaging processing software (National Institutes of Health) was used. To quantify lesion size, area of collagen (picrosirius red staining), necrosis (haematoxylin and eosin staining), lipid (oil red-o staining) and antigens of interests (CD68, α-SMA and MCP1), an area of positive staining was measured, and in some experiments, normalised to plaque size.

2.5 Statistical Analysis

When two groups of continuous variables were compared, and the data distribution was normally distributed, student's t-test was used. If the distribution was not Gaussian, then the non-parametric Mann-Whitney U test was used. In cases where three or more variables were compared, then Analysis of Variance (ANOVA) was used for normally distributed variables and the non-parametric Kruskal-Wallis test used for non-Gaussian distributed variables. When a significant difference was detected between groups, a post-hoc analysis using either Tukey or Dunn's methods were used to compare subgroups. When repeated measurements were taken, then non-parametric Wilcoxson signed-rank test was used. $P<0.05$ was deemed statistically significant. Data was presented as mean ± SEM unless otherwise specified.

Table 2-1. Buffers and media used in this study.

Name	Composition and final concentration
Hanks balanced salt solution (HBSS)	Double distilled water 0.137M Sodium chloride (Sigma-Aldrich) 5.4mM Potassium chloride (Sigma-Aldrich) 0.25mM Disodium phosphate (Sigma-Aldrich) 6mM D-Glucose (Sigma-Aldrich) 0.44 mM Monopotassium phosphate (Sigma-Aldrich) 1.3 mM Calcium chloride (Sigma-Aldrich) 1.0 mM Magnesium sulfate (Sigma-Aldrich)
10x Tyrode's buffer	Double distilled water 4.2 mM Monosodium phosphate (Sigma-Aldrich) 120 mM Sodium bicarbonate (Sigma-Aldrich) 100 mM Hepes (Sigma-Aldrich) 1.37 mM Sodium chloride (Sigma-Aldrich) 27 mM Potassium chloride (Sigma-Aldrich) 55 mM D-Glucose (Sigma-Aldrich)
Platelet Wash Buffer (PWB)	Double distilled water 4.3 mM Dipotassium phosphate (Sigma-Aldrich) 4.3 mM Disodium phosphate (Sigma-Aldrich) 24.3 mM Monosodium phosphate (Sigma-Aldrich) 113 mM Sodium chloride (Sigma-Aldrich) 5.5 mM D-Glucose (Sigma-Aldrich) 10 mM Theophylline (Sigma-Aldrich) 0.5% w/v Bovine serum albumin (BSA; Sigma-Aldrich) 0.02% w/v Enoxaparin (Sanofi) 1% u/v Apyrase (Sigma Aldrich)
Magnetic immuno-selection buffer	PBS (Baker) 0.5% v/w BSA (Sigma Aldrich) 2mM EDTA (pH 7.2; Sigma Aldrich)
Fluorescent-activated cell sorting (FACS) buffer	PBS (Baker) 0.5% w/v BSA 2mM Ethylenediaminetetraacetic acid

Table 2-2. Antibodies for flow cytometry used in this study.

Target stain	Antibody	Clone	Source
Depletion Experiments (Neutrophils and Monocytes)	CD11b-FITC	M1/70	BD Bioscience
	CD45-APC	30-F11	eBioscience
	Ly6C-V450	AL-21	BD Bioscience
Platelet Activation Experiments	CD41-APC	MWReg30	BioLegend
	CD62P-BV421	RB40.34	BD Biosciences
Assessment for Neutrophil Purity Platelets	CD11b-PerCP/Cy5.5	M1/70	BioLegend
	Ly6G-PE	RB6-8C5	eBioscience
	CD41-APC	MWReg30	BioLegend
	CD62P-PerCP-eFluor 710	Psel.KO2.3	eBioscience
Monocytes	CD11b-FITC	M1/70 (RUO)	BD Biosciences
	CD45-APC	30-F11	eBioscience
	Ly6C-V450	AL-21	BD Biosciences
Lymphocytes	CD4-V450	1D3 (RUO)	BD Biosciences
	CD8a-PerCP	53-6.7 (RUO)	BD Biosciences
	TCRβ-FITC	553170	BD Biosciences
Blocking	CD16-CD32 (Fc block)	30	eBioscience

Table 2-3. Antibodies for immunohistochemistry used in this study.

Primary antibodies				
Antigen	**Clone**	**Dilution**	**Incubation conditions**	**Source**
CD86	FA-11	1:100	4°C overnight	BioRad
MCP1	Polyclonal	1:50	4°C overnight	Abcam
α-SMA	Polyclonal	1:100	room temp. overnight	Abcam
Secondary antibodies				
Primary antibody	**Matching Secondary**	**Species of Normal Serum**	**Source**	
α-CD86	Anti-Rat IgG	Rabbit	Vector Laboratories	
α-MCP1	Anti-Rabbit IgG	Goat	Vector Laboratories	
α-α-SMA	Anti-Rat IgG	Rabbit	Vector Laboratories	

Table 2-4. Absorbance frequency to measure cholesterol concentration

	Cobra Integra 400 System (Roche Diagnostics)	LX20PRO Analyser (Beckman Coulter)
Total cholesterol	512 nm	520 nm
Triglyceride	512 nm	520 nm
HDL-Cholesterol	583 nm	560 nm

Table 2-5. Histochemistry stains used in this study.

Stain	Solution	Active Ingredients		Source
Haematoxylin & Eosin	Harris Haematoxylin			Amber Scientific
	Eosin 1% alcoholic			Amber Scientific
Oil Red-O	Oil-Red O	Oil Red-O	0.3g	Sigma-Aldrich
		99% Isopropanol	30mL	Merck
		dH_2O	20mL	
	Mayers Haematoxylin			Sigma-Aldrich
Picrosirius Red	0.1% Picrosirius	Sirius red	0.5g	Sigma-Aldrich
		Picric acid	500mL	Thermo-Fisher Scientific
Martius Scarlett Blue	Martius Yellow	Martius Yellow	0.5g	Sigma-Aldrich
		Phosphotungstic acid	2g	Sigma-Aldrich
		95% Ethanol	98mL	Sigma-Aldrich
	Brilliant crystal scarlet	Brilliant crystal scarlet	1g	Sigma-Aldrich
		Acetic acid	2.5mL	Sigma-Aldrich
		dH_2O	97.5mL	
	Weigert's iron hematoxylin			Sigma-Aldrich
	Phosphotungstic acid 1%			EMS
	Aniline Blue	Aniline Blue	1g	Sigma-Aldrich
		Acetic acid	1mL	Sigma-Aldrich
		dH_2O	99mL	

Table 2-6. Computer software used in this study.

Software	Version	Vendor
Fiji	2.0	National Institutes of Health
LabChart	7	ADInstruments
GraphPad Prism	7	GraphPad Company
FlowJo	10	FlowJo, LLC
Flowlogic	7.2.1	Inivai Technologies
Optimas	6.2	Meyer Instrument

Table 2-7. Suppliers used in this study.

Company	Location
Abcam	Cambridge, United Kingdom
ADInstruments	Sydney, New South Wales, Australia
Agilent Dako	Santa Clara, California, USA
Amber Scientific	Midvale, Western Australia, Australia
Amgen	Thousand Oaks, California, USA
Andor	Belfast, United Kingdom
BD Biosciences	Franklin Lakes, New Jersey, USA
Beckman Coulter	Pasadena, California, USA
Bio X Cell	West Lebanon, New Hampshire, USA
Bristol-Myers Squibb	New York City, New York, USA
Clodronate Liposomes	Haarlem, The Netherlands
Covidien	Dublin, The Republic of Ireland
EMS	Hatfield, Pennsylvania, USA
Ethilon	Cornelia, Georgia, USA
FlowJo, LCC	Ashland, Oregon, USA
GE Healthcare Life Sciences	Marlborough, Massachusetts, USA
GraphPad Company	La Jolla, California, USA
Helena Laboratories	Mount Waverly, Victoria, Australia
Inivai Technologies	Mentone, Victoria, Australia
Leica	Wetzler, Germany
Life Technologies	Carlsbad, California, USA
Merck	Kenilworth, New Jersey, USA
Meyer Instruments	Houston, Texas, USA
Miltenyi Biotec	Bergisch Gladbach, Germany
National Institutes of Health	Bethesda, Maryland, USA
Neuvitro Corporation	Vancouver, Washington, USA
Nikon	Tokyo, Japan
Olympus	Tokyo, Japan
Perkin Elma	Waltham, Massachusetts, USA
Pfizer	New York City, New York, USA
R&D Systems	Minneapolis, Minnesota, USA
Roche	Basel, Switzerland
Sakura Finetek Europe B.V.	Alphen aan den Riji, The Netherlands
Sanofi	Paris, France

Siemens	Munich, Germany
Sigma-Aldrich	St Louis, Missouri, USA
Stago	Wicklow, Ireland
Sysmex	Norderstedt, Germany
Takeda	Linz, Austria
Terumo	Tokyo, Japan
Thermo Fisher Scientific	Waltham, Massachusetts, USA
TransnetXY	Cordova, Tennessee, USA
Transonic	Ithaca, New York, USA
Vector Laboratories	Burlingame, CA, USA
Zoetis	Parsippany, NJ, USA

CHAPTER 3

HMGB1 Neutralisation Safely and Effectively Prevents Arterial Thrombosis Through Inhibition of NET Formation

3.1 Introduction

Haemostasis is the orchestrated physiological response to stop bleeding. Thrombosis is the pathological deviation of haemostasis. It is characterised by inappropriate intravascular clot formation with acute vascular occlusion. In Australia, >33,000 lives and >200,000 hospital admissions are attributed to thrombotic disease every year[215]. In particular, arterial thrombotic disease, which includes stroke and myocardial infarction, is the leading cause of mortality and morbidity both in Australia and worldwide[5,216]. Arterial thrombosis occurs when artherosclerotic plaques rupture or erode, exposing thrombogenic material within plaques to the lumen, and results in activation of platelets and formation of fibrin. Recognition of the critical contribution of acute and subacute thrombosis in stroke and myocardial infarction has led to development of antiplatelets and anticoagulants that transformed modern medicine[217]. However, current antithrombotic therapies are limited by their suboptimal efficacy and notable bleeding risks, pointing to a unmet medical need[218].

Traditionally, antithrombotic therapeutics target either platelets or coagluation factors. Over the last decade, accumulating evidence has implicated the role of neutrophils in acute thrombosis. Neutrophils can secrete tissue factors that trigger the extrinsic coagulation pathway[107]. Neutrophils can also, upon activation, release neutrophil extracellular traps (NET), lattices of free DNA with histones and neutrophil proteases[109]. NET formation, or NETosis, provides a scaffold that allows interactions between platelets, von Willebrand factor and fibrinogen[219]. Further, it promotes platelet activation, directly triggers the intrinsic pathway through factor XII, and it indirectly initiates the extrinsic pathway through inactivation of TF pathway inhibitor[220]. NET formation has been detected in acute human coronary thrombi[192], and dismantling NET formation may enhance the potency of fibirinolytic therapy[124].

High mobility group protein B1 (HMGB1) is a 25-kDa protein of 215 amino acids with a highly-conserved primary sequence, being 99% identical in all mammalian species. As a non-histone nuclear protein, its primary intracellular function is modulation of DNA structures, through which, it regulates transcription, recombination and DNA replication[140]. In addition, it serves as a DAMP that is released upon infection and sterile inflammation to signal cell death and injury. Extracellular HMGB1 binds to pattern-recognition receptors on the surface of immune cells, and partakes in a myriad of immune, repair and regenerative processes,

depending on its redox status and the molecular partner it engages. In a partially reduced form, it binds to TLR4 and causes cytokine induction[146]. Conversely, when released in a fully-oxidised form, as in the setting of apoptosis, it generates immunotolerance and does not trigger an inflammatory response[153].

Previous mechanistic and clinical investigations have implicated a role for HMGB1 in thrombosis and haemostasis. HMGB1 has been detected in coronary and peripheral arterial thrombi[191,193], and plasma HMGB1 levels were found to be elevated in patients with stroke and myocardial infarction. In STEMI patients, HMGB1 independently predicts adverse clinical outcomes, suggesting a pathogenic role[184]. Experimental studies have shown that, while being enucleate, platelets contain HMGB1 which is exported to the cell surface for release upon platelet activation[197]. HMGB1 binds to TLR4 or receptor of advanced glycation product (RAGE) on activated platelets[191,195]. However, by itself, HMGB1 does not cause platelet activation or aggregation[191], raising the possibility that platelet-derived HMGB1 may promote thrombosis in a cytokine or paracrine fashion[191,195]. One potential mediator is neutrophil. HMGB1 is a known inducer of NET formation[169] and it has been shown to colocalise with NET formation in human coronary thrombi[192]. Based on this, it was hypothesised that inhibition of NET formation through HMGB1 neutralisation represents a novel and effective antithrombotic strategy.

The first aim of this project was to assess antithrombotic effects of HMGB1 neutralisation. The second aim was to determine the principal mechanism through which HMGB1 neutralisation prevents thrombosis. The third aim of this thesis was to assess the safety profile and translational potential of HMGB1 neutralisation as an anti-thrombotic strategy.

3.2 Results

3.2.1 HMGB1 neutralisation prevents FeCl3-induced carotid arterial thrombosis (Fig. 3-1)

To investigate if HMGB1 neutralisation is an effective strategy in preventing arterial thrombosis, male C57Bl6 mice were pre-treated with either α-HMGB1 mAb or an isotype control before they were subjected to $FeCl_3$, a chemical that induces thrombosis. Carotid artery blood flow was used as a readout of thrombus formation, as thrombosis would lead to lumenal obstruction and limitation or complete cessation of blood flow. Carotid blood flow was monitored over a 30-minute period, and the area-under-the-curve (AUC) was calculated, which represented the average blood flow over the monitoring period. In mice which received α-HMGB1 mAb, the average carotid artery blood flow after $FeCl_3$ application was preserved throughout the 30-minute monitored period. In contrast, average carotid artery flow in control mice was reduced to zero after exposure to $FeCl_3$, indicating vessel occlusion due to thrombosis (Fig. 3-1A). Aggregate blood flow over the 30-minute monitored period was calculated by measuring the area-under-the-curve (AUC) of the carotid flow diagram (Fig. 3-1A). HMGB1 neutralisation had higher, thus, better preserved aggregate carotid arterial flow during the monitored period (Fig. 4-1B, $p<0.01$). With HMGB1 neutralisation, the carotid artery remained patent for significantly longer (Fig. 4-1C; patency time, control vs. α-HMGB1 mAb; mean ± SEM, 10.3±2.3 vs. 23.1±3.1 minutes, $p<0.01$). To investigate how HMGB1 neutralisation affected the kinetics of thrombus formation, time to occlusion was determined. Time-to-occlusion is the first time point where blood flow ceases completely. Time-to-occlusion was the same as patency time, indicating the antithrombotic effect of HMGB1 neutralisation was in preventing the initiation of thrombus formation, rather than promoting recanalisation after thrombus occludes the vessel.

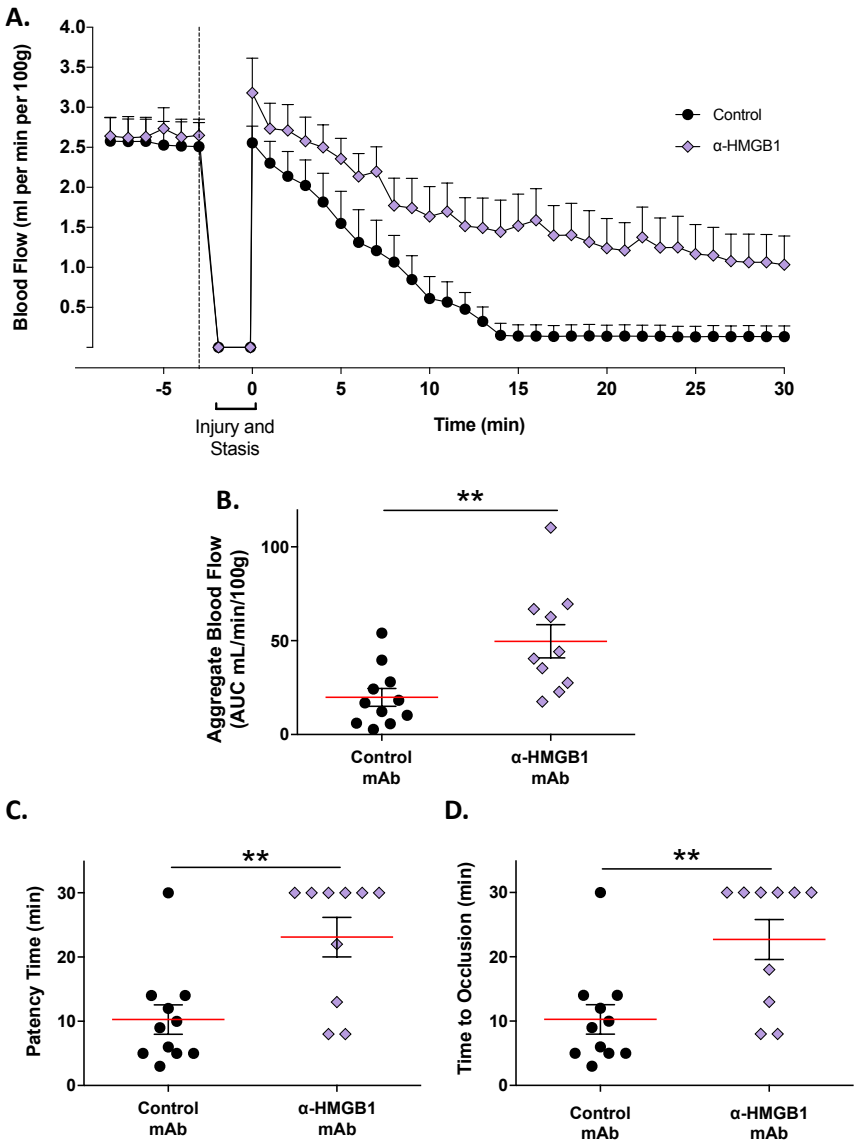

Figure 3-1. HMGB1 neutralisation inhibits $FeCl_3$-induced carotid arterial thrombosis. Male C57Bl6 (aged >6 weeks, weight>22g) mice were pre-treated with HMGB1-specific neutralising monoclonal antibody (α-HMGB1 mAb; 200µg i.v.) or isotype control antibody (α-KLH; 200µg i.v.) before $FeCl_3$ was applied to the left carotid artery. (A) HMGB1 neutralisation better preserved carotid artery blood flow and had (B) higher aggregate carotid blood flow over 30 minutes (measured by area-under-the-curve, AUC). (C, D) α-HMGB1 mAb prolonged patency time and time to occlusion. Data was analysed using non-parametric Mann-Whitney U test, **p<0.01. Error bars represent mean ± SEM.

3.2.2. HMGB1 neutralisation prevents laser-induced mesenteric arterial thrombosis (Fig. 3-2)

To confirm the antithrombotic effects of HMGB1 neutralisation, a second model of thrombosis was used. In this model, mouse mesenteric arterial endothelium was injured using pulsed laser, which caused thrombus formation that was visualised using intravital microscopy. The baseline experiment was performed in the first vessel, and thrombus size measured. Then, treatment (either isotype control or α-HMGB1 mAb) was given, and experiments performed in a different artery of the same mice. Post-treatment thrombus size was compared to the baseline. By comparing the post-treatment to baseline, rather than between mice that received isotype and α-HMGB1 mAb, the inter-individual difference was eliminated.

In mice that received the isotype control, thrombus size did not change between baseline and when laser injury was repeated after injection of the isotype control. (baseline vs. isotype control; mean ± SEM, 760.8±437.6 vs. 385.7±103.8μm^2, $p>0.99$). In contrast, following administration of α-HMGB1 mAb, the thrombi became significantly smaller (baseline vs. α-HMGB1; mean ± SEM, 518.6±129.3 vs. 142.6±50.4μm^2, $p<0.05$), confirming α-HMGB1 mAb's efficacy in preventing arterial thrombosis.

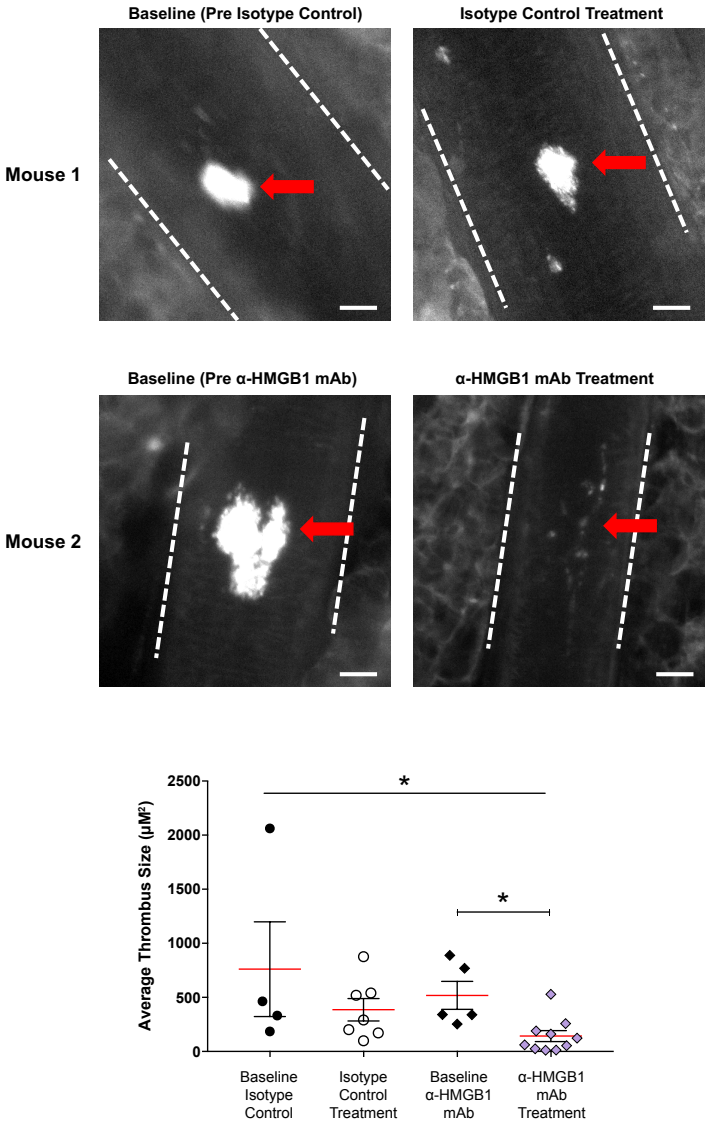

Figure 3-2. HMGB1 neutralisation inhibits laser-induced mesenteric arterial thrombosis. Male C57Bl6 mice weighed 18-23g were subjected to laser-induced thrombosis at their mesenteric arteries before and after treatment. (A) Representative intravital photomicrographs of laser-induced thrombus in mouse before and after treatment (isotype control or α-HMGB1 mAb, both at the dose of i.v. 200μg). (B) Quantification of thrombus size in mice before and after their respective treatment. Data was analysed with non-parametric Kruskal-Wallis test and subgroup comparison was made using Dunn's multiple comparison test, *$p<0.05$; error bars represent the mean ± SEM. Scale bar represents 50μM

3.2.3 Successful induction of human neutrophil NETosis (Fig 3-3 and Fig 3-4)

HMGB1 is reported to be an inducer of NETosis[169]. To verify this, optimisation experiments were carried out to (1) isolate neutrophils of high purity and viability, (2) induce NETosis with PMA, the classic agonist that induces NETosis and (3) to quantify NETosis. This set of optimisation experiments were first carried out using human neutrophils. Human neutrophils were isolated using differential density gradient method. These isolated cells were then examined with flow cytometry, where DNA-binding fluorescent stain, DAPI, was used to determine viability (viability was defined as $DAPI^-$, Fig. 3-3A). Purity of isolated cells were determined using automated blood cell counter (Sysmex XS-100). It was found high purity ($92.2 \pm 1.8\%$) and viability ($98.4 \pm 0.5\%$) were consistently achieved (Fig. 3-3A).

Having determined high purity and viability, isolated neutrophils were incubated with PMA to induce NETosis. Two methods were used to detect NETosis. Firstly, SYTOX® Green, a nuclei-acid dye was used. SYTOX® Green is impermanent to live cells and emits green fluorescence when bound to DNA. Thus, it was used to quantify extracellular DNA, a constituent thus a marker of NETosis. It was found extracellular DNA increased by 2.6-fold ($p<0.05$) after PMA exposure, indicating successful induction of NETosis (Fig. 3-3B).

Alternatively, NET formation can be identified using fluorescently-conjugated antibodies against neutrophil proteases including MPO, which can then be visualised with a confocal microscope. Following incubation with PMA, neutrophils were stained with Hoechst 33342, a nucleic acid stain, and α-MPO antibodies. NET formation was characterised as a speculated structure that stained positive for both DNA (Hoechst positive, in blue) and MPO (in purple). Such structure was readily identifiable in neutrophils stimulated with PMA (Fig. 3-4A iii to Fig. 3-4A v and magnified view shown in Fig. 3-4B) but not in those without PMA exposure (Fig. 3-4Ai). To confirm the specificity of the primary antibody (α-MPO mAb) used, a matching isotype was used, which did not stain the speculated structure (Fig. 3-4Aii). To determine the optimal concentration for the primary and secondary antibodies, two concentrations (1:200 and 1:500) were used. As shown in Fig. 3-4Aiii to Fig. 3-4Av, both NETosis was well visualised using either concentration.

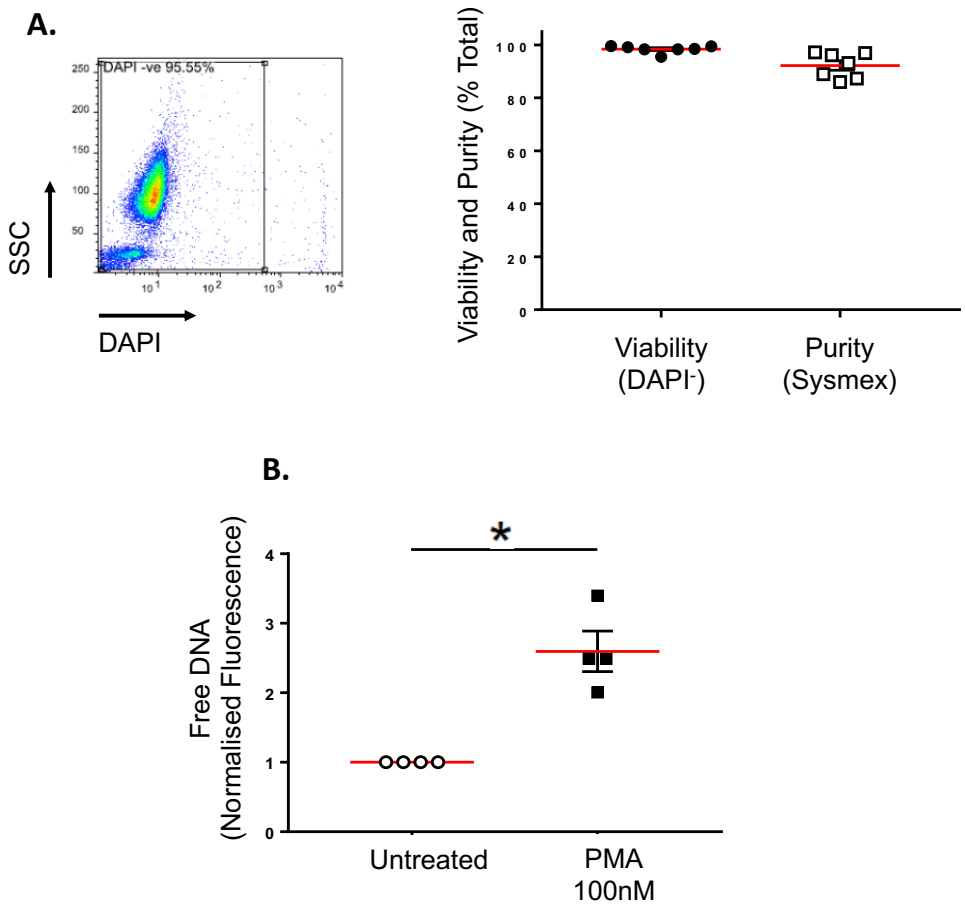

Figure 3-3. Successful human neutrophil isolation and NET induction. (A) Neutrophils isolated were of high specificity and viability (both >90%). Human neutrophils were isolated using density gradient separation method. Viability was determined using flow cytometry, defined as $DAPI^-$. Gating strategy and quantification are shown here. Purity was determined using automated blood cell counter. (B) Human NETosis can be successfully induced with PMA. Human neutrophils were seeded at a density of $1x10^5$ cells per well, and incubated with PMA 100nM for 3 hours, at 37°C, 5% CO_2. Cell-free DNA, thus NETosis, was assessed using SYTOX® Green and fluorescence normalised to untreated cells. Data was analysed with non-parametric Mann-Whitney U test, *$p<0.05$. Error bars represent mean ± SEM.

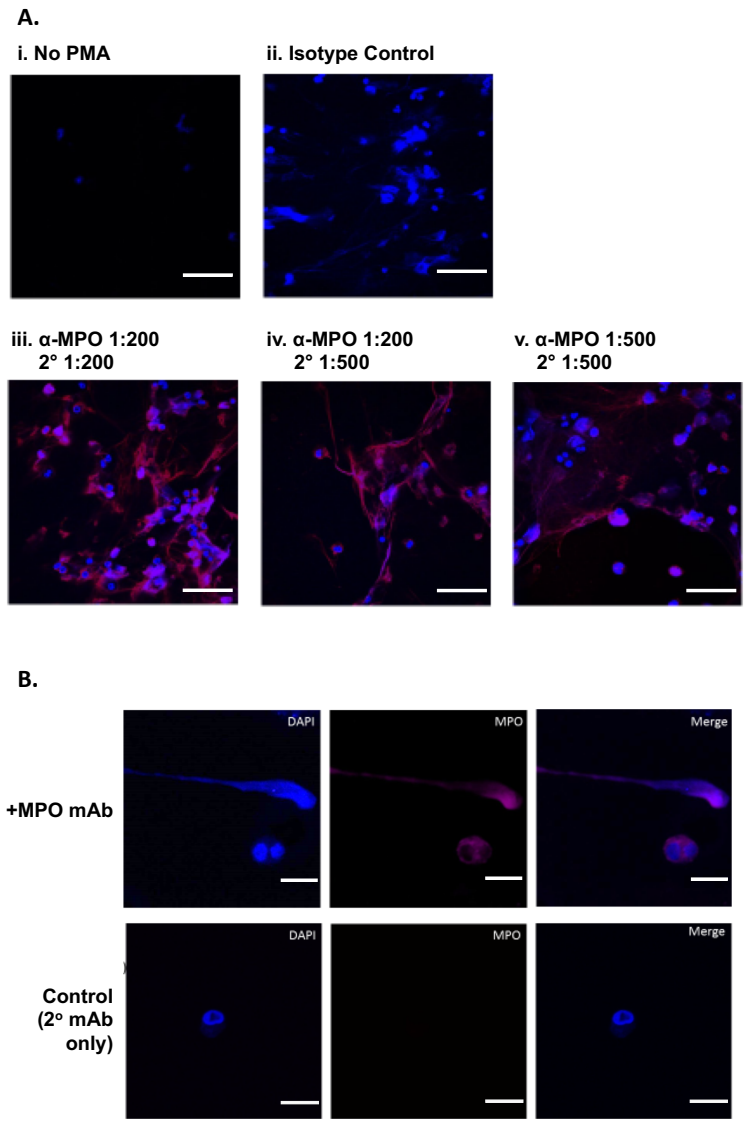

Figure 3-4. Successful induction and detection of human neutrophil NETosis. Human neutrophils were plated onto lysine-coated cover slips and incubated at 37°C, 5% CO_2 overnight. PMA, at final concentration of 10nM, was added and neutrophils were further incubated for 3 hours. Cells were then fixed with 4% PFA, stained with (1) Hoechst 33342 and (2) α-MPO or matching isotype. Two concentrations (1:200 and 1:500) of α-MPO and secondary antibodies were used to determine optimal staining concentrations. (A) Confocal microscopy at 40x magnification showing Hoechst in blue and MPO in purple, scale bar represents 50 µm. (i) No NETosis without PMA. (ii) No purple staining with isotype control, demonstrating specificity of primary antibody. (iii-v) Successful staining at both 1:200 and 1:500 antibody concentrations. (B) Nyquist magnified view of human NETosis, scale bar represents 10µm.

3.2.4 Successful induction of mouse neutrophil NETosis (Fig. 3-5 and Fig. 3-6)

Mouse bone marrow neutrophils were isolated using 2 different methods, (1) using Histopaque®-based, differential density gradient method and (2) negative immunomagnetic selection (MACS) methods. Then, flow cytometry was used to determine purity and viability of isolated cells. Neutrophils were identified as $CD45^+CD11b^+Ly6G^+$ cells, and viability was defined as $DAPI^-$ cells. (Gating strategy, Appendix 3-1). Cells yielded using immunomagnetic selection were of a higher purity ($p<0.01$), and cells yielded using these two methods were of similar viability ($p=0.59$), shown in Fig. 3-5A and B. Based on this, immunomagnetic selection method was used to purify neutrophils for further experiments.

To induce mouse NETosis, mouse bone marrow neutrophils isolated were incubated with PMA, and NETosis was quantified, first using SYTOX® Green. Multiple doses of PMA were used, and it was found high dose PMA (100μM) increased free DNA by 5.8-fold ($p<0.05$) compared to the control, demonstrating successful NET induction. On the other hand, at lower doses (0.1-10μM), PMA had no appreciable effects on NET induction (Fig. 3-5C). In addition to the SYTOX® Green method, NETosis can also be detected using immunofluorescence. PMA-treated neutrophils were stained with fluorescence-conjugated antibody against MPO and either DAPI or Hoechst 33342 to probe for DNA. Using confocal microscopy, NETosis was identified as the speculated structure that stained positive for DAPI (blue colour, Fig. 3-6A) or Hoechst (blue colour, Fig. 3-6B), as well as MPO (green), as shown in Fig. 3-6 (A, 40x magnification, B, 60x and Nyquist magnification). The specificity of primary antibody, α-MPO mAb, was also examined. Absence of signals in FITC channel in samples stained with isotype control confirmed specificity of α-MPO mAb (Fig. 3-6). Due to its ease and quantitative nature, SYTOX® Green was used to measure NETosis in the next experiment.

3.2.5 Recombinant HMGB1 induces mouse NETosis (Fig. 3-7)

Mouse bone marrow neutrophils were isolated using negative immunomagnetic selection method and incubated with recombinant HMGB1. In the time course experiment, high dose recombinant HMGB1 (10μg/mL) was used to induce NETosis, which was detected and quantified using the SYTOX® Green method. As shown in Figure 3-7A, NETosis started to emerge at 3 hours, and became significant at 4 hours ($p<0.01$). When incubated with different concentrations of HMGB1 for 4 hours, a dose-response was observed. In particular, at 10μg/mL, recombinant HMGB1 increased free DNA by 30% ($p<0.05$; Fig. 3-7B).

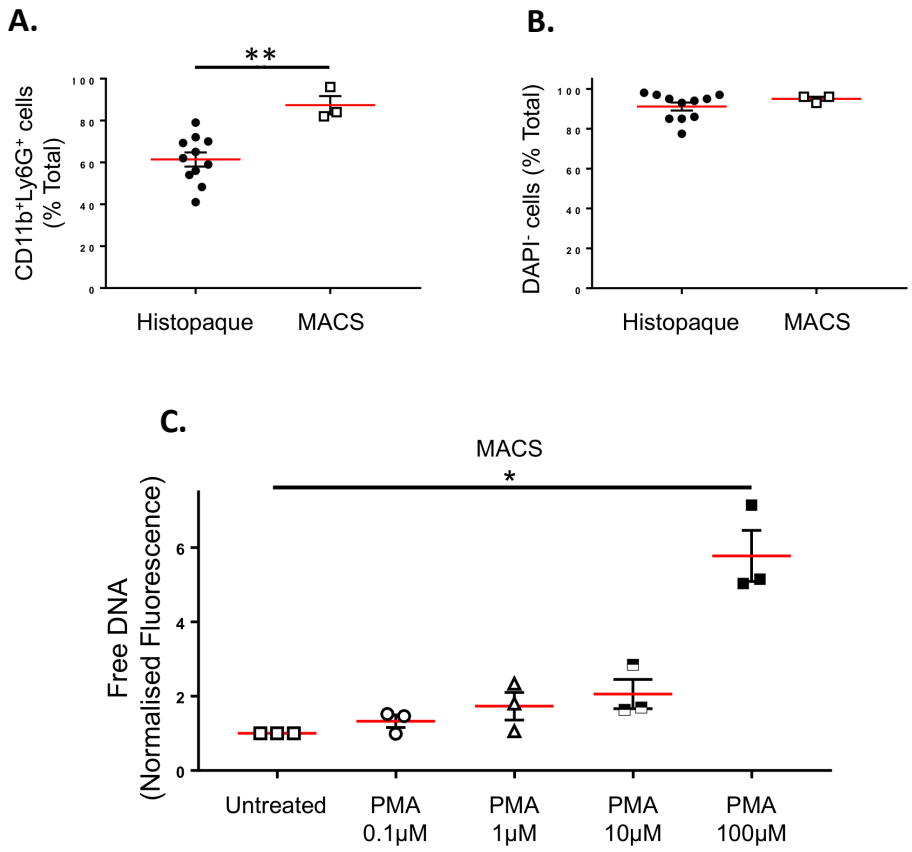

Figure 3-5. Successful induction of mouse NETosis. Mouse bone marrow cells were isolated using either differential density medium (Histopaque®) or negative immunomagnetic selection (MACS) methods, followed by flow cytometric analysis to determine the purity and viability of isolated neutrophils. (A) Immunomagnetic selection method (MACS) yielded higher purity and comparable viability. Data were analysed using non-parametric Mann-Whitney U test, **$p<0.01$. Error bars represent mean ± SEM. (B) PMA-induced NETosis was measured using SYTOX® Green and fluorescence normalised to untreated cells. Statistical analysis was performed with non-parametric Kruskal-Wallis test followed by Dunn's multiple subgroup comparisons test, *$p<0.05$. Error bars represent mean ± SEM.

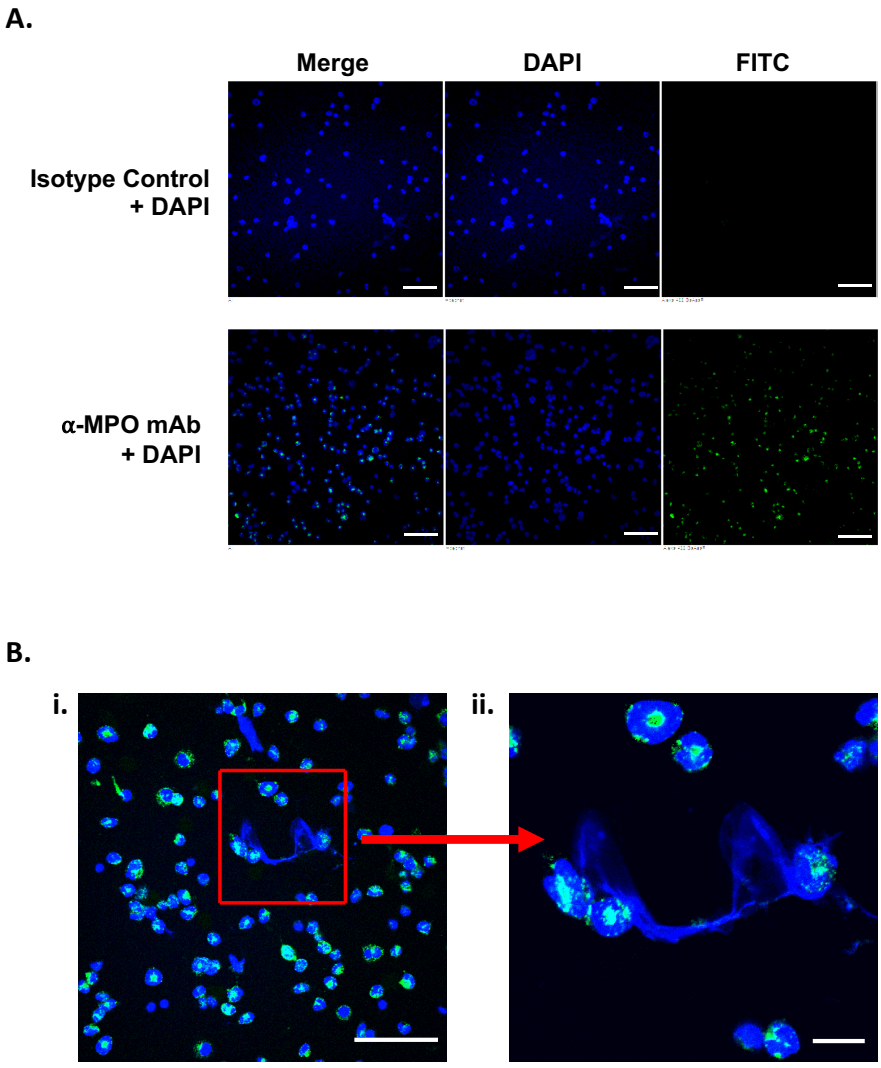

Figure 3-6. Successful detection of NETosis in murine bone marrow derived neutrophils using immunofluorescence and confocal microscopy. Mouse bone marrow neutrophils were plated onto lysine-coated cover slips, and incubated at 37C, 5% CO_2 for 3.5 hours. Neutrophils were then fixed with 4% PFA and stained with (1) Hoechst and (2) FITC-conjugated MPO or matching isotype control. (A) Confocal microscopy at 40x magnification, where DAPI stains blue and α-MPO stains green. Absence of green fluorescence in cells stained with isotype control demonstrated specificity of α-MPO mAb. Scale bar represents 50 µm. (B) Magnified view of confocal microscopy where NETosis was visualised at (i) 60x, scale bar represents 50 µm and (ii) Nyquist magnification, where scale bar represents 10 µm. In both (Bi) and (Bii), Blue represented Hoechst and green represented MPO stain.

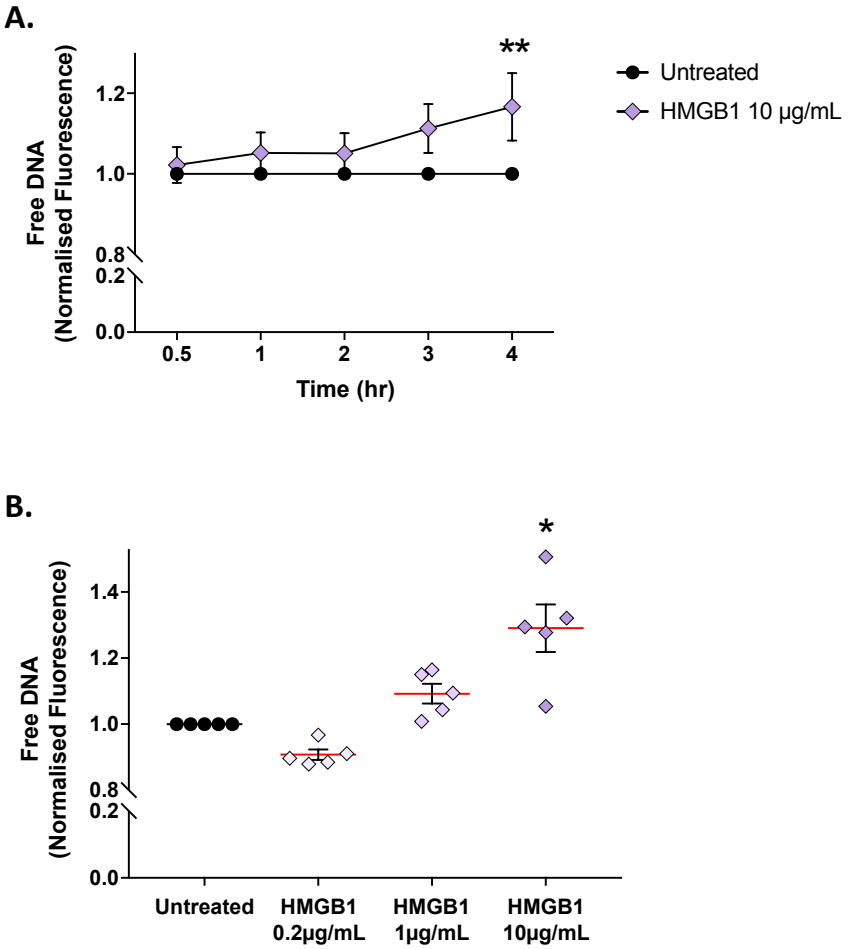

Figure 3-7. Recombinant HMGB1 induces mouse NETosis. Mouse bone marrow neutrophils were isolated using negative immunomagnetic selection and incubated with recombinant HMGB1. SYTOX® Green was used to quantify cell free DNA, and fluorescence was normalised to that of untreated cells. (A) Bone marrow neutrophils were incubated with 10µg/mL recombinant HMGB1 and the fluorescence intensity was read at 0.5, 1, 2, 3 and 4 hours. Normalised fluorescence is significantly higher at 4 hours than at 0.5 hour, indicating NETosis induction. Error bar represents 95% confidence interval. (B) Bone marrow neutrophils were incubated with recombinant HMGB1 for 4 hours, at final concentrations of 0, 0.2, 1 and 10 µg/mL. Fluorescence intensity was normalised to that of untreated cells. Data was analysed using non-parametric Kruskal-Wallis test, followed by Dunn's subgroup analysis. *$p<0.05$, **$p<0.01$. Error bars represent mean ± SEM.

3.2.6 α-Ly6G antibody successfully depletes neutrophils *in vivo* (Fig. 3-8)

Having established HMGB1 induces NETosis *in-vitro*, the next step was to determine if HMGB1-induced NETosis contributes to thrombosis *in vivo*. To investigate this, it was reasoned that if HMGB1 neutralisation mediates its actions through inhibition of NET formation, neutrophil depletion would prevent NET-mediated thrombosis in mice that received isotype control. However, it would not change the antithrombotic effects of HMGB1 neutralisation, as NET-mediated thrombosis would already be inhibited by α-HMGB1 mAb.

To carry out this set of investigations, experiments were conducted to ensure murine neutrophils can be successfully depleted. Neutrophil depletion was achieved by using α-Ly6G mAb, 1A8. This clone is specific to neutrophils and does not affect monocytes[221]. Neutrophils were defined as $CD45^{+}CD11b^{+}Ly6C^{int}$ cells. Ly6G, a commonly used marker of neutrophils, was not used to identify neutrophils in this study because the depleting (α-Ly6G mAb, 1A8) and staining antibodies (α-L6yG mAb, RB6-8C5) target the same epitope. It was found mouse neutrophils were reduced significantly by 72% ($p<0.01$).

3.2.7 Neutrophil depletion impairs $FeCl_3$-induced carotid artery thrombosis (Fig. 3-9)

It was important to first establish if neutrophils made any contribution to $FeCl_3$-induced thrombosis. Mice were neutrophil-depleted and subjected to $FeCl_3$-induced carotid artery thrombosis. Compared to the historical control (male C57Bl6 mice treated with α-KLH isotype control), aggregate carotid blood flow appears to be higher in neutrophil-depleted mice, though this did not reach statistical significance (Fig. 3-9A and B, $p=0.08$). However, neutrophil depletion significantly prolonged patency time and time to occlusion (Fig. 3-9C, $p<0.05$), indicating neutrophils made a significant contribution to $FeCl_3$-induced carotid thrombosis.

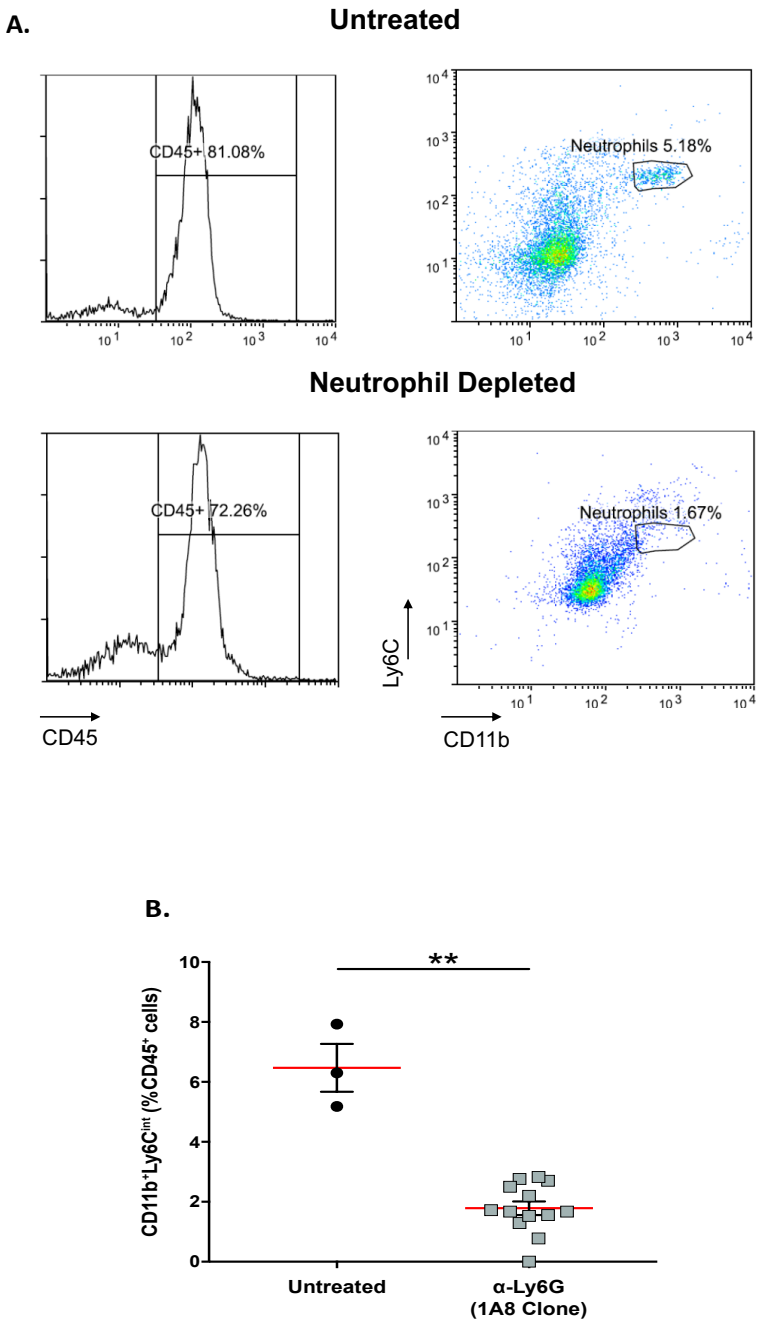

Figure 3-8. Mouse neutrophils were effectively depleted using α-Ly6G antibody (1A8 clone). Mice were injected with α-Ly6G (1A8 clone) 0.5mg i.p. and blood collected for flow cytometric analysis 19 hour later. (A) Neutrophils were defined as $CD45^{+}CD11b^{+}Ly6C^{int}$ cells. (B) Mice receiving α-Ly6G antibody had significantly reduced numbers of neutrophils. Statistical analysis was performed using non-parametric Mann-Whitney U test, **p<0.01. Error bars represent mean ± SEM.

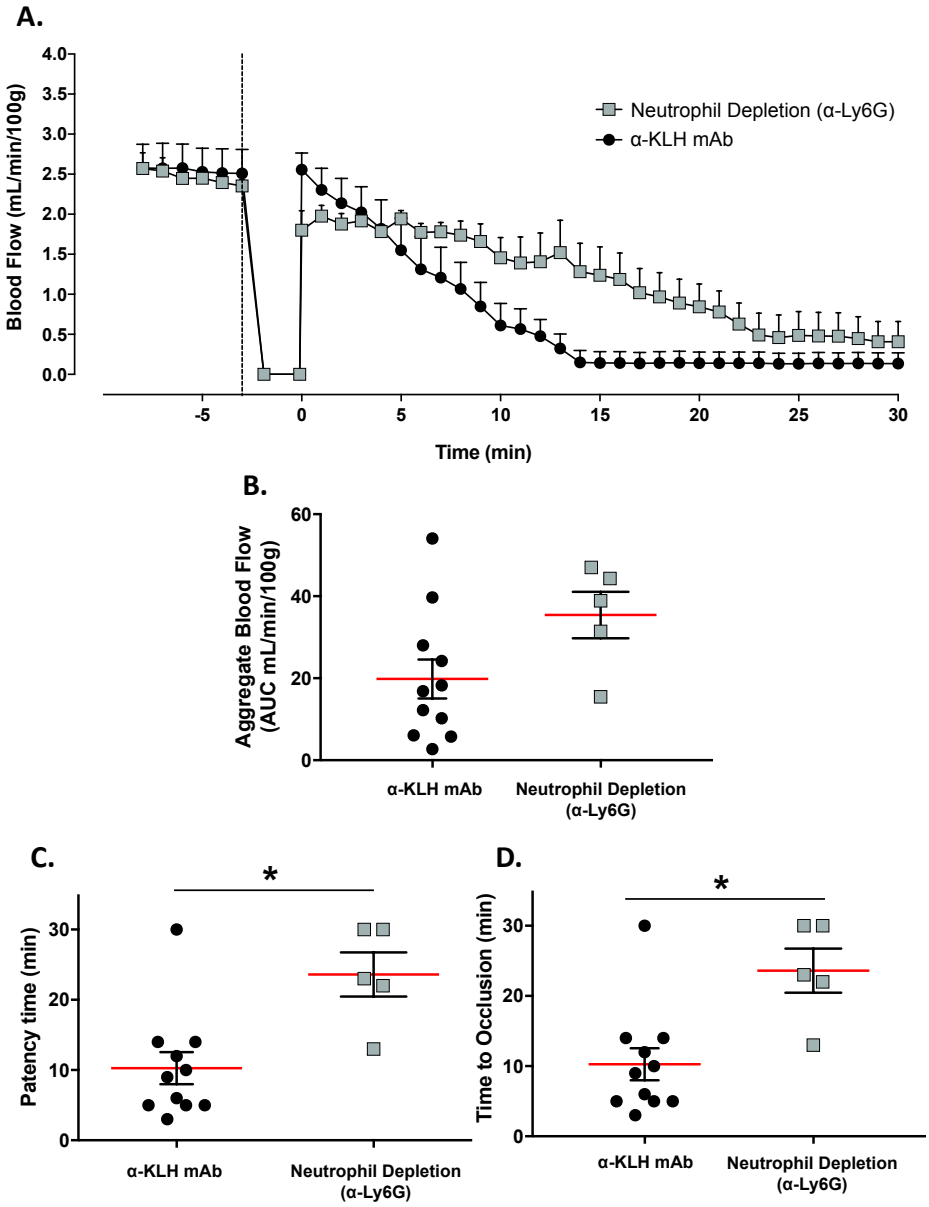

Figure 3-9. Neutrophils contribute significantly to $FeCl_3$-induced carotid artery thrombosis. Mice were injected with α-Ly6G (1A8 clone) 0.5mg i.p to deplete neutrophils and were subjected to $FeCl_3$. (A, B) This did not change aggregate carotid blood flow significantly, but it (C) prolonged patency time and (D) time to occlusion. Statistical analysis was performed using non-parametric Mann-Whitney U test, where *$p<0.05$. Error bars represent mean ± SEM.

3.2.8 Neutrophil depletion eliminates antithrombotic benefits of HMGB1 neutralisation (Fig. 3-10)

The next experiment assessed how neutrophil depletion affected the antithrombotic actions of α-HMGB1 mAb. As eluded to before, if HMGB1 neutralisation mediates its antithrombotic effects through inhibition of NETosis, then neutrophil depletion and α-HMGB1 mAb would work through the same pathway and produce similar antithrombotic effects (e.g., no change in patency time). However, neutrophil depletion would have an antithrombotic effect in mice receiving the isotype control (e.g., longer patency time than mice without neutrophil depletion). As expected, with neutrophil depletion, the difference in $FeCl_3$-induced carotid thrombosis between mice receiving isotype control and α-HMGB1 mAb was abolished.

3.2.9 DNase abolishes the antithrombotic benefits of HMGB1 neutralisation (Fig. 3-11)

In addition to NETosis, neutrophils can also promote thrombosis through the release of TF[107]. To establish that the antithrombotic effect of α-HMGB1 mAb was specific to NETosis, DNase, an enzyme that degrades DNA thus NET formation, was administered to mice before they received α-HMGB1 mAb or isotype control. These mice were then subjected to $FeCl_3$-induced carotid artery thrombosis. Similar to the neutrophil depletion experiment, if HMBG1 principally exerts its prothrombotic effects through NETosis, DNase would confer an antithrombotic effect in mice receiving isotype but make no difference to mice receiving α-HMGB1 mAb. As expected, DNase eliminated the difference between the two treatment groups with respect to carotid artery blood flow, patency time and time to occlusion.

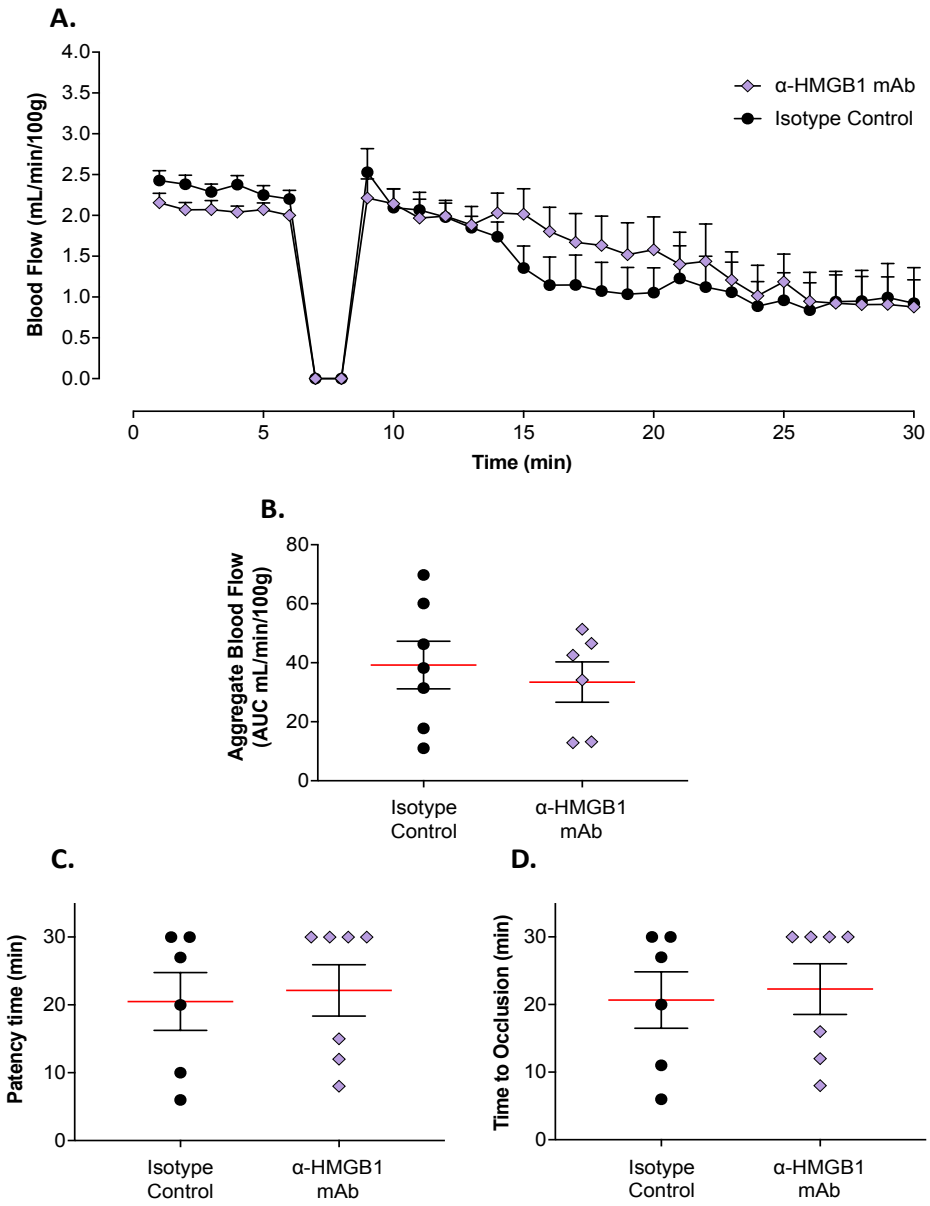

Figure 3-10. Neutrophil depletion abolishes the antithrombotic benefits of α-HMGB1 mAb in $FeCl_3$-induced carotid arterial thrombosis. Mice were depleted with neutrophils using α-Ly6G mAb, then received isotype control or α-HMGB1 (both i.v. 200μg) before subjected to FeCl3-induced carotid thrombosis, (A, B) carotid artery blood flow, (C) patency time and (D) time to occlusion were no longer different between mice that received isotype control and those that received α-HMGB1 mAb. Statistical analysis was performed using non-parametric Mann-Whitney U test. Error bars represent mean ± SEM.

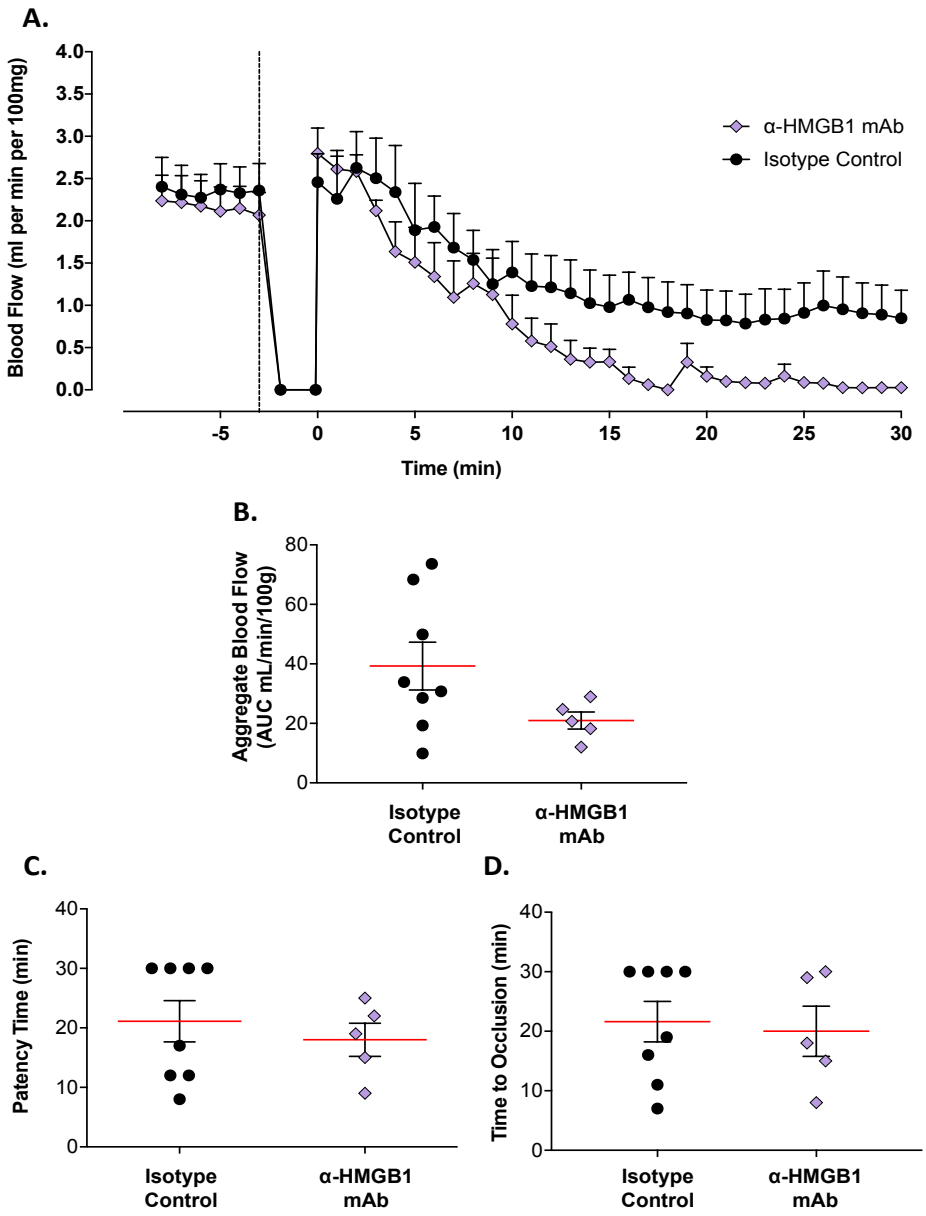

Figure 3-11. DNase abolishes the antithrombotic benefits of α-HMGB1 mAb in $FeCl_3$-induced carotid arterial thrombosis. Mice first received DNase (1500u i.v.), followed by isotype control or α-HMGB1 mAb (i.v. 200μg), before being subjected to $FeCl_3$-induced carotid artery thrombosis. After DNase treatment, there were no longer significant differences in (A, B) carotid artery blood flow, (C) patency time or (D) time to occlusion between the 2 groups. Statistical analysis was performed using non-parametric Mann-Whitney U test. Error bars represent mean ± SEM.

3.2.10 HMGB1 neutralisation has no effect in a neutrophil-independent model of thrombosis (Fig. 3-12)

It had been reported that neutrophils do not contribute to thrombosis in a deep vein thrombosis model of the inferior vena cava (IVC) ligation[222]. If α-HMGB1 mAb mediates its action principally through NETosis, one would expect that administration of α-HMGB1 mAb would have no effect in this model. To test this concept, the first step was to establish a model, where flow stasis was achieved through ligation of IVC and closure of all branches through diathermy or ligation (Appendix 3-2). Then, mice were first treated with either isotype control or α-HMGB1 mAb and then subjected to IVC ligation surgery. Regardless of the route of delivery (s.c. vs. i.v.), frequency of administration (single dose vs. divided dose) or dose of α-HMGB1 (200μg vs. 400μg), HMGB1 neutralisation did not change the size of IVC thrombus when compared to those administered isotype control or received no treatment.

3.2.11 Liposomal clodronate effectively depletes monocytes (Fig. 3-13)

HMGB1 induces TF expression on monocytes *in vitro*[135,223], and this is a potential mechanism through which HMGB1 promotes thrombosis. However, it is unclear if monocytes make significant contribution to $FeCl_3$-induced carotid artery thrombosis. To address this issue, the impact of monocyte depletion in $FeCl_3$-induced carotid artery thrombosis was assessed. The first step was to ensure effective depletion of monocytes. This was achieved through the use of i.v. liposomal clodronate, a pharmacological approach that selectively ablates monocytes but does not affect neutrophil number or function[224]. Compared to mice that received liposomal PBS, liposomal clodronate significantly reduced monocyte numbers by 64% ($p<0.05$).

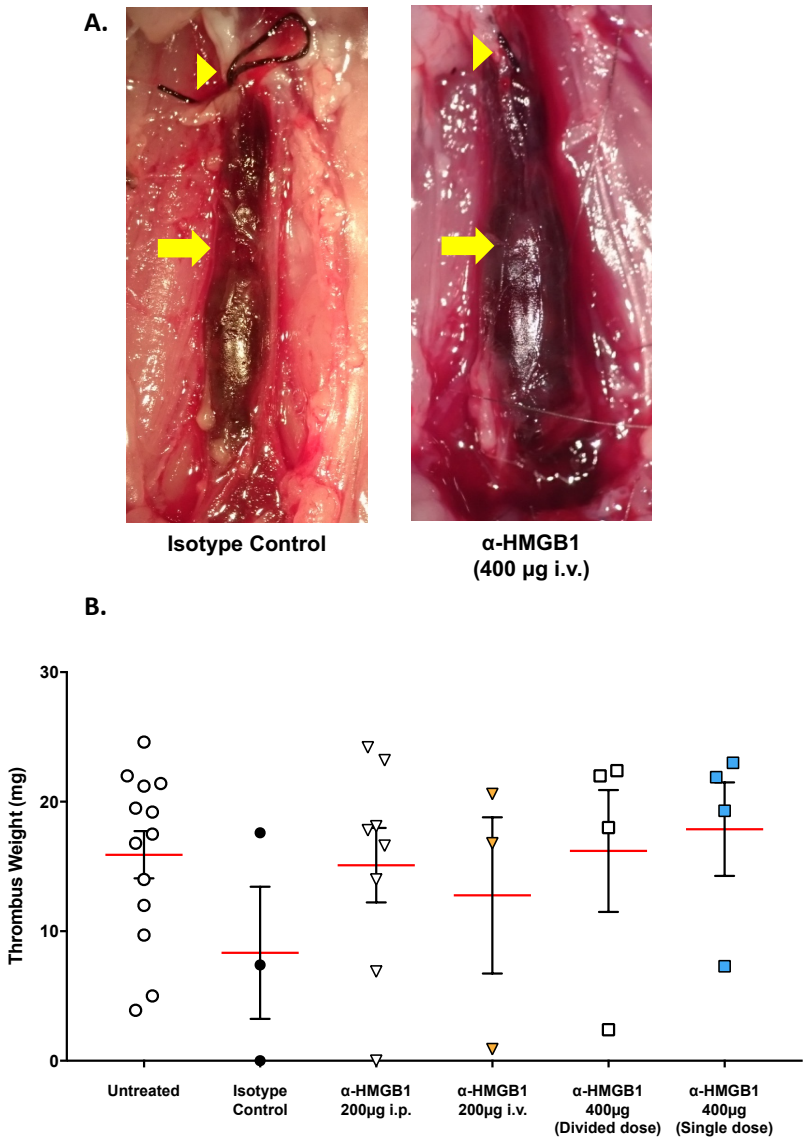

Figure 3-12. α-HMGB1 mAb does not reduce thrombus size in a neutrophil-independent model of venous thrombosis. Mice were treated with either isotype control or α-HMGB1 mAb at escalating doses before IVC ligation surgery. (A) Representative photomicrograph of IVC ligation (yellow arrowhead) and thrombi (yellow arrow) from mice pre-treated with either 400µg i.v. α-HMGB1 mAb or isotype control. (B) α-HMGB1 mAb did not reduce IVC thrombosis. Data were analysed using non-parametric Kruskal-Wallis test. Error bars represent mean ± SEM.

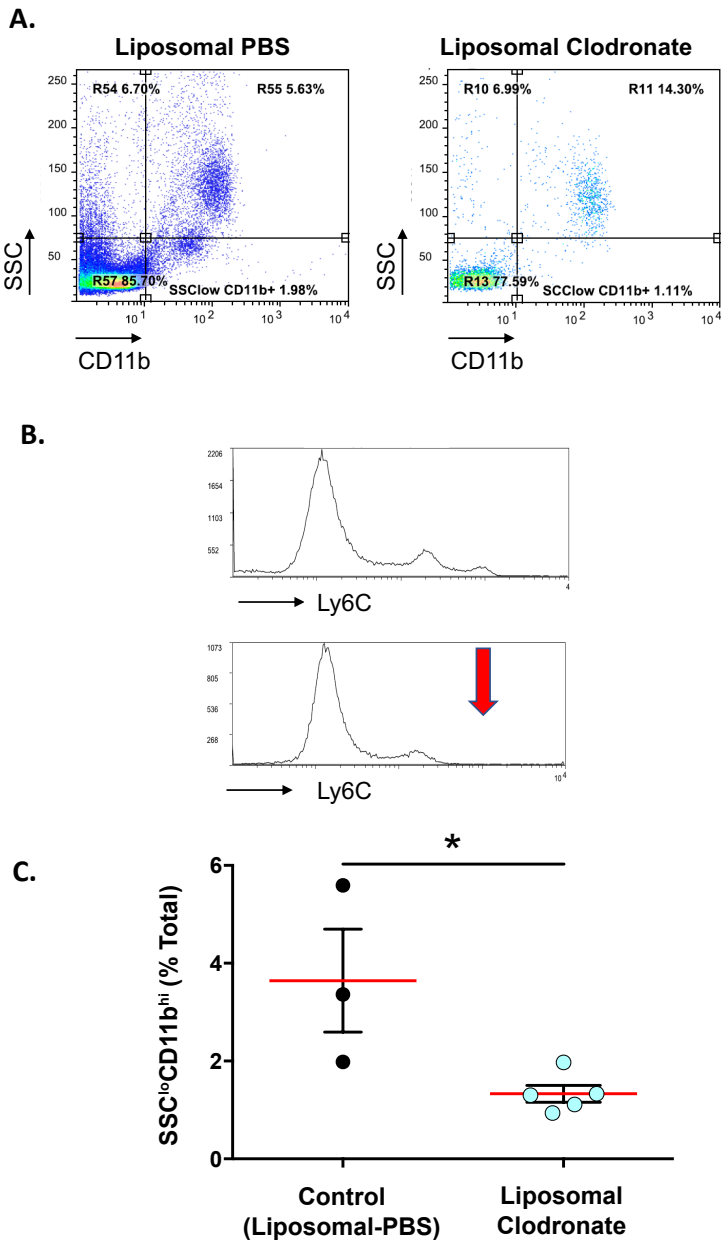

Figure 3-13. Successful monocyte depletion following i.v. liposomal clodronate. Mice received i.v. liposomal clodronate (5µg/mg weight), or liposomal PBS as control, and depletion was verified using flow cytometry, where monocytes were defined as $SSC^{low}CD11b^{+}$ cells. (A) Gating strategy (B) Compared to control (top panel), liposomal clodronate depleted $Ly6C^{hi}$ cells (bottom panel). (C) Circulating monocyte counts were significantly lower in mice that received liposomal clodronate. Statistical analysis was performed using non-parametric Mann-Whitney U test, where *$p<0.05$. Error bars represent mean ± SEM.

3.2.12 Monocyte depletion does not affect $FeCl_3$-induced carotid thrombosis (Fig. 3-14)

Following successful monocyte depletion, male C57Bl6 mice were subjected to $FeCl_3$-induced carotid artery thrombosis. Compared to control mice that received liposomal PBS, monocyte depletion did not affect any of the parameters examined including carotid blood flow, patency time or time to occlusion. As monocytes are irrelevant in $FeCl_3$-induced carotid thrombosis, by inference, α-HMGB1 mAb antithrombotic effects are independent of monocytes.

3.2.13 HMGB1 neutralisation does not affect platelet aggregation (Fig. 3-15)

Previous studies from this laboratory have shown that HMGB1 binds to activated platelets[191]. Thus, it is plausible the antithrombotic actions of α-HMGB1 mAb was due, at least in part, to platelet function. However, pre-incubating platelets with α-HMGB1 mAb did not prevent platelet aggregation in response to 3 common platelet agonists including ADP ($p>0.99$), thrombin ($p=0.20$) and collagen ($p=0.10$).

3.2.14 HMGB1 neutralisation does not affect platelet responsiveness (Fig. 3-16)

In addition to platelet aggregation, the effect of α-HMGB1 mAb in platelet responsiveness was also examined. It was found that for platelets from male C57Bl6 mice, pre-treatment with α-HMGB1 mAb did not prevent platelet activation (defined as $CD41^+CD62P^+$, for gating strategy, refer to Appendix 3-3) in response to ADP ($p=0.89$) or thrombin ($p=0.20$).

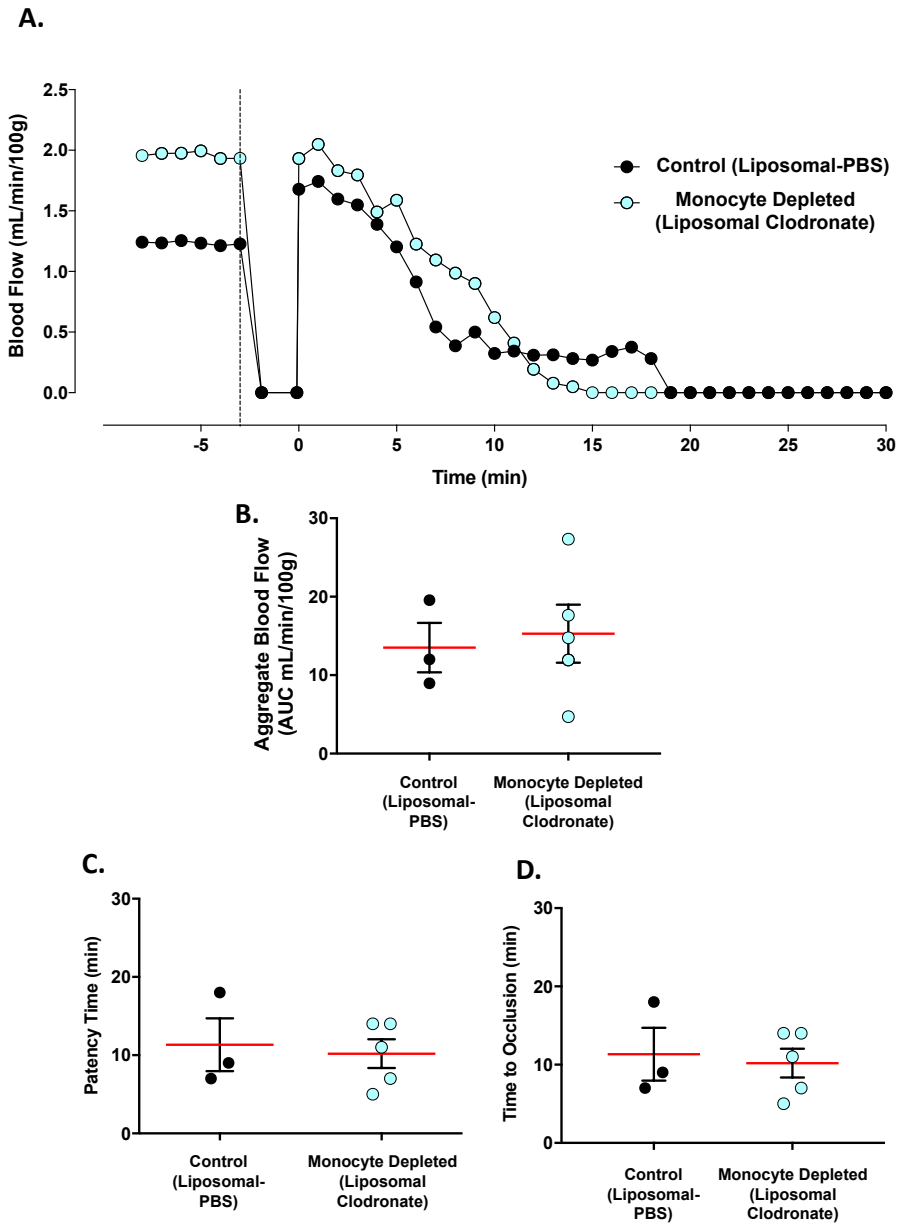

Figure 3-14. Monocyte depletion does not affect $FeCl_3$-induced carotid arterial thrombosis. Mice were subjected to $FeCl_3$-induced carotid artery thrombosis after successful monocyte depletion. Compared to control mice (liposomal-PBS), monocyte-depleted mice had similar (A, B) carotid artery blood blow, (C) patency time and (D) time to occlusion. Statistical analysis was performed using non-parametric Mann-Whitney U test. Error bars represent mean ± SEM.

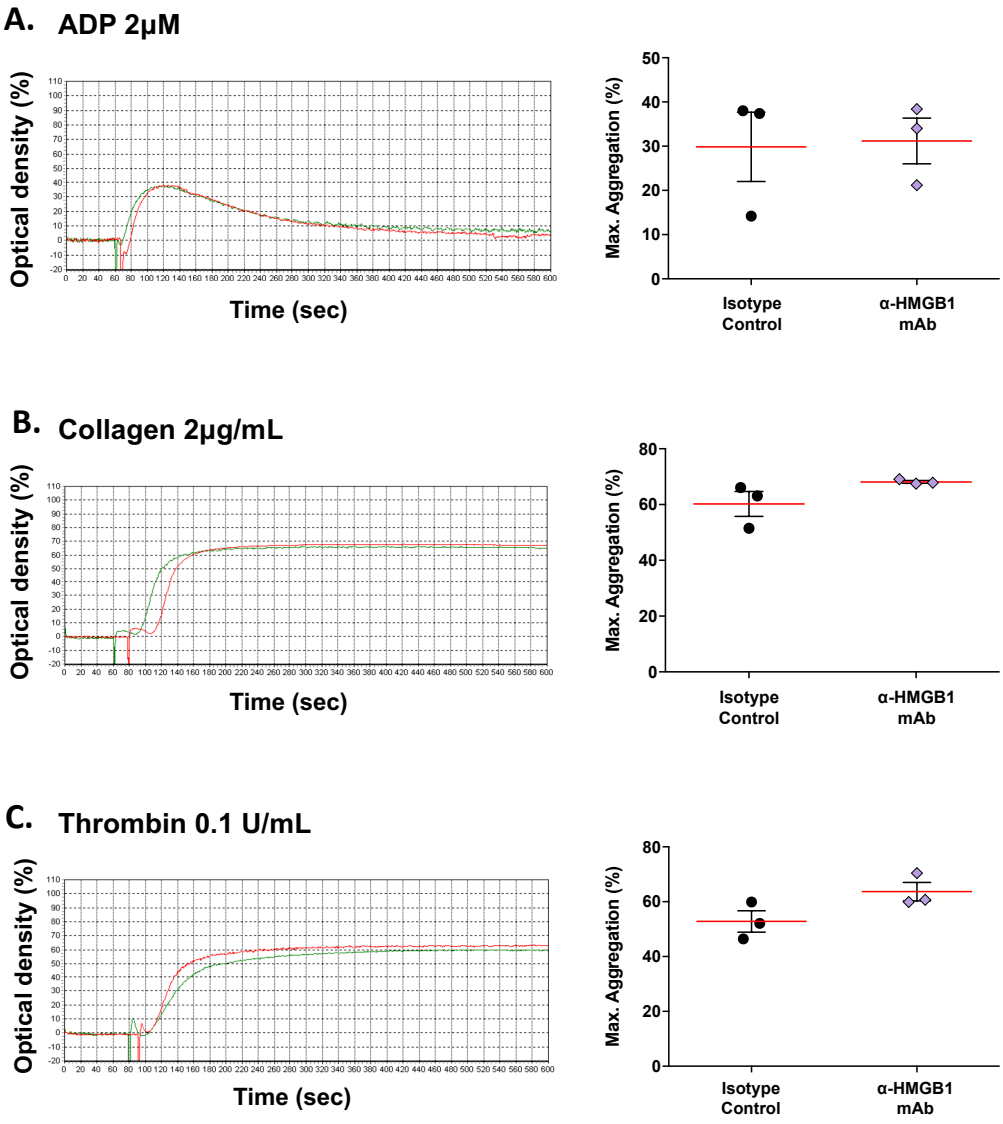

Figure 3-15. HMGB1 neutralisation does not affect *ex-vivo* platelet aggregation. Platelet-rich plasma was incubated with isotype control (final concentration 100µg/mL) or α-HMGB1 mAb (final concentration 100µg/mL) for 30 minutes prior to being stimulated with either (A) ADP 2µM, or (B) collagen 2µg/mL. For experiments with thrombin stimulation (C), washed platelets were used and incubated with isotype control or α-HMGB1 (both at final concentration 100µg/mL). They were then stimulated with thrombin 0.1U/mL. Data was analysed using non-parametric Mann-Whitney U test. Error bars represent mean ± SEM.

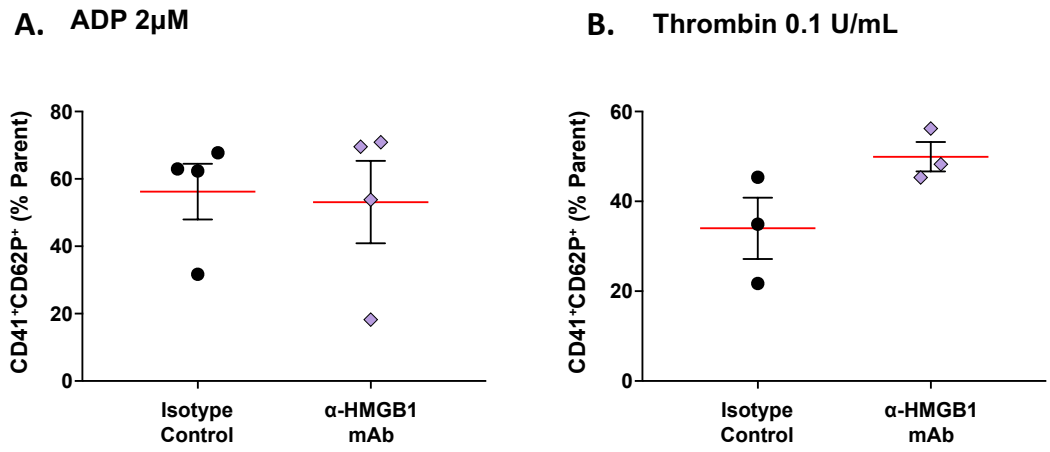

Figure 3-16. HMGB1 neutralisation does not affect ADP- or thrombin-induced platelet activation. Mice platelets were incubated with isotype control or α-HMGB1 mAb (both at final concentration of 100µg/mL) for 30 minutes prior to being stimulated with either (A) ADP 2µM or (B) thrombin 0.1U/mL. Data was analysed using non-parametric Mann-Whitney U test. Error bars represent the mean ± SEM.

3.2.15 HMGB1 neutralisation does not affect haemostasis (Fig. 3-17)

Bleeding is a significant risk of common antiplatelet and antithrombotic agents. To assess the translational potential of HMGB1 neutralisation in preventing arterial thrombosis, it was important to examine its impacts on haemostasis. α-HMGB1 mAb did not affect platelet count ($p=0.40$) or 3mm tail bleeding time ($p=0.64$), an accepted marker of haemostatic function. HMGB1 interacts with different components of the coagulation cascade and fibrinolytic system, including tissue factor and thrombomodulin[199]. This can potentially affect bleeding diathesis. However, compared to isotype control, α-HMGB1 did not alter the activated partial thrombin time (APTT) or prothrombin time (PT), two parameters that reflects alteration in the intrinsic and extrinsic pathways of the coagulation cascade.

3.2.16 HMGB1 neutralisation is equally effective but safer than antithrombotic agents used clinically (Fig. 3-18)

The utility of a clinical therapeutic depends on both efficacy and safety, and for any novel therapeutics, it is important to compare it to current therapeutics. When evaluating antithrombotic drugs, carotid artery patency time in response to $FeCl_3$ can be used as a measure of efficacy, and 3mm tail bleeding time as a surrogate for safety. Compared to the control (isotype control), α-HMGB1 was both effective (longer patency time) and safe (similar bleeding time). In contrast, clopidogrel significantly prolonged bleeding time, even at a dose (1mg/kg) too low to prevent arterial thrombosis. Enoxaparin, at a high dose of 10mg/kg, was effective (longer patency time, $p<0.01$) yet caused bleeding diathesis (prolonged tailed bleeding time, $p<0.05$). In summary, α-HMGB1 compared favourably to clinical antithrombotic therapy.

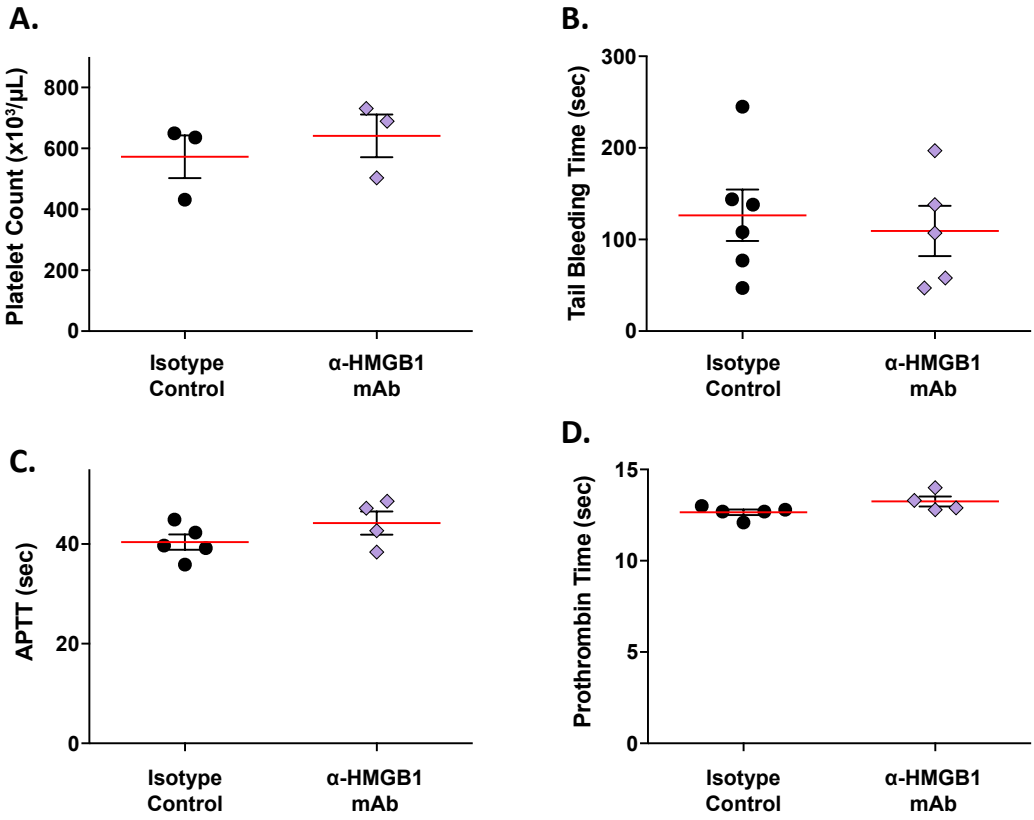

Figure 3-17. HMGB1 neutralisation does not affect haemostasis. Mice were injected with i.v. isotype control or α-HMGB1 mAb (200µg for both) and allowed 30 minutes circulation before blood was drawn for analysis. (A) Platelet count was determined using an automated blood cell counter. (B) To determine tail bleeding time, mouse tails were resected distally at 3mm from the tip of the tail and immersed in pre-warmed PBS. Bleeding time is taken as the point bleeding stopped. If bleeding continued for >30 minutes, mice were culled, and 30 minutes was taken as the bleeding time. (C) APPT and (D) PT were determined using commercial assays as per manufacturer instruction. Data was analysed using non-parametric Mann-Whitney U test. Error bars represent mean ± SEM.

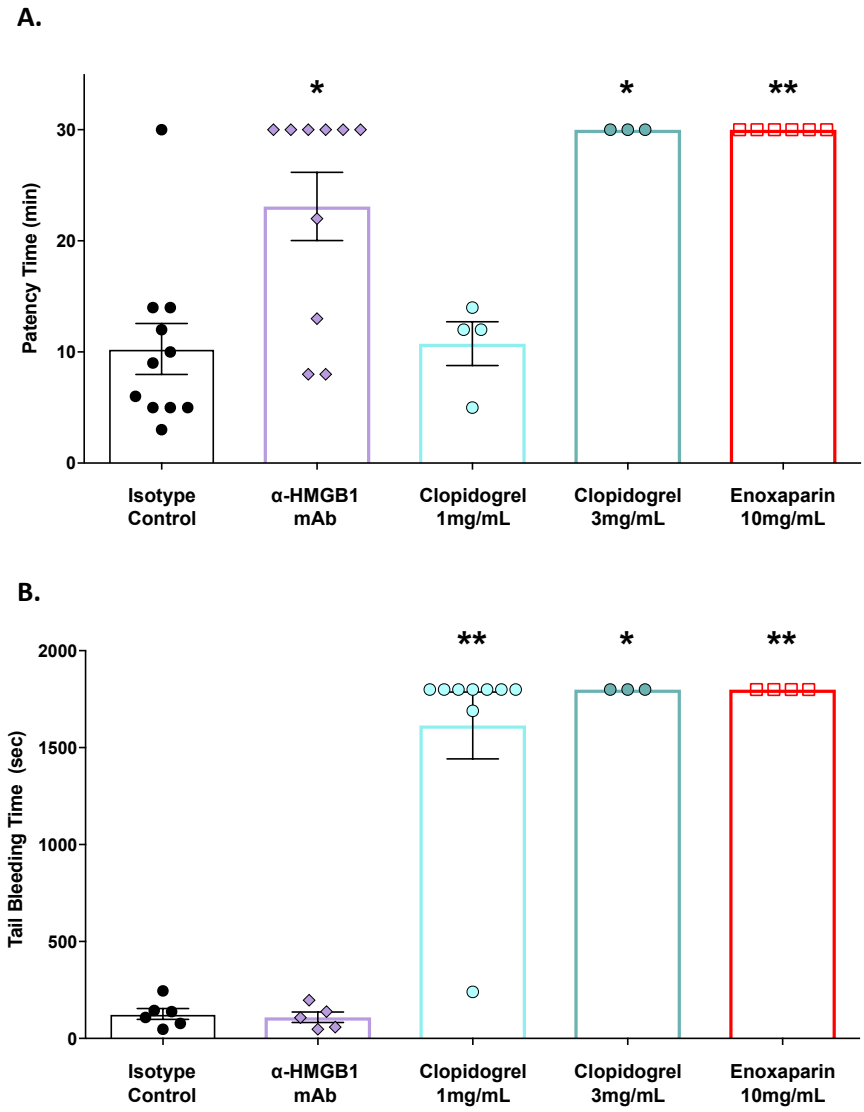

Figure 3-18. HMGB1 neutralisation compares favourably to other clinical antithrombotic drugs. Mice received either isotype control, α-HMGB1 mAb (described in detail in Fig. 3-1), 1mg/kg or 3mg/kg gavage of clopidogrel or 10mg/kg i.v. enoxaparin. (A) Mice then underwent $FeCl_3$-induced carotid thrombosis experiments or (B) 3mm tail bleeding time experiments. Data was analysed using non-parametric Kruskal-Wallis test, and subgroup analysis was performed using Dunn's subgroup analysis, *$p<0.05$ and **$p<0.01$ (each compared to isotype control). Error bars represent mean ± SEM.

3.3 Discussion

The main findings of this investigation were schematically represented in Fig. 3-19 and include, (1) an antibody-based approach to neutralise HMGB1 is an effective antithrombotic strategy, as demonstrated by preserved carotid artery flow after $FeCl_3$ exposure and smaller thrombi in mesenteric arteries following laser injury. (2) The antithrombotic actions of HMGB1 neutralisation were mediated through inhibition of NET formation, independent of monocytes and platelets. (3) HMGB1 neutralisation did not affect normal haemostatic function, as indicated by the normal tail bleeding time and coagulation parameters. (4) Compared to clinical antithrombotics, HMGB1 neutralisation had a favourable efficacy/safety profile, i.e., a wider therapeutic window.

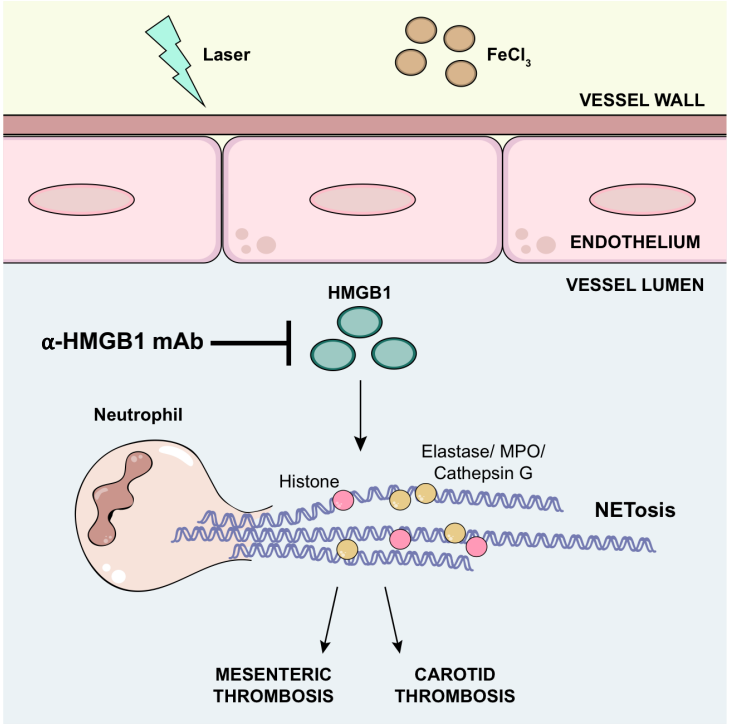

Figure 3-19. Schematic illustration – antithrombotic actions of α-HMGB1 mAb. HMGB1 neutralisation with α-HMGB1 mAb inhibits NETosis and thus prevents $FeCl_3$-induced carotid arterial thrombosis and laser-induced mesenteric arterial thrombosis. Modified from Huang et al[122].

Thrombosis, in particular, arterial thrombosis, is a major cause of mortality and morbidity[5]. Currently, all clinical antithrombotic therapeutics target platelets or the coagulation cascade. Development of more potent antithrombotic agents were accompanied with higher bleeding risks[225], calling for a new strategy to treat thromboembolism. NET formation is increasingly being implicated in arterial and venous thrombosis[137]. It provides a scaffold to facilitate interactions between platelets, coagulation factors and erythrocytes, and neutrophil proteases including MPO and elastase can also promote thrombosis through activation of platelets, the extrinsic and intrinsic coagulation pathways[220]. Clinical investigations have extended these observations and lend support to the clinical significance of these experimental findings[192]. Results from this thesis have shown that inhibition of NET formation not only is effective, but it also appeared to be a safe therapeutic strategy. Compared to other means of inhibiting NETosis, targeting HMGB1 offers unique advantages. Recently, it was reported that humanised α-HMGB1 mAb had been developed[204], taking this therapeutic strategy one step closer to clinical translation. Secondly, in addition to its antithrombotic effects, HMGB1 blockade has been shown to be protective in ischemia-reperfusion injury[186]. Compared to agents that acts solely on NET inhibition, the additive or even synergistic benefits of HMGB1 blockade could confer further protective advantages in patients suffering from stroke or myocardial infarction. Thirdly, the excellent haemostatic profile shown in this thesis will facilitate its clinical application.

The importance of HMGB1 in mediating arterial and venous thrombosis has been demonstrated by other investigators too. Vogel et al. has demonstrated that platelet-specific ablation of HMGB1 in mice resulted in a phenotype with reduced thrombosis, as indicated by longer time to occlusion when mouse mesenteric artery was exposed to $FeCl_3$[195]. They also reported diminished NET formation in these mice. This is in agreement with the findings of our current investigation. However, in contrast to our study, Vogel et al. found that platelet-specific ablation of HMGB1 affects platelet function including platelet aggregation in response to collagen, and it also affects haemostasis, as reflected by prolonged tail bleeding time[195]. The difference between the study of Vogel et al. and this study is that this study employed antibody-based HMGB1 inhibition, whereas Vogel et al. utilised mice with platelet-specific, genetic knock-out of HMGB1. Therefore, the discrepancies may relate to the means in which HMGB1 was inhibited, where genetic deletion likely ablates HMGB1 to a greater extent than antibody-based neutralisation. Stark et al. have shown that pharmacological inhibition (using HMGB1

Box A) or platelet-specific genetic depletion of HMGB1 reduced thrombus size in an IVC flow stenosis model of deep vein thrombosis[196]. This is in contrast to our current data, where HMGB1 neutralisation did not reduce deep vein thrombosis, using an IVC ligation model of deep vein thrombosis. These conflicting results are most likely due to different animal model used, as the IVC stenosis model used by Stark et al. is NET-dependent[113], whereas the IVC total ligation model was deliberately chosen in this project for its neutrophil-independent nature[222]. Indeed, among the 4 mouse models of DVT, the IVC stenosis model is the only model where NETosis plays a role[113,132,133,222]. It suggests the IVC stenosis model may reflect limited aspects of DVT physiology and may not be generalisable. However, Dyers et al. have recently reported that platelet-specific deletion of HMGB1 results in a reduction in deep vein thrombi, using the IVC ligation model[226], different to the findings in this investigation. The reason for these conflicting results is not clear, but it may relate to the different study durations. In this thesis, IVC thrombus was examined at 48 hours, whereas Dyers et al. examined the thrombus at day 1 and 7.

One other novelty of this investigation is that it provides evidence that NET formation is the principal mechanism through which HMGB1 neutralisation inhibits thrombosis. Previous studies have shown that HMGB1 promotes NET formation[169], induces monocyte and endothelial expression of tissue factors[223,227] and changes platelet phenotypes[195]. While these *in vitro* studies provide plausible mechanisms to account for the prothrombotic actions of HMGB1, this thesis examined their relative importance and showed that *in vivo*, prothrombotic effects of HMGB1 is chiefly attributed to NET formation. Indeed, this study showed that inhibition of NET formation alone is an effective antithrombotic strategy. Secondly, extending previous studies, this study further explored the translational potential of HMGB1 neutralisation. Results here demonstrated that HMGB1 neutralisation is not only effective, but also safe, as it does not affect any haemostatic parameters. Indeed, it compares favourably to antithrombotic agents used currently.

This study has a number of limitations. Firstly, the effects of HMGB1 neutralisation in platelets were examined *in vitro* only. Platelet-depleting antibody was not used in this study, as it would completely abolish the haemostatic and thrombotic machinery. Lockyers et al. have shown that in the $FeCl_3$ model of thrombosis, carotid artery remained patent (for the entire 60-minute monitoring period) when platelets were depleted[228]. Secondly, to translate current findings clinically, detailed information regarding the cellular source of HMGB1, and the post-

modifications required for HMGB1 to induce NETosis would be important, as they would allow more precise targeting of any therapeutics designed.

In conclusion, HMGB1 neutralisation is an effective antithrombotic strategy. In addition, this thesis extends findings from previous studies and demonstrated that HMGB1 exerts its prothrombotic effects principally through inhibition of NET formation, and its effects on platelets and monocytes are not significant. In broader terms, it also highlights the feasibility and efficacy of NET inhibition as a novel antithrombotic strategy. This study is clinically relevant, as antibody-based therapeutics, a clinically-acceptable means of interventions, was used in this study, and superior safety profile of HMGB1 neutralisation was demonstrated. Together, this should pave the way for clinical translation.

CHAPTER 4

Effects of PCSK9 Inhibition in a Mouse Model of Atherosclerotic Plaque Rupture

4.1 Introduction

The "lipid hypothesis" postulates that atherosclerosis is caused by hypercholesterolaemia and in particular, an elevation in LDL cholesterol. With accumulating evidence from basic, clinical and population studies, it is now widely accepted[30,229]. In experimental studies, dietary supplementation of cholesterol induced atherosclerotic lesions in rabbits[229]. In addition, in mice, manipulation of the mouse genome (e.g., deletion of *apoE* and *Ldlr* genes) results in chronic hypercholesterolaemia and also causes atherosclerosis[37,39]. Supporting this, epidemiological studies have consistently demonstrated a strong correlation between hypercholesterolaemia and coronary artery disease[230-232]. The most compelling evidence has arisen from Mendelian randomisation and intervention studies where all effective LDL-lowering measures, whether due to genetic variation, pharmacological intervention, or surgical treatment, concordantly reduce cardiovascular risks[30]. Remarkably, despite disparate modes of intervention, the magnitude of benefit is similar: for every 1 mmol/L reduction in LDL cholesterol, there is an approximate 20% relative reduction in cardiovascular risks[30].

Over the last 2 decades, HMG-CoA reductase inhibitors, or statins, have been the mainstay of treatment for hypercholesterolaemia[233]. Statins inhibit cholesterol biosynthesis, which, through the transcription factor SREBP, lead to the upregulation of hepatic LDLR and increased uptake of plasma LDL[77,234]. Despite marked clinical benefits of statins, they have very modest effects on plaque regression[235]. Instead, statins exert their protective effects through stabilisation of atherosclerotic plaques, as they change plaque biochemical and cellular composition. Crisby et al. has shown that following three months of statin treatment, carotid plaques from patients who underwent carotid endarterectomy had a higher collagen and lower lipid content[236]. Using IVUS, investigators demonstrated that atorvastatin increased plaque hyperechogeneity, consistent with an increase in fibrous tissue[237]. Animal studies have extended these observations by providing mechanistic insights into the action of statins. Monkeys treated with pravastatin have reduced intimal macrophage infiltration and neovascularisation, despite unchanged cholesterol levels[58], and simvastatin reduced the frequency of atherosclerotic intraplaque haemorrhage in apoE$^{-/-}$ mice, even with a paradoxical increase in plasma cholesterol[238]. These observations raise the question whether the protective effects of statins are chiefly mediated through its lipid-lowering or lipid-independent pleiotropic effects.

Recently, inhibition of PCSK9 has been validated in clinical studies to be effective in lowering cholesterol and cardiovascular risks[66]. PCSK9 is a 22kDa protein expressed in the liver, kidney and small intestine. It binds to the LDLR and mediates lysosomal degradation of LDLR[239]. This results in decreased LDLR thus reduced hepatic uptake of cholesterol. Clinical significance of PCSK9 was first demonstrated in genetic epidemiology studies. In one study, it was shown a loss-of-function mutation in the PCSK9 gene led to a 28% reduction in LDL cholesterol and a 88% reduction in cardiovascular risk[93]. Recently, two large clinical trials have shown that antibody-based inhibition of PCSK9 reduced relative cardiovascular risk by approximately 15% in secondary prevention settings[66,67]. Similar to statin, PCSK9 inhibition only regresses established plaques modestly[240]. This raises the question if PCSK9 also reduces cardiovascular events by strengthening plaque stability. So far, there is a paucity of mechanistic studies that address this question. In addition, a recent study suggests that PCSK9 inhibition may have anti-inflammatory actions in apoE$^{-/-}$ mice[241], and this could also impact on plaque stability. Lastly, it remains possible that α-PCSK9 mAb may have yet-unknown off-target effects that provide clinical benefits.

This laboratory has previously established a mouse model of atherosclerotic plaque rupture/instability. In this model, two stenoses in tandem are created surgically at the carotid artery of apoE$^{-/-}$ mice fed a high fat diet. This generated an environment with low shear and high tensile stress, two important precipitants of plaque rupture[242,243], which favours the development of an unstable phenotype at the atherosclerotic lesion in the mouse carotid artery. This model uniquely reproduces many features of ruptured plaques including lesions rich in necrosis, the presence of lumenal thrombosis, disrupted fibrous caps and intraplaque haemorrhage[63]. Further, its response to clinical therapeutics mirrors those observed clinically[63].

In this study, the aim was to determine the effect of evolocumab, a human monoclonal antibody against PCSK9, in plaque stabilisation, using the tandem stenosis model. Currently, using apoE$^{-/-}$ mice, there is conflicting evidence on the effect of PCSK9 inhibition in atherosclerosis. Denis et al. reported that deletion of PCSK9 did not change cholesterol or atherosclerotic plaque burden[89]. On the other hand, Tang et al. recently demonstrated that silencing PCSK9 could reduce atherosclerotic plaque sizes[241]. Both studies, however, examined plaques in aortic sinus, which seldom develop into unstable and clinically relevant atherosclerotic lesions. Given carotid tandem stenosis model has the unique advantage of creating lesions that resemble

human ruptured plaques, it was hypothesised that by using this model, this study would provide definite evidence with direct clinically relevance. Secondarily, the aim was to assess PCSK9 inhibition in atherogenesis and its impact on platelets and immune cells, both can contribute to atherosclerotic plaque stability and development.

4.2. Results

4.2.1 Evolocumab does not change body or spleen weight (Fig. 4-1)

Male apoE$^{-/-}$ mice aged 6 weeks or older were fed a high fat diet for 6 weeks before they were subjected to tandem stenosis surgery. After surgery, they continued on high fat diet for a further 7 weeks and concomitantly received weekly i.v. injections of either evolocumab or PBS (Fig. 2-2). Eight mice were randomly assigned to the evolocumab group and 5 mice to the control group, and all survived until the end of the study. There was no significant difference in body weight between the two groups (p=0.23). Spleen weight was also examined as it is an important immune organ and may affect plasma cholesterol and atherosclerotic lesion size in mice[244]. No difference between the two groups was observed.

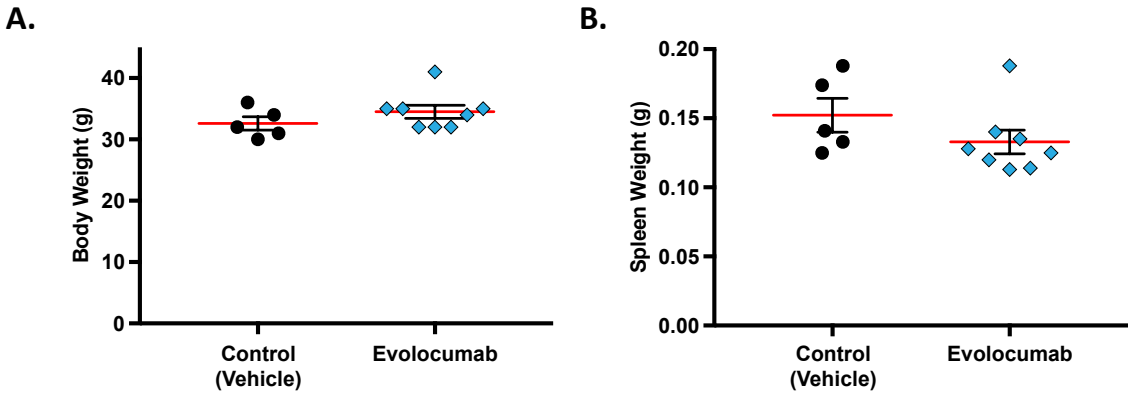

Figure 4-1. Average body and spleen weight do not differ between control and evolocumab-treated apoE$^{-/-}$ mice. Male apoE$^{-/-}$ mice aged 6 weeks or older were fed a high fat diet for 6 weeks and then subjected to carotid tandem stenosis surgery. After surgery, mice received i.v. PBS or evolocumab (10 mg/kg) weekly while continuing on high fat diet for a further 7 weeks. Data was analysed using the non-parametric Mann-Whitney U test. Error bars represents mean ± SEM.

4.2.2 Evolocumab does not change plasma cholesterol profile (Fig. 4-2)

Plasma cholesterol was measured once only, at the end of the study. Total plasma cholesterol concentration did not differ between control and evolocumab-treated mice (control vs.

evolocumab; mean ± SEM, 28.0 ± 1.7 vs. 32.8 ± 1.5mmol/L, p=0.13). Similarly, plasma triglyceride concentration did not differ between control and evolocumab-treated mice (control vs. evolocumab; mean ± SEM, 1.2 ± 0.2 vs. 1.8 ± 0.3mmol/L, p=0.11).

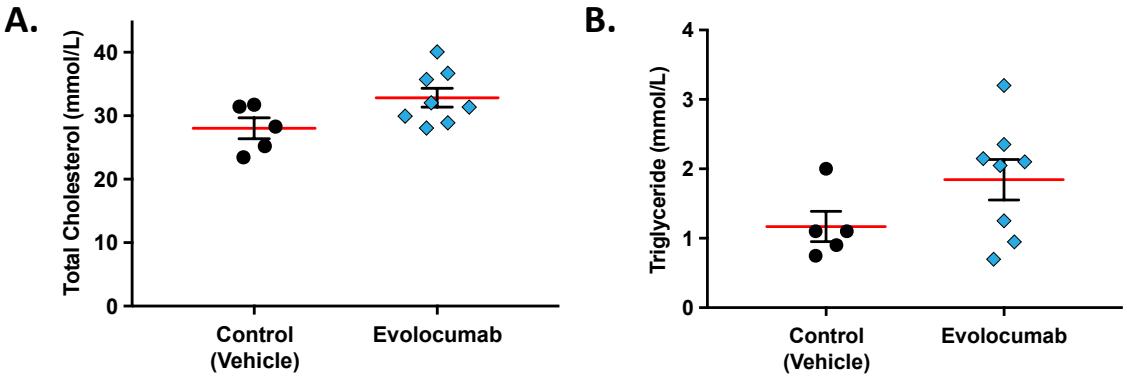

Figure 4-2. Evolcoumab does not change cholesterol profile of male apoE$^{-/-}$ mice fed a high fat diet. Plasma obtained at the end of the study period was analysed using the Roche Cobas immunochemistry system. Compared to control, evolocumab did not change total cholesterol or triglyceride concentrations significantly. Statistical analysis was performed using non-parametric Mann-Whitney U test. Error bars represents mean ± SEM.

4.2.3 Evolocumab does not change lipid content in carotid segment I (Fig. 4-3)

It was previously established that carotid segment I, defined as the segment between the origin of the carotid artery and the proximal narrowing suture, is the section with the most unstable phenotype and resembles vulnerable human atherosclerotic plaques[63]. Thus, histochemical analysis of the carotid tandem stenosis lesion was limited to segment I. Plaque lipid content was first examined as it is an indicator of plaque instability and responds to lipid-lowering therapy[236]. Average lipid content of the 3 sampled frozen sections (taken to represent the proximal, middle and distal carotid segment I), when normalised to carotid plaque size, did not differ between mice treated with PBS or evolocumab (p=0.62). No differences between the 2 groups were detected in any of the 3 sections (Appendix 4.1)

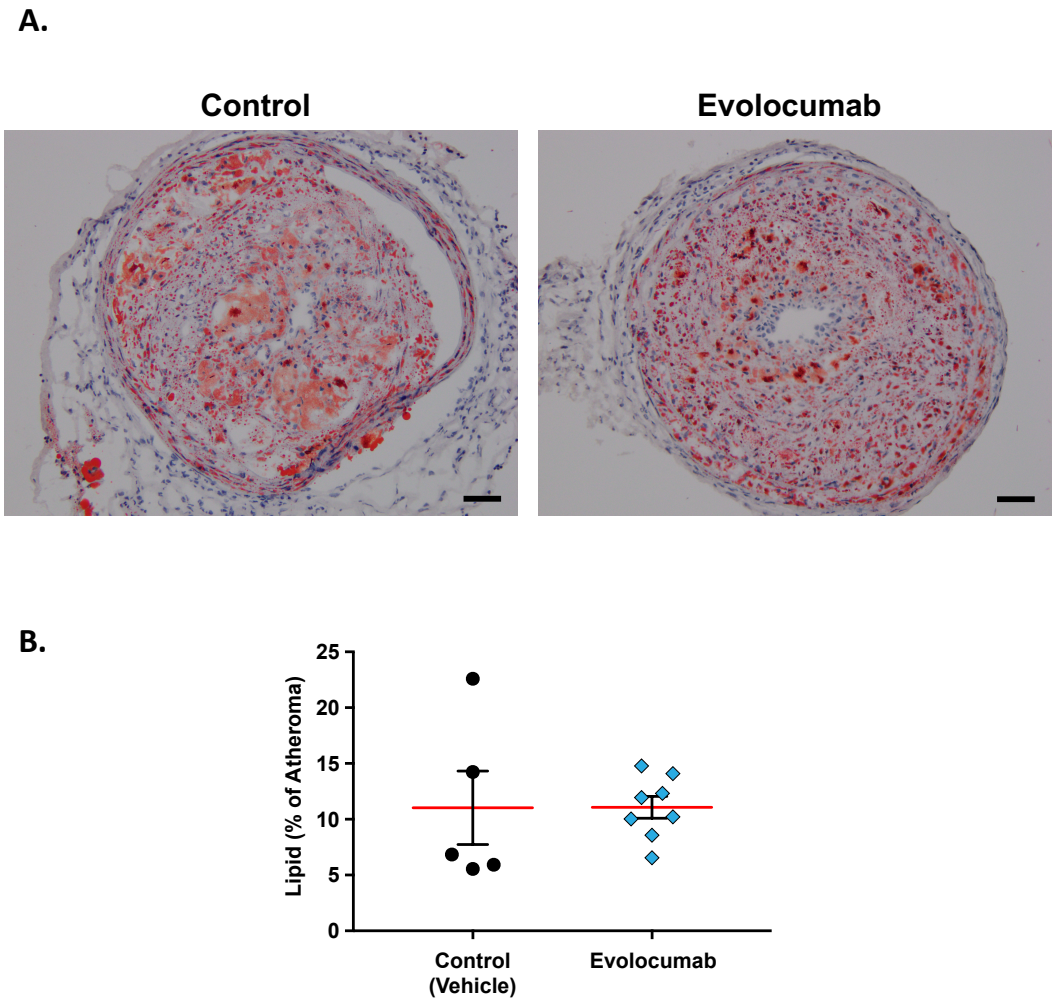

Figure 4-3. Evolocumab does not change the lipid content in carotid segment I in male apoE$^{-/-}$ mice fed a high fat diet. Frozen sections of carotid segment I, defined as the section between the origin of carotid artery and the first stenosing ligature, were stained with oil red-o, where neutral lipid stained red. (A) Representative photomicrograph and (B) quantification of proportion of atheroma containing lipid. Data was analysed using non-parametric Mann-Whitney U test. Error bars represent mean ± SEM. Scale bar represents 50 μm.

4.2.4 Evolocumab does not change collagen content in carotid segment I (Fig. 4-4)

Collagen content in carotid segment I was next examined, as collagen abundance is associated with plaque stability[15] and changes in response to pharmacotherapy[236]. Compared to control, evolocumab-treated apoE$^{-/-}$ mice had similar collagen content (p=0.52) in carotid segment I. Normalised collagen content between control and evolocumab-treated mice were comparable in proximal, middle and distal carotid segment I (Appendix 4-2).

4.2.5 Evolocumab does not reduce the size of atherosclerotic lesions in aortic sinus (Fig. 4-5)

Thus far, it has been shown that evolocumab does not change any of the stability parameters at carotid segment I. Next, aortic sinus atheroma were examined to determine if evolocumab impacted on the development and progression of atherosclerosis. Frozen sections from the proximal, middle and distal parts of aortic sinus were stained with haematoxylin and eosin (H&E) and lesion size was measured. Compared to control, evolocumab did not reduce the size of the atherosclerotic lesion in aortic sinus (control vs. evolocumab; mean ± SEM, 394,570±53,043 vs. 441,719±45,813μm^2, p=0.62). Though there was heterogeneity in lesion size at different levels, no between-group difference was detected at any of the 3 levels (Appendix 4-3 A).

4.2.6 Evolocumab does not change the extent of necrosis in aortic sinus atheroma (Fig. 4-6)

Progression in atherosclerotic lesions are often accompanied by changes in plaque composition including the extent of necrosis, abundance of collagen and the amount of lipid [8-10]. These changes can also affect plaque stability[245]. Area of necrosis was defined as acellular space (characterised by the absence of nuclei) on frozen sections stained with H&E. Evolocumab did not change the extent of necrosis, whether measured in absolute terms (p=0.83) or as a percentage of atheroma (p=0.94). No difference was found at any of the levels examined (Appendix 4-3 B)

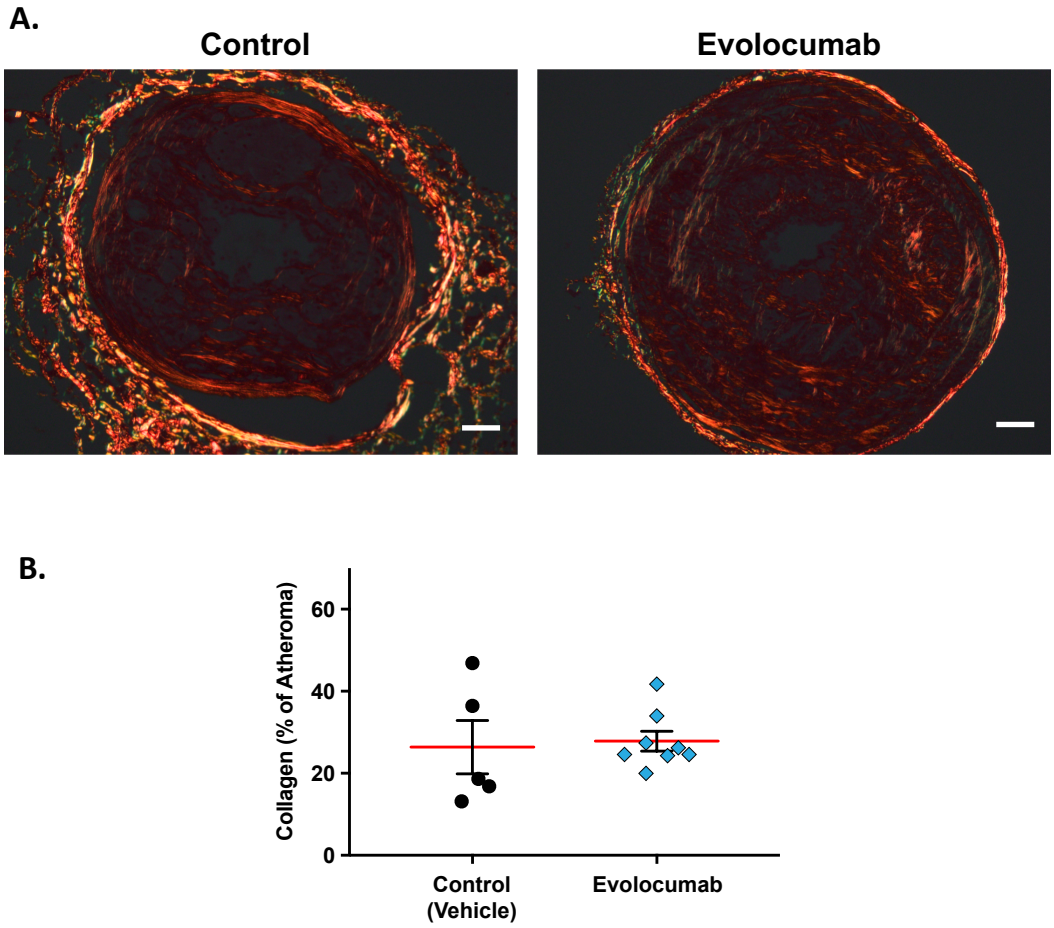

Figure 4-4. Evolocumab does not change the collagen content in carotid segment I in male apoE$^{-/-}$ mice fed a high fat diet. Frozen sections of carotid segment I was stained with picrosirius red and examined under polarised light, where collagen stained orange-red. (A) Representative photomicrograph and (B) quantification of proportion of atheroma containing collagen. Data was analysed using non-parametric Mann-Whitney U test. Error bars represent mean ± SEM. Scale bar represents 50 μm.

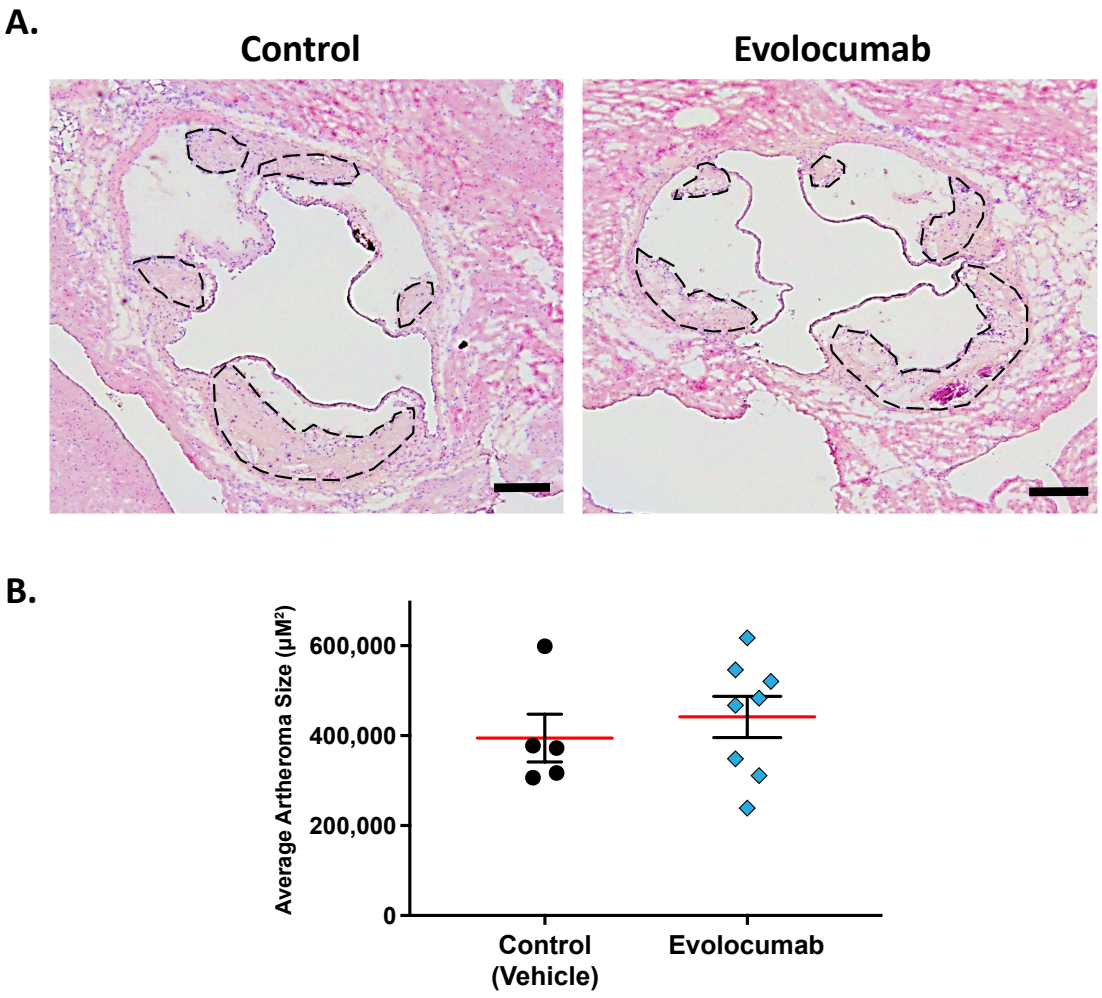

Figure 4-5. Evolocumab does not change the size of atherosclerotic lesions in aortic sinus in male apoE$^{-/-}$ mice fed a high-fat diet. Frozen sections of the aortic sinus were stained with H&E and lesion area (circled in dotted line) was measured. Data was analysed using non-parametric Mann-Whitney U test. Error bars represent mean ± SEM, scale bar represents 200µm.

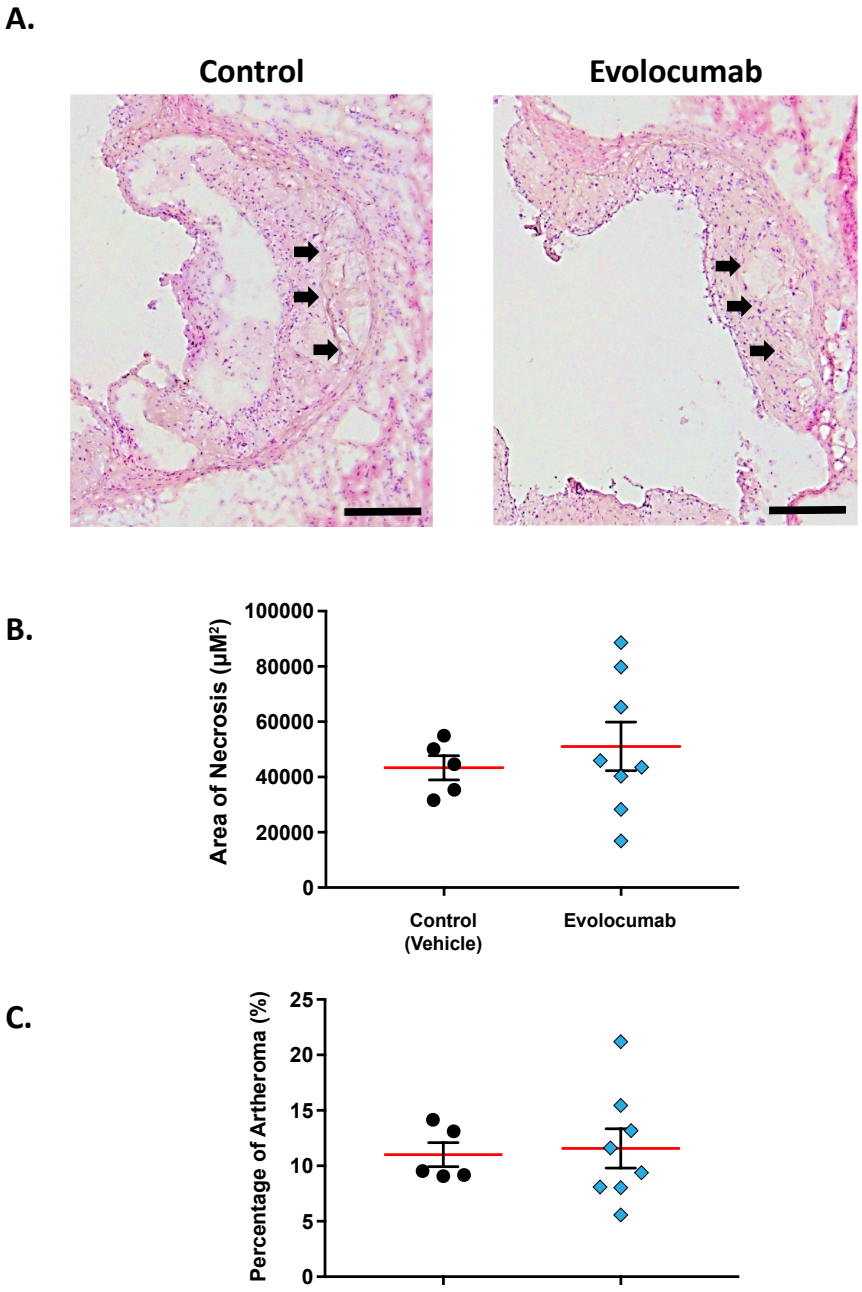

Figure 4-6. Evolocumab does not change the extent of necrosis in aortic sinus atheroma in male apoE$^{-/-}$ mice fed a high fat diet. Necrosis was defined as acellular area in H&E-stained sections (black arrow). (A) Representative photomicrograph and quantification of (B) absolute area of necrosis and (C) necrosis as a percentage of atheroma. Data was analysed using non-parametric Mann-Whitney U test. Error bars represent mean ± SEM. Scale bar represents 200µm.

4.2.7 Evolocumab does not change lipid content in aortic sinus atheroma (Fig. 4-7)

To examine the lipid content within the atherosclerotic plaques, frozen sections of atheroma in aortic sinus were stained with oil red-o. Average lipid content within the plaques did not differ between mice that received PBS or evolocumab ($p=0.94$ and 0.22 respectively). No difference was detected at any of the three levels (Appendix 4-4 A).

4.2.8 Evolocumab does not change collagen content in in aortic sinus atheroma (Fig. 4-8)

To assess collagen content, frozen sections of aortic sinus were stained with picrosirius red and examined under polarised light. Mice that received PBS and evolocumab had similar amounts of collagen within aortic sinus atheroma, both in absolute terms and when normalised to plaque area ($p=0.62$ and $p>0.99$ respectively). No difference between the two groups was detected at any of the 3 levels (Appendix 4-4 B).

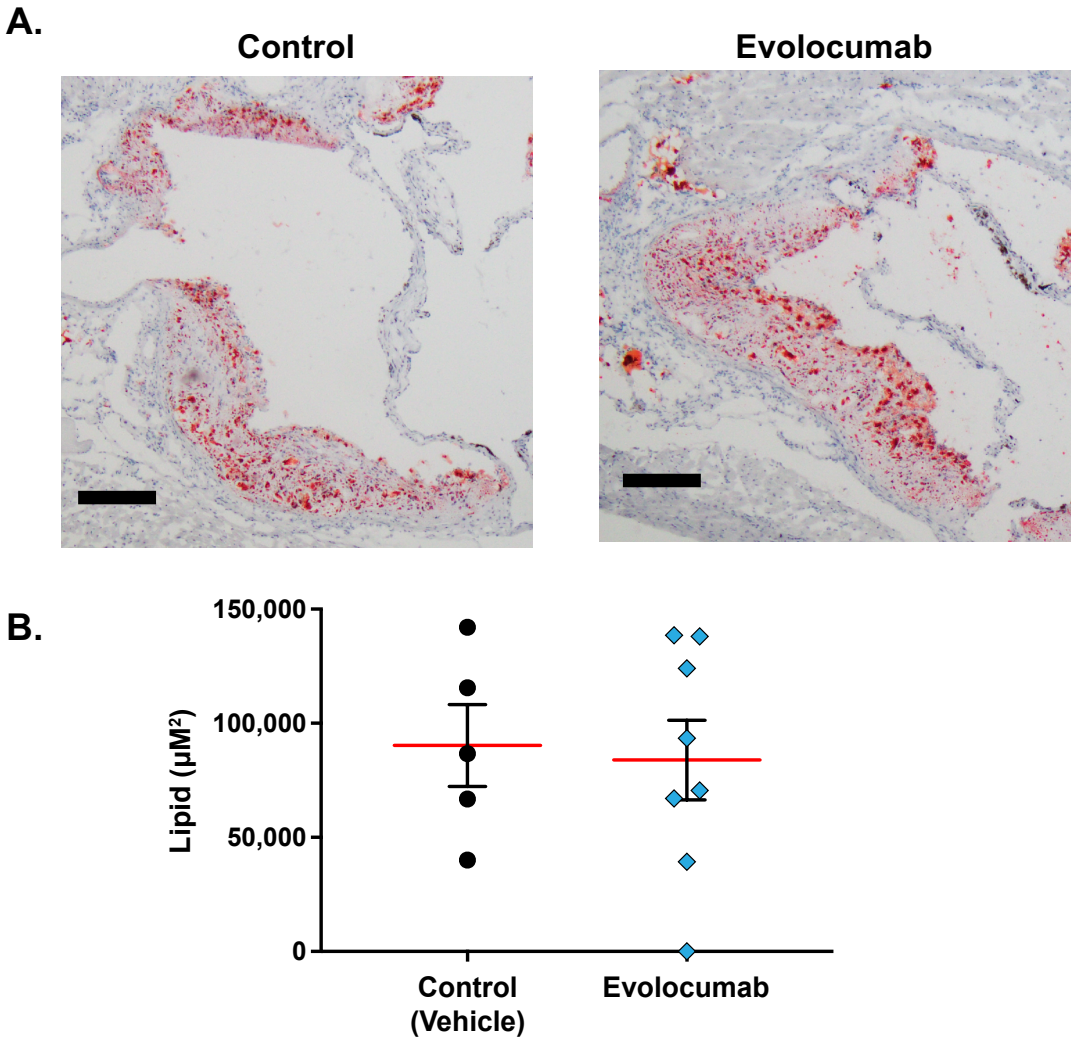

Figure 4-7. Evolocumab does not change the lipid content in aortic sinus atheroma in male apoE$^{-/-}$ mice fed a high fat diet. Frozen sections of aortic sinus were stained with oil red-o, where neutral lipid stained red. (A) Representative photomicrograph and (B) quantification of area of lipid in aortic sinus atheroma were shown. Data was analysed using non-parametric Mann-Whitney U test. Error bar represents mean ± SEM. Scale bar represents 200µm.

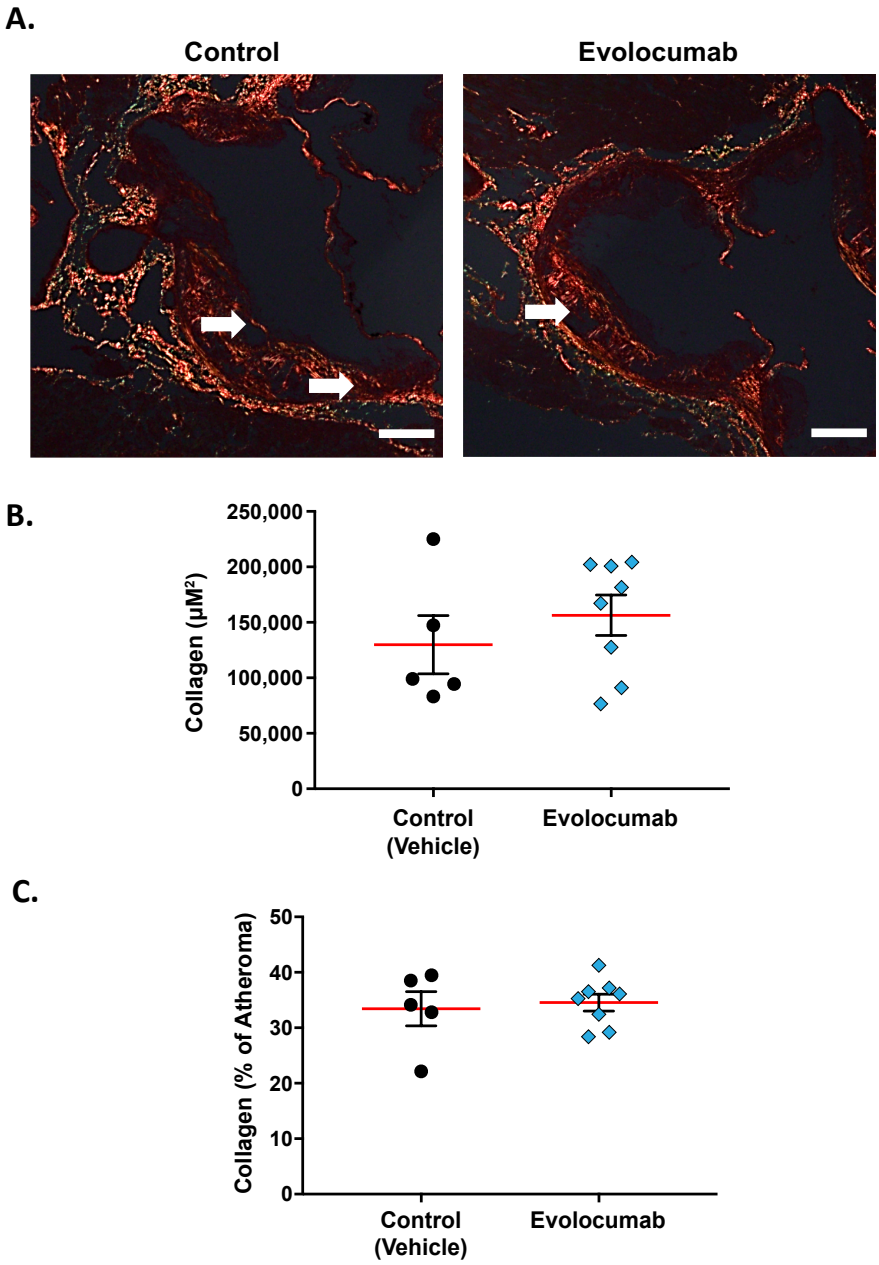

Figure 4-8. Evolocumab does not change collagen content (white arrow) in aortic sinus atheroma in male apoE$^{-/-}$ mice fed a high fat diet. Frozen sections of aortic sinus were stained with picrosirius red and examined under polarised light, where collagen stained orange-red. (A) Representative photomicrograph and quantification of (B) absolute area of collagen in or (C) area of collagen normalised to aortic sinus atheroma were shown. Data was analysed using non-parametric Mann-Whitney U test. Error bar represents mean ± SEM. Scale bar represents 200μm.

4.2.9. Evolocumab does not change spleen or circulating monocyte populations (Fig. 4-9)

In apoE$^{-/-}$ mice, high fat diet leads to Ly6C^{hi} monocytosis which contributes to lesion macrophages[246]. To investigate if evolocumab reverses this change, blood and spleen cells were examined using flow cytometry, where monocytes were defined as CD45^{+}CD11b^{+} cells and subcategorised based on their Ly6C status (Appendix 4-5 for gating strategy). Evolocumab did not change the frequency of monocytes count in blood (p=0.17) or abundance in spleen (p=0.27). Similarly, no significant difference in relative number of the Ly6C^{hi} subpopulation of monocytes in mice that received PBS or evolocumab was seen in blood (p=0.09) or spleen (p=0.27).

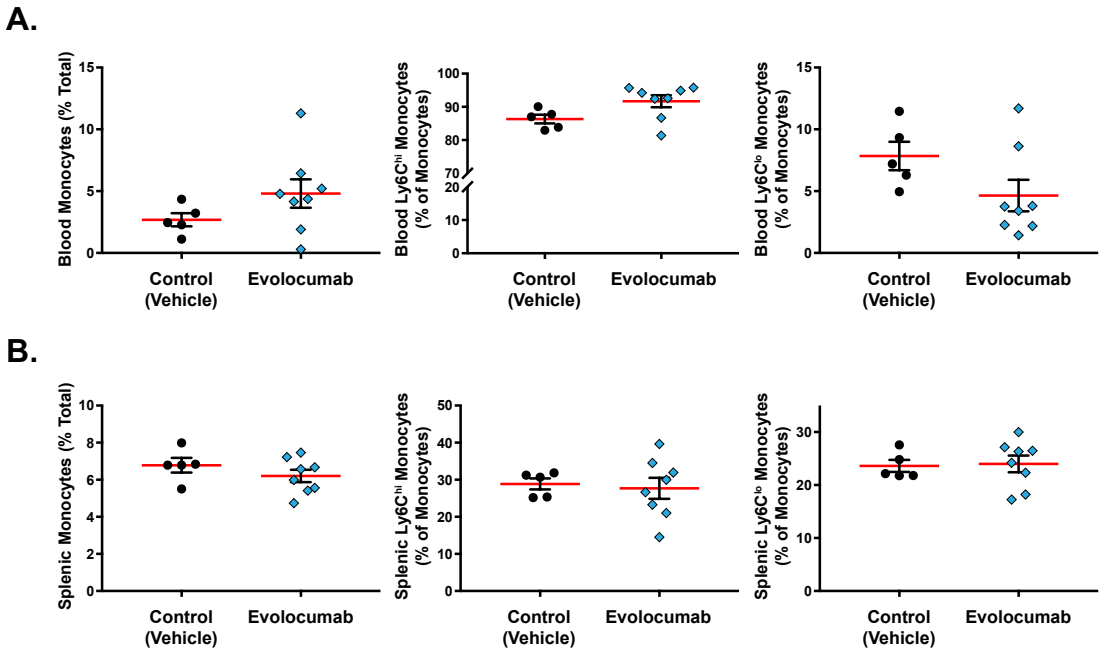

Figure 4-9. Evolocumab does not change circulating or splenic monocytes, or their Ly6C^{hi} subpopulations, in apoE$^{-/-}$ mice fed a high fat diet. Blood and spleen were haemolysed, homogenised and suspended in FACS buffer, then subjected to flow cytometric examination. Monocytes were defined as CD45^{+}CD11b^{+} cells and subdivided according to their Ly6C status. Quantification of (A) blood (B) spleen monocytes. Data was analysed using non-parametric Mann-Whitney U test. Error bars represent mean ± SEM.

4.2.10. Evolocumab does not change lymphocyte frequencies and their subpopulations (Fig. 4-10)

Lymphocytic cells, including both T and B cells, have been implicated in atherosclerosis[247]. Flow cytometry was used to examine the relative frequency of lymphocytes and their subpopulations in the blood, spleen and lymph nodes. Lymphocytes were identified by their forward and sideward scatter characteristics, and then B lymphocytes were defined as $CD19^+$ cells, and T lymphocytes as $TCR\beta^+$ cells. T lymphocytes were subdivided into $TCR\beta^+CD4^+$ cell and $TCR\beta^+CD8^+$ cells (Gating strategy was depicted in Appendix 4-6). No difference was detected in any of the 3 subpopulations between mice treated with PBS and evolocumab in any of the 3 compartments examined.

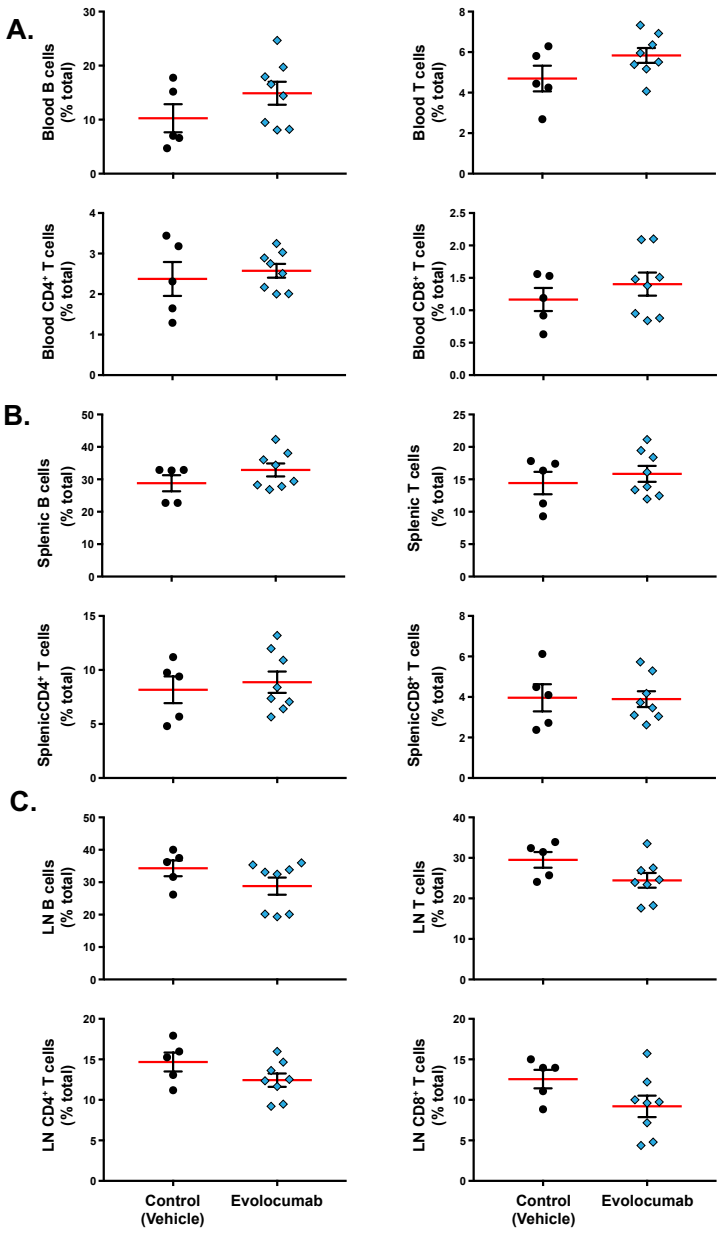

Figure 4-10. Evolocumab does not change circulating, splenic or lymph node lymphocytes or their subpopulations in male apoE$^{-/-}$ mice fed a high fat diet. Blood, spleen and lymph nodes were haemolysed, homogenised and suspended in FACS buffer, then subjected to flow cytometric examination. B lymphocytes were defined as CD19^{+} cells, and T lymphocytes as TCRβ^{+} cells. T cells were subdivided into TCRβ^{+}CD4^{+} and TCRβ^{+}CD8^{+} T cells. Quantification of (A) blood (B) spleen (C) lymph node lymphocytes. Data was analysed using non-parametric Mann-Whitney U test. Error bars represent mean ± SEM.

4.2.11 Evolocumab does not change platelet responsiveness (Fig. 4-11)

Clinical studies have shown that the PCSK9 level is associated with platelet activity and may predict adverse clinical outcomes[248]. Based on this, platelet activation in response to ADP was examined. Platelets were defined as $CD41^+$ cells and activation status was defined by $CD62P^+$ expression (Gating strategy was depicted in Appendix 4-7). There was no difference in the percentage of platelets being activated between control and evolocumab-treated mice (p=0.13).

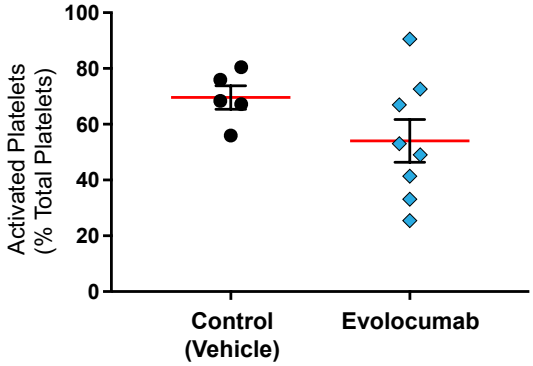

Figure 4-11. Evolocumab does not lower ADP-induced platelet activation in male apoE$^{-/-}$ mice fed a high fat diet. Platelet rich plasma was stimulated with ADP 20μM and examined with flow cytometry. Platelets were defined as $CD41^+$ cells and activation status defined by $CD62P^+$ expression. Data was analysed using non-parametric Mann-Whitney U test. Error bars represent mean ± SEM.

4.2.12 Evolocumab requires apoE to function (Fig. 4-12)

So far, evolocumab showed null effects in all the parameters examined. Potential reasons for this include, (1) inadequate dose, (2) cross-species differences making evolocumab, a human α-PCSK9 mAb, ineffective in mice, or (3) apoE is required for normal functioning of PCSK9 or evolocumab. To answer the first question, a much higher dose of evolocumab was injected i.v. into the male apoE$^{-/-}$ mice. No difference in plasma cholesterol was noted, despite changes in the dose of evolocumab (p=0.35). To address the latter two questions, evolocumab was administered i.v. into male C57Bl6 mice, at a dose of 10mg/kg. Evolocumab significantly lowered total cholesterol in these mice (baseline vs. post-evolocumab; mean ± SEM, 2.7±0.3 vs. 1.7±0.1mmol/L, p=0.02). A significant reduction in plasma triglyceride level was also seen

(p=0.03). This demonstrated that evolocumab was effective in wild-type mice and provided supporting evidence that the null-effect seen in apoE$^{-/-}$ mice was due to apoE deficiency, as other likely causes were excluded.

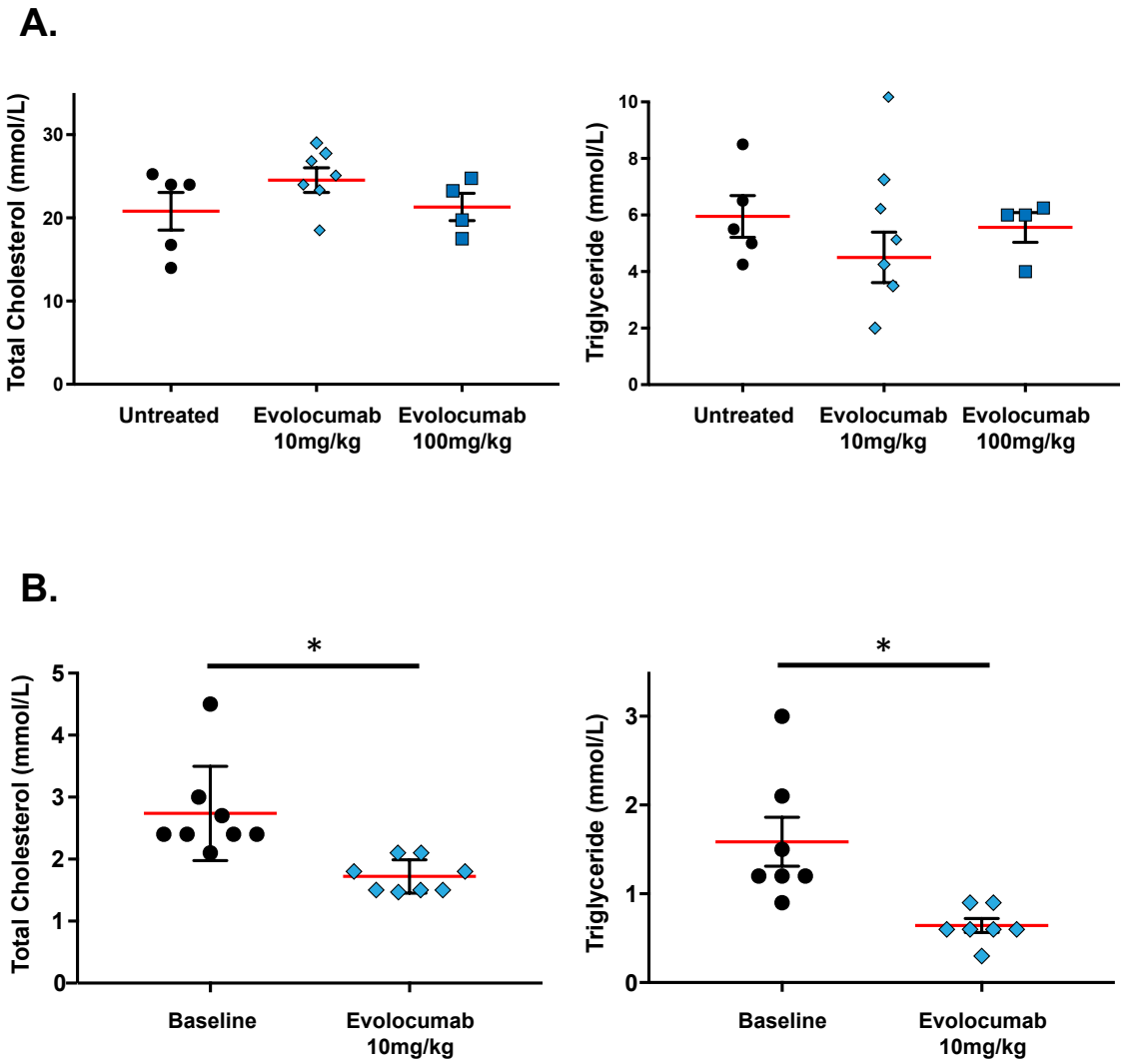

Figure 4-12. Evolocumab or PCSK9 requires apoE to mediate lipid-lowering actions. (A) Evolocumab at variable doses was injected i.v. into male apoE$^{-/-}$ mice and cholesterol levels were examined at 72 hours. Data was analysed using non-parametric Kruskal-Wallis test. (B) Male C57Bl6 mice were injected i.v. with evolocumab and plasma cholesterol and triglyceride were examined before and 72 hours after treatment. Data analysed using paired, non-parametric Wilcoxson's test, *p<0.05. Error bars represent mean ± SEM.

4.3 Discussion

In this study, it was found evolocumab did not change plasma cholesterol or plaque stability in the apoE$^{-/-}$-based, tandem stenosis model of plaque instability/rupture. No difference in atherogenesis, including the size and composition of atherosclerotic plaques in aortic sinus was detected. Evolocumab did not change platelet function or the relative abundance of monocytes or lymphocytes in the blood or spleen.

There are a few potential reasons as to why evolocumab did not affect any of the parameters measured. Firstly, the dose of evolocumab may be too low to effectively lower plasma cholesterol. However, at 10 mg/kg, evolocumab was sufficient to lower plasma cholesterol effectively in C57Bl6 mice and increasing the dose by 10-fold did not change plasma cholesterol levels in apoE$^{-/-}$ mice, making this an unlikely cause. Secondly, evolocumab is a human α-PCSK9 mAb, so it may not be effective in mice. However, it was highly effective in C57Bl6 mice, demonstrating that evolocumab works in both species. A recent clinical trial has revealed problems in using antibodies raised in other species. In the SPIRE trial, incompletely humanised α-PCSK9 mAb was associated with the development of antidrug antibodies and loss of clinical efficacy[249]. However, antidrug antibodies tend to develop over time, after repeated exposure[249]. In this study, evolocumab had no effect in apoE$^{-/-}$ mice that had no previous exposure to evolocumab, making this a very unlikely cause. Based on results from our study (Fig 4-13), the most likely reason is that evolocumab or PCSK9 requires apoE to function. This is consistent with previous reports that neither genetic ablation nor pharmacological inhibition of PCSK9 lower cholesterol in apoE$^{-/-}$ mice[55,89]. At odds with these studies, Tang et al[241] recently showed silencing PCSK9 led to a reduction in atherosclerotic lesions in apoE$^{-/-}$ mice. The reason for the discrepancy is not clear.

ApoE is a 34kDa glycoprotein with 299 amino acid residues. It is synthesised primarily in the liver, but is also found in kidney, brain and spleen. It serves as a ligand for two receptors, one is LDLR, and the other being LRP[35]. ApoE-containing lipoproteins bind to either receptors and mediate hepatic clearance of remnant lipoproteins[250]. In apoE$^{-/-}$ mice, hypercholesterolaemia results from accumulation of VLDL cholesterol in the plasma, as ligand deficiency leads to impaired uptake by LDLR and LRP. One may speculate that evolocumab does not lower cholesterol in apoE$^{-/-}$ mice as it upregulates LDLR, a pathway that was not used in apoE$^{-/-}$ mice. If this is the case, one would expect that evolocumab could still upregulate hepatic LDLR. On

the other hand, if evolocumab fails to lower cholesterol in apoE$^{-/-}$ mice because PCSK9 requires apoE to function, then LDLR expression would remain unchanged with evolocumab. One limitation of this project is that hepatic LDLR expression was not assessed. However, it had been reported that the expression of hepatic LDLR in apoE$^{-/-}$ mice did not change with either pharmacological inhibition or genetic deletion of PCSK9[55]. This suggests apoE is involved in the intrinsic functioning of PCSK9. The mechanism through which apoE affects the actions of PCSK9 is unclear. As plasma PCSK9 levels are similar between apoE$^{-/-}$ mice and C57Bl6 mice[55], it seems unlikely that apoE affects the production or degradation of PCSK9. Instead, as both apoE and PCSK9 are ligands of LDLR, one may speculate apoE may be required for LDLR-PCSK9 binding on cell membrane. Alternatively, apoE could also affect the affinity of LDLR to PCSK9 in the endosome.

While this investigation could not determine the effects of PCSK9 inhibition on plaque stability, it has clinical implications. ApoE is deficient or defective in patients with type III hyperlipoproteinemia, and these patients have an increased risk of premature atherosclerotic vascular disease. This investigation suggests monoclonal antibodies against PCSK9 may not be effective in this population, and careful monitoring of treatment response is required. A second implication is that evolocumab does not have any PCSK9-independent off-target effects, which is consistent with excellent safety profile of evolocumab reported in FOURIER trial[66].

Due to the limitation of the mouse model, it was not possible to evaluate the impact of PCSK9 inhibition in atherogenesis and plaque stability. Thus, a different mouse model of atherosclerotic plaque rupture is required. As PCSK9 exerts most, if not all, of its actions through LDLR[55], atherosclerosis models using LDLR$^{-/-}$ mice would once again negate all effects of PCSK9 inhibition. Recently, Bjorklund et al. and Roche-Molina et al. described the induction of atherosclerosis using a recombinant adenovirus-associated vector carrying a mutant human PCSK9 gene[251,252]. While this model is relatively easy, cheap and offers unique advantages of not needing germ-line genetic engineering, this model is based solely on PCSK9-driven hypercholesterolaemia, thus would not be suitable for the next study. A third genetically-engineered mouse used in atherosclerosis study that may be suitable for next investigation is apoE*3-Leiden.CETP (E3LC) mice. This mouse line expresses two human transgenes that result in a more human-like cholesterol profile and have been shown to be responsive to various lipid-lowering agents[253]. Thus, this mouse was chosen for the next investigation.

CHAPTER 5

Establishing a Model of Atherosclerotic Plaque Rupture in ApoE*3-Leiden.CETP Mice

5.1 Introduction

Atherosclerotic plaque rupture, defined as the disruption of the fibrous capsule overlying the plaque necrotic core[16], is the pivotal event that transitions atherosclerosis from a silent pathology to its dreaded clinical manifestations, most notably, myocardial infarction and sudden cardiac death. Autopsy series of victims of sudden cardiac death and clinical imaging studies of patients presented with myocardial infarction both show that plaque rupture accounts for approximately 50-70% of acute coronary events[15,254], and it is the most common cause of coronary thrombosis irrespective of patient age, gender or geographic location[18]. Careful post-mortem examination has identified characteristic features of ruptured plaques, including thin fibrous caps (<65μm), lumenal thrombosis, intraplaque haemorrhage and a large necrotic core abundantly infiltrated with macrophages but scant in collagen fibre[15]. Though the importance of plaque rupture is well appreciated, and plaque stabilisation is well-accepted as a promising therapeutic strategy, there has been limited advances in this field. One reason is the lack of a good animal model. Ideally, this model recapitulates human pathology, has identical or similar disease processes to the ones that drive human plaque rupture, and it should also have the ability to accurately predict clinical responses to novel pharmaceuticals. From a pragmatic standpoint, this model should be easy to use. This means that the species or strains used should be readily available, induction of plaque rupture requires minimal genetic or surgical manipulation, and plaque rupture can be achieved within a reasonable time frame[255].

Over the last decade, much effort had been invested into development of suitable mouse models to study plaque rupture. However, the uptake of these models has been slow, because they may require prolonged experimental time (> 1 year)[256], complex interventions[60] or have an underlying process that is dissimilar to human pathophysiology[257,258]. Our laboratory has previously described a novel mouse model of plaque rupture, where tandem stenosis was created at the right common carotid artery in apoE$^{-/-}$ mice fed a high fat diet[63]. This model induces an environment of low shear and high tensile stress, and it faithfully reproduces many features of human ruptured plaque, including disruption of fibrous caps, lumenal thrombosis and intraplaque haemorrhage. Importantly, atorvastatin, a lipid-lowering medication known to stabilise atherosclerotic plaques, also changes plaque phenotype in this model.

However, models using apoE$^{-/-}$ mice have limitations. Firstly, the lipid profile of apoE$^{-/-}$ mice is noticeably different to that of patients with atherosclerotic vascular disease. In mice, apoE

deficiency leads to significant elevation in VLDL, IDL and chylomicron remnants[37], whereas clinically, LDL is the main lipoprotein that is elevated in human atherosclerosis. Secondly, in addition to its role in lipoprotein metabolism, apoE has pleiotropic effects affecting inflammation and diverse immune cell functions, including macrophage cholesterol efflux, lymphocyte proliferation and vascular smooth muscle migration[259]. These cholesterol-independent effects have been shown to have significant impacts on atherogenesis[260]. Thirdly, apoE$^{-/-}$ mice do not respond to many lipid-lowering agents. For example, statin and monoclonal antibodies against PCSK9 do not lower plasma cholesterol in apoE$^{-/-}$ mice[55,238]. Thus, validation of the tandem stenosis model in another mouse line may provide complementary information and address some limitations of the current apoE$^{-/-}$-based atherosclerosis mouse model.

ApoE*3-Leiden.CTEP (E3LC) is another mouse model of atherosclerosis with unique advantages over apoE$^{-/-}$-based models. The first human transgene in this mouse, apoE*3-Leiden (E3-Leiden), is a variant of normal human apoE that was first identified in a Dutch family of type III familial hyperlipoproteinaemia. This variant has defective binding to LDL receptor (approximately 25% of normal) thus cause attenuated plasma clearance of apoB-containing lipoproteins[48]. It is important to note that E3-Leiden binding to LDLR remains partially functioning, in contrast to complete deficiency as in the case of apoE$^{-/-}$ mice. This low level of apoE-LDLR binding may be sufficient for PCSK9 to exert its actions, allowing experiments studying effects of PCSK9 inhibition in atherosclerosis to be conducted. The second transgene, human CETP, codes for cholesterol ester transfer protein. This protein transfers cholesteryl ester and triglyceride between VLDL/LDL and HDL. It remodels HDL and is crucial in cholesterol reverse transport[261]. As rodents are deficient in CETP, introduction of CETP to E3-Leiden transgenic mice moves cholesterol from the HDL fraction to VLDL. So E3LC have the advantage of a more human-like cholesterol profile. Secondly, E3LC mice develop hypercholesterolemia and atherosclerosis with high fat diet, and the response can be titrated by changing the composition of the high fat diet, for example, adding cholate, or lengthening the duration of the high fat diet. Lutgens et al. demonstrated that feeding E3-Leiden mice (without the CETP transgene) high fat diet for 4 months induces extensive atherosclerosis that progresses in a cranial to caudal fashion. Importantly, at 4 months, atheroma was already present (AHA type IV), and they can progress to complex type V lesions if fed a high fat diet for 12 months[49]. While such characterisation studies have not been reported for E3LC mice, Westerterp et al. showed that expression of CETP in E3-Leiden mice was associated with a 7-

fold increase in atherosclerotic lesion area and more advanced lesions, suggesting an even more accelerated process of atherosclerosis[50]. Thus, even though their hypercholesterolaemic response to high fat diet may not be as exaggerated as that in apoE$^{-/-}$ mice, E3LC mice do develop extensive and complex lesions, a pre-requisite for plaque rupture. A third advantage of E3LC mice lies in their responsiveness to a myriad of cholesterol-lowering therapeutics including statins[51], fibrates[53], niacin[52], CETP inhibitors[54] and α-PCSK9 mAb[90].

In this study, the aim was to apply the principle of carotid tandem stenosis to E3LC mice to establish a model of atherosclerotic plaque rupture. The study is similar to the tandem stenosis model described previously[63] with two important differences. Firstly, female mice are used in this study, as male E3LC mice developed metabolic syndrome rather than atherosclerosis in response to high fat diet (personal communication, Dr. Jimmy Berbee, Leiden University). Secondly, considering E3LC mice have lower plasma cholesterol levels in response to high fat diet, the duration of study was increased to 19 weeks (by extending high fat feeding after surgery from 7 to 13 weeks, refer to Fig. 2-3).

5.2 Results

5.2.1 Phenotypic characterisation of E3LC mice underwent tandem stenosis surgery (Table 5-1 and Fig. 5-1)

Ten female E3LC mice aged 13-17 weeks were fed a high fat diet for 19 weeks and underwent tandem stenosis surgery at the end of week 6. One mouse was culled at week 18 due to a severe skin lesion. Body weight of E3LC mice increased steadily with high fat diet, starting from mean ± SEM of 21.0±0.4 g at baseline to 30.9±1.2 g at the end of the study (Table 5-1 and Fig. 5-1). To characterise the phenotype of E3LC pertinent to atherosclerotic studies, E3LC mice were compared to historical apoE$^{-/-}$ control mice. Control mice underwent standard treatment for tandem stenosis model, i.e., they received high fat diet for a total of 13 weeks. They underwent carotid tandem stenosis surgery at week 6, and after surgery, they received weekly i.v. injection of PBS for 7 weeks (Fig. 2-3). At the end of the study period, E3LC and apoE$^{-/-}$ mice had similar body weights. The spleen was examined due to its importance in immune regulation of cholesterol and atherosclerosis[244]. There was no significant difference in spleen weight between E3LC and apoE$^{-/-}$ mice.

Table 5-1. Body weight, organ weight and cholesterol profile of E3LC mice.

	Mean	SD	SEM	Median	Interquartile Range
Weight (g)					
Baseline	21.0	1.4	0.4	21.0	20.0-22.0
At Tandem Stenosis Surgery	26.3	4.2	1.3	26.7	22.0-29.3
Study End Point	30.9	3.6	1.2	31.0	28.0-34.5
Organ weight (g; study end point)					
Liver	2.55	0.76	0.25	2.35	2.0-3.0
Spleen	0.14	0.03	0.01	0.13	0.12-0.18
Kidney	0.31	0.04	0.01	0.31	0.28-0.34
Cholesterol Profile (mmol/L; study end point)					
Total Cholesterol	8.0	1.4	0.5	8.1	6.8-9.6
Triglyceride	1.9	0.5	0.2	2.1	1.5-2.4
HDL Cholesterol	1.2	0.3	0.1	1.4	0.8-1.5
Non-HDL Cholesterol	6.8	1.2	0.4	6.6	5.7-8.1
LDL Cholesterol	5.9	1.2	0.4	6.1	4.0-7.1

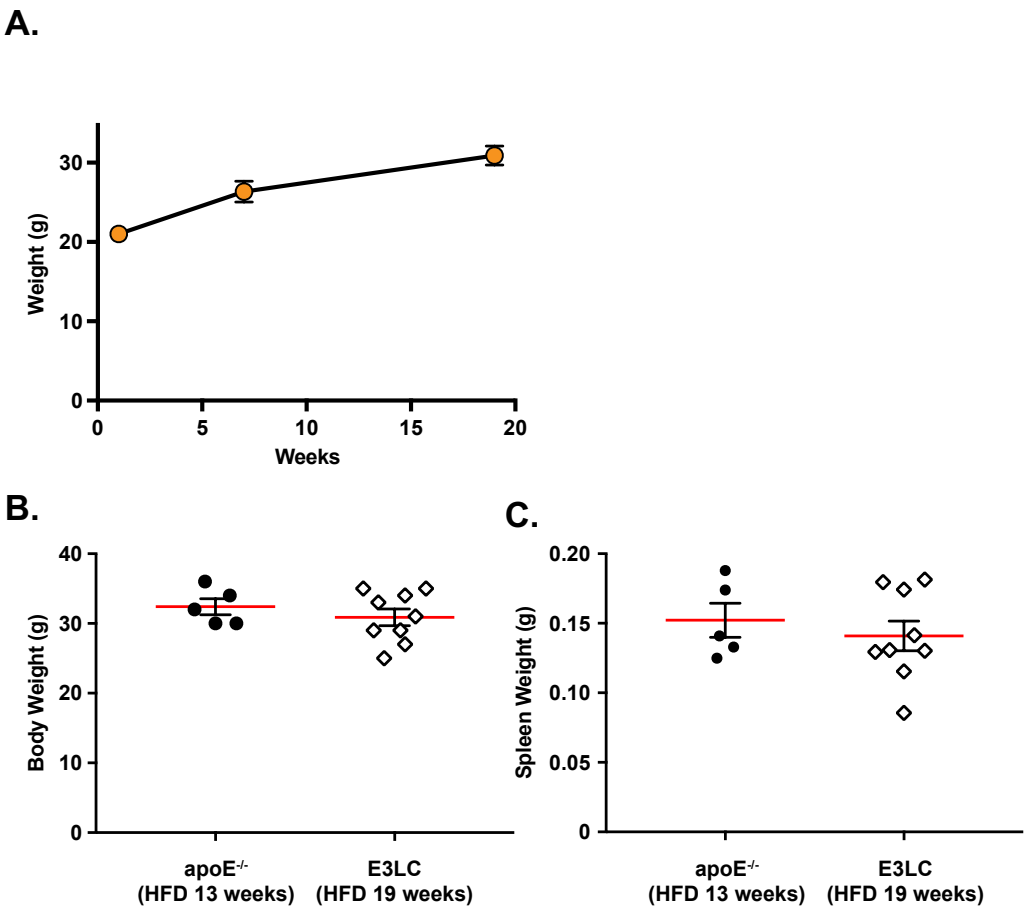

Figure 5-1. Female E3LC mice fed a high fat diet for 19 weeks have similar body and organ weights as male apoE$^{-/-}$ mice fed a high fat diet for 13 weeks. (A) E3LC mice body weight increased steadily over the study period. (B, C) At the end of the study period, female E3LC had similar average body and spleen weights as male apoE$^{-/-}$ mice fed a high fat diet for 13 weeks. Data was analysed using non-parametric Mann-Whitney U test. Error bars represent mean ± SEM.

5.2.2 Diet-induced hypercholesterolaemia is less severe in E3LC than apoE$^{-/-}$ mice (Fig. 5-2)

The average plasma total cholesterol of E3LC mice at the end of the study was 8.0±0.5 mmol/L, with an average plasma triglyceride level of 1.9±0.2 mmol/L. Most cholesterol was distributed in the non-HDL fraction of lipoproteins, in particular, the VLDL/LDL fraction. Despite a longer duration of high fat feeding, E3LC mice had significantly lower plasma total cholesterol than apoE$^{-/-}$ mice (apoE$^{-/-}$ vs. E3LC; mean ± SEM, 28.0±1.7 vs. 8.0±0.5mmol/L, $p<0.001$). However, E3LC mice had slightly higher plasma triglyceride than apoE$^{-/-}$ mice (apoE$^{-/-}$ vs. E3LC; mean ± SEM, 1.2±0.2 vs. 1.9±0.2 mmol/L, $p<0.05$).

5.2.3 E3LC mice have smaller atherosclerotic lesions than apoE$^{-/-}$ mice (Fig. 5-3)

In most mouse models of atherosclerosis, the aortic sinus is the first site to develop atherosclerotic plaques, and it remains the most common site for assessment of atherogenesis in mouse models[262]. The average plaque size at the aortic sinus was much smaller in E3LC than that of apoE$^{-/-}$ mice (apoE$^{-/-}$ vs. E3LC; mean ± SEM, 394,570±53,043 vs. 67,163 ±10,732 μm^2 vs., $p<0.001$), even though the duration of high fat feeding was much longer. The significant difference in lesion size between E3LC and apoE$^{-/-}$ mice was seen at all 3 levels examined (Appendix 5-1).

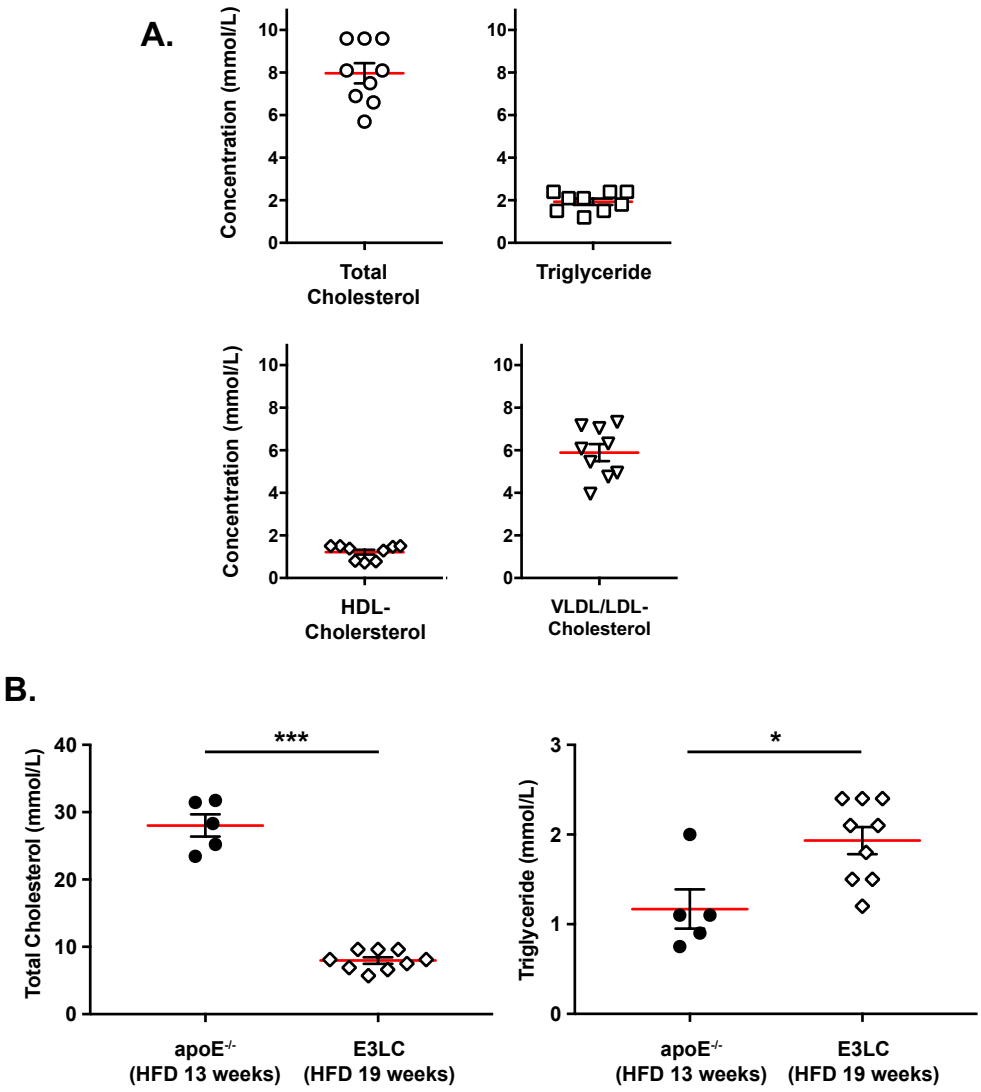

Figure 5-2. Plasma total cholesterol is significantly lower in female E3LC mice fed a high fat diet for 19 weeks than male apoE$^{-/-}$ mice fed a high fat diet for 13 weeks. Concentrations of plasma total cholesterol, triglyceride and different fractions (HDL- and VLDL/LDL-cholesterol) were measured using an enzymatic colorimetric method. (A) Cholesterol profile of E3LC mice at the end of the study. Cholesterol was mainly transported in VLDL/LDL lipoproteins. (B) E3LC mice had a much lower plasma cholesterol though slightly higher plasma triglyceride than apoE$^{-/-}$ mice. Data was analysed using non-parametric Mann-Whitney U test. *$p<0.05$, ***$p<0.001$. Error bars represent mean ± SEM.

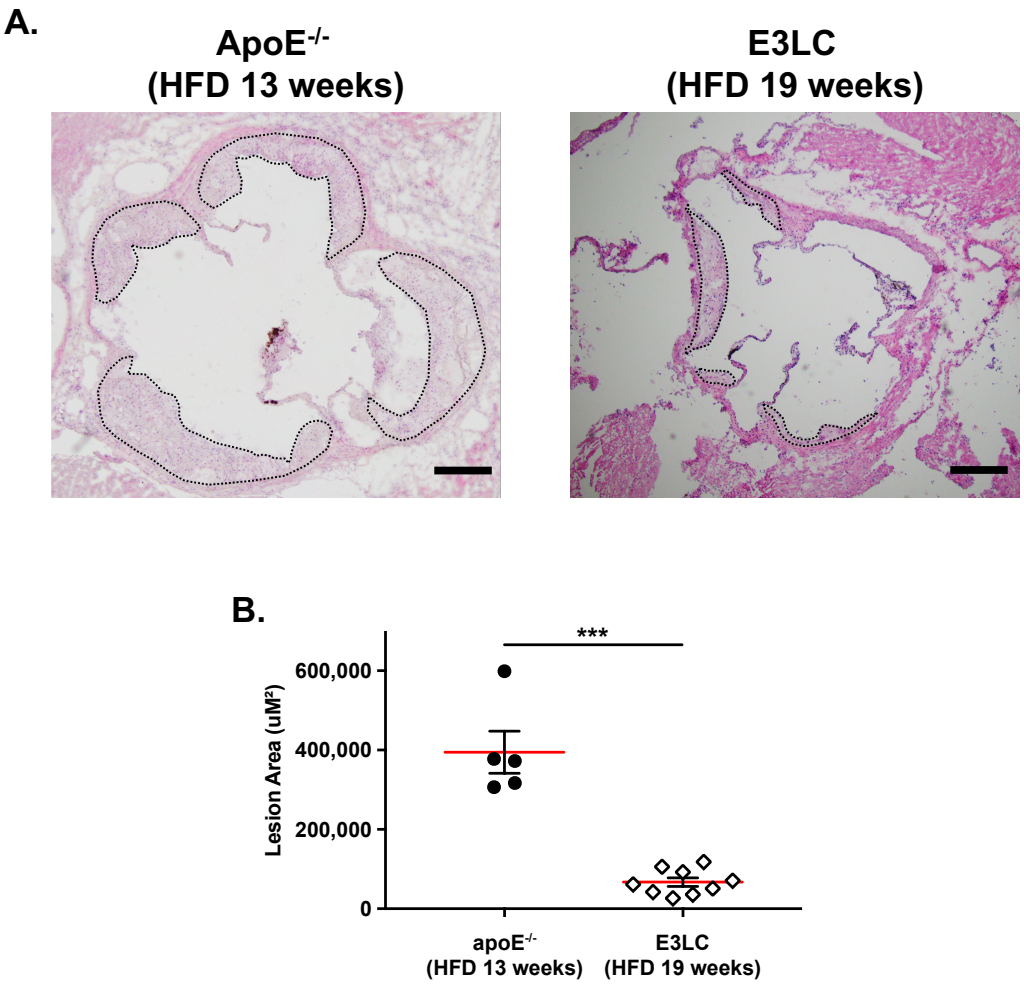

Figure 5-3. Female E3LC mice fed a high fat diet (HFD) for 19 weeks have significantly smaller atherosclerotic lesions in aortic sinus than that of male apoE$^{-/-}$ mice fed a high fat diet for 13 weeks. Three frozen sections of aortic sinus were stained with H&E and the size of the lesion was measured. (A) Representative photomicrograph, where the dotted black line indicates atherosclerotic lesion. (B) Quantification of lesion area. Data was analysed using non-parametric Mann-Whitney U test, ***$p<0.001$. Error bars represent mean ± SEM. Scale bar represents 1mm.

5.2.4 Carotid segment I in E3LC mice has the morphology of early-stage lesions (Fig. 5.4)

As carotid segment I is the region with the most unstable phenotype in the apoE$^{-/-}$ tandem stenosis model, this segment was examined first. Of the 9 mice that survived until the experiment end date, only 8 mouse aortic sinus were available for analysis. One was lost during retrieval of the carotid artery. Previous investigation (Chapter 4) showed that plaque composition in carotid segment I was quite homogenous with little spatial variation, so for each histochemical assessment, only 1 section was examined.

Frozen sections of E3LC carotid segment I was stained with H&E. First, the severity of the lesion was examined. Severity of the lesion was based on the degree of lumenal obstruction. If plaques caused >50% stenosis, a criterium commonly used clinically[263], then they were classified as severe. Of the 8 samples available for analysis, it was found 4 mice (50%) had severe lesions, and 4 (50%) had non-severe lesions. Secondly, the morphology of every carotid segment I was examined. It was found that 3 of the 8 (38%) carotid segment I had hypocellular and amorphous intima that raised suspicion for fatty streak or intermediate lesions. The intima of the other 5 (62%), on the other hand, appeared hypercellular that could be neointimal hyperplasia. These general impressions need to be confirmed with immunohistochemistry. Next, carotid segment I was examined for hallmark features of atherosclerotic plaque rupture. No lumenal thrombi or fibrous cap fissuring/ruptures were observed. These plaques had no features of advanced plaques such as large, convalescent necrotic cores, cholesterol clefts, thin fibrous capsules or obvious intraplaque haemorrhage. Collectively, the atherosclerotic plaques at segment I had a morphology of early-stage atherosclerotic lesions.

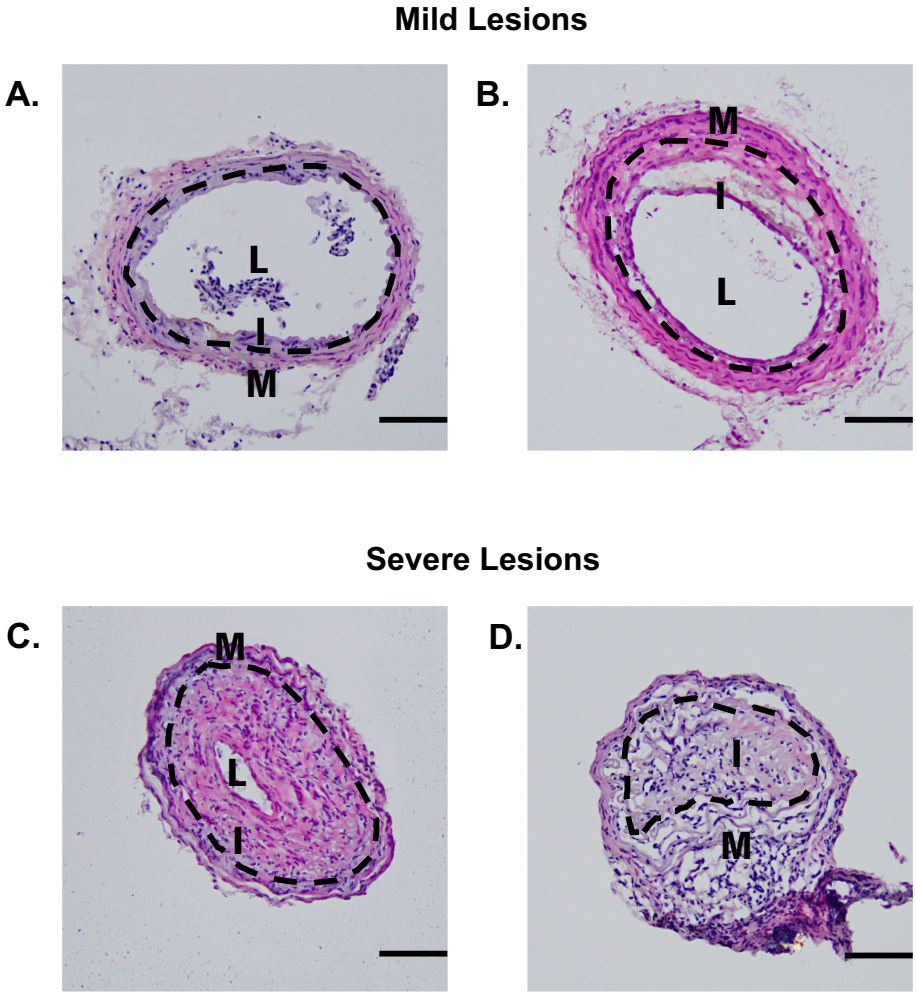

Figure 5-4. Carotid segment I in female E3LC mice fed a high fat diet has a morphology of early-stage atherosclerotic lesions. Carotid segment I was stained with H&E, and representative images are shown here. There were significant variations in severity (degree of lumenal stenosis). (A, B) Four out of 8 (50%) had mild lesions and (C, D) the other 4 out of 8 (50%) had severe lesions. Lesion morphology also varies. (B) Three out of 8 (38%) had amorphous, hypocellular intima whereas (A, C, D) the other 5 out of 8 (62%) had a hypercellular morphology. Characteristic features of unstable plaques were not seen in any of the carotid segment I examined. These sections were taken from the same level of carotid segment I. Scale bar represents 50 µm. Key: L - lumen, I – intima, M – media.

5.2.5 Carotid segment I in E3LC were fatty streaks/intermediate lesions or neointimal hyperplasia (Fig. 5.5)

To confirm the suspicion that these lesions were either fatty streaks/intermediate lesions or neointimal hyperplasia, carotid segments from the 8 mice were stained with oil red-o (to identify neutral lipid) and immunohistochemistry with antibodies against α-SMA (to identify vascular smooth muscle cells). Lesions suspected to be fatty streaks/intermediate lesions were rich in lipid and scant in vascular smooth muscle cells, consistent with fatty streaks/intermediates lesions. On the other hand, hypercellular lesion were rich in vascular smooth muscle cells but relatively devoid of lipid, consistent with neointimal hyperplasia.

5.2.6 Carotid segment I in E3LC has minimal necrosis (Fig. 5-6)

Plaque composition is an important determinant of plaque vulnerability[15]. In mice, atherosclerotic lesions at the aortic sinus are considered to have a stable phenotype. Even with advanced disease, plaques in aortic sinus do not rupture, thrombose or fissure[264]. Intraplaque haemorrhage is extremely rare too. To assess the stability of carotid segment I, plaque composition including necrosis, lipid and collagen were compared with lesions in aortic sinus. Area of necrosis, defined as acellular area on H&E staining (absence of cell nuclei), was readily identifiable in aortic sinus lesions. In carotid segment I, there was virtually no area of necrosis. Clearly, there was significantly more necrosis in the aortic sinus than carotid segment I (mean ± SEM, aortic sinus vs. carotid segment I, 32.8±2.2% vs. 0.6±0.2%, $p<0.01$).

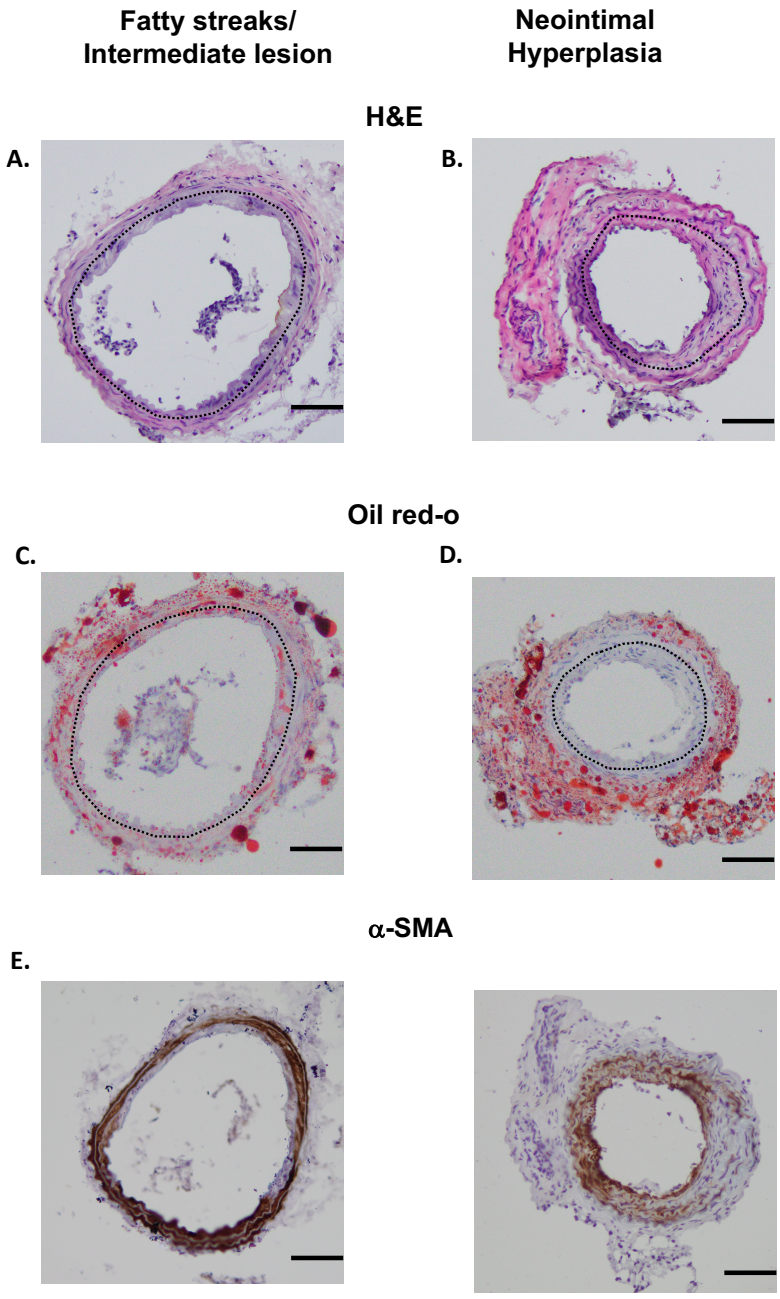

Figure 5-5. Carotid segment I in female E3LC fed a high fat diet are fatty streaks/intermediate lesions or neointimal hyperplasia. Representative images from two mice. Three frozen sections of carotid segment I were taken (24μm apart) from the same mouse and stained with H&E, oil red-o and α-SMA antibody. (A, C, E) The intimal lesion (dotted line) was high in lipid and low in smooth muscle cells, confirming it was a fatty streak/intermediate lesion. (B, D, F) In this mouse, the intimal lesion (dotted line) had abundant smooth muscle cells but little lipid, consistent with intimal hyperplasia. Scale bar represents 50 μum.

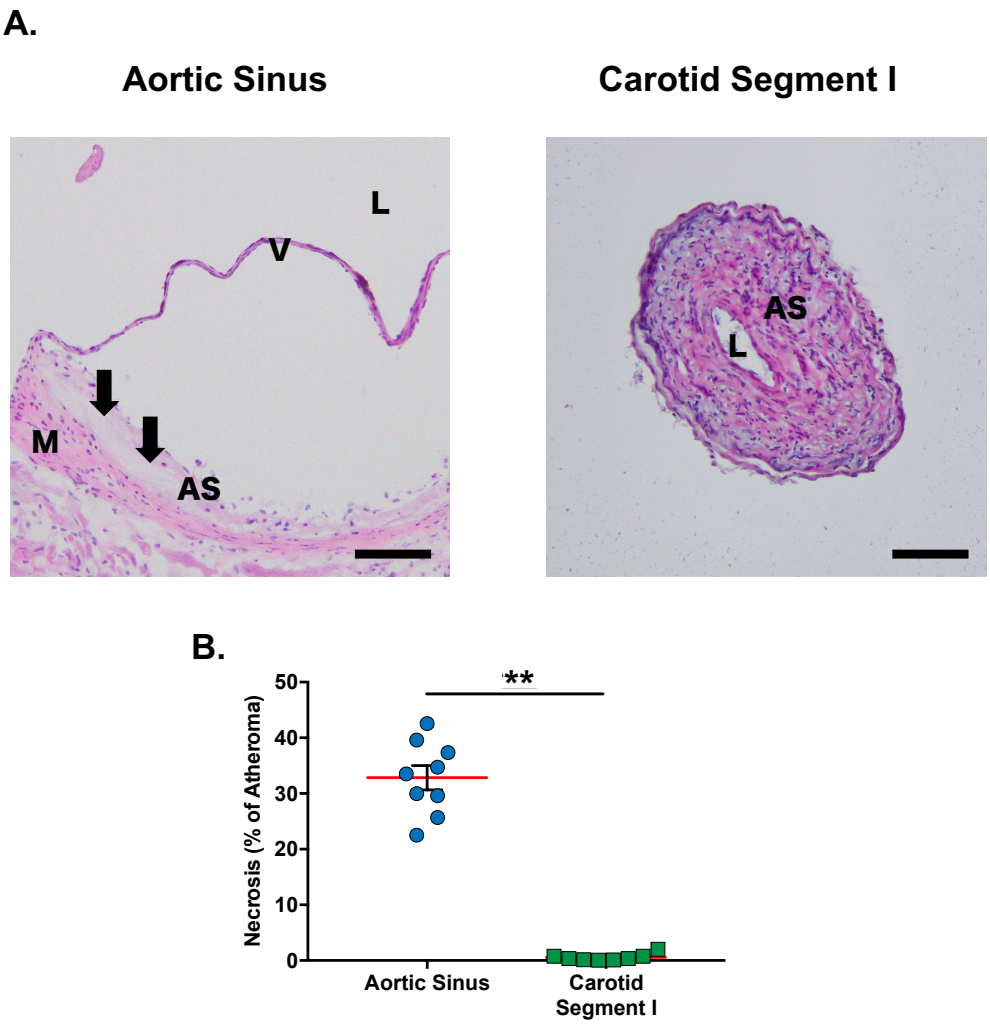

Figure 5-6. Carotid segment I in female E3LC mice fed a high fat diet has minimal necrosis. Frozen sections of carotid segment I and aortic sinus were stained with H&E. (A) Representative photomicrographs. Necrotic area, defined as acellular area (black arrow), was readily identifiable in atherosclerotic lesion in aortic sinus, but virtually absent in carotid segment I. (B) Quantification of necrosis. Data was analysed using non-parametric Wilcoxon matched-pair rank test, ***$p<0.001$. Error bars represent mean ± SEM. Scale bar represents 50µm. Key: L - lumen, AS – atherosclerotic lesion, V – valve, M – media.

5.2.7 Carotid segment I and aortic sinus lesion in E3LC have similar lipid content (Fig. 5-7)

Oil red-o stain was used to identify lipid content within the plaque. In E3LC mice, the normalised lipid content of the aortic sinus lesion and that of carotid segment I were similar (p=0.38).

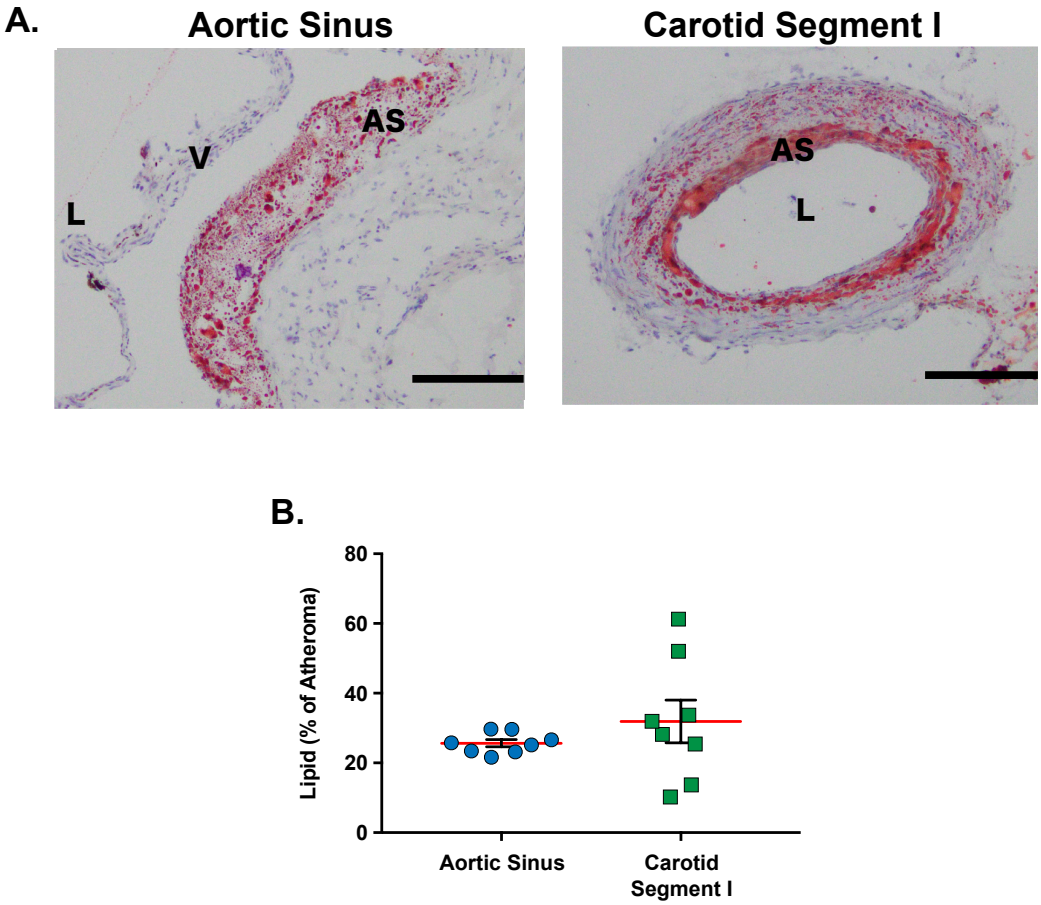

Figure 5-7. In female E3LC mice fed a high fat diet, carotid segment I and atherosclerotic lesion in aortic sinus have similar lipid content. Frozen sections of carotid segment I and aortic sinus were stained with oil red-o, where neutral lipid stained red. (A) Representative photomicrograph and (B) quantification of normalised lipid content are shown here. Data was analysed using non-parametric Wilcoxon matched-pair rank test. Error bars represent mean ± SEM. Scale bar represents 100μm. Keys: L - lumen, AS – atherosclerotic lesion, V – valve.

5.2.8 Collagen content in carotid segment I and aortic sinus lesions were similar (Fig. 5-8)

Picrosirius red was used to identify collagen within the plaque. No significant difference was found between normalised collagen content in aortic sinus lesions and carotid segment I in female E3LC mice ($p<0.95$).

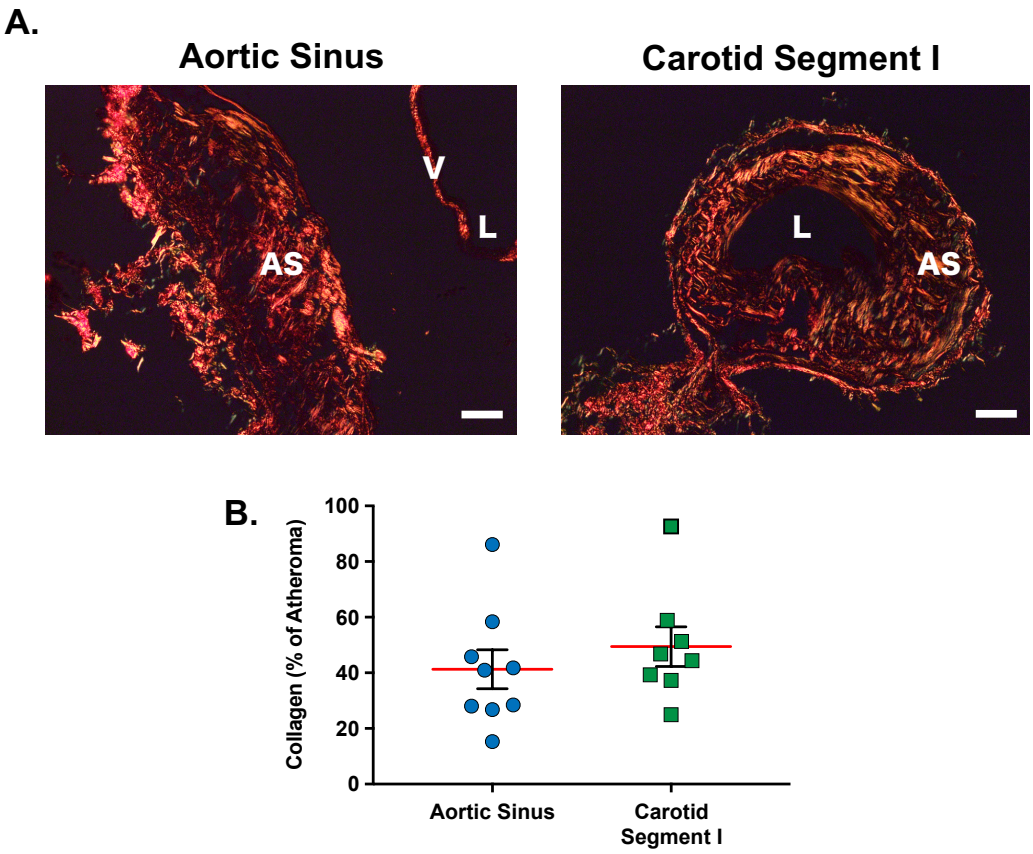

Figure 5-8. In female E3LC mice fed a high fat diet, carotid segment I and atherosclerotic lesions in aortic sinus have similar collagen content. Frozen sections of carotid segment I and aortic sinus were stained with picrosirius red and examined under polarised light, where collagen stained orange-red. (A) Representative photomicrograph and (B) quantification of normalised collagen content are shown here. Data was analysed using non-parametric Wilcoxon matched-pair rank test. Error bars represent mean ± SEM. Scale bar represents 200µm. Keys: L - lumen, AS – atherosclerotic lesion, V – valve.

5.3 Discussion

In this study, the findings are, (1) in female E3LC mice fed a high fat diet, carotid segment I did not display an unstable phenotype. (2) Compared to apoE$^{-/-}$ mice that displayed ruptured plaques (tandem stenosis model), E3LC mice had much a lower plasma cholesterol. (3) E3LC mice also had much smaller plaques at the aortic sinus. (4) In E3LC mice, the plaques at aortic sinus had the morphology of fatty streak/intermediate type lesion or neointimal proliferation.

The clinical implication of atherosclerotic plaque rupture is well appreciated[265]. Accordingly, much effort has been directed towards the development of suitable animal models of plaque rupture to advance our understanding and facilitate therapeutic testing. Despite a myriad of genetic, pharmacological and surgical manipulations used to trigger plaque rupture (reviewed by Veseli et al.[62]), one prerequisite is the presence of advanced atherosclerotic plaques, usually achieved with severe and prolonged hypercholesterolaemia. This is also the most obvious difference between apoE$^{-/-}$ mice and E3LC mice. While fed the same diet, plasma cholesterol levels in apoE$^{-/-}$ mice was >3 times that of E3LC mice, and plaque size at the aortic sinus was almost 8 times bigger. In addition, in apoE$^{-/-}$ mice, features of advanced plaque including necrotic core and cholesterol clefts were often present in the atheroma in aortic sinus, manifesting an accelerated process of atherogenesis.

E3LC mice had a much lower plasma cholesterol than apoE$^{-/-}$ mice, as apoE*3-Leiden has defective but partially functional binding to LDLR, whereas apoE$^{-/-}$ mice have complete deficiency of apoE. Further, E3LC mice have one functional apoE allele, as homozygous apoE*3-Leiden mice are not viable (personal communication, Dr. Jimmy Berbee, Leiden University Medical Centre). As E3LC are responsive to dietary changes, this is one way to induce severe hypercholesterolaemia. In this study, a diet regimen of 22% fat and 0.15% cholesterol was used. This is commonly used in apoE$^{-/-}$ and Ldlr$^{-/-}$ mice to induce hypercholesterolaemia and atherosclerosis, but it appears to be too mild to achieve severe hypercholesterolaemia in E3LC mice. One strategy to elevate cholesterol level is to supplement mouse diet with cholate, an important component of the so-called "Paigen diet"[266,267]. Cholate is a constituent of bile acid and enhances absorption of fat and cholesterol in enterohepatic circulation. Cholate has also been shown to inhibit 7α-hydroxylase, the rate-limiting enzyme in bile acid biosynthesis where cholesterol is converted to 7-hydroxycholesterol[268]. Using a diet consisting of 15% fat, 1% cholesterol and 0.1% cholate, van Vlijmen et al. showed that

E3-Leiden transgenic mice could develop severe hypercholesterolemia, with average plasma total cholesterol as high as 43.7±13.2 mmol/L[48]. When cholate dose was increased to 0.5%, plasma total cholesterol was further accentuated to an average of 59.1±9.8 mmol/L. Though effective, cholate was not used in this project for a number of reasons. Firstly, cholate increases the incidence of skin xanthoma in mice[40]. Secondly, cholate has multiple actions. It is a ligand for the nuclear hormone receptor, farnesoid X receptor (FXR), an essential regulator in lipoprotein, glucose and bile acid metabolism[269]. It also lowers plasma triglyceride and induces hepatic genes related to fibrosis[270]. Given these complex metabolic effects, the decision was made at the planning stage of the experiment that a cholate-free diet should be used. Another strategy to increase plasma cholesterol is to increase cholesterol content in high fat diet. Westerterp et al. has shown that, when fed a diet containing 15% fat and 0.25% cholesterol for 19 weeks, the plasma total cholesterol in E3LC mice can be elevated to 23±6 mmol/L[50]. This strategy could be used in future experiments.

Another strategy to increase plasma cholesterol and accelerate atherosclerotic plaque development is to increase the duration of the high fat diet. In previous investigations where tandem stenosis was being established in apoE$^{-/-}$ mice, apoE$^{-/-}$ mice were culled at several time points after surgery. At 2 weeks, carotid segment I had a stable phenotype, but they had abundant CD68^{+} macrophages. At 4 weeks, features of advanced plaques including large necrotic cores and cholesterol clefts were evident. But characteristic features of plaque rupture did not appear until after 7 weeks[63]. Similarly, both plasma cholesterol and atherosclerotic plaque severity were increased with prolonged feeding of high fat diet in apoE*3-Leiden mice[49]. However, E3LC mice have a biphasic response to high fat diet, where total and non-HDL cholesterol peak at 16-20 weeks of high fat diet, and both decline after 20 weeks[271]. In this study, E3LC mice were fed a high fat diet for 19 weeks. Therefore, further lengthening in the duration of high fat diet may only provide marginal benefits in raising plasma cholesterol, and from a logistic point of view, the study period becomes be too long.

Small lesion size may have contributed to the failure to induce plaque rupture in E3LC mice too. Atherosclerotic lesions are known to change local rheology by causing stenosis and flow limitation. In our model, low shear stress was created by two non-occlusive stenoses. However, low shear stress alone, without pre-existing atherosclerotic plaques, were insufficient to cause plaque rupture[272]. In wild-type mice with no pre-existing atherosclerosis, low shear stress induced by either ligation or placement of perivascular nonconstructive cuff cause neointima

formation[273,274], similar to the morphology of carotid segment I in E3LC mice. This raises the question whether there were atherosclerotic plaques present in carotid artery at the time of tandem stenosis surgery. Thus, in contrast to apoE$^{-/-}$ mice, longer duration (>6 weeks) of high fat feeding may be required before application of the tandem stenosis procedure. Perhaps more importantly is how advanced the plaques are. Our study indicated lesions in carotid segment I were predominantly early-stage lesions, thus unlikely to lead to plaque rupture. So, lesions present at the time of tandem stenosis procedure were likely too early in the process to have plaque ruptures, even with surgical manipulation. In addition to plasma cholesterol, it may also relate to the immune and inflammatory response of E3LC. In carotid segment I, E3LC had much less necrosis. One may speculate this could be due to a more proliferative response to injury, or it could also be due to lesser apoptosis.

In addition to local haemodynamic factors, systemic influence of hypertension also promotes plaque rupture[272]. In a mouse model of plaque rupture, use of a vasoconstrictor, phenylephrine, significantly augmented the action of smooth muscle cell overexpression of p53 and induced plaque rupture in 40% of the mice[60]. This illustrates a potential approach to accentuate the occurrence of plaque rupture.

One limitation of our study is that immunohistochemical methods were not used to definitively exclude the presence of intraplaque haemorrhage and intramural or lumenal thrombosis. However, examination of H&E-stained samples did not reveal lesions suggestive any of these features. Further, the overall morphology at carotid segment I were early-stage, and it would be unusual to see features of advanced or ruptured plaques in early lesions.

In summary, despite applying the same principle through identical surgical intervention, having the same dietary regimen, and fed an even longer duration of high fat diet, carotid segment I of E3LC did not show evidence of plaque instability. Instead, a morphology of early lesions including fatty streaks, intermediate type lesion or neointimal hyperplasia was detected. This is likely to be due to E3LC mice having a much lower plasma cholesterol and consequently, much smaller and less advanced plaques. A diet supplemented with higher cholesterol, a deferred time point for tandem stenosis surgery and the use of a vasoconstrictor may be required for successful induction of plaque rupture in E3LC mice.

CHAPTER 6

Effects of PCSK9 Inhibition in Atherogenesis and Plaque Stability in a Mouse Model of Atherosclerosis

6.1 Introduction

Atherosclerosis is a disease of the medium and large arteries characterised by a progressive build-up of intimal plaques consisting of cholesterol esters, foam cells and extracellular matrix. It is the underlying pathology of myocardial infarction, stroke and sudden cardiac death. Despite its complex pathogenesis, basic and clinical investigations have elucidated aspects of disease processes, identified therapeutic opportunities and improved patient outcomes. In particular, the role of hypercholesterolaemia in atherosclerosis is well-established[30]. Observational studies have shown a robust correlation between hypercholesterolaemia and ischemic heart disease[275], and numerous large-scale randomised trials have demonstrated the benefits of lowering cholesterol, with a remarkably consistent dose-response[276]. This led many investigators to conclude that hypercholesterolaemia is the cause of atherosclerosis[30].

Mechanistic studies have shown that hypercholesterolaemia contributes to all stages of atherosclerosis. Passive diffusion of cholesterol into and the subsequent retention of apoB-containing lipoproteins in subendothelial intima are the sentinel event that initiate atherosclerosis[277]. Bound to subendothelial proteoglycan, these lipoproteins are modified through oxidation or acetylation, which creates a proinflammatory environment and modulates the phenotypes of different vascular cells[278]. Hypercholesterolaemia induced by western diet causes Ly6C^{hi} monocytosis, a monocyte subpopulation with a proinflammatory phenotype that gives rise to lesional macrophages and is associated with plaque development[246]. Lesional macrophages take up oxidised or acetylated LDL via scavenger receptors (SR) including SRA and CD36, and secretes cytokines (IL-1, IL-6 and TNF) and chemokines (CCL2 and CCL5) that promote further recruitment of inflammatory cells[13]. In addition, hypercholesterolaemia and oxidised LDL lead to decreased nitric oxide bioavailability, endothelial activation and increased vascular permeability, which augments subendothelial uptake and retention of LDL[12]. Later in the disease process, accumulation of lipid in atheroma changes plaque biomechanics; it stimulates the secretion of proteolytic enzymes by macrophages and decreases collagen production as it induces apoptosis of vascular smooth muscle cells[279,280]. These changes compromise the integrity of atherosclerotic plaques and increase their propensity to rupture. Further, hypercholesterolaemia enhances platelet biogenesis and activity, thus accentuating prothrombotic propensity and amplifies thrombotic complications[281].

Proprotein convertase subtilisin/kexin type 9, PCSK9, is a protein of 692 amino acid residues expressed in the liver, kidney and intestines. In cells, it is first synthesised at the endoplasmic reticulum, then undergoes a series of modifications including cleavage of the prodomain via its catalytic domain at residues 152-153 ($FAQ_{152}\downarrow SIP$), before being secreted into the circulation[68]. In plasma, PCSK9 can exist as a free molecule or bind to LDL. It can be further cleaved by furin in the circulation, which attenuates its activity[72]. On the cell surface of hepatocytes, PCSK9 binds to LDLR at the epidermal growth factor like-(EGF) A domain, and this LDL-PCSK9 complex is internalised together[78,282]. PCSK9 keeps LDLR in an open conformation, and chaperones LDLR to the lysosome for degradation. Therefore, PCSK9 decreases the availability of LDLR and elevates plasma cholesterol levels. Genetic studies have confirmed that gain-of-function mutations of PCSK9 lead to hypercholesterolaemia, and loss-of-function mutations cause hypocholesterolaemia and confer protection against atherosclerotic vascular disease[93]. Following this, two monoclonal antibodies against PCSK9 have been developed and their efficacy in improving clinical outcomes was demonstrated recently in two large-scale clinical trials[66,67].

While the clinical benefits of PCSK9 inhibition are now established, the mechanisms through which it confers protection are not fully appreciated. Clinical studies have shown that, similar to statin, PCSK9 inhibition also induces modest plaque regression[240]. It remains unknown, however, if PCSK9 changes plaque composition and stability. It is also unclear if PCSK9 inhibition reverses many adverse systemic effects of hypercholesterolaemia, such as $Ly6C^{hi}$ monocytosis and platelet hyperreactivity. In particular, in previous preclinical studies of PCSK9, PCSK9 was either genetically ablated at birth or pharmacologically inhibited at the onset or soon after commencing high fat diet[55,89,90]. These studies do not simulate the clinical scenario where treatment is usually applied after hypercholesterolaemia or even atherosclerosis is established.

The aim of this study was to investigate the impact of PCSK9 inhibition in atherosclerosis in hypercholesterolaemic E3LC mice. Specifically, the effects of PCSK9 inhibition on plaque size, plaque composition, and immune cells were examined. In this study (Fig. 2-4), E3LC were fed a high fat diet for a total of 19 weeks. Mice also underwent carotid tandem stenosis surgery at the end of week 6, followed by weekly s.c. injections of α-PCSK9 mAb treatment for the remaining 13 weeks (refer to Fig. 2-4). As the tandem-stenosis surgery did not reproduce unstable plaque phenotypes in E3LC mice, carotid artery was not examined.

6.2 Results

6.2.1 PCSK9 does not change mouse body or organ weight (Fig. 6-1)

Female E3LC aged 13-17 weeks were fed a high fat diet for a total of 19 weeks and weighed at different study time points. Ten mice were assigned to the control group and 11 to the α-PCSK9 mAb group. During the study period, one mouse in the α-PCK9 mAb treatment group was culled due to severe skin lesion. The aortic sinus of one mouse in the α-PCK9 group was lost during processing, thus only 9 from the α-PCSK9 group were available for analysis.

Compared to E3LC that received control antibody, mice treated with the α-PCSK9 mAb had similar weights at baseline ($p=0.57$), prior to commencing the high fat diet ($p=0.88$) and at the study end point (control vs. α-PCSK9 mAb; mean ± SEM, 28.7±0.6 vs. 30.2±1.4g, $p=0.19$). The two groups did not differ significantly in organ weights at the end of the study period, for liver ($p=0.850$), kidney ($p=0.95$) or spleen ($p=0.81$).

6.2.2 PCSK9 inhibition lowers plasma cholesterol concentration but not glucose concentration (Fig. 6-2)

At the study end point, total plasma cholesterol was modestly (22%) but significantly lower in mice treated with α-PCSK9 mAb (control vs. α-PCSK9 mAb; mean ± SEM, 5.8±0.4 vs. 4.5±0.5mmol/L, $p<0.05$), whereas plasma triglyceride levels did not differ between the two groups ($p=0.21$). PCSK9 inhibition did not alter plasma HDL-cholesterol significantly ($p=0.21$), however, it significantly lowered the LDL/VLDL- cholesterol levels in these mice (-29%, $p<0.05$,). PCSK9 inhibition did not change plasma glucose levels significantly ($p=0.15$).

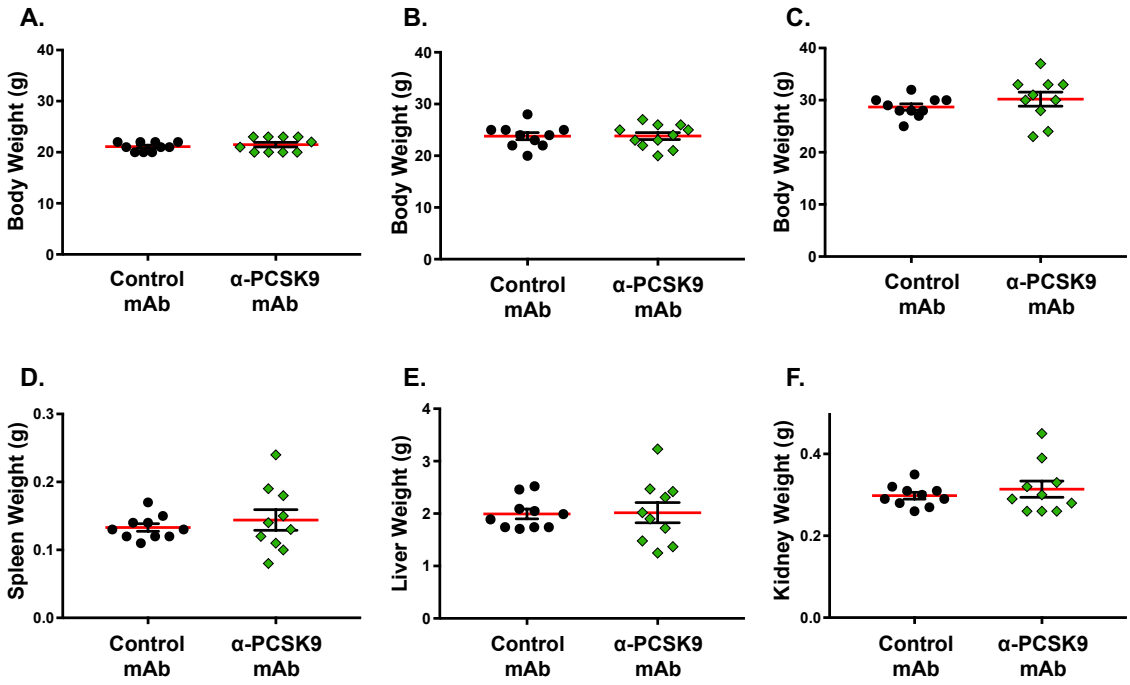

Figure 6-1. PCSK9 inhibition does not change average body or organ weight of female E3LC mice fed a high fat diet. Mice were weighed at different time points including (A) baseline (B) before receiving α-PSCK9 mAb or control (C) at study end point. At study end point, organs were retrieved and weighed, including (D) spleen (E) liver and (F) kidney. Data was analysed using non-parametric Mann-Whitney U test. Error bars represent mean ± SEM.

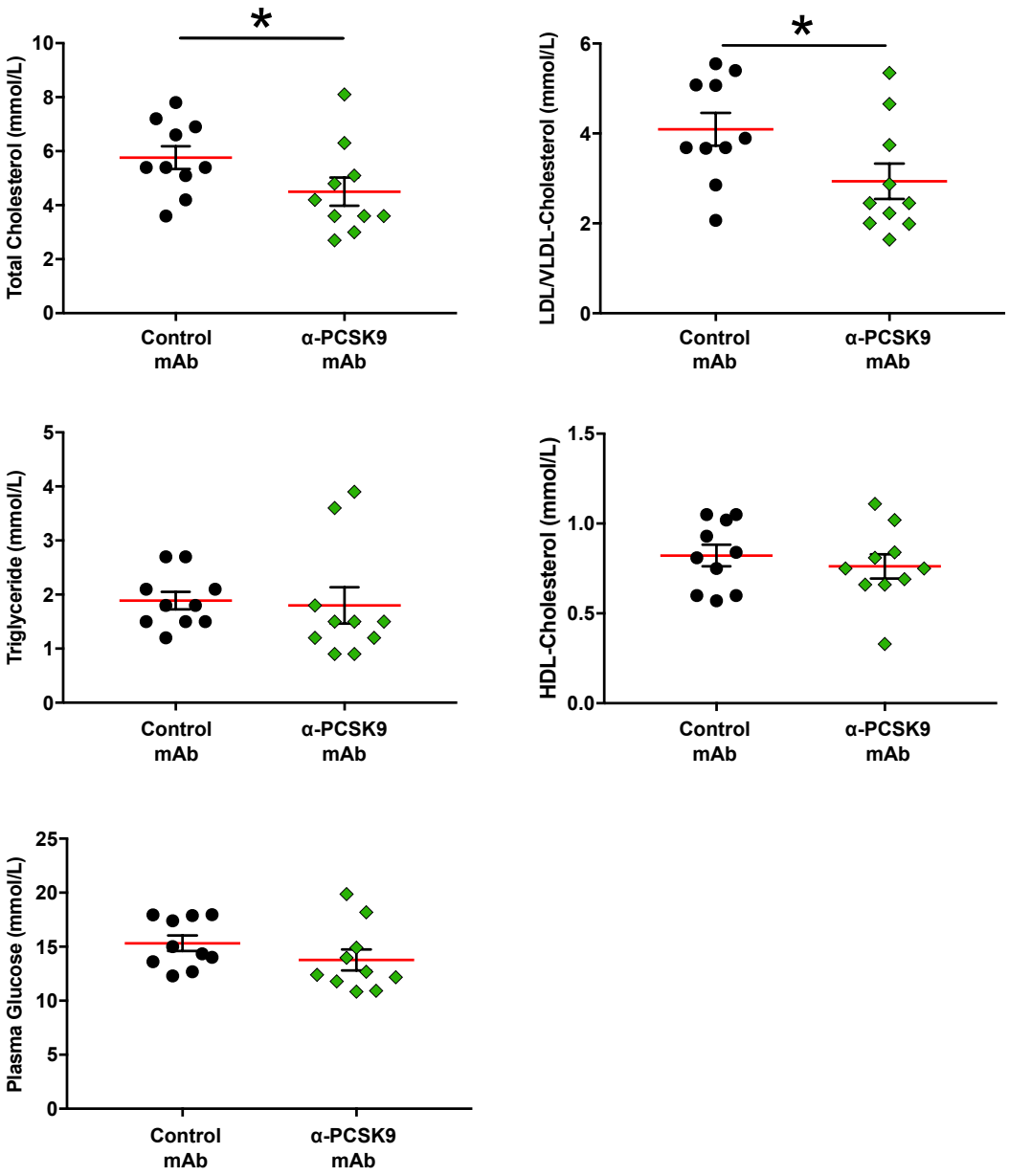

Figure 6-2. PCSK9 inhibition significantly lowers total and LDL/VLDL-cholesterol in female E3LC mice fed a high fat diet, but not triglycerides, HDL-cholesterol or glucose. Plasma cholesterol profile and glucose at study end point were determined using the enzymatic colorimetric method. Data was analysed using non-parametric Mann-Whitney U test, *$p<0.05$. Error bars represent mean ± SEM.

6.2.3 PCSK9 reduces the size of atherosclerotic lesions in aortic sinus (Fig.6-3)

Three frozen sections of aortic sinus covering proximal, middle and distal atheroma in aortic sinus were stained with oil red-o, and lesion area measured. In E3LC mice treated with α-PCSK9 mAb, average plaque area was significantly smaller than mice treated with control antibody (control vs. α-PCSK9 mAb; mean ± SEM, 264,383±33,267 vs. 116,763±22,572 μm^2, $p<0.01$). This represented a 56% reduction in average lesion size. The difference in plaque area between the two groups were seen at all 3 levels (proximal, middle and distal), with similar magnitude of difference (54-59%, Appendix 6-1).

6.2.4 PCSK9 reduces lipid content in aortic sinus atheroma (Fig. 6-4)

Composition of atherosclerotic plaques including lipid content affects stability and clinical manifestation[283]. PCSK9 inhibition reduced the lipid content in the plaque substantially (by 74.3%, $p<0.001$). To account for the difference in plaque size, lipid content was normalised to plaque area. It was found that percentage lipid content was also lower in mice treated with α-PCSK9 mAb (control vs. α-PCSK9 mAb; mean ± SEM, 24.7±1.7 vs. 13.8±1.4%, $p<0.001$). This significant between-group difference was seen at all 3 levels examined (Appendix 6-2).

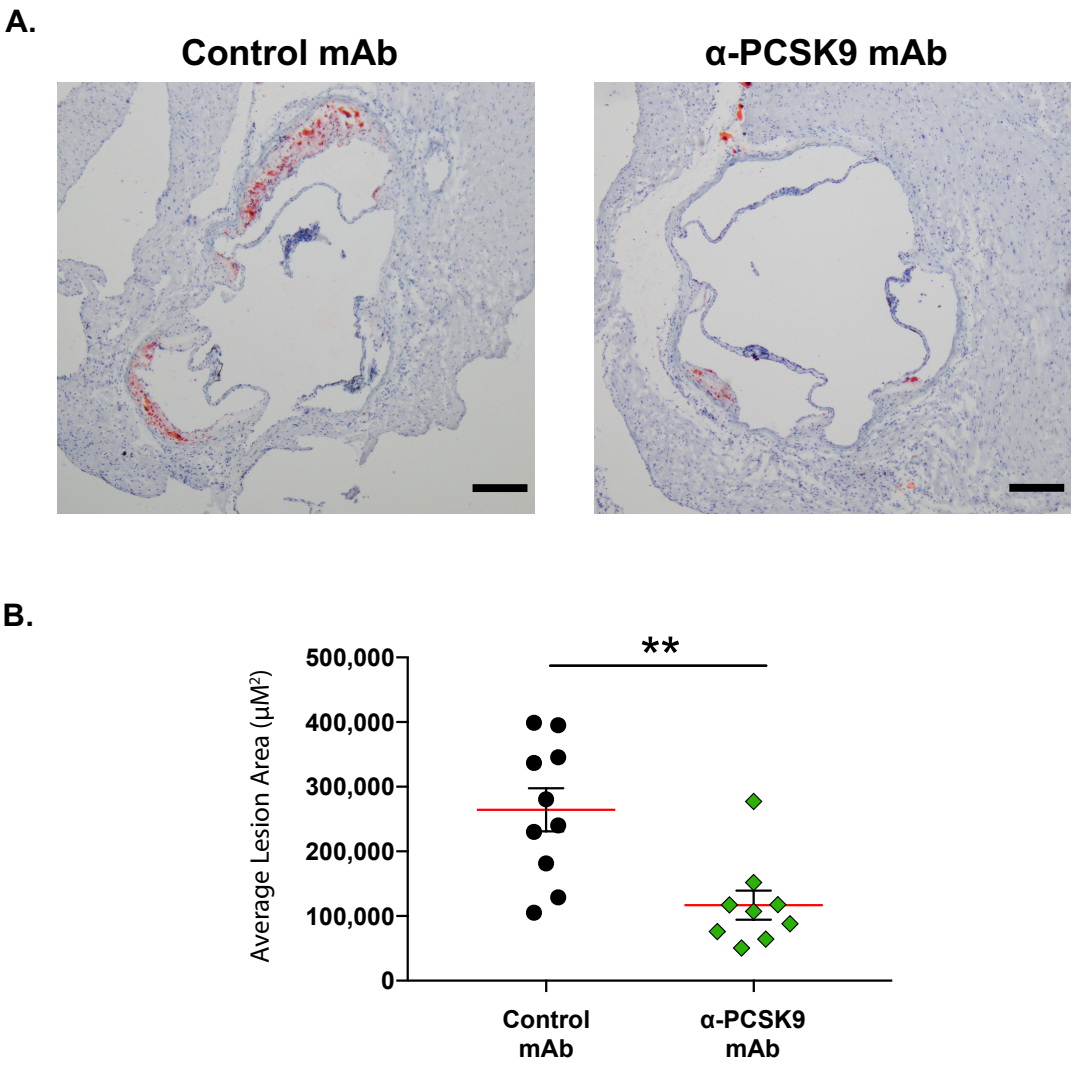

Figure 6-3. PCSK9 inhibition significantly reduces the size of atherosclerotic lesions in aortic sinus in female E3LC mice fed a high fat diet. Frozen sections of aortic sinus were stained with oil red-o and lesion area was measured. (A) Representative photomicrograph and (B) quantification of lesion size. Data was analysed using non-parametric Mann-Whitney U test, **p<0.01. Error bars represent mean ± SEM. Scale bar represents 200μm.

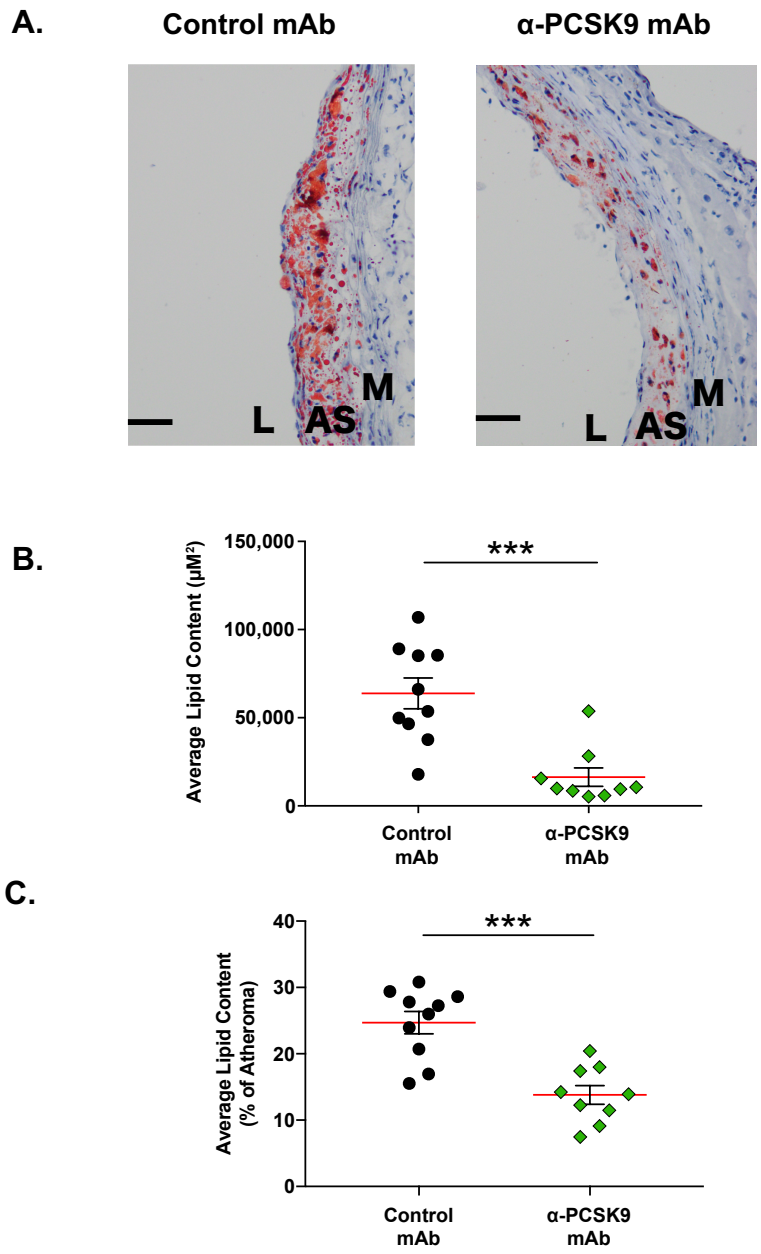

Figure 6-4. PCSK9 inhibition reduces lipid content in aortic sinus atheroma in female E3LC mice fed a high fat diet. Frozen sections of aortic sinus were stained with oil red-o, where neutral lipid stained red. (A) Representative photomicrograph, (B) quantification of average lipid content in and (C) lipid content normalised to plaque size. Data was analysed using non-parametric Mann-Whitney U test, ***$p<0.001$. Error bars represent mean ± SEM. Scale bar represents 50µm. Key: L - lumen, AS - atherosclerotic lesion and M - media.

6.2.5 PCSK9 inhibition does not reduce percentage necrosis in aortic sinus atheroma (Fig. 6-5)

Area of necrosis, especially when forming a confluent core, is a cardinal feature of advanced atherosclerotic plaques and independently predicts worse patient outcomes[15,256,284]. Frozen sections of aortic sinus were stained with H&E, and area of necrosis, defined as acellular region free of cell nuclei was measured. Female E3LC mice treated with α-PCSK9 mAb had a smaller area of necrosis (-51%, $p<0.01$). However, when normalised to plaque area, this difference was no longer significant ($p=0.07$). So, the reduction in necrotic area in the treatment group was due to their smaller plaque size, rather than a true change in plaque composition. The difference in necrosis between the 2 groups was seen in some but not all sections examined (Appendix 6-3).

6.2.6 PCSK9 inhibition does not change collagen content in aortic sinus atheroma (Fig. 6-6)

Collagen provides structural integrity and stability to atherosclerotic plaques. Frozen sections of aortic sinus were stained with picrosirius red and examined under polarised light. Collagen content did not differ between mice treated with control and α-PCSK9 mAb, whether in absolute area measured ($p=0.13$) or when normalised to plaque area ($p=0.55$). No difference between the two groups was found at any of the 3 levels examined (Appendix 6-4).

6.2.7 Validation of specificity of antibodies used in immunohistochemistry (Fig. 6-7)

Problems in antibodies, including cross-reactivity and variability, can lead to false and irreproducible results[285-287]. In accordance with a recent consensus statement[262], antibodies to be used in immunohistochemistry experiments were first validated. Adjacent frozen sections of atherosclerotic plaque were incubated with either (1) primary antibodies against CD68, α-SMA, MCP1, or (2) matching isotype control or (3) no primary antibodies. All three antibodies demonstrated binding specificity.

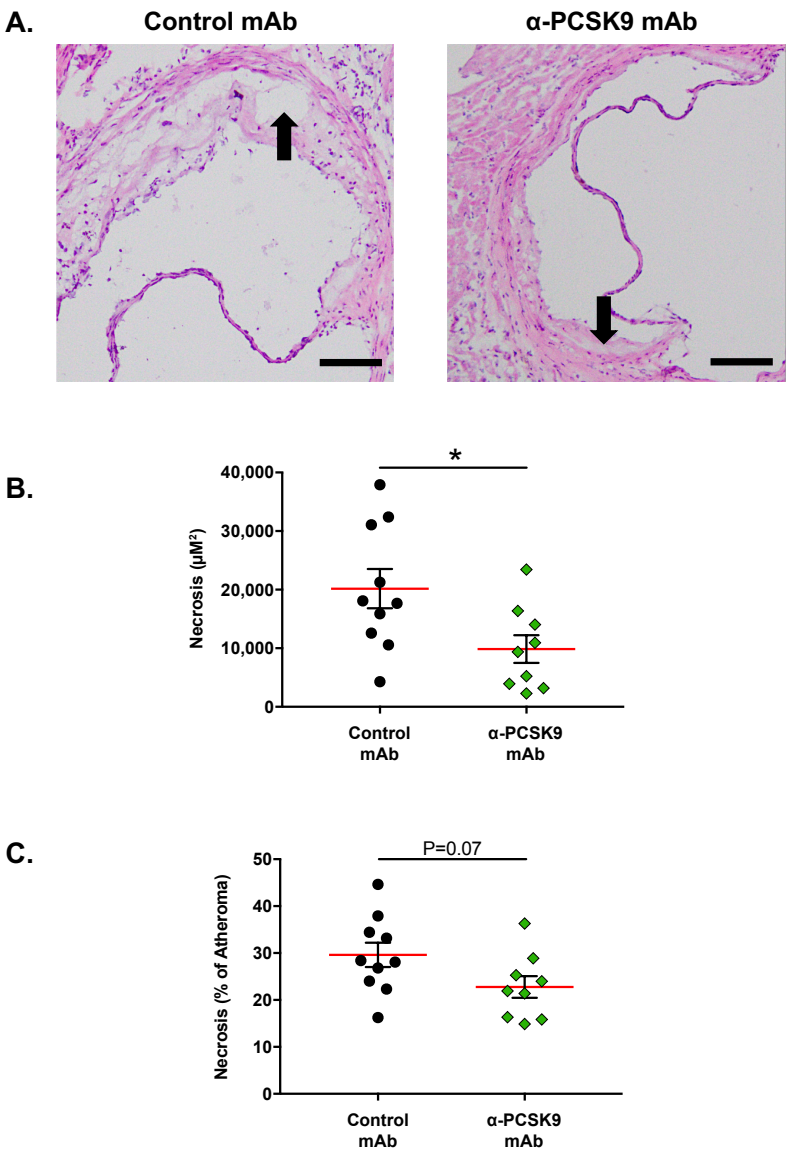

Figure 6-5. PCSK9 inhibition appears to reduce the area of necrosis within aortic sinus atheroma in female E3LC mice fed a high fat diet, but this is due to difference in plaque size. Area of necrosis were identified as acellular space with no cell nuclei (black arrow) on H&E-stained frozen sections of aortic sinus. (A) Representative photomicrograph showing necrosis (black arrow), and quantification of (B) area of necrosis and (C) normalised area of necrosis. Data was analysed using non-parametric Mann-Whitney U test, *$p<0.05$. Error bars represent mean ± SEM. Scale bar represents 100μm.

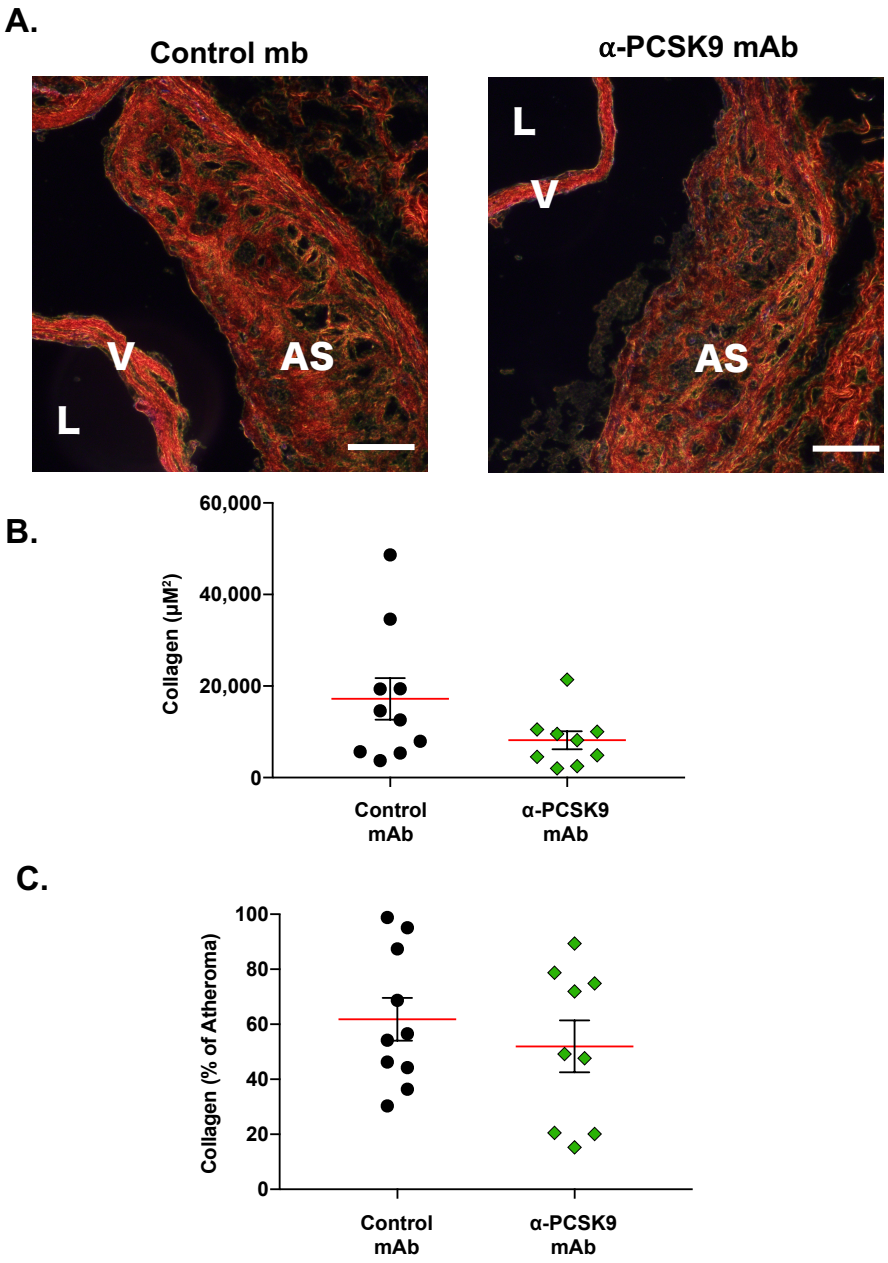

Figure 6-6. PCSK9 inhibition does not change collagen content in aortic sinus atheroma in female E3LC mice fed a high fat diet. Frozen sections of aortic sinus were stained with picrosirius red and examined under polarised light, where collagen stained orange-red. (A) Representative photomicrograph, quantification of (B) area of collagen and (C) collagen content normalised to plaque area. Data was analysed using non-parametric Mann-Whitney U test, Error bars represent mean ± SEM. Scale bar represents 100μm. Key: L - lumen, AS - atherosclerotic lesion and V – valve.

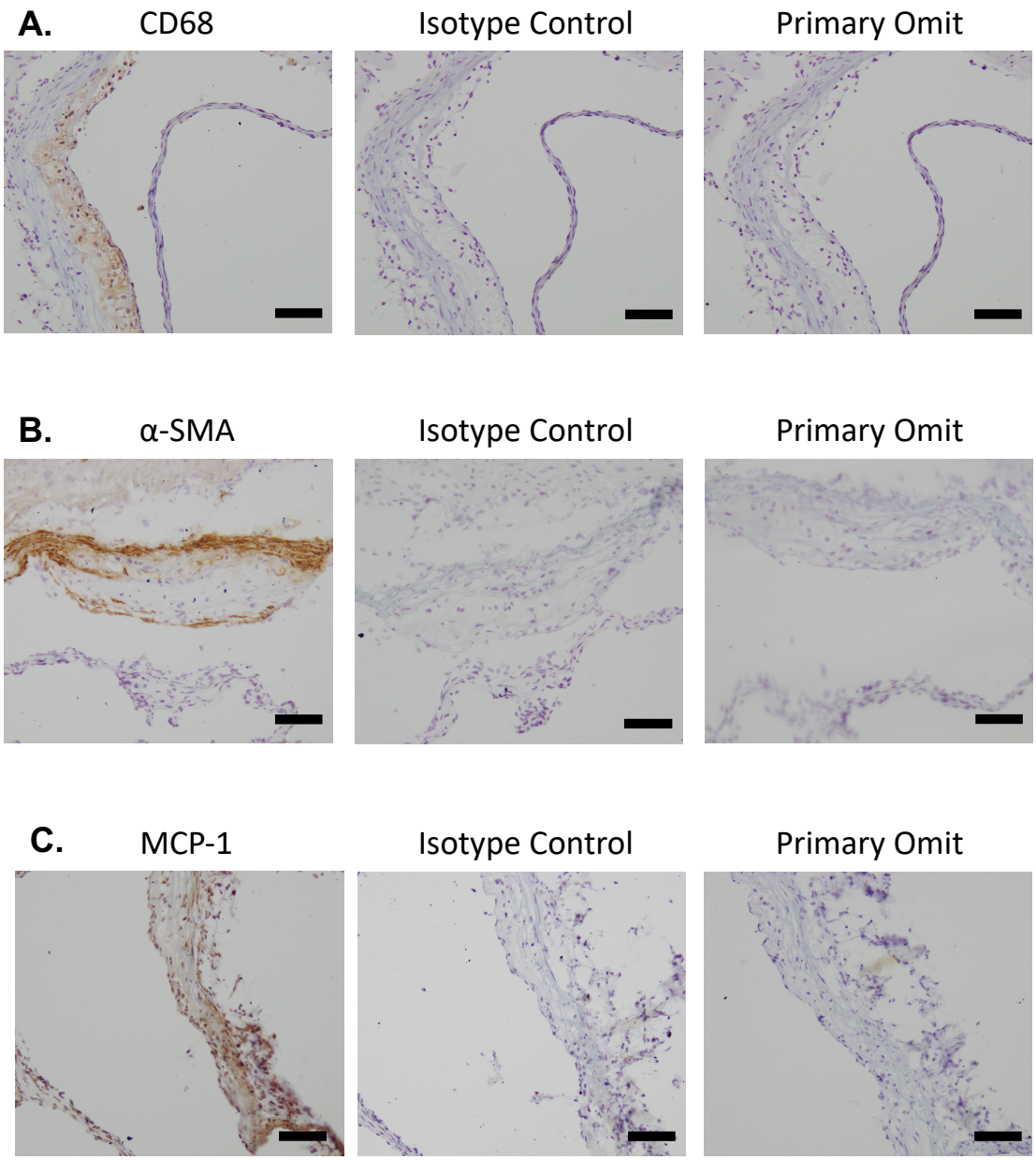

Figure 6-7. Validation of primary antibodies used in immunohistochemistry staining. Shown here are optimised immunohistochemistry staining of (A) CD68 at 1:100 dilution; (B) α-SMA at 1:100 dilution and (C) MCP-1 at 1:50 dilution, their respective isotype controls and when primary antibodies were omitted and stained with secondary antibodies only. Scale bar represents 50μm.

6.2.8 PCSK9 inhibition significantly reduces plaque macrophage infiltration (Fig. 6-8)

Macrophages ingest plaque lipid and cholesterol, and they secrete inflammatory cytokines and proteolytic enzymes[13]. These processes are intimately related to hypercholesterolaemia, atherogenesis and plaque stability. Using immunohistochemistry, macrophages were identified as $CD68^+$ cells. It was found the area of atheroma stained positive for $CD68^+$, in both absolute and normalised terms, was significantly smaller in female E3LC mice treated with α-PCSK9 mAb ($p<0.0001$ and $p<0.05$ respectively) than mice treated with isotype control.

6.2.9 PCSK9 inhibition increases vascular smooth muscle cell abundance in atheroma (Fig. 6-9)

Vascular smooth muscle cells synthesise and secrete constituents of extracellular matrix including collagen, fibronectin and proteoglycan, and their abundance in atherosclerotic plaque is often regarded as a feature of plaque stability[15]. Immunohistochemistry staining of frozen sections of aortic sinus, using primary antibodies against α-SMA showed that the area stained positive for α-SMA were similar between the 2 groups. However, when normalised to the plaque size, the α-SMA-stained area was significantly larger in mice treated with α-PCSK9 mAb ($p<0.05$).

6.2.10 PCSK9 inhibition does not change MCP-1 expression in atheroma (Fig. 6-10)

MCP-1 is an important cytokine in the initiation and development of atherosclerosis, and it mediates recruitment of immune cells[288]. Using immunohistochemistry, it was found there was no between-group difference in the absolute area stained positive for MCP-1 ($p=0.15$) or when MCP-1 stained area is normalised to atheroma ($p=0.51$)

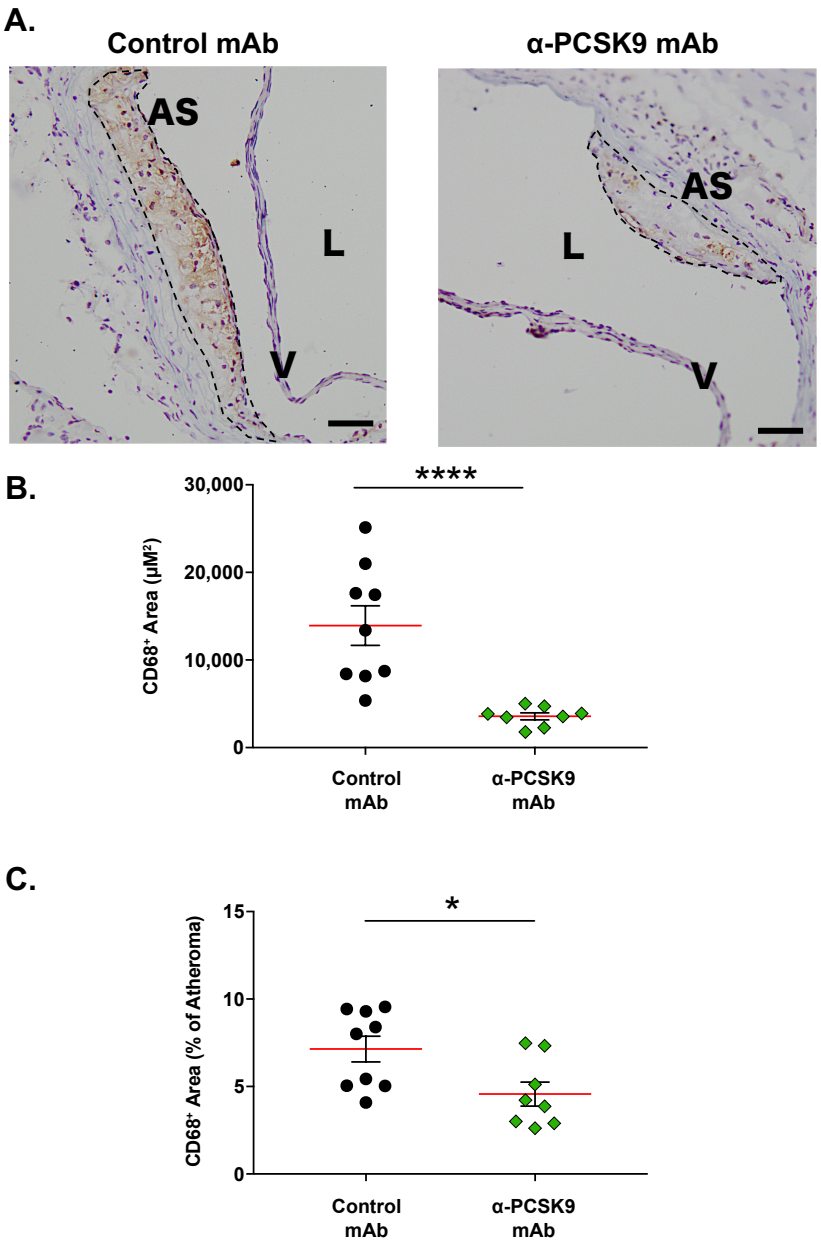

Figure 6-8. PCSK9 inhibition significantly reduces macrophage infiltration in aortic sinus atheroma in female E3LC mice fed a high fat diet. Frozen sections of aortic sinus were stained with primary antibody against CD68. (A) Representative photomicrograph, $CD68^+$ area was outlined in dotted line, and quantification of (B) $CD68^+$ area and (C) $CD68^+$ area normalised to atheroma. Data was analysed using non-parametric Mann-Whitney U test, *$p<0.05$ and ****$p<0.0001$. Error bars represent mean ± SEM. Scale bar represents 50µm. Key: L -lumen, AS - atherosclerotic lesion, V - valve.

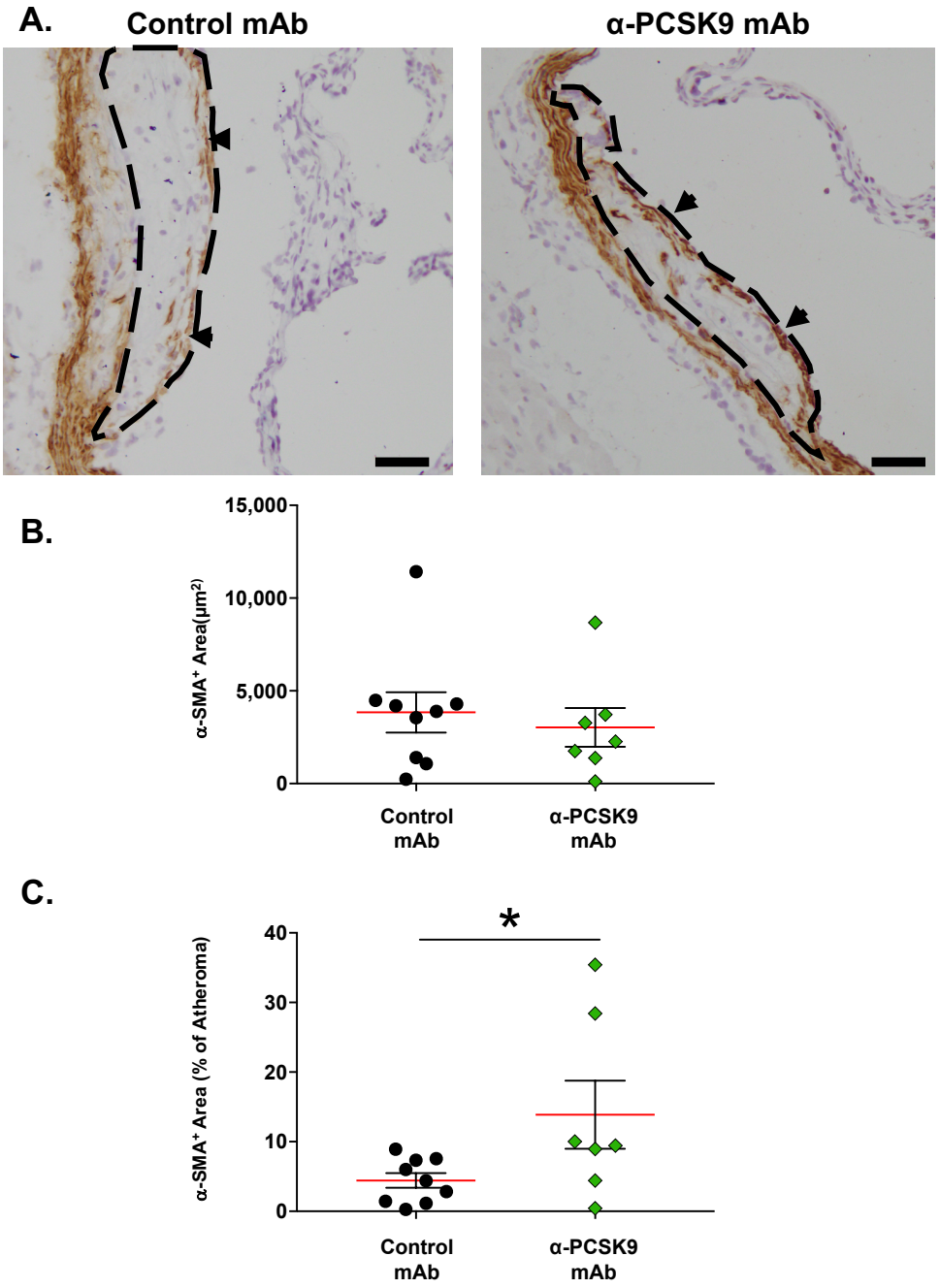

Figure 6-9. PCSK9 inhibition increases relative abundance of vascular smooth muscle cells in aortic sinus atheroma in female E3LC mice fed a high fat diet. (A) Representative photomicrograph, and quantification of (B) area stained positive for α-SMA and (C) area of α-SMA$^+$ area normalised to plaque area. Data was analysed with non-parametric Mann-Whitney U test, *p<0.05. Error bars represent mean ± SEM. Scale bar represents 50μm. Key: AS – atherosclerotic lesion.

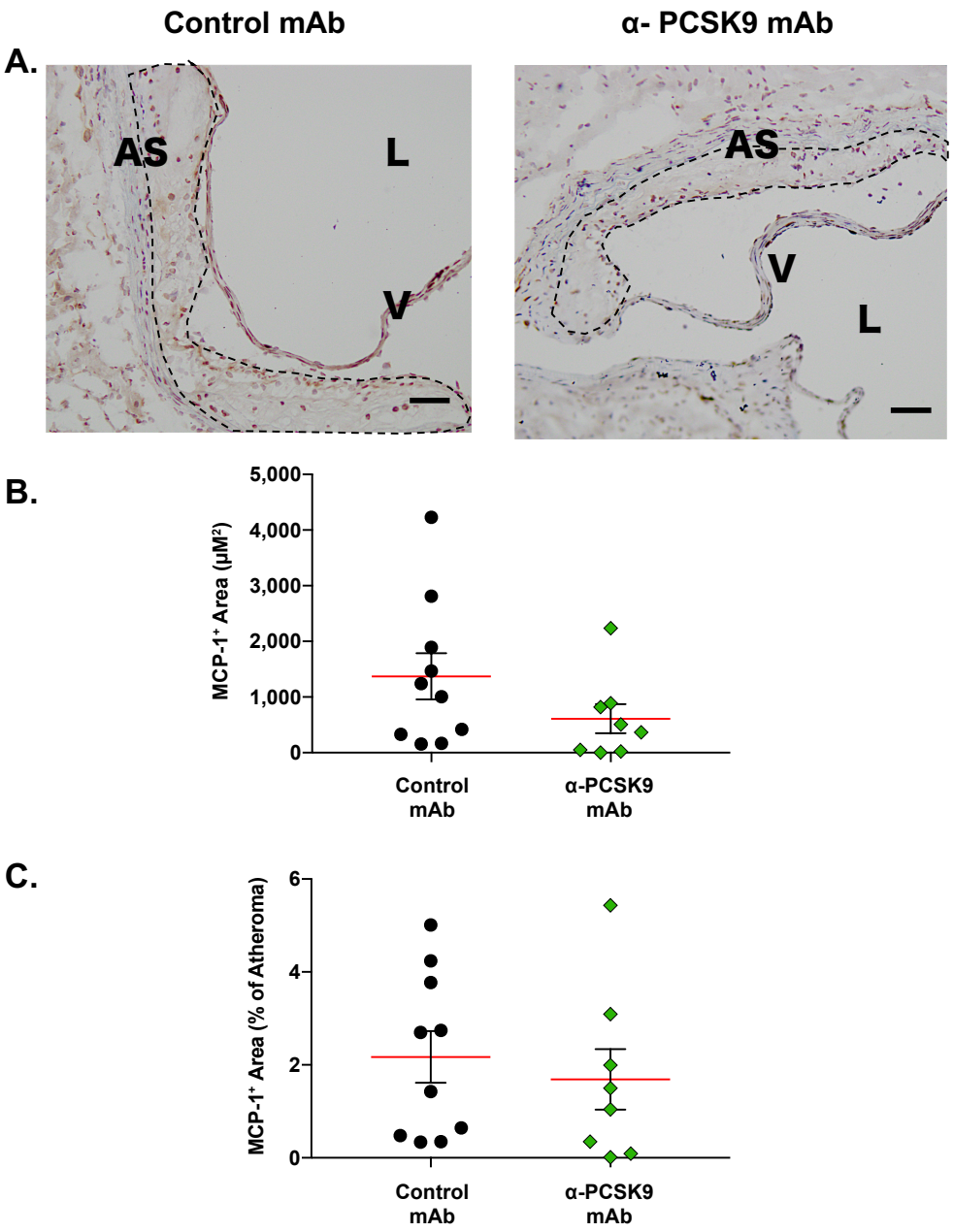

Figure 6-10. PCSK9 inhibition does not change expression of MCP-1 in aortic sinus atheroma in female E3LC mice fed a high fat diet. (A) Representative photomicrograph, lesion is outlined in dotted line. Quantification of (B) absolute MCP-1$^+$ area and (C) MCP-1$^+$ area normalised to plaque area. Data was analysed with non-parametric Mann-Whitney U test. Error bars represent mean ± SEM. Scale bar represents 50µm. Key: AS – atherosclerotic lesion, V – valve, L - lumen

6.2.11 PCSK9 inhibition does not change monocyte abundance (Fig. 6-11)

High fat diet induces proinflammatory Ly6C^{hi} monocytosis that is reversible with statins[246]. To determine if PCSK9 inhibition had similar effects, blood cells and splenocytes were examined with flow cytometry. Monocytes were defined as CD45^{+}CD11b^{+} cells, then subdivided according to Ly6C expression (for gating strategy, Appendix 6-5). No significant difference was found in the frequency of monocytes in either blood (p=0.09) or spleen (p=0.87) between female E3LC mice treated with control and those treated with α-PCSK9 mAb. No significant difference in the relative frequency of Ly6C^{hi} and Ly6C^{lo} monocytes was detected in blood (p=0.09) or spleen (p>0.99).

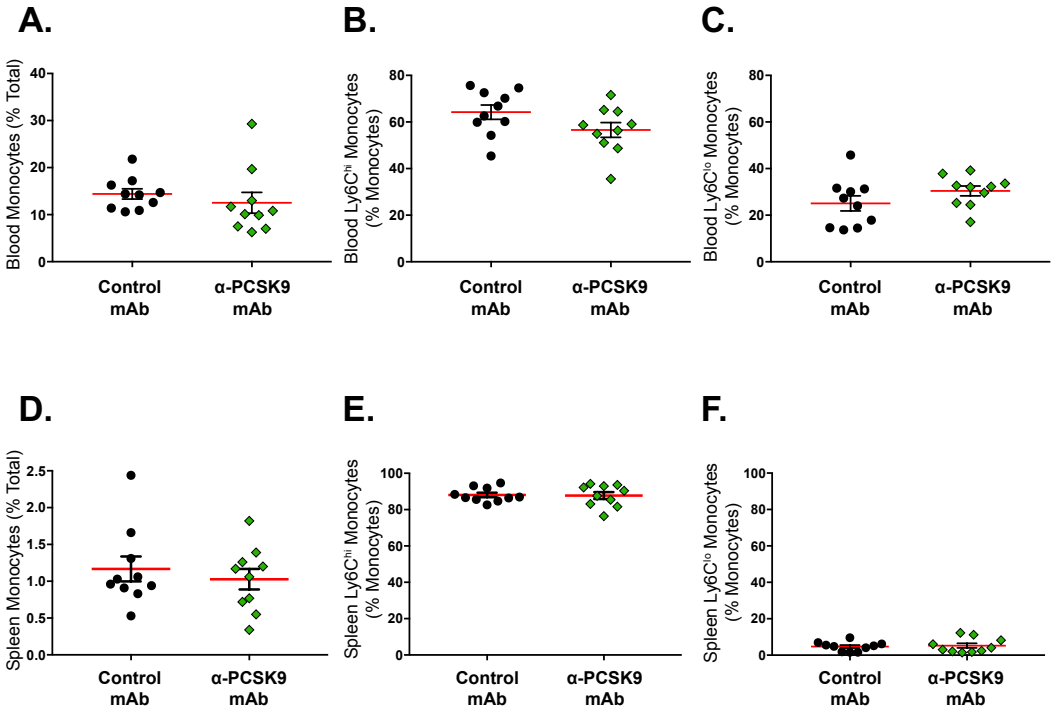

Figure 6-11. PCSK9 inhibition does not change relative abundance of monocytes. Blood and spleen were haemolysed, homogenised and suspended in FACS buffer, then subjected to flow cytometric examination. Monocytes were defined as CD45^{+}CD11b^{+} cells and further subdivided according to Ly6C expression. Their relative abundance in (A, B, C) blood and (D, E, F) spleen were examined. Data analysed using non-parametric Mann-Whitney U test. Error bars represent mean ± SEM.

6.2.12 PCSK9 inhibition increases the frequency of spleen and lymph node B cells (Fig. 6-12 to Fig. 6-14)

Lymphocytes have been implicated in the pathogenesis of atherosclerosis, and they can be activated by hypercholesterolaemia[289]. To investigate if PCSK9 inhibition changes lymphocyte populations, cells from blood, spleen and lymph nodes were examined using flow cytometry (Figs. 6-12, 6-13 and 6-14 respectively). B cells, defined by $CD19^+$ status, were modestly but significantly higher in the spleen (control vs. α-PCSK9 mAb; mean ± SEM, 42.9±1.1 vs. 47.8±1.5%, $p<0.05$) and lymph nodes (control vs. α-PCSK9 mAb; mean ± SEM, 42.2±1.1 vs. 47.1±1.5%, $p<0.05$) in mice treated with α-PCSK9 mAb. There were no differences in the frequency of B cells in the blood. No difference in the frequency of T lymphocytes (defined as $TCR\beta^+$) or $TCR\beta^+CD4^+$ and $TCR\beta^+CD8^+$ T lymphocyte subpopulations were found between mice treated with control and α-PCSK9 mAb (for gating strategy, see Appendix 6-6).

6.2.13 PCSK9 inhibition does not change platelet responsiveness (Fig. 6-15)

Clinical investigations suggest PCSK9 inhibition may reduce platelet responsiveness[290], and this offers another plausible mechanism where α-PCSK9 mAb reduces cardiovascular risks. Platelet-rich plasma from E3LC mice was incubated with ADP, a known agonist of platelet activation. Platelets were defined as $CD41^+$ cells and the status of activation was defined by $CD62P^+$ expression. No difference in platelet responsiveness to ADP was detected between the two groups ($p=0.89$).

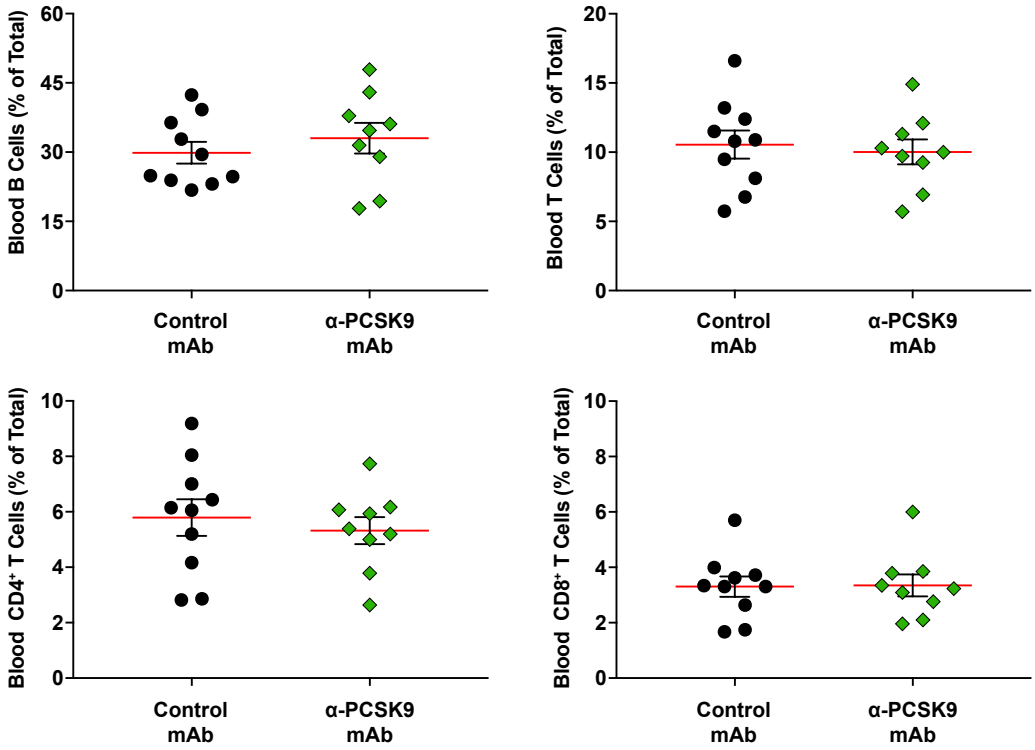

Figure 6-12. PCSK9 inhibition does not change relative frequency of circulating lymphocytes and its subpopulations in female E3LC mice fed a high fat diet. Blood from mice were haemolysed and resuspended in FACS buffer. B lymphocytes were defined as $CD19^+$ cells, and T lymphocytes were defined as $TCR\beta^+$ cells, then subdivided into $TCR\beta^+CD4^+$ and $TCR\beta^+CD8^+$ cells. Data was analysed using non-parametric Mann-Whitney U test. Error bars represent mean ± SEM.

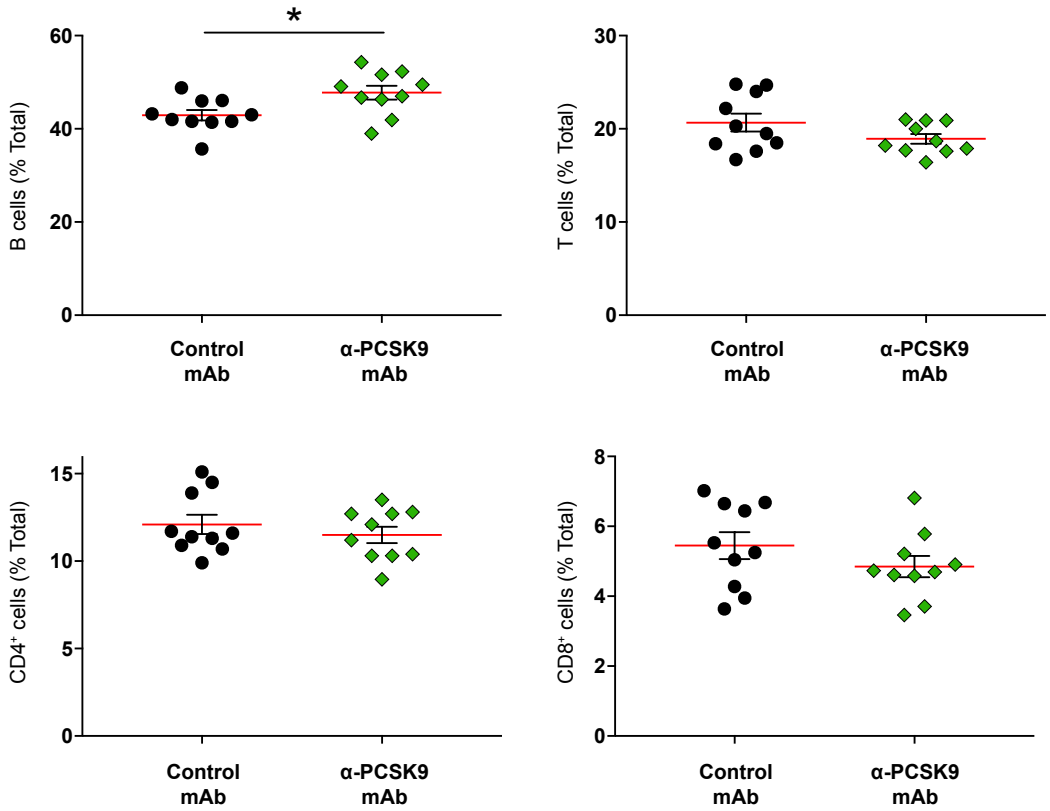

Figure 6-13. PCSK9 inhibition increases relative frequency of splenic B cells in female E3LC mice fed a high fat diet. Mouse spleens were haemolysed, homogenised and resuspended in FACS buffer before subjected to flow cytometry. B lymphocytes were defined as $CD19^+$ cells, and T lymphocytes were defined as $TCR\beta^+$ cells, then subdivided into $TCR\beta^+CD4^+$ and $TCR\beta^+CD8^+$ cells. Data was analysed using non-parametric Mann-Whitney U test, *$p<0.05$. Error bars represent mean ± SEM.

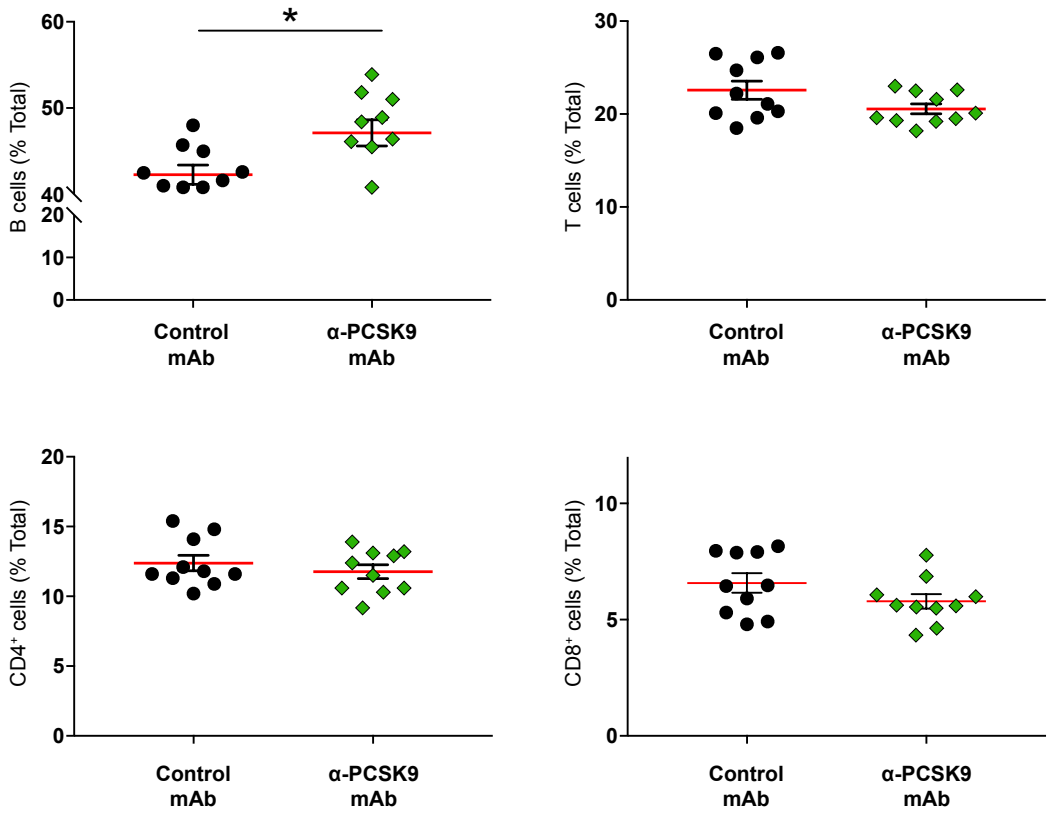

Figure 6-14. PCSK9 inhibition increases relative frequency of lymph node B cells in female E3LC mice fed a high fat diet. Lymph nodes were haemolysed, homogenised and resuspended in FACS buffer before subjected to flow cytometry. B lymphocytes were defined as $CD19^+$ cells, and T lymphocytes were defined as $TCR\beta^+$ cells, then subdivided into $TCR\beta^+CD4^+$ and $TCR\beta^+CD8^+$ cells. Data was analysed using non-parametric Mann-Whitney U test, *$p<0.05$. Error bars represent mean ± SEM.

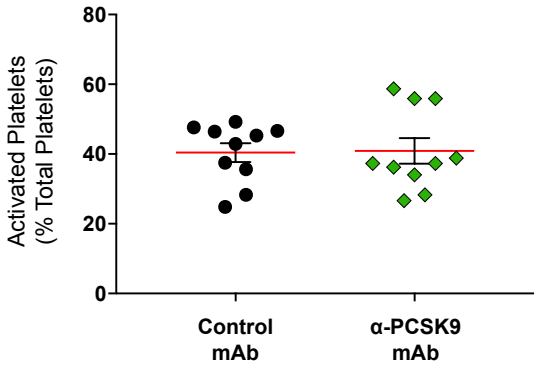

Figure 6-15. PCSK9 inhibition does not change platelet ADP-induced platelet activation. Platelet rich plasma was isolated from E3LC mouse blood and subjected to flow cytometry before and after ADP stimulation, at the dose of 20μM. Platelets were defined as $CD41^+$ cells and $CD62P^+$ expression was used as the platelet activation marker. Data was analysed using Mann-Whitney U test. Error bars represent mean ± SEM.

6.3 Discussion

In this study, the major findings in female E3LC mice with chronic (6 weeks) hypercholesterolaemia are the following, (1) PCSK9 inhibition modestly but significantly lowered plasma cholesterol concentration, and in particular, the atherogenic LDL/VLDL-cholesterol. (2) PCSK9 inhibition reduced atherosclerotic plaque size in aortic sinus. (3) PCSK9 inhibition stabilised atherosclerotic plaques through changing plaque cellular and chemical composition. (4) PCSK9 inhibition led to increased B cell population in spleen and lymph nodes. Compared to other studies, the novelty of this project is that α-PCSK9 mAb was administered after 6 weeks of high fat diet, simulating the clinical scenario of primary prevention in the setting of chronic hypercholesterolaemia.

Recently, two large-scale clinical trials (enrolling >18,000 and >27,000 patients with known atherosclerotic vascular diseases) have showed that, antibody-based PCSK9 inhibition reduced the risk of adverse cardiovascular events by approximately 15%[66,67]. In the GLAGOV study, PCSK9 inhibition was associated with a 0.95% reduction in the volume of atheroma, and 64.3% of patients had plaque regression[240]. This is one mechanism where PCSK9 inhibition offers atheroprotective effects. Consistent with clinical observations, this study found that PCSK9 inhibition was associated with smaller plaque burden, which could result from either plaque regression or retarded plaque growth.

In female E3LC mice fed a high diet, it was found PCSK9 inhibition was associated with a more favourable plaque phenotype, containing less lipid content, less extensive macrophage infiltration and more vascular smooth muscle. Denis et al. has also shown that, genetic depletion of PCSK9 in mice with either C57Bl6 or apoE$^{-/-}$ background led to a reduction in the amount of cholesterol ester in mouse aorta, however, no changes in atherosclerotic plaque size in apoE$^{-/-}$ mice was detected[89]. Current findings were comparable with Kuhnast et al. and Ason et al., who reported that pharmacological inhibition in PCSK9 in female E3LC mice was associated with smaller plaque sizes and a more stable lesion phenotype[55,90]. However, Kuhnast et al., observed that PCSK9 inhibition was associated with a reduction in circulating monocytes[90]. In contrast, no difference in the abundance of CD45^{+}CD11b^{+} monocytes or the CD45^{+}CD11b^{+}Ly6C^{hi} monocyte subpopulation were seen in this investigation. This may be related to the timing of intervention in relation to disease processes. In their study, α-PCSK9 mAb was initiated at the same time as commencement of high fat diet, whereas in this study,

PCSK9 inhibition was deferred for 6 weeks to simulate chronic, untreated hypercholesterolaemia. Hypercholesterolaemia affects haematopoiesis including Ly6C^{hi} monocytosis, which are recruited to and contribute to the macrophage population in atherosclerotic plaques[246]. Recent studies have implicated that this process may be more important in earlier stages of atherosclerosis, whereas in later stages, local proliferation of lesional macrophages may be more important[13]. Further, while monocyte depletion is associated with reduced plaque size and altered plaque composition in early-stage atherosclerosis, it did not impact on plaque inflammation or rupture in established disease[291]. This highlights the importance of understanding different disease stages and how it may result in different treatment responses.

This investigation provides evidence of the plaque stabilising effects of PCSK9 inhibition in atherogenesis, as PCSK9 was associated with reduced macrophage in the atheroma. This could result from decreased recruitment, decreased local macrophage proliferation or increased macrophage death. In this study, PCSK9 inhibition did not change circulating and spleen monocyte numbers, and there were no changes in the expression of monocyte recruiting cytokine, MCP-1 in atheroma. Taken together, these findings suggest that reduced lesional macrophage may result from either increased local proliferation or reduced apoptosis. Mechanistically, lowering cholesterol induces macrophages into a less inflammatory phenotype, which may slow disease progression. For example, cholesterol crystal induces neutrophil NET formation, which primes the macrophage inflammasome NLRP3 to secretes IL-1β[292], an important mediator of atherosclerosis whose clinical significance has recently been validated[26]. Indeed, inhibition of PCSK9 through vaccination has been shown to reduce NLRP3 activation[91]. On the other hand, it was found that there was an increase in vascular smooth muscle cells within atheroma, which is a marker of plaque stability. Vascular smooth muscle cells undergo apoptosis with hypercholesterolaemia in advanced lesions, and defective removal of apoptotic vascular smooth muscle cells is a source of inflammation and plaque propagation[293]. It is possible PCSK9 inhibition retards this process. Vascular smooth muscle cells secrete collagen to strengthen atherosclerotic plaques. In this and other studies, plaque collagen content was similar between control and α-PCSK9 mAb-treated mice[90]. However, vascular smooth muscles also secrete proteoglycan and fibronectin, express LDL and VLDL receptors and promote macrophage survival, all of which may contribute to plaque stability[14].

One unexpected finding from this investigation is the increased splenic and lymph node B lymphocytes. B lymphocytes are subdivided into IgM-producing B1 cells and IgG-producing B2 cells. Interestingly, B cells have been reported to both protect against and promote atherosclerosis. For example, B1 cells have been shown to be atheroprotective, while B2 cells exert deleterious effects and promote the development of atherosclerosis[247]. Recently, Nus et al. reported that when fed a high fat diet, marginal zone B cells in the spleen of apoE$^{-/-}$ mice were upregulated[294]. These cells control the migration and differentiation of follicular T cells, thus limiting follicular T cell proatherosclerotic activity. The significance of increased B cell abundance when treated with α-PCSK9 mAb is unknown and additional experiments are needed to confirm these findings.

In this investigation, atherosclerotic lesion size was quantified using frozen sections stained with oil red-o. This is different to previous chapters where the quantification of frozen sections was based on sections stained with H&E. This change was made in accordance with a recent recommendation statement[262]. Further, oil red-o provides better contrast thus allows easier quantification of smaller lesions[295].

Lastly, there were four limitations to this study. The carotid tandem stenosis surgery was performed but carotid segments were not analysed, as previous investigations demonstrated that they did not display unstable phenotypes. It is possible, though unlikely, that the carotid tandem stenosis surgery could affect atherogenesis. Secondly, only female E3LC mice were used, as male E3LC mice do not respond well to high fat diet and have very limited lesion development. This limits the generalisability of the current study. Thirdly, atherosclerotic lesions in aortic sinus tend to be early-stage lesions with a stable phenotype, thus this mouse model may not be as sensitive as other models designed to recapitulate human plaque rupture. Lack of certain features of plaque rupture such as lumenal thrombosis or intraplaque haemorrhage limits detailed assessment of the effects of PCSK9 inhibition on plaque stability. However, there was sufficient evidence in this study to conclude that PCSK9 inhibition changes plaque composition to a more favourable, stable phenotype. Lastly, PCSK9 inhibition had dual lipid-lowering and anti-inflammatory effects, as indicated reduced lesional lipid and macrophages. The relative contribution of each to plaque stabilisation is unknown, and it remains possible that the favourable changes in plaque composition was principally driven by LDL-cholesterol reduction.

In summary, this investigation provides strong evidence demonstrating the favourable effects of PCSK9 inhibition in limiting plaque development, reducing localised intraplaque inflammation, and promoting systemic changes in immune cell populations e.g. B cells. However, further and more in-depth analysis is required to delineate the molecular mechanisms of PCSK9 in atherosclerosis, and to assess the significance of the increased B cell populations in spleen and lymph nodes. Future studies addressing these issues will yield novel insights into the atheroprotective effects of PCSK9 inhibition and may lead to the development of other novel therapies.

CHAPTER 7

General Discussion and Future Directions

Atherosclerosis is a complex disease that involves multiple pathological processes and diverse cellular players. Further, the chronicity of the disease, and the heterogeneity in its temporal course, anatomical distribution and patient population have added further complexity in understanding and management of this disease. This is reflected by the sobering fact that despite our significantly improved understanding and development of successful therapeutic interventions, which has resulted in the dramatic improvement in the prognosis of myocardial infarction and stroke over the last 4 decades[296], atherosclerotic vascular disease remains the leading cause of death worldwide[5]. This highlights the continuing challenges of atherosclerosis and calls for novel strategies to effectively prevent and treat atherosclerotic vascular disease and its complications due to plaque rupture and/or "erosion". Research over the last 2 decades had elucidated many aspects of the disease mechanisms and has uncovered novel contributing factors. However, data from autopsy series[18] and clinical investigations[99,254] has highlighted the importance of atherosclerotic plaque rupture and ensuing thrombosis. As plaque rupture and thrombosis represent the final common pathway that precipitates the devastating clinical manifestations of myocardial infarction and stroke[297], prevention of these occurrences should avert a significant portion of adverse clinical events. Of note, plaque rupture and thrombosis are related but not necessarily consequential. Thus, targeting development/progression as well as rupture and thrombosis would likely have additive or even synergistic benefits. Based on this, this thesis investigated novel strategies of plaque stabilisation and the prevention of arterial thrombosis.

To better understand the underlying processes of atherosclerotic plaque rupture, Chapter 4 of this thesis focused on the development of a mouse model of plaque rupture, using E3LC mice. The rationale and experimental design were based on a previously established plaque rupture model that used apoE$^{-/-}$ mice[63]. It was found that even though the same principle - creating an environment of low shear and high tensile stress - was applied to hypercholesterolaemic mice, the carotid segment I of E3LC mice did not display an unstable plaque phenotype. Compared to apoE$^{-/-}$ mice, E3LC mice had lower plasma cholesterol levels and smaller and less advanced atherosclerotic plaques (fatty streak/intermediate lesions or neointimal hyperplasia). These differences are likely, at least in part, to account for to account for the finding that plaque instability/rupture could not be induced in E3LC mice. Genetic studies have demonstrated that cardiovascular risk is a function of both the level of as well as the duration of exposure to plasma cholesterol[93]. Atherosclerotic lesions can adversely affect vascular rheology, which in turn remodels vasculature, propagates lesion development and induces plaque rupture[243].

Lastly, progression of atherosclerosis is generally associated with the development of advanced lesions, which are prone to rupture. Whilst E3LC mice are relatively poorly studied when compared to apoE$^{-/-}$ mice, it is tempting to speculate that other factors such as potential baseline differences between apoE$^{-/-}$ and E3LC mice in cellular responses to hypercholesterolaemia, the activation status of the immune system, and the vulnerability of vascular cells (e.g., smooth muscle cells) to apoptosis may contribute to the lower propensity of plaque rupture in E3LC mice. The design of future experiments would need to take these factors into consideration. Using immunohistochemistry to examine, compare and contrast cell markers of proliferation, activation and apoptosis within atherosclerotic plaques between E3LC and apoE$^{-/-}$ mice would be an informative starting point. This should be followed by further studies (e.g., changing high fat diet) to assess how E3LC and apoE$^{-/-}$ respond differently to high fat diet. These experiments are crucial to successfully induce plaque rupture in E3LC and would likely yield novel insights into the pathophysiology of plaque rupture.

Recently, Veseli et al. reviewed 10 mouse models of atherosclerotic plaque rupture[62]. A myriad of interventions that alters haemodynamic conditions (e.g., administration of phenylnephrine[60] or partial renal artery ligation[298]), impairs vascular structural integrity (e.g., macrophage overexpression of uPA[61] or MMP-9[59], elastin fragmentation[64]) or ageing alone[57] were used to induce plaque rupture. However, the ability to successfully induce plaque rupture was low in most studies, with plaque rupture seen in <50% of mice[62]. But for mechanistic studies a rupture frequency of >90% would be required to definitively identify specific mechanisms that contribute to plaque rupture. These data suggest that plaque rupture has a multi-factorial aetiology and may require a "perfect storm" situation where a constellation of conditions needs to be present to reach the tipping point for plaque rupture. Consistent with this, in human, plaque rupture is often silent, suggesting other local (shear stress) or systemic factors (thrombotic tendency) are at work and they are involved in determining if episodes of plaque rupture manifest clinically. In corollary, removing one insulting stimulus or restoring one perturbed pathophysiology may be sufficient to prevent plaque rupture in some scenarios. One such example is hypercholesterolaemia, where effective treatment such as statins has been shown to reduce cardiovascular risk through stabilisation of atherosclerotic plaques[236]. Recently, another class of highly effective hypolipidaemic agents, monoclonal antibodies against PCSK9 including evolocumab and alirocumab, have been added to the armamentarium against atherosclerosis. The development of a PCSK9 inhibitor is a remarkable example of how informative genetic epidemiology studies are used to guide the selection of therapeutic targets.

Equally astonishingly, it only took 13 years between the first report linking PCSK9 to cholesterol metabolism[65] and the approval of first α-PCSK9 mAb[299]. Though much of the basic biology of PCSK9 has been elucidated already, much more remains to be learned. One important question, especially in light of recent findings from the FOURIER[66] and ODYSSEY-Outcome trials[67], is whether PCSK9 inhibition affects plaque stability.

To address this question, an apoE$^{-/-}$ mouse model of plaque rupture was used (Chapter 4). It was found that in apoE$^{-/-}$ mice, PCSK9 inhibition did not change plasma cholesterol, plaque size or composition. After excluding other potential causes for these results, including insufficient dosing, loss of antibody specificity when used in different species or the development of immunity against cross-species antibodies, it was concluded that PCSK9 requires apoE to mediate its function. How apoE affects and enables PCSK9 to function remains unclear. It is possible apoE may modulate LDLR and PCSK9 binding, either on cell surface or in endosomes. From a clinical perspective, the results from this investigation have two implications. Firstly, PCSK9 inhibition may not be as effective in patients with type III hyperlipoproteinemia, where apoE has defective binding to LDLR. As some of the apoE isoforms in these patients still have partial function, these patients may respond to PCSK9 inhibition, but to a lesser extent[300]. Secondly, it can be inferred from our findings that, evolocumab does not have significant off-target effects. The safety signals from the FOURIER trial corroborate this finding[66].

In this thesis, a second mouse model of diet-induced atherosclerosis was used to investigate the effects of PCSK9 in atherogenesis and plaque stability (Chapter 6). It was found that, in female E3LC mice with chronic (6 week) hypercholesterolaemia, PCSK9 inhibition resulted in smaller plaques containing less lipid. PCSK9 inhibition was also associated with reduced local inflammation evidenced by a reduced infiltration of lesional macrophages, and improved plaque stability as seen with more vascular smooth muscle cells. Taken together, this indicates a change in plaque composition to a more stable phenotype. In this study, the magnitude of cholesterol reduction from PCSK9 inhibition was fairly modest (approximately 20%), and it raises the question whether PCSK9 has any cholesterol-independent pleiotropic effects. This notion is supported by some reported experimental studies. Compared to apoE$^{-/-}$ mice, apoE$^{-/-}$ mice expressing transgenic PCSK9 had bigger atherosclerotic plaques and increased deposition of cholesterol ester in mouse aorta, despite minimal changes in plasma cholesterol levels[89]. In

a mouse model of atherosclerosis, Giunzioni et al. demonstrated the presence of bone marrow-derived PCSK9 within atherosclerotic lesions, and expression of PCSK9 in plaques promoted accumulation of Ly6C^{hi} monocytes [301]. Ricci et al. have also shown *in vitro* that PCSK9 exerts pro-inflammatory actions on monocytes and upregulates mRNA expression of IL-1β, IL-6, TNF-α, CXCL2, and MCP-1[302]. Investigators also found that vascular smooth muscle cells secreted PCSK9, especially in an environment of low shear stress[303], and the secreted PCSK9 reduced LDLR expression in macrophages[304]. However, clinical investigations have shown that after adjusting for cholesterol and triglyceride levels, PCSK9 did not independently predict adverse cardiovascular events[305,306]. Further, in patients treated with α-PCSK9 mAb, there were no significant changes in c-reactive protein levels in the blood[307]. Therefore, it appears PCSK9 does not have significant immunomodulatory effects independent of cholesterol-lowering. Clearly, there are conflicting results between the experimental and clinical literature, and further investigations are required to reconcile these differences.

Given that in mice, diet-induced atherosclerosis requires at least 8 weeks of high fat feeding[308], E3LC mice in this investigation simulates the setting of chronic hypercholesterolaemia without established atherosclerosis. Results from this investigation suggest that cholesterol-lowering at such an early stage of disease slows down progression of atherosclerosis. So, should cholesterol-lowering therapy such as PCSK9 inhibitors be started in primary prevention instead of secondary prevention where disease has already progressed? Three lines of evidence from clinical studies lend support to this concept. Firstly, the seminal observation by Cohen et al. demonstrates that a lifelong reduction in cholesterol, as seen in subjects carrying the loss-of-function PCSK9 mutation, was associated with a significant reduction in cardiovascular risks[93]. Importantly, the magnitude of benefits is larger than expected or observed from clinical trials. Secondly, meta-analysis of statin trials has shown that patients with lower cardiovascular risk (by inference, less advanced disease) derive more benefit from statins than patients with established disease[309]. Thirdly, in the WOSCOP trial, one of the large statin trials, patients that were assigned to statin continued to have better outcomes, even at the 20-year extended follow up (the trial duration was 5 years)[310]. This is coined the "legacy effect". Taken together, these observations suggest the duration of hypercholesterolaemia is also important, and earlier intervention will likely provide greater benefit in the long run. Some investigators even advocate for aggressive interventions at adolescence or early adulthood to induce plaque stabilisation, followed by long-term maintenance with statin[311]. Important to consider though

are the potential risks of long-term cholesterol-lowering therapy (e.g., a small but significant increased risk of diabetes[312]), the prohibitive cost of α-PCSK9 mAb and patient reluctance for very long-term preventative treatments. This means such an aggressive approach is unlikely to be adopted. However, newer agents such as PCSK9-targeting vaccines[91], which are currently undergoing clinical testing, may be a feasible way to implement early interventions in the future.

While plaque rupture is the most common trigger of sudden coronary deaths[18], it is not the only precipitant. Plaque erosion is another pathology that leads to coronary thrombosis and accounts for approximately 30% of acute coronary syndrome[19]. Thus, it is important to also prevent the downstream event of thrombosis. Current anti-thrombotic therapeutics target platelets or coagulation factors. While they are effective in preventing the occurrence and limiting the extent of thrombotic events, they also carry significant bleeding risks. This may be particularly challenging in clinical situations where combination anti-thrombotic therapy is required[313], or in the elderly population who are susceptible to major bleeding[218].

Over recent years, a deeper understanding of the contribution of leukocytes and how they interact with other players of the haemostasis system, have offered another potential therapeutic opportunity[314]. In particular, NETosis, a DNA scaffold lattice with histones and neutrophil proteases[109], have garnered much interest. Preclinical studies have shown that NETosis is involved in arterial[120] and venous[127] thrombosis. Clinical investigations have demonstrated the presence of NETosis in human arterial[192] and venous thrombi[128], providing clinical validation of animal studies. As NETosis is a novel therapeutic target, development of NETosis inhibition agents may provide complementary actions when added to anti-thrombotic therapies routinely used. Previous studied have provided supporting evidence for this. DNase, which dismantles DNA and NETosis, was effective in breaking down arterial thrombi resistant to fibrinolytic therapy[124]. Of interest, NETosis can be induced by activated platelets[315], LPS[315] and HMGB1[169]. In this investigation, a strategy of targeting NETosis through HMGB1 neutralisation was tested. HMGB1 was chosen as studies have implicated its role in thrombosis [195,196], and it has been shown to co-localise with NETosis in human coronary thrombi[192], suggesting a participating role. Indeed, as shown in this study, HMGB1 neutralisation was an effective strategy in preventing arterial thrombosis in two mouse models of thrombosis. This investigation also demonstrated that HMGB1 neutralisation principally exerts its

antithrombotic actions through inhibition of NETosis, rather than via monocytes or platelets. Lastly, HMGB1 neutralisation appeared to be safe with no bleeding risks, and it compared favourably to current anti-thrombotic treatments. As treatment with anti-HMGB1 antibodies is also known to attenuate atherosclerosis, targeting HMGB1 in atherosclerosis may be highly beneficial in atherosclerosis by preventing both upstream development of atherosclerosis and downstream thrombosis due to plaque rupture/erosion[178].

To translate current findings to bedside, a few issues need to be resolved. Firstly, HMGB1 has diverse and sometimes seemingly opposite biological actions. On the one hand, in the setting of ischemia-reperfusion injury, HMGB1 acts as a DAMP that recruits immune cells and can cause severe organ damage[200]. On the other hand, HMGB1 can signal and prepare for regenerative processes[190]. Indiscriminate inhibition of HMGB1 may lead to unpredictable responses and is potentially harmful. This issue may be overcome by better understanding of HMGB1 biology. In the case of thrombosis, strong evidence has shown that NETosis induction results from platelet-derived rather than neutrophil-derived HMGB1[196]. Conceivably, a targeted delivery of HMGB1 antagonist using nanoparticles or antibodies specific to activated platelets would allow more precise drug targeting[316]. As HMGB1 is subjected to redox modifications, this offers another opportunity for specific targeting of HMGB1. In thrombosis, disulphide bonds bind HMGB1 to TLR4 and induces NETosis[196]. Investigators have developed a tetramer (P5779) that specifically antagonises TLR4-disulphide HMGB1 interactions[152], and this tetramer maybe effective in interfering with HMGB1-mediated thrombosis too. Further, by understanding HMGB1 biology better, it may be possible to take advantage of its diverse functions. For example, in a mouse model of myocardial ischaemia-reperfusion injury, inhibition of HMGB1 results in smaller infarct size[186]. Thus, in the setting of myocardial infarction, it may be possible to achieve both anti-thrombotic and cardioprotective benefits through careful choosing of the timing, duration and dose of HMGB1 inhibition,

In the basic science literature, different methods were used to antagonise HMGB1. These strategies include neutralising antibodies (as used in this study), thrombomodulin, HMGB1 box A, small molecule inhibitors and cognate receptor antagonists. As thrombomodulin also has antithrombotic actions, administrating thrombomodulin may provide additive or synergistic anti-thrombotic actions. Box A of HMGB1 acts as an antagonist to full-length HMGB1 and was used in a number of animal studies. One challenge with this approach is that

the mechanism of action remains unknown, making it difficult to predict potential off-target toxicity. A third approach is to design competitive or non-competitive inhibitors that bind to cognate receptors of HMGB1. For example, the small molecule eritoran has been used in mice as a specific TLR4 inhibitor[317]. However, TLR4 and RAGE both have multiple ligands and biological actions, thus how to ensure precision targeting so not to have off-target effects would be challenging. A neutralising antibody was used in this thesis. Recently, a patent application for human α-HMGB1 neutralising antibody was filed, taking this approach one step closer to the clinic[204]. One challenge of antibody-based therapies, however, is the low bioavailability. From a pragmatic standpoint, this restricts the mode of delivery to subcutaneous or intravenous routes and excludes oral formulation. However, this is balanced by the long half-life of IgG, which reduces dosing frequency and enhances patient adherence. Lastly, small molecules inhibitors are another alternative. Researchers have previously screened drug libraries and developed specific small-molecule inhibitors that were effective in limiting HMGB1-mediated hepatic ischaemic-reperfusion injury[152]. This is an attractive option as the cost of manufacturing is lower compared to that of biologics.

Thrombosis is an unpredictable event, thus effective prevention often requires long-term use of antithrombotic therapy. However, the long-term risk of HMGB1 neutralisation was not assessed in this thesis. Considering HMGB1's role as a DAMP, chronic HMGB1 depletion could potentially compromise immunity and increase the risk of infection. Although in preclinical studies where α-HMGB1 mAb was administered for a prolonged period of time (> 4 weeks), mice did not show an increased vulnerability to infection[179]. This suggests there is sufficient redundancy in the immune system such that HMGB1 neutralisation does not grossly impair overall immunity. In particular, due to the high mortality rate of 7-10% within the first 30 days of an episode of acute coronary syndrome, it would be beneficial to intensify treatment with additional antithrombotic therapies during this window[318]. This is a potential niche for HMGB1 neutralisation treatment.

In summary, two strategies to prevent atherosclerotic complications were assessed in this thesis. The first approach targeted the upstream event of plaque rupture and demonstrated that PCSK9 can stabilise atherosclerotic plaques by changing plaque composition. The second approach targeted the downstream event of arterial thrombosis, through the neutralisation of HMGB1 and inhibition of NETosis. Taken together, these approaches are

highly-promising and if they are successfully translated to a clinical setting, they may lead to improved patient outcomes.

APPENDIX

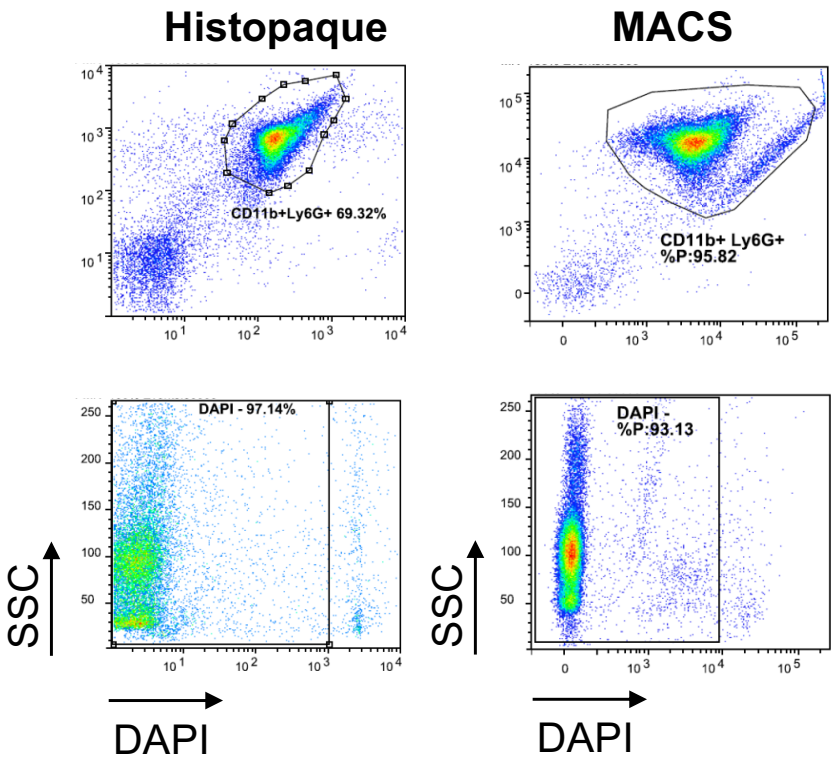

Appendix 3-1 Gating strategy to assess purity and viability of neutrophils isolated. Mouse neutrophils isolated using differential density gradient and negative immunomagnetic selection methods were examined using flow cytometry. Neutrophils were defined as $CD11b^{+}Ly6G^{+}$ cells, and viability was defined as $DAPI^{-}$.

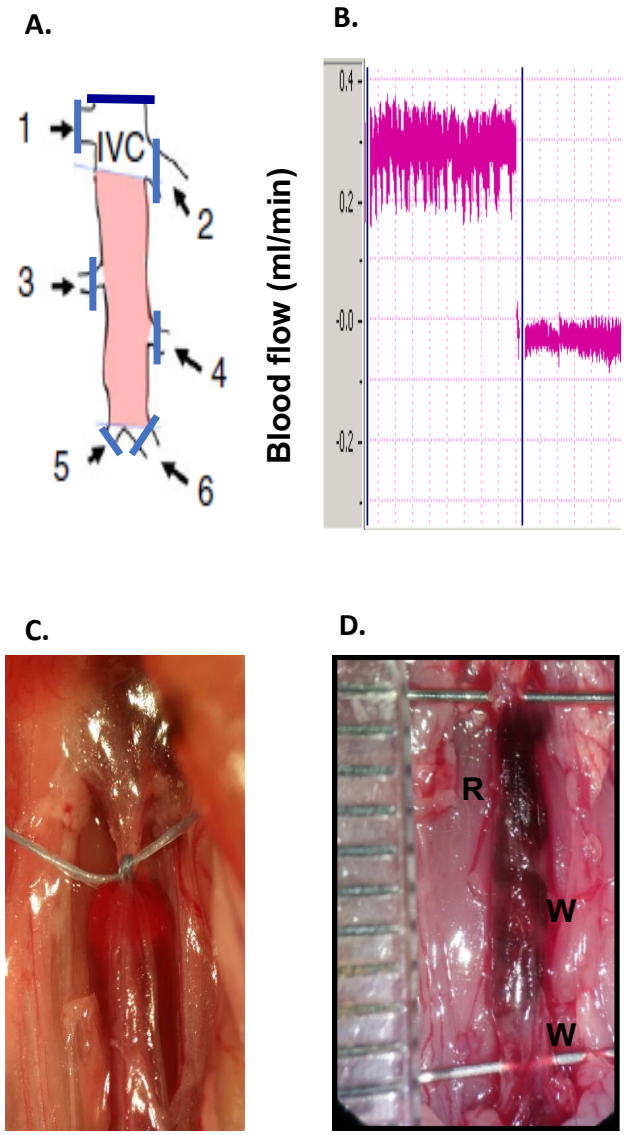

Appendix 3-2. Establishing the IVC-ligation deep vein thrombosis model. (A) A schema showing the model design. In this model, IVC was ligated below the renal vein, and all branches were ligated to achieve complete flow stasis (modified from Diaz et al.[210]). (B) Flow stasis was confirmed using Doppler ultrasound. Shown is blood flow (ml/min) before (on the left) and after ligation of IVC (right) (C) Thrombosis occurred from below the renal vein and extended to the inguinal arteries. (D) This model produced a thrombus of heterogeneous composition with both white (W) and red (R) thrombus, recapitulating human pathology of deep vein thrombosis.

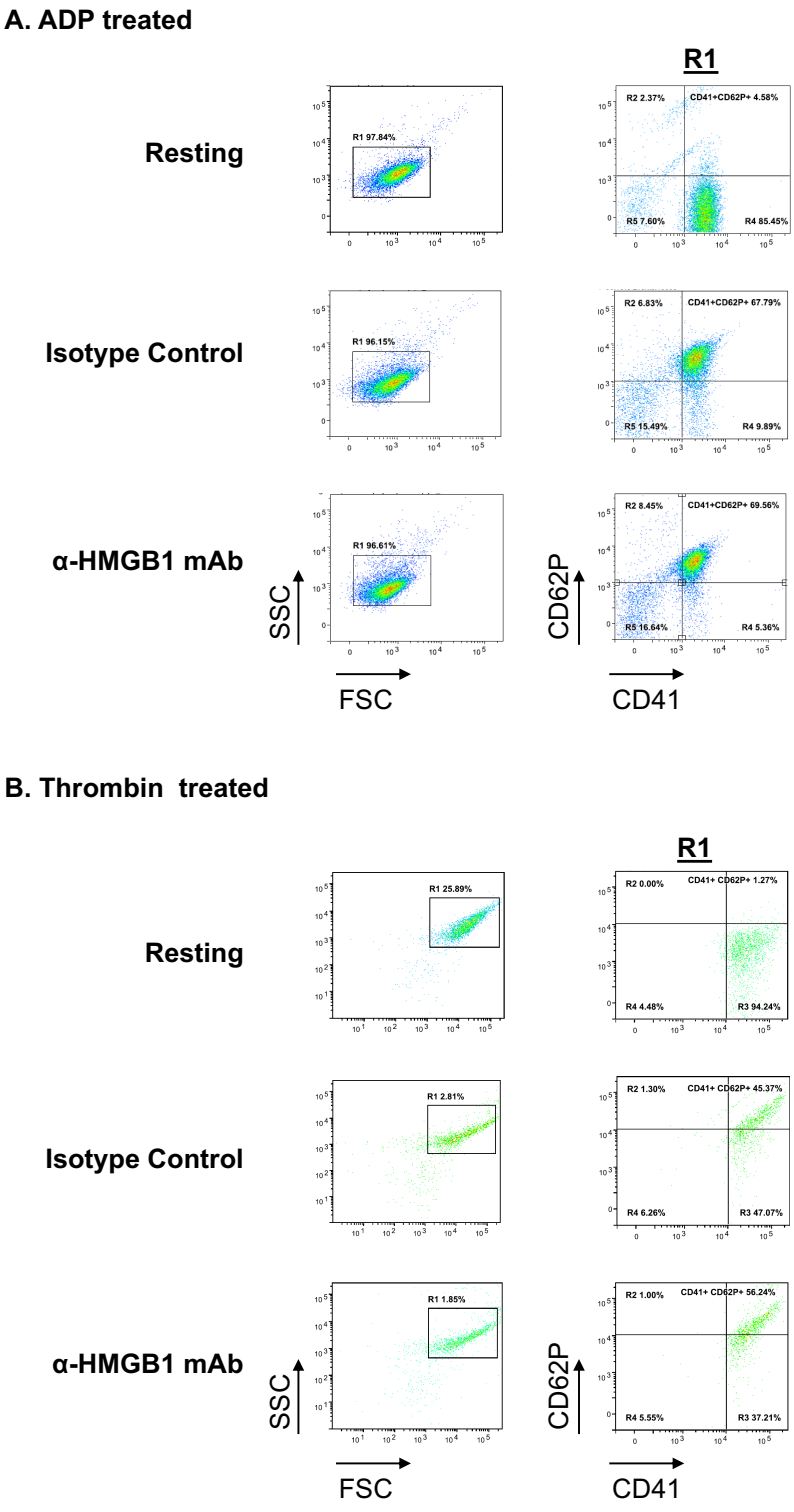

Appendix 3-3. Gating strategy for activated platelets. Platelets were defined as $CD41^{+}$ cells and activation status defined by CD62P expression. For both (A) and (B), resting cells were not treated with the platelet agonists (ADP or thrombin); isotype control and α-HMGB1 represented their respective pre-treatment before platelet agonists were added.

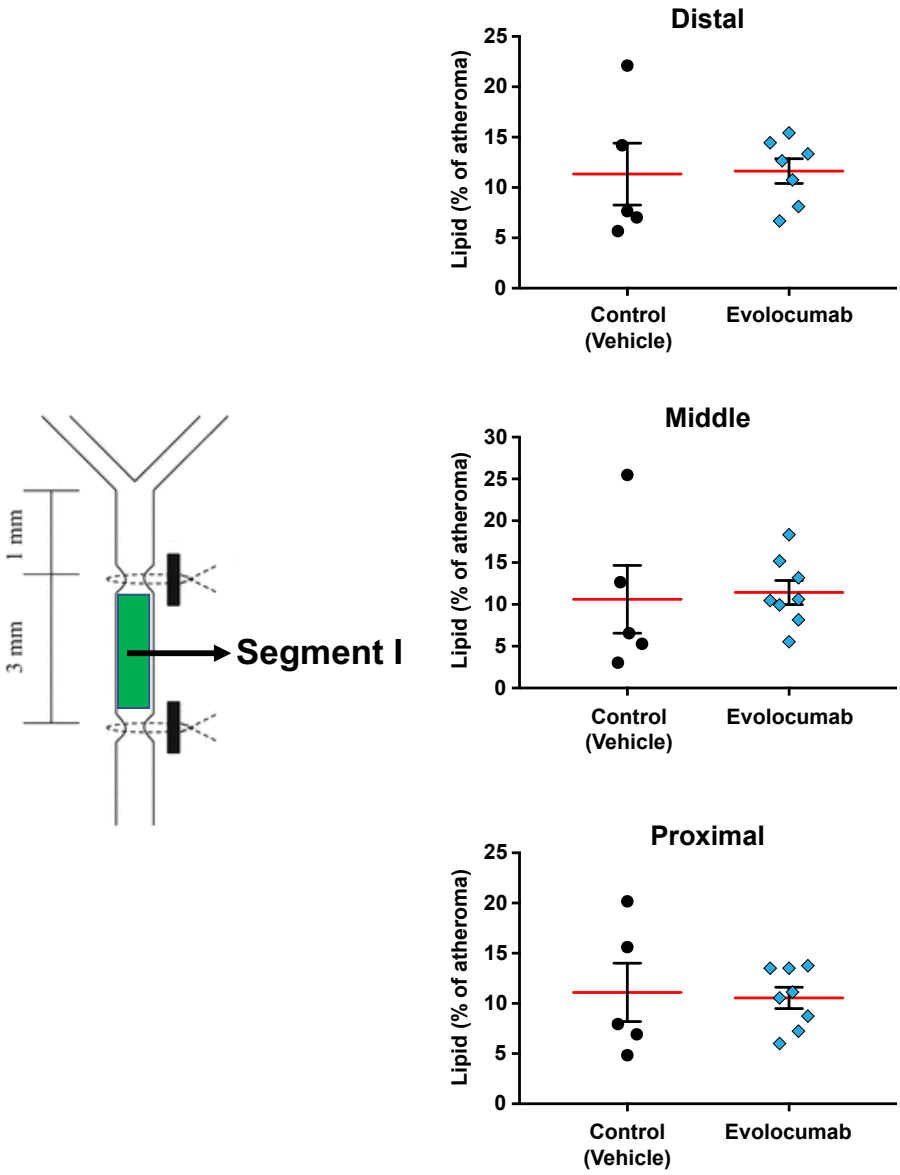

Appendix 4-1. Evolocumab does not change the lipid content at any of the 3 carotid segment I levels. Three frozen sections, each taken from the proximal, middle and distal parts of carotid segment I in male apoE$^{-/-}$ mice fed a high fat diet, were stained with oil red-o, where neutral lipid stained red. Data was analysed using non-parametric Mann-Whitney U test. Error bars represent mean ± SEM.

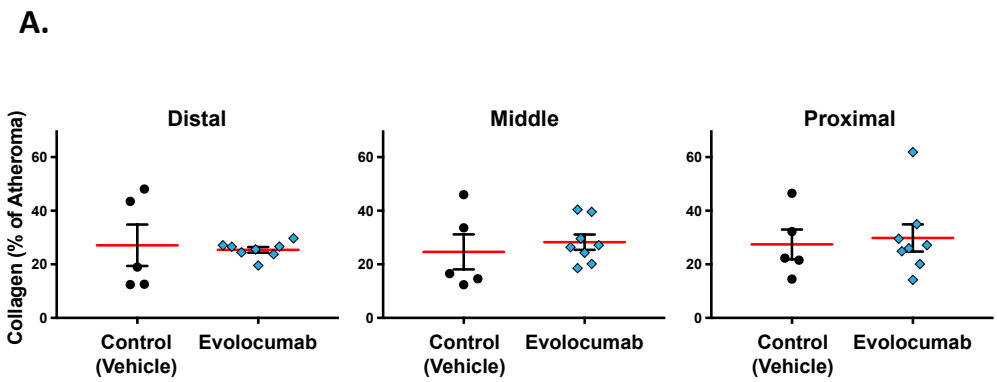

Appendix 4-2. Evolocumab does not change the collagen content in any of the carotid segment I sections. Frozen sections of proximal, middle and distal carotid segment I in male apoE-/- mice fed a high fat diet were stained with picrosirius red and examined under polarised light. Data was analysed using non-parametric Mann-Whitney U test. Error bars represent mean ± SEM.

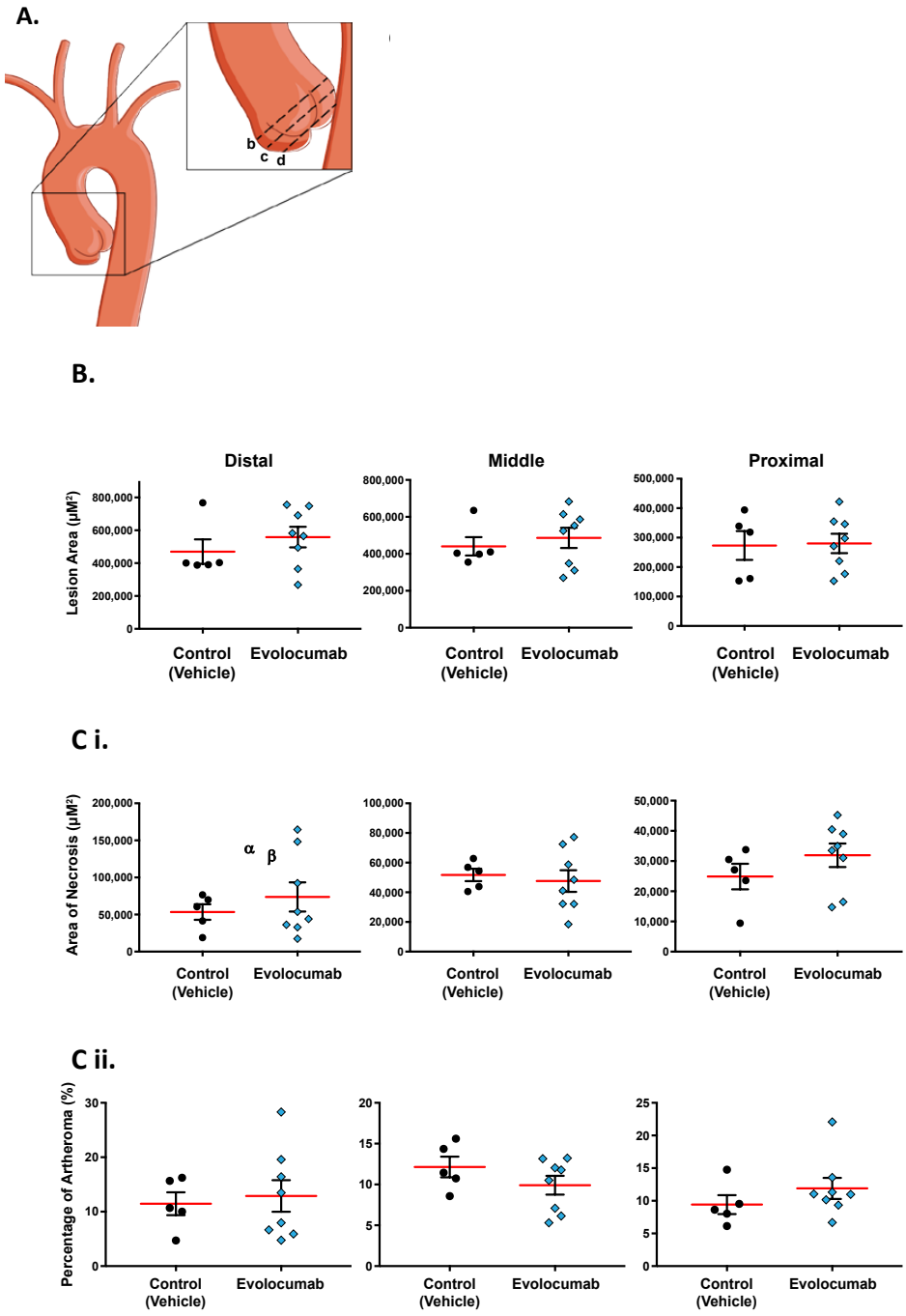

Appendix 4-3. Evolocumab does not change the lesion size or extent of necrosis at any of the 3 levels of aortic sinus atheroma. Three frozen sections were taken, one each from the proximal, middle and distal parts of the atheroma in aortic sinus in male apoE$^{-/-}$ mice fed a high fat diet. and stained with H&E. (A) Schematic of (b) distal, (c) middle and (d) proximal sections in aortic sinus. No difference in (B) lesion area, (C i) area of necrosis (C ii) percentage of necrosis was detected at any level. Data was analysed using non-parametric Mann-Whitney U test. Error bars represent mean ± SEM.

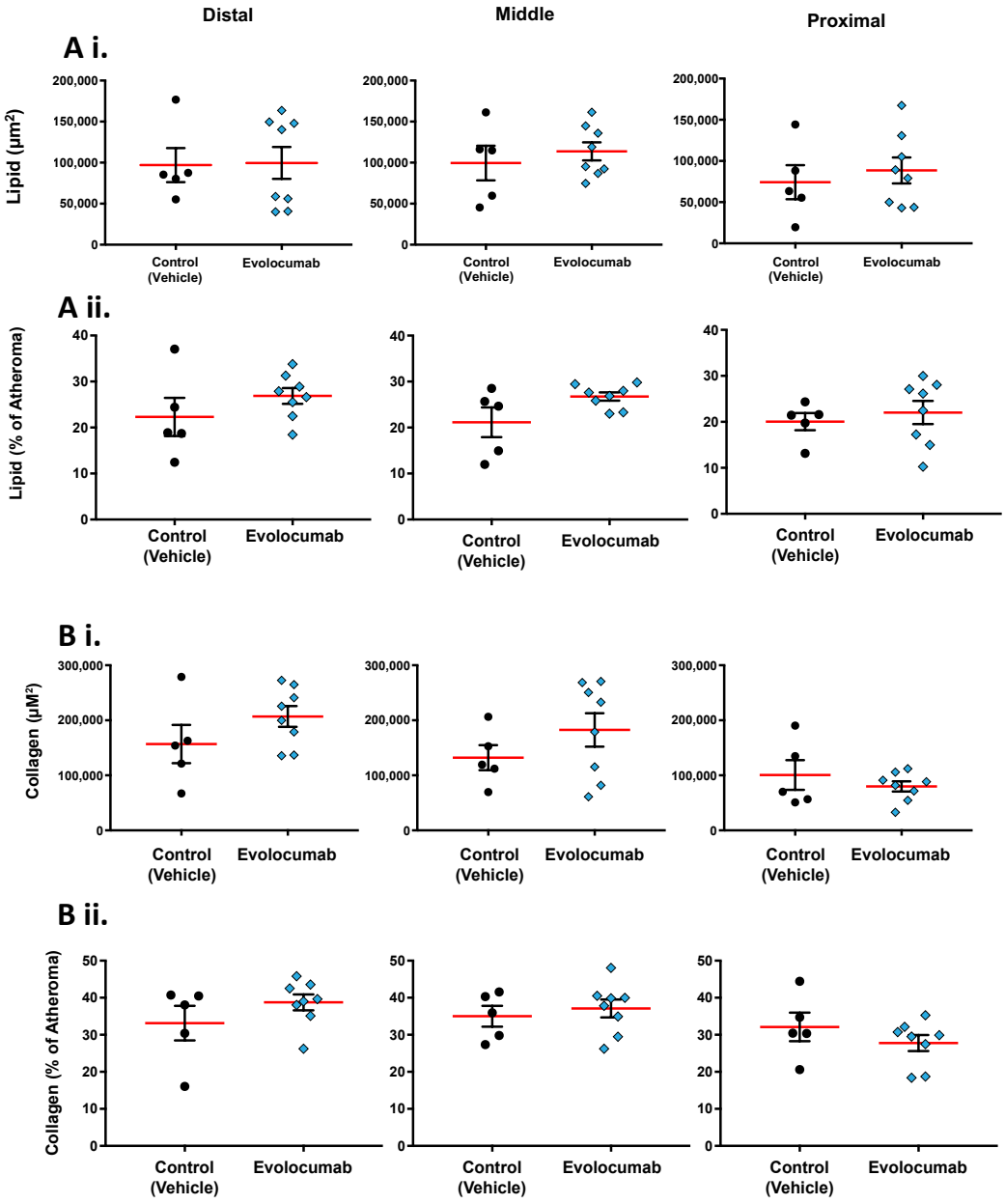

Appendix 4-4. Evolocumab does not change the lipid or collagen content at any of the 3 levels of aortic sinus atheroma. Frozen sections, one each was taken from the proximal, middle and distal parts of the atheroma in aortic sinus in male apoE$^{-/-}$ mice fed high fat diet and stained with oil red-o or picrosirius red. (A i) Area of lipid and (A ii) area of lipid normalised to plaque size; (B i) area of collagen and (B ii) area of collagen normalised to plaque size. Data was analysed using non-parametric Mann-Whitney U test. Error bars represent mean ± SEM.

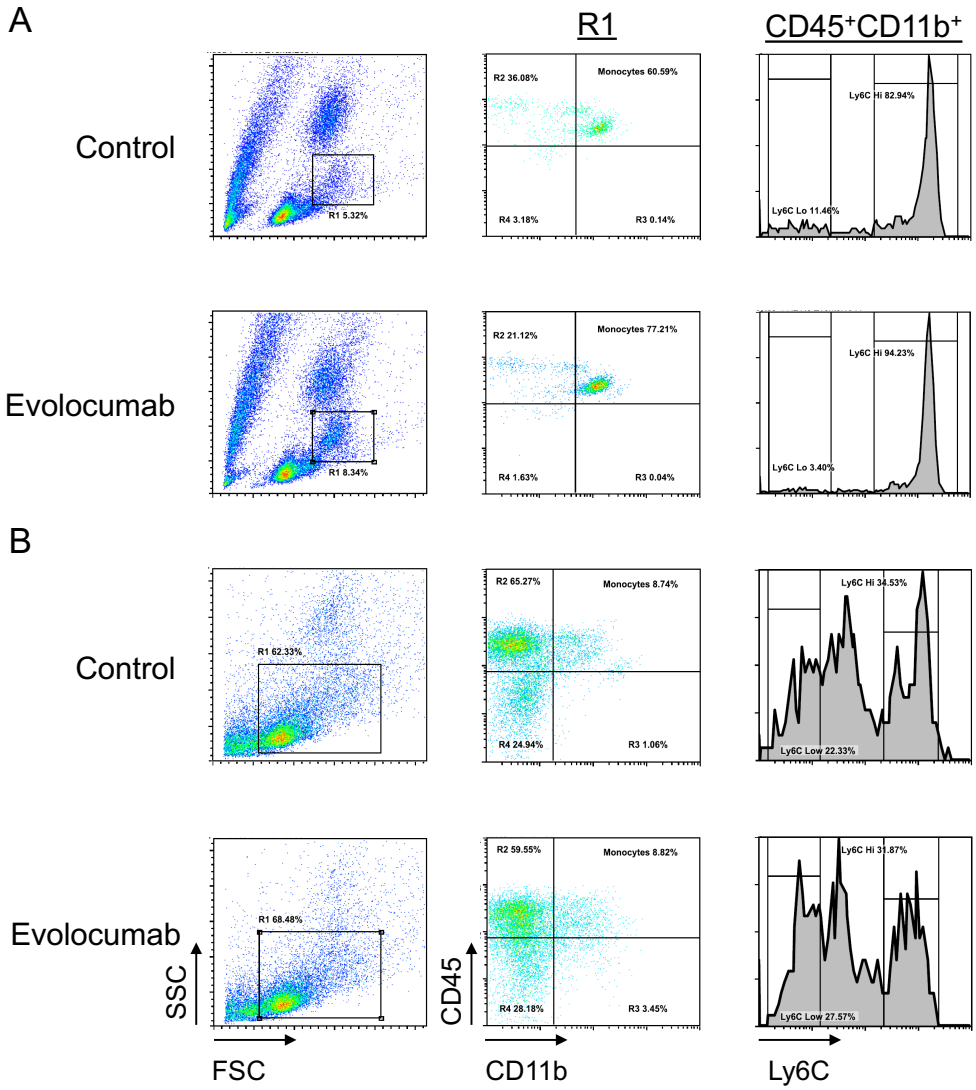

Appendix 4-5. Gating strategy for flow cytometric examination of (A) blood and (B) spleen monocytes. Monocytes were gated as $CD45^{+}CD11b^{+}$ cells, then subdivided according to Ly6C expression.

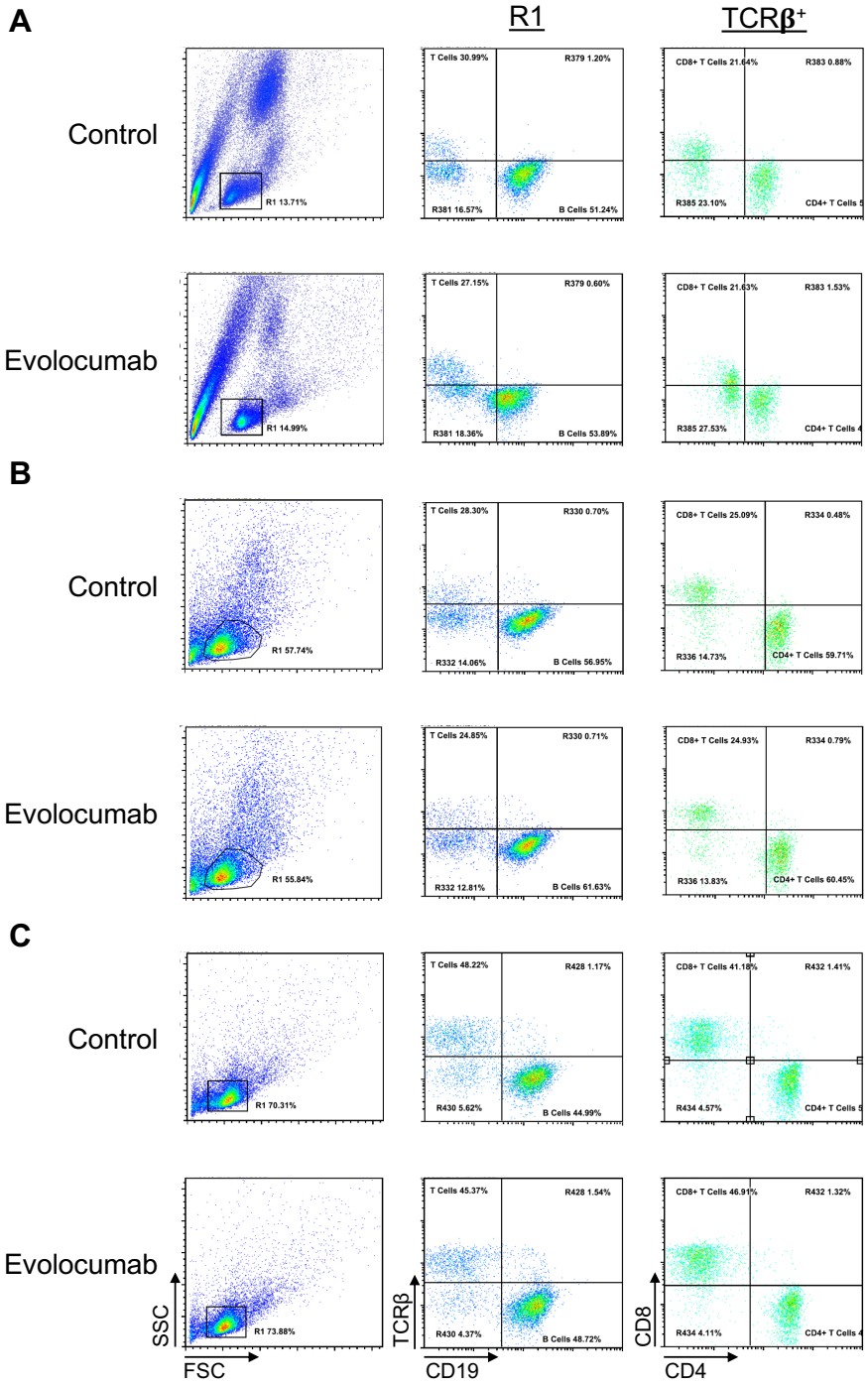

Appendix 4-6. Gating strategy for flow cytometric examination of (A) blood (B) spleen and (C) lymph node lymphocytes. Lymphocytes were identified by their characteristic forward- and side-scatter profiles. B lymphocytes were defined as $CD19^+$ cells, and T cells as $TCR\beta^+$ cells. T lymphocytes were subdivided into $TCR\beta^+CD4^+$ and $TCR\beta^+CD8^+$ cells.

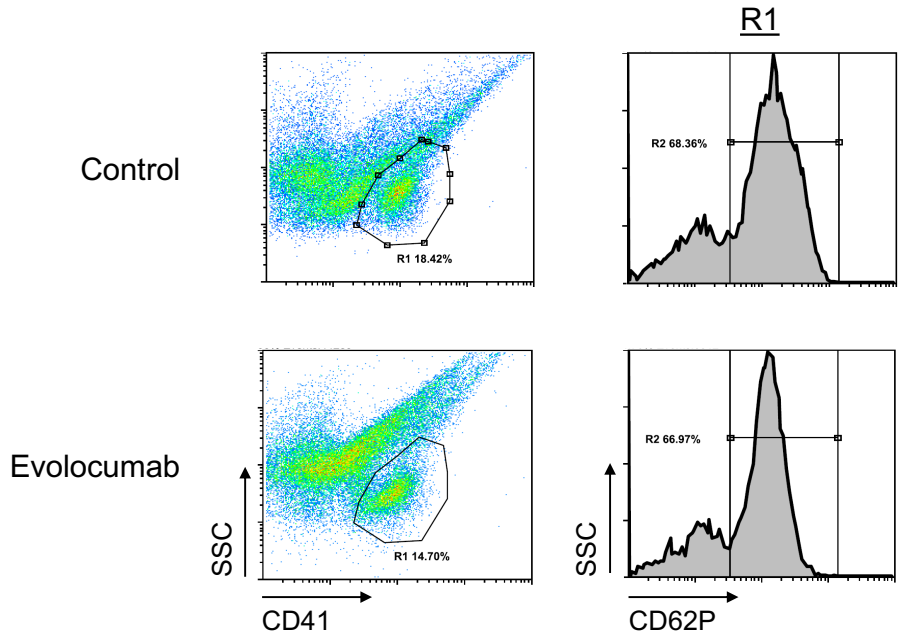

Appendix 4-7. Gating strategy for flow cytometric examination of platelet activation. Platelets were defined as $CD41^{+}$ cells and activation status identified by CD62P expression.

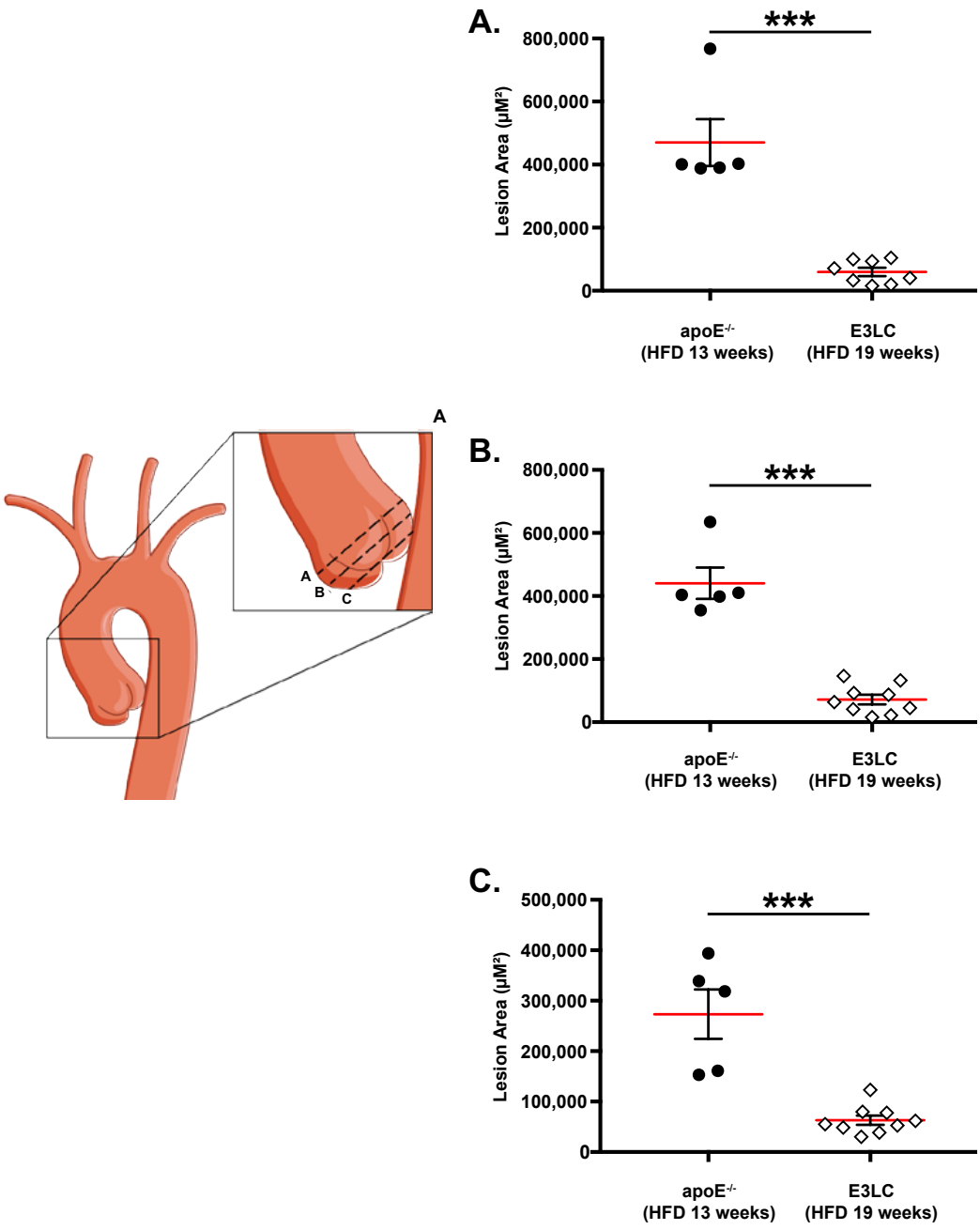

Appendix 5-1. Smaller diet-induced atherosclerotic plaques in female E3LC mice than apoE-/- mice at all 3 levels of aortic sinus atheroma. Frozen sections of aortic sinus atheroma were stained with H&E and lesion area quantified at different levels, (A) distal (B) middle (C) proximal of the aortic sinus. Data was analysed using non-parametric Mann-Whitney U test. *** $p<0.001$. Error bars represent mean ± SEM.

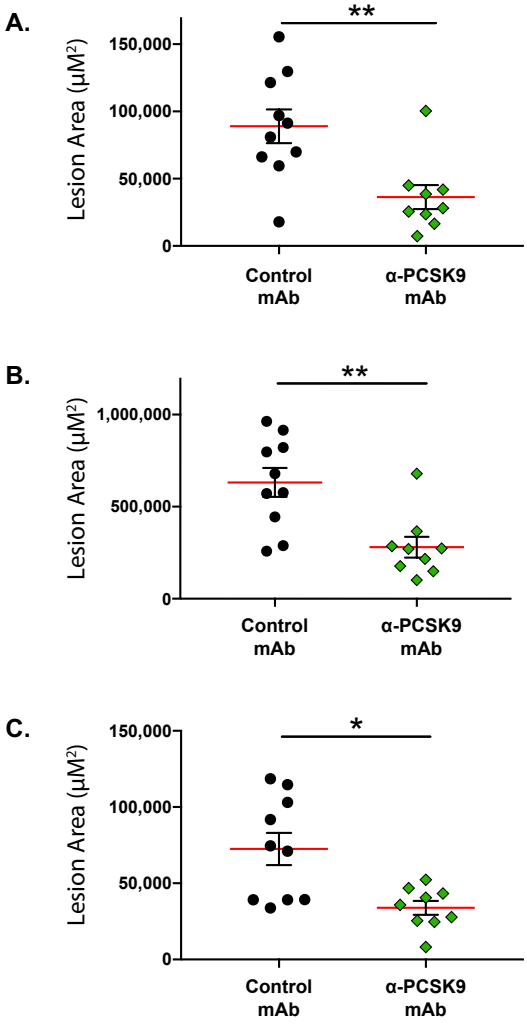

Appendix 6-1. PCSK9 inhibition significantly reduces the size of aortic sinus plaques in all 3 segments examined. Frozen sections of aortic sinus in female E3LC fed a high fat diet were stained with oil red-o and lesion area was measured at (A) distal (B) middle and (C) proximal levels (Appendix 5-1 for schema). Data was analysed using non-parametric Mann-Whitney U test, *$p<0.05$, **$p<0.01$. Error bars represent mean ± SEM.

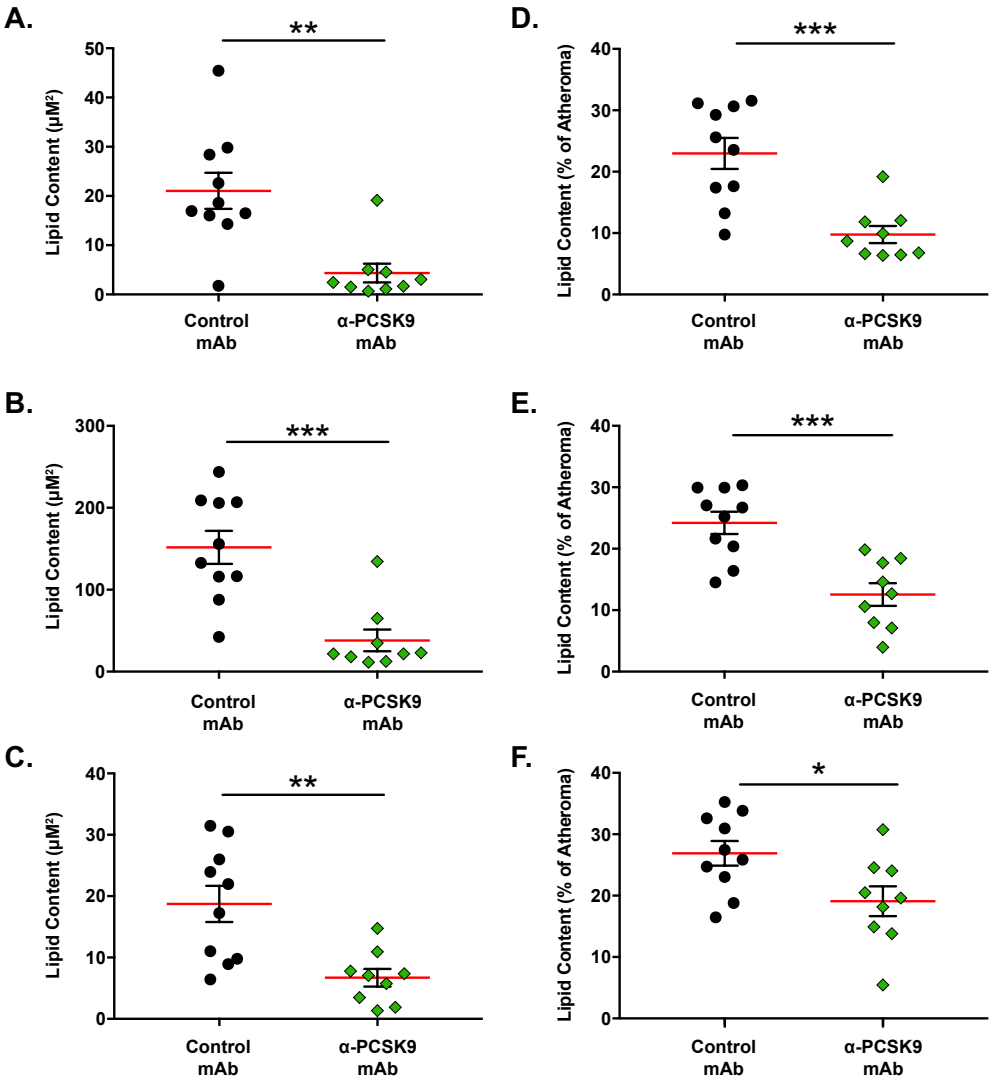

Appendix 6-2. PCSK9 inhibition significantly reduces the lipid content at all 3 levels of aortic sinus atheroma. Frozen sections of aortic sinus in female E3LC mice fed a high fat diet were stained with oil red-o, where neutral lipid stained red. Quantification of area of lipid and percentage lipid content in (A, D) distal, (B, E) middle (C, F) proximal part of the aortic sinus. Data was analysed using non-parametric Mann-Whitney U test, *$p<0.05$, **$p<0.01$, ***$p<0.001$. Error bars represent mean ± SEM.

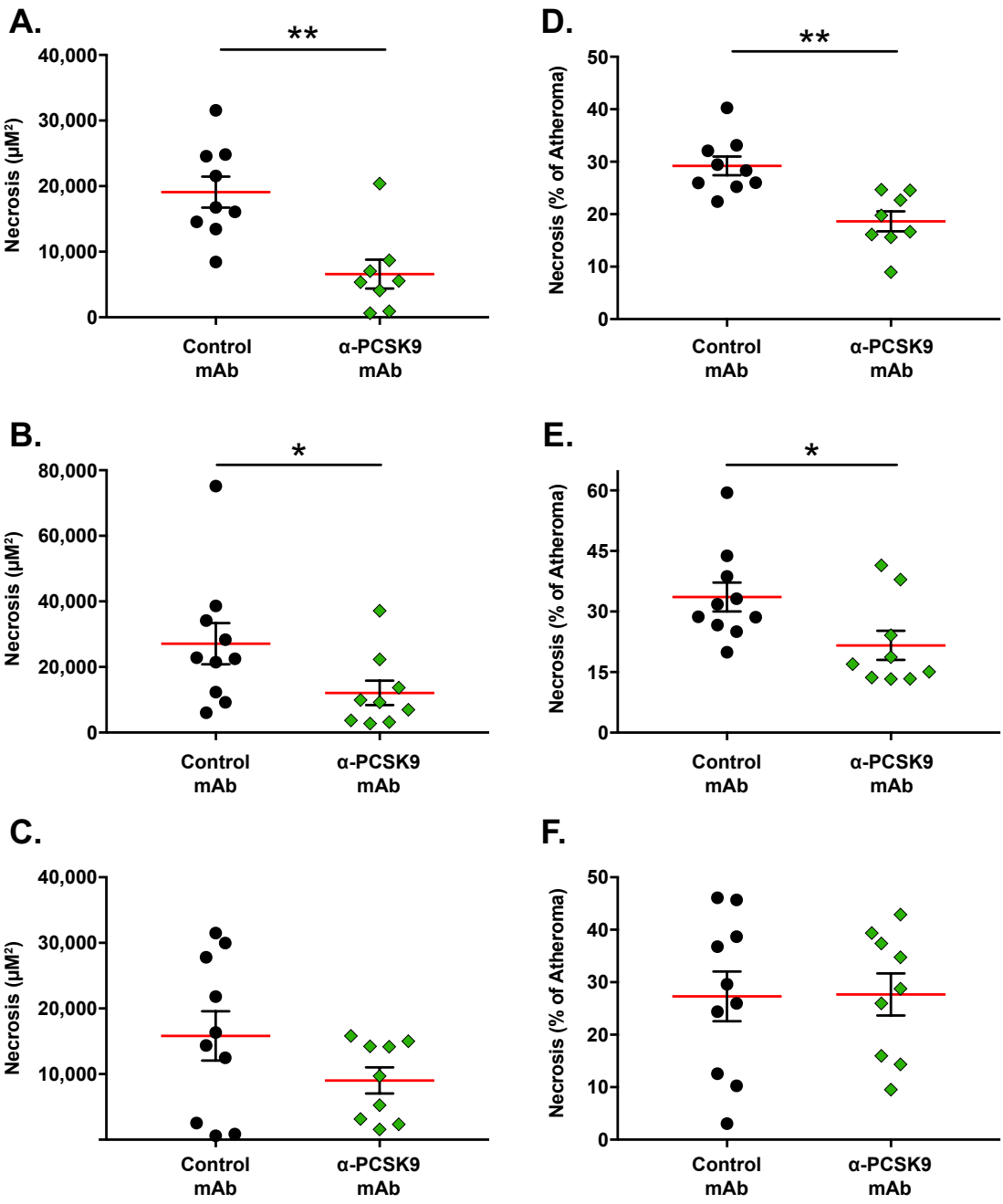

Appendix 6-3. PCSK9 inhibition inconsistently reduces the area of necrosis at the 3 levels of aortic sinus atheroma. Frozen sections of aortic sinus in female E3LC mice fed a high fat diet were stained with H&E, where neutral lipid stained red. Quantification of area of necrosis and percentage necrotic area in (A, D) distal, (B, E) middle (C, F) proximal parts of the aortic sinus. Data was analysed using non-parametric Mann-Whitney U test, *p<0.05, **p<0.01. Error bar represents mean ± SEM.

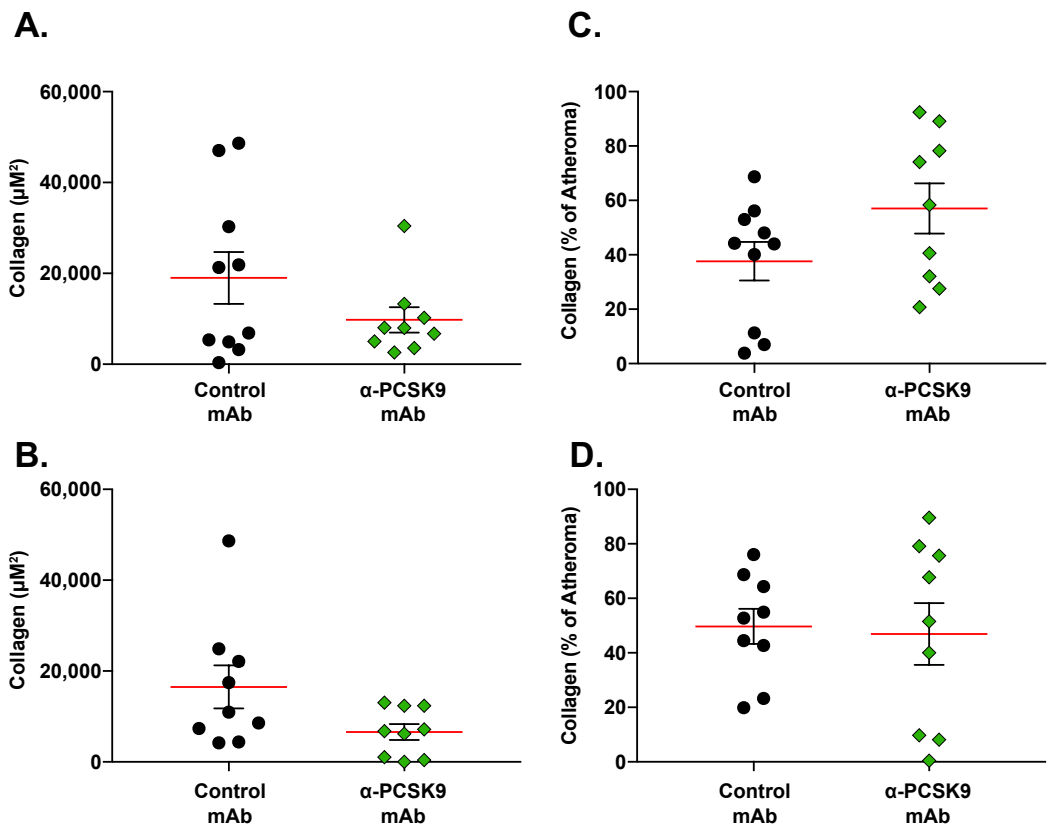

Appendix 6-4. PCSK9 inhibition does not change collagen content at the 2 levels of aortic sinus atheroma. Frozen sections of aortic sinus in female E3LC mice fed a high fat diet were stained with picrosirius red and examined under polarised light. Quantification of collagen content measured in absolute area and when normalised to atheroma at (A, C) distal and (B, D) proximal sections. Data was analysed using non-parametric Mann-Whitney U test. Error bar represents mean ± SEM.

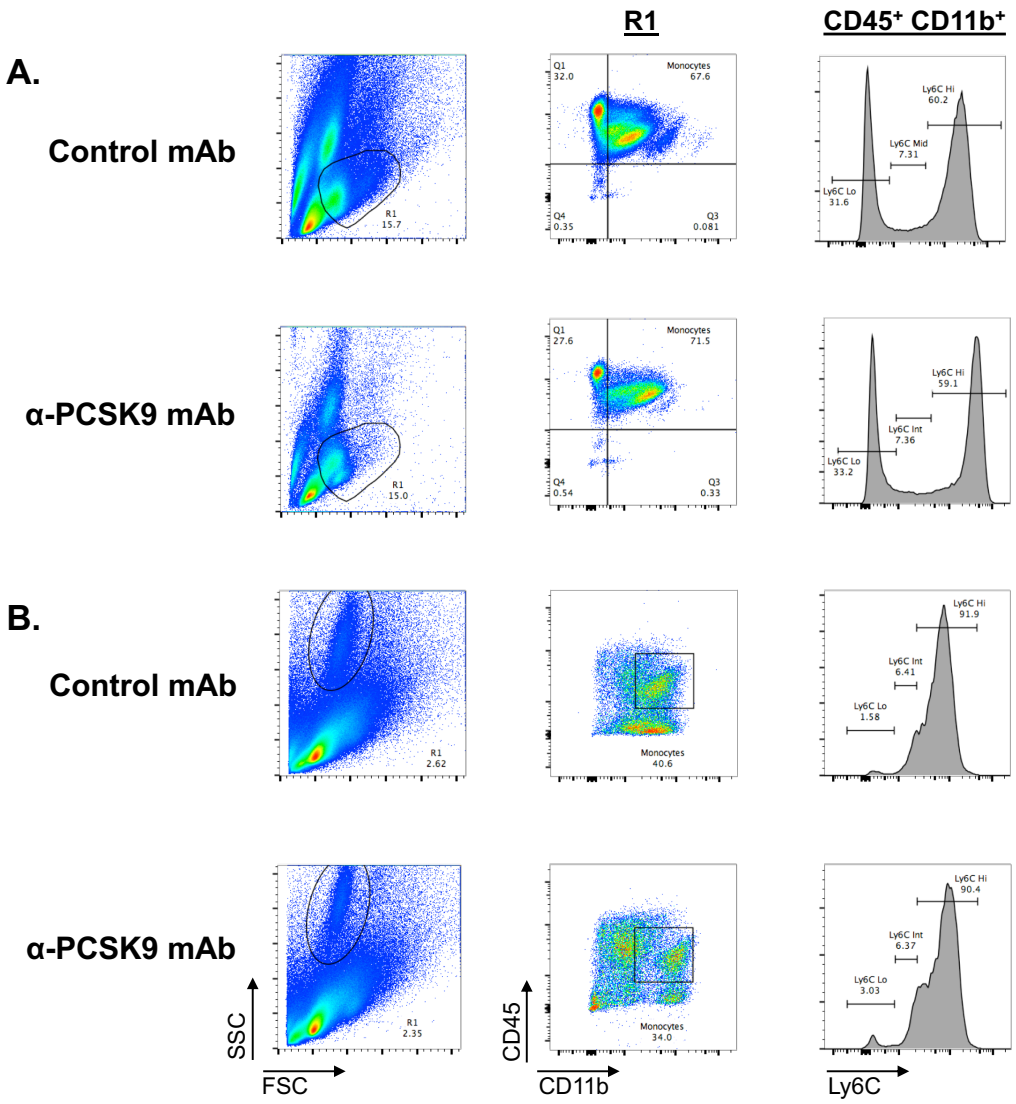

Appendix 6-5. Gating strategy for monocytes and its subpopulations in the (A) blood and (B) spleen. Monocytes were defined as $CD45^{+}CD11b^{+}$ cells, then subdivided according to their Ly6C expression.

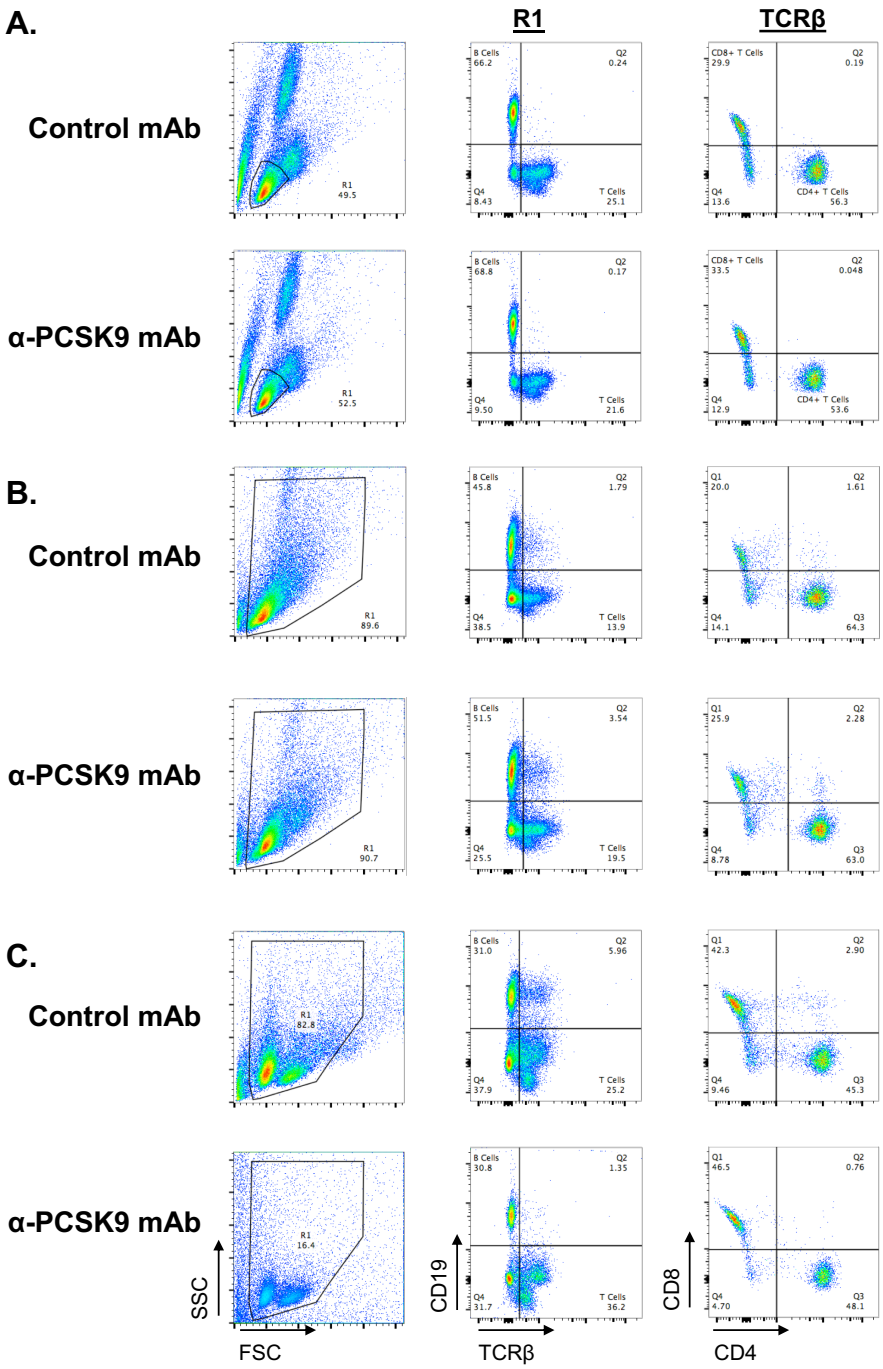

Appendix 6-6. Gating strategy for lymphocytes and its subpopulations in (A) blood (B) spleen and (C) lymph nodes. Lymphocytes were first identified based on characteristic forward and side scatter profiles. B lymphocytes were defined as $CD19^+$ cells, and T lymphocytes as $TCR\beta^+$ cells. T lymphocytes were subdivided into $TCR\beta^+CD4^+$ and $TCR\beta^+CD8^+$ cells.

BIBLIOGRAPHY

1 Napoli, C. *et al.* Fatty streak formation occurs in human fetal aortas and is greatly enhanced by maternal hypercholesterolemia. Intimal accumulation of low density lipoprotein and its oxidation precede monocyte recruitment into early atherosclerotic lesions. *J. Clin. Invest.* **100**, 2680-2690, doi:10.1172/JCI119813 (1997).

2 Virmani, R. *et al.* Atherosclerotic plaque progression and vulnerability to rupture: angiogenesis as a source of intraplaque hemorrhage. *Arterioscler. Thromb. Vasc. Biol.* **25**, 2054-2061 (2005).

3 Kolodgie, F. D. *et al.* Intraplaque hemorrhage and progression of coronary atheroma. *N. Engl. J. Med.* **349**, 2316-2325 (2003).

4 Falk, E. Pathogenesis of atherosclerosis. *J. Am. Coll. Cardiol.* **47**, C7-12, doi:10.1016/j.jacc.2005.09.068 (2006).

5 Collaborators, G. B. D. C. o. D. Global, regional, and national age-sex specific mortality for 264 causes of death, 1980-2016: a systematic analysis for the Global Burden of Disease Study 2016. *Lancet* **390**, 1151-1210, doi:10.1016/S0140-6736(17)32152-9 (2017).

6 Ohsfeldt, R. L., Gandhi, S. K., Fox, K. M., Bullano, M. F. & Davidson, M. Medical and cost burden of atherosclerosis among patients treated in routine clinical practice. *J. Med. Econ.* **13**, 500-507, doi:10.3111/13696998.2010.506348 (2010).

7 Moran, A. *et al.* Future cardiovascular disease in china: markov model and risk factor scenario projections from the coronary heart disease policy model-china. *Circ. Cardiovasc. Qual. Outcomes* **3**, 243-252, doi:10.1161/CIRCOUTCOMES.109.910711 (2010).

8 Stary, H. C. *et al.* A definition of the intima of human arteries and of its atherosclerosis-prone regions. A report from the Committee on Vascular Lesions of

the Council on Arteriosclerosis, American Heart Association. *Circulation* **85**, 391-405 (1992).

9 Stary, H. C. *et al.* A definition of advanced types of atherosclerotic lesions and a histological classification of atherosclerosis. A report from the Committee on Vascular Lesions of the Council on Arteriosclerosis, American Heart Association. *Circulation* **92**, 1355-1374 (1995).

10 Stary, H. C. *et al.* A definition of initial, fatty streak, and intermediate lesions of atherosclerosis. A report from the Committee on Vascular Lesions of the Council on Arteriosclerosis, American Heart Association. *Circulation* **89**, 2462-2478 (1994).

11 Schwartz, S. M., deBlois, D. & O'Brien, E. R. The intima. Soil for atherosclerosis and restenosis. *Circ. Res.* **77**, 445-465 (1995).

12 Gimbrone, M. A., Jr. & Garcia-Cardena, G. Endothelial Cell Dysfunction and the Pathobiology of Atherosclerosis. *Circ. Res.* **118**, 620-636, doi:10.1161/CIRCRESAHA.115.306301 (2016).

13 Moore, K. J., Sheedy, F. J. & Fisher, E. A. Macrophages in atherosclerosis: a dynamic balance. *Nat. Rev. Immunol.* **13**, 709-721, doi:10.1038/nri3520 (2013).

14 Doran, A. C., Meller, N. & McNamara, C. A. Role of smooth muscle cells in the initiation and early progression of atherosclerosis. *Arterioscler. Thromb. Vasc. Biol.* **28**, 812-819, doi:10.1161/ATVBAHA.107.159327 (2008).

15 Virmani, R., Kolodgie, F. D., Burke, A. P., Farb, A. & Schwartz, S. M. Lessons from sudden coronary death: a comprehensive morphological classification scheme for atherosclerotic lesions. *Arterioscler. Thromb. Vasc. Biol.* **20**, 1262-1275 (2000).

16 Schaar, J. A. *et al.* Terminology for high-risk and vulnerable coronary artery plaques. Report of a meeting on the vulnerable plaque, June 17 and 18, 2003, Santorini, Greece. *Eur. Heart J.* **25**, 1077-1082, doi:10.1016/j.ehj.2004.01.002 (2004).

17 Bentzon, J. F., Otsuka, F., Virmani, R. & Falk, E. Mechanisms of plaque formation and rupture. *Circ. Res.* **114**, 1852-1866, doi:10.1161/CIRCRESAHA.114.302721 (2014).

18 Falk, E., Nakano, M., Bentzon, J. F., Finn, A. V. & Virmani, R. Update on acute coronary syndromes: the pathologists' view. *Eur. Heart J.* **34**, 719-728, doi:10.1093/eurheartj/ehs411 (2013).

19 Jia, H. *et al.* In vivo diagnosis of plaque erosion and calcified nodule in patients with acute coronary syndrome by intravascular optical coherence tomography. *J. Am. Coll. Cardiol.* **62**, 1748-1758, doi:10.1016/j.jacc.2013.05.071 (2013).

20 Hao, H. *et al.* Phenotypic modulation of intima and media smooth muscle cells in fatal cases of coronary artery lesion. *Arterioscler. Thromb. Vasc. Biol.* **26**, 326-332, doi:10.1161/01.ATV.0000199393.74656.4c (2006).

21 Kramer, M. C. *et al.* Relationship of thrombus healing to underlying plaque morphology in sudden coronary death. *J. Am. Coll. Cardiol.* **55**, 122-132, doi:10.1016/j.jacc.2009.09.007 (2010).

22 Kojima, S. *et al.* Is preinfarction angina related to the presence or absence of coronary plaque rupture? *Heart* **83**, 64-68 (2000).

23 Farb, A. *et al.* Coronary plaque erosion without rupture into a lipid core. A frequent cause of coronary thrombosis in sudden coronary death. *Circulation* **93**, 1354-1363 (1996).

24 Xu, Y. *et al.* Prevalence, distribution, predictors, and outcomes of patients with calcified nodules in native coronary arteries: a 3-vessel intravascular ultrasound analysis from Providing Regional Observations to Study Predictors of Events in the Coronary Tree (PROSPECT). *Circulation* **126**, 537-545, doi:10.1161/CIRCULATIONAHA.111.055004 (2012).

25 Kirii, H. *et al.* Lack of interleukin-1beta decreases the severity of atherosclerosis in ApoE-deficient mice. *Arterioscler. Thromb. Vasc. Biol.* **23**, 656-660, doi:10.1161/01.ATV.0000064374.15232.C3 (2003).

26 Ridker, P. M. *et al.* Antiinflammatory Therapy with Canakinumab for Atherosclerotic Disease. *N. Engl. J. Med.* **377**, 1119-1131, doi:10.1056/NEJMoa1707914 (2017).

27 Ginsberg, H. N. Lipoprotein physiology. *Endocrinol. Metab. Clin. North Am.* **27**, 503-519 (1998).

28 Feingold, K. a. G., C. . *Introduction to Lipids and Lipoproteins*, <http://mdanderson.libanswers.com/faq/26219> (2018).

29 Rosenson, R. S. *et al.* Cholesterol efflux and atheroprotection: advancing the concept of reverse cholesterol transport. *Circulation* **125**, 1905-1919, doi:10.1161/CIRCULATIONAHA.111.066589 (2012).

30 Ference, B. A. *et al.* Low-density lipoproteins cause atherosclerotic cardiovascular disease. 1. Evidence from genetic, epidemiologic, and clinical studies. A consensus statement from the European Atherosclerosis Society Consensus Panel. *Eur. Heart J.*, doi:10.1093/eurheartj/ehx144 (2017).

31 Investigators, A.-H. *et al.* Niacin in patients with low HDL cholesterol levels receiving intensive statin therapy. *N. Engl. J. Med.* **365**, 2255-2267, doi:10.1056/NEJMoa1107579 (2011).

32 Musunuru, K. & Kathiresan, S. Surprises From Genetic Analyses of Lipid Risk Factors for Atherosclerosis. *Circ. Res.* **118**, 579-585, doi:10.1161/CIRCRESAHA.115.306398 (2016).

33 Tall, A. R. & Rader, D. J. Trials and Tribulations of CETP Inhibitors. *Circ. Res.* **122**, 106-112, doi:10.1161/CIRCRESAHA.117.311978 (2018).

34 Berberich, A. J. & Hegele, R. A. The complex molecular genetics of familial hypercholesterolaemia. *Nat. Rev. Cardiol.*, doi:10.1038/s41569-018-0052-6 (2018).

35 Ishibashi, S., Herz, J., Maeda, N., Goldstein, J. L. & Brown, M. S. The two-receptor model of lipoprotein clearance: tests of the hypothesis in "knockout" mice lacking the low density lipoprotein receptor, apolipoprotein E, or both proteins. *Proc. Natl. Acad. Sci. U. S. A.* **91**, 4431-4435 (1994).

36 Mahley, R. W., Huang, Y. & Rall, S. C., Jr. Pathogenesis of type III hyperlipoproteinemia (dysbetalipoproteinemia). Questions, quandaries, and paradoxes. *J. Lipid Res.* **40**, 1933-1949 (1999).

37 Plump, A. S. *et al.* Severe hypercholesterolemia and atherosclerosis in apolipoprotein E-deficient mice created by homologous recombination in ES cells. *Cell* **71**, 343-353 (1992).

38 Rader, D. J. & FitzGerald, G. A. State of the art: atherosclerosis in a limited edition. *Nat. Med.* **4**, 899-900 (1998).

39 Ishibashi, S. *et al.* Hypercholesterolemia in low density lipoprotein receptor knockout mice and its reversal by adenovirus-mediated gene delivery. *J. Clin. Invest.* **92**, 883-893, doi:10.1172/JCI116663 (1993).

40 Getz, G. S. & Reardon, C. A. Diet and murine atherosclerosis. *Arterioscler. Thromb. Vasc. Biol.* **26**, 242-249, doi:10.1161/01.ATV.0000201071.49029.17 (2006).

41 Piedrahita, J. A., Zhang, S. H., Hagaman, J. R., Oliver, P. M. & Maeda, N. Generation of mice carrying a mutant apolipoprotein E gene inactivated by gene targeting in embryonic stem cells. *Proc. Natl. Acad. Sci. U. S. A.* **89**, 4471-4475 (1992).

42 Zhang, S. H., Reddick, R. L., Burkey, B. & Maeda, N. Diet-induced atherosclerosis in mice heterozygous and homozygous for apolipoprotein E gene disruption. *J. Clin. Invest.* **94**, 937-945, doi:10.1172/JCI117460 (1994).

43 Fazio, S. *et al.* Increased atherosclerosis in mice reconstituted with apolipoprotein E null macrophages. *Proc. Natl. Acad. Sci. U. S. A.* **94**, 4647-4652 (1997).

44 Kockx, M., Traini, M. & Kritharides, L. Cell-specific production, secretion, and function of apolipoprotein E. *J. Mol. Med. (Berl.)* **96**, 361-371, doi:10.1007/s00109-018-1632-y (2018).

45 Havekes, L. *et al.* Apolipoprotein E3-Leiden. A new variant of human apolipoprotein E associated with familial type III hyperlipoproteinemia. *Hum. Genet.* **73**, 157-163 (1986).

46 Wardell, M. R., Weisgraber, K. H., Havekes, L. M. & Rall, S. C., Jr. Apolipoprotein E3-Leiden contains a seven-amino acid insertion that is a tandem repeat of residues 121-127. *J. Biol. Chem.* **264**, 21205-21210 (1989).

47 van den Maagdenberg, A. M. *et al.* Transgenic mice carrying the apolipoprotein E3-Leiden gene exhibit hyperlipoproteinemia. *J. Biol. Chem.* **268**, 10540-10545 (1993).

48 van Vlijmen, B. J. *et al.* Diet-induced hyperlipoproteinemia and atherosclerosis in apolipoprotein E3-Leiden transgenic mice. *J. Clin. Invest.* **93**, 1403-1410, doi:10.1172/JCI117117 (1994).

49 Lutgens, E. *et al.* Atherosclerosis in APOE*3-Leiden transgenic mice: from proliferative to atheromatous stage. *Circulation* **99**, 276-283 (1999).

50 Westerterp, M. *et al.* Cholesteryl ester transfer protein decreases high-density lipoprotein and severely aggravates atherosclerosis in APOE*3-Leiden mice. *Arterioscler. Thromb. Vasc. Biol.* **26**, 2552-2559, doi:10.1161/01.ATV.0000243925.65265.3c (2006).

51 Delsing, D. J. *et al.* Differential effects of amlodipine and atorvastatin treatment and their combination on atherosclerosis in ApoE*3-Leiden transgenic mice. *J. Cardiovasc. Pharmacol.* **42**, 63-70 (2003).

52 Kuhnast, S. *et al.* Niacin Reduces Atherosclerosis Development in APOE*3Leiden.CETP Mice Mainly by Reducing NonHDL-Cholesterol. *PLoS One* **8**, e66467, doi:10.1371/journal.pone.0066467 (2013).

53 Bijland, S. *et al.* Fenofibrate increases very low density lipoprotein triglyceride production despite reducing plasma triglyceride levels in APOE*3-Leiden.CETP mice. *J. Biol. Chem.* **285**, 25168-25175, doi:10.1074/jbc.M110.123992 (2010).

54 de Haan, W. *et al.* Torcetrapib does not reduce atherosclerosis beyond atorvastatin and induces more proinflammatory lesions than atorvastatin. *Circulation* **117**, 2515-2522, doi:10.1161/CIRCULATIONAHA.107.761965 (2008).

55 Ason, B. *et al.* PCSK9 inhibition fails to alter hepatic LDLR, circulating cholesterol, and atherosclerosis in the absence of ApoE. *J. Lipid Res.* **55**, 2370-2379, doi:10.1194/jlr.M053207 (2014).

56 Gijbels, M. J. *et al.* Progression and regression of atherosclerosis in APOE3-Leiden transgenic mice: an immunohistochemical study. *Atherosclerosis* **143**, 15-25 (1999).

57 Calara, F. *et al.* Spontaneous plaque rupture and secondary thrombosis in apolipoprotein E-deficient and LDL receptor-deficient mice. *J. Pathol.* **195**, 257-263, doi:10.1002/path.915 (2001).

58 Williams, H., Johnson, J. L., Carson, K. G. & Jackson, C. L. Characteristics of intact and ruptured atherosclerotic plaques in brachiocephalic arteries of apolipoprotein E knockout mice. *Arterioscler. Thromb. Vasc. Biol.* **22**, 788-792 (2002).

59 Gough, P. J., Gomez, I. G., Wille, P. T. & Raines, E. W. Macrophage expression of active MMP-9 induces acute plaque disruption in apoE-deficient mice. *J. Clin. Invest.* **116**, 59-69, doi:10.1172/JCI25074 (2006).

60 von der Thusen, J. H. *et al.* Induction of atherosclerotic plaque rupture in apolipoprotein E-/- mice after adenovirus-mediated transfer of p53. *Circulation* **105**, 2064-2070 (2002).

61 Hu, J. H. *et al.* Overexpression of urokinase by plaque macrophages causes histological features of plaque rupture and increases vascular matrix metalloproteinase activity in aged apolipoprotein e-null mice. *Circulation* **121**, 1637-1644, doi:10.1161/CIRCULATIONAHA.109.914945 (2010).

62 Emini Veseli, B. *et al.* Animal models of atherosclerosis. *Eur. J. Pharmacol.* **816**, 3-13, doi:10.1016/j.ejphar.2017.05.010 (2017).

63 Chen, Y. C. *et al.* A novel mouse model of atherosclerotic plaque instability for drug testing and mechanistic/therapeutic discoveries using gene and microRNA expression profiling. *Circ. Res.* **113**, 252-265, doi:10.1161/CIRCRESAHA.113.301562 (2013).

64 Van der Donckt, C. *et al.* Elastin fragmentation in atherosclerotic mice leads to intraplaque neovascularization, plaque rupture, myocardial infarction, stroke, and sudden death. *Eur. Heart J.* **36**, 1049-1058, doi:10.1093/eurheartj/ehu041 (2015).

65 Abifadel, M. *et al.* Mutations in PCSK9 cause autosomal dominant hypercholesterolemia. *Nat. Genet.* **34**, 154-156, doi:10.1038/ng1161 (2003).

66 Sabatine, M. S. *et al.* Evolocumab and Clinical Outcomes in Patients with Cardiovascular Disease. *N. Engl. J. Med.* **376**, 1713-1722, doi:10.1056/NEJMoa1615664 (2017).

67 Kumbhani, D. *Evaluation of Cardiovascular Outcomes After an Acute Coronary Syndrome During Treatment With Alirocumab - ODYSSEY OUTCOMES*, <http://www.acc.org/latest-in-cardiology/clinical-trials/2018/03/09/08/02/odyssey-outcomes> (2018, March 10).

68 Seidah, N. G. *et al.* The secretory proprotein convertase neural apoptosis-regulated convertase 1 (NARC-1): liver regeneration and neuronal differentiation. *Proc. Natl. Acad. Sci. U. S. A.* **100**, 928-933, doi:10.1073/pnas.0335507100 (2003).

69 Seidah, N. G., Awan, Z., Chretien, M. & Mbikay, M. PCSK9: a key modulator of cardiovascular health. *Circ. Res.* **114**, 1022-1036, doi:10.1161/CIRCRESAHA.114.301621 (2014).

70 Dewpura, T. *et al.* PCSK9 is phosphorylated by a Golgi casein kinase-like kinase ex vivo and circulates as a phosphoprotein in humans. *FEBS J* **275**, 3480-3493, doi:10.1111/j.1742-4658.2008.06495.x (2008).

71 Benjannet, S., Rhainds, D., Hamelin, J., Nassoury, N. & Seidah, N. G. The proprotein convertase (PC) PCSK9 is inactivated by furin and/or PC5/6A: functional consequences of natural mutations and post-translational modifications. *J. Biol. Chem.* **281**, 30561-30572, doi:10.1074/jbc.M606495200 (2006).

72 Lipari, M. T. *et al.* Furin-cleaved proprotein convertase subtilisin/kexin type 9 (PCSK9) is active and modulates low density lipoprotein receptor and serum cholesterol levels. *J. Biol. Chem.* **287**, 43482-43491, doi:10.1074/jbc.M112.380618 (2012).

73 Horton, J. D., Cohen, J. C. & Hobbs, H. H. PCSK9: a convertase that coordinates LDL catabolism. *J. Lipid Res.* **50 Suppl**, S172-177, doi:10.1194/jlr.R800091-JLR200 (2009).

74 Dadu, R. T. & Ballantyne, C. M. Lipid lowering with PCSK9 inhibitors. *Nat. Rev. Cardiol.* **11**, 563-575, doi:10.1038/nrcardio.2014.84 (2014).

75 Maxwell, K. N. & Breslow, J. L. Adenoviral-mediated expression of Pcsk9 in mice results in a low-density lipoprotein receptor knockout phenotype. *Proc. Natl. Acad. Sci. U. S. A.* **101**, 7100-7105, doi:10.1073/pnas.0402133101 (2004).

76 Park, S. W., Moon, Y. A. & Horton, J. D. Post-transcriptional regulation of low density lipoprotein receptor protein by proprotein convertase subtilisin/kexin type 9a in mouse liver. *J. Biol. Chem.* **279**, 50630-50638, doi:10.1074/jbc.M410077200 (2004).

77 Goldstein, J. L. & Brown, M. S. A century of cholesterol and coronaries: from plaques to genes to statins. *Cell* **161**, 161-172, doi:10.1016/j.cell.2015.01.036 (2015).

78 Zhang, D. W. *et al.* Binding of proprotein convertase subtilisin/kexin type 9 to epidermal growth factor-like repeat A of low density lipoprotein receptor decreases receptor recycling and increases degradation. *J. Biol. Chem.* **282**, 18602-18612, doi:10.1074/jbc.M702027200 (2007).

79 Poirier, S. *et al.* The proprotein convertase PCSK9 induces the degradation of low density lipoprotein receptor (LDLR) and its closest family members VLDLR and ApoER2. *J. Biol. Chem.* **283**, 2363-2372, doi:10.1074/jbc.M708098200 (2008).

80 Canuel, M. *et al.* Proprotein convertase subtilisin/kexin type 9 (PCSK9) can mediate degradation of the low density lipoprotein receptor-related protein 1 (LRP-1). *PLoS One* **8**, e64145, doi:10.1371/journal.pone.0064145 (2013).

81 Lagace, T. A. *et al.* Secreted PCSK9 decreases the number of LDL receptors in hepatocytes and in livers of parabiotic mice. *J. Clin. Invest.* **116**, 2995-3005, doi:10.1172/JCI29383 (2006).

82 Rashid, S. *et al.* Decreased plasma cholesterol and hypersensitivity to statins in mice lacking Pcsk9. *Proc. Natl. Acad. Sci. U. S. A.* **102**, 5374-5379, doi:10.1073/pnas.0501652102 (2005).

83 Dubuc, G. *et al.* Statins upregulate PCSK9, the gene encoding the proprotein convertase neural apoptosis-regulated convertase-1 implicated in familial

hypercholesterolemia. *Arterioscler. Thromb. Vasc. Biol.* **24**, 1454-1459, doi:10.1161/01.ATV.0000134621.14315.43 (2004).

84 Welder, G. *et al.* High-dose atorvastatin causes a rapid sustained increase in human serum PCSK9 and disrupts its correlation with LDL cholesterol. *J. Lipid Res.* **51**, 2714-2721, doi:10.1194/jlr.M008144 (2010).

85 Zaid, A. *et al.* Proprotein convertase subtilisin/kexin type 9 (PCSK9): hepatocyte-specific low-density lipoprotein receptor degradation and critical role in mouse liver regeneration. *Hepatology* **48**, 646-654, doi:10.1002/hep.22354 (2008).

86 Labonte, P. *et al.* PCSK9 impedes hepatitis C virus infection in vitro and modulates liver CD81 expression. *Hepatology* **50**, 17-24, doi:10.1002/hep.22911 (2009).

87 Mbikay, M. *et al.* PCSK9-deficient mice exhibit impaired glucose tolerance and pancreatic islet abnormalities. *FEBS Lett.* **584**, 701-706, doi:10.1016/j.febslet.2009.12.018 (2010).

88 Chogtu, B., Magazine, R. & Bairy, K. L. Statin use and risk of diabetes mellitus. *World J. Diabetes* **6**, 352-357, doi:10.4239/wjd.v6.i2.352 (2015).

89 Denis, M. *et al.* Gene inactivation of proprotein convertase subtilisin/kexin type 9 reduces atherosclerosis in mice. *Circulation* **125**, 894-901, doi:10.1161/CIRCULATIONAHA.111.057406 (2012).

90 Kuhnast, S. *et al.* Alirocumab inhibits atherosclerosis, improves the plaque morphology, and enhances the effects of a statin. *J. Lipid Res.* **55**, 2103-2112, doi:10.1194/jlr.M051326 (2014).

91 Landlinger, C. *et al.* The AT04A vaccine against proprotein convertase subtilisin/kexin type 9 reduces total cholesterol, vascular inflammation, and atherosclerosis in APOE*3Leiden.CETP mice. *Eur. Heart J.* **38**, 2499-2507, doi:10.1093/eurheartj/ehx260 (2017).

92 Abifadel, M. *et al.* Living the PCSK9 adventure: from the identification of a new gene in familial hypercholesterolemia towards a potential new class of anticholesterol drugs. *Curr Atheroscler Rep* **16**, 439, doi:10.1007/s11883-014-0439-8 (2014).

93 Cohen, J. C., Boerwinkle, E., Mosley, T. H., Jr. & Hobbs, H. H. Sequence variations in PCSK9, low LDL, and protection against coronary heart disease. *N. Engl. J. Med.* **354**, 1264-1272, doi:10.1056/NEJMoa054013 (2006).

94 Abboud, S. *et al.* Proprotein convertase subtilisin/kexin type 9 (PCSK9) gene is a risk factor of large-vessel atherosclerosis stroke. *PLoS One* **2**, e1043, doi:10.1371/journal.pone.0001043 (2007).

95 Folsom, A. R., Peacock, J. M., Boerwinkle, E. & Atherosclerosis Risk in Communities Study, I. Variation in PCSK9, low LDL cholesterol, and risk of peripheral arterial disease. *Atherosclerosis* **202**, 211-215, doi:10.1016/j.atherosclerosis.2008.03.009 (2009).

96 Kathiresan, S. & Myocardial Infarction Genetics, C. A PCSK9 missense variant associated with a reduced risk of early-onset myocardial infarction. *N. Engl. J. Med.* **358**, 2299-2300, doi:10.1056/NEJMc0707445 (2008).

97 Schneider, D. J. Factors contributing to increased platelet reactivity in people with diabetes. *Diabetes Care* **32**, 525-527, doi:10.2337/dc08-1865 (2009).

98 Chen, K. & Keaney, J. F., Jr. Evolving concepts of oxidative stress and reactive oxygen species in cardiovascular disease. *Curr Atheroscler Rep* **14**, 476-483, doi:10.1007/s11883-012-0266-8 (2012).

99 DeWood, M. A. *et al.* Prevalence of total coronary occlusion during the early hours of transmural myocardial infarction. *N. Engl. J. Med.* **303**, 897-902, doi:10.1056/NEJM198010163031601 (1980).

100 Wallentin, L. *et al.* Ticagrelor versus clopidogrel in patients with acute coronary syndromes. *N. Engl. J. Med.* **361**, 1045-1057, doi:10.1056/NEJMoa0904327 (2009).

101 Yusuf, S. *et al.* Effects of clopidogrel in addition to aspirin in patients with acute coronary syndromes without ST-segment elevation. *N. Engl. J. Med.* **345**, 494-502, doi:10.1056/NEJMoa010746 (2001).

102 Linden, M. D. Platelet physiology. *Methods Mol. Biol.* **992**, 13-30, doi:10.1007/978-1-62703-339-8_2 (2013).

103 Denis, C. V. & Wagner, D. D. Platelet adhesion receptors and their ligands in mouse models of thrombosis. *Arterioscler. Thromb. Vasc. Biol.* **27**, 728-739, doi:10.1161/01.ATV.0000259359.52265.62 (2007).

104 Jackson, S. P. Arterial thrombosis--insidious, unpredictable and deadly. *Nat. Med.* **17**, 1423-1436, doi:10.1038/nm.2515 (2011).

105 Versteeg, H. H., Heemskerk, J. W., Levi, M. & Reitsma, P. H. New fundamentals in hemostasis. *Physiol. Rev.* **93**, 327-358, doi:10.1152/physrev.00016.2011 (2013).

106 Morrissey, J. H., Choi, S. H. & Smith, S. A. Polyphosphate: an ancient molecule that links platelets, coagulation, and inflammation. *Blood* **119**, 5972-5979, doi:10.1182/blood-2012-03-306605 (2012).

107 Darbousset, R. *et al.* Tissue factor-positive neutrophils bind to injured endothelial wall and initiate thrombus formation. *Blood* **120**, 2133-2143, doi:10.1182/blood-2012-06-437772 (2012).

108 Maugeri, N. *et al.* Human polymorphonuclear leukocytes produce and express functional tissue factor upon stimulation. *J. Thromb. Haemost.* **4**, 1323-1330, doi:10.1111/j.1538-7836.2006.01968.x (2006).

109 Brinkmann, V. *et al.* Neutrophil extracellular traps kill bacteria. *Science* **303**, 1532-1535, doi:10.1126/science.1092385 (2004).

110 Fuchs, T. A. *et al.* Novel cell death program leads to neutrophil extracellular traps. *J. Cell Biol.* **176**, 231-241, doi:10.1083/jcb.200606027 (2007).

111 Papayannopoulos, V., Metzler, K. D., Hakkim, A. & Zychlinsky, A. Neutrophil elastase and myeloperoxidase regulate the formation of neutrophil extracellular traps. *J. Cell Biol.* **191**, 677-691, doi:10.1083/jcb.201006052 (2010).

112 Li, P. *et al.* PAD4 is essential for antibacterial innate immunity mediated by neutrophil extracellular traps. *J. Exp. Med.* **207**, 1853-1862, doi:10.1084/jem.20100239 (2010).

113 von Bruhl, M. L. *et al.* Monocytes, neutrophils, and platelets cooperate to initiate and propagate venous thrombosis in mice in vivo. *J. Exp. Med.* **209**, 819-835, doi:10.1084/jem.20112322 (2012).

114 Semeraro, F. *et al.* Extracellular histones promote thrombin generation through platelet-dependent mechanisms: involvement of platelet TLR2 and TLR4. *Blood* **118**, 1952-1961, doi:10.1182/blood-2011-03-343061 (2011).

115 Ammollo, C. T., Semeraro, F., Xu, J., Esmon, N. L. & Esmon, C. T. Extracellular histones increase plasma thrombin generation by impairing thrombomodulin-dependent protein C activation. *J. Thromb. Haemost.* **9**, 1795-1803, doi:10.1111/j.1538-7836.2011.04422.x (2011).

116 Semeraro, F., Ammollo, C. T., Esmon, N. L. & Esmon, C. T. Histones induce phosphatidylserine exposure and a procoagulant phenotype in human red blood cells. *J. Thromb. Haemost.* **12**, 1697-1702, doi:10.1111/jth.12677 (2014).

117 Xu, J. *et al.* Extracellular histones are major mediators of death in sepsis. *Nat. Med.* **15**, 1318-1321, doi:10.1038/nm.2053 (2009).

118 Allen, D. H. & Tracy, P. B. Human coagulation factor V is activated to the functional cofactor by elastase and cathepsin G expressed at the monocyte surface. *J. Biol. Chem.* **270**, 1408-1415 (1995).

119 Gale, A. J., Cramer, T. J., Rozenshteyn, D. & Cruz, J. R. Detailed mechanisms of the inactivation of factor VIIIa by activated protein C in the presence of its cofactors, protein S and factor V. *J. Biol. Chem.* **283**, 16355-16362, doi:10.1074/jbc.M708985200 (2008).

120 Massberg, S. *et al.* Reciprocal coupling of coagulation and innate immunity via neutrophil serine proteases. *Nat. Med.* **16**, 887-896, doi:10.1038/nm.2184 (2010).

121 Jochum, M., Lander, S., Heimburger, N. & Fritz, H. Effect of human granulocytic elastase on isolated human antithrombin III. *Hoppe Seylers Z. Physiol. Chem.* **362**, 103-112 (1981).

122 Huang, A. L., Bosco, J. J. & Peter, K. Mast Cell: An Unexpected Villain in Venous Thromboembolism? *Circ. Res.* **121**, 899-901, doi:10.1161/CIRCRESAHA.117.311777 (2017).

123 Knight, J. S. *et al.* Peptidylarginine deiminase inhibition reduces vascular damage and modulates innate immune responses in murine models of atherosclerosis. *Circ. Res.* **114**, 947-956, doi:10.1161/CIRCRESAHA.114.303312 (2014).

124 Mangold, A. *et al.* Coronary neutrophil extracellular trap burden and deoxyribonuclease activity in ST-elevation acute coronary syndrome are predictors of ST-segment resolution and infarct size. *Circ. Res.* **116**, 1182-1192, doi:10.1161/CIRCRESAHA.116.304944 (2015).

125 Riegger, J. *et al.* Histopathological evaluation of thrombus in patients presenting with stent thrombosis. A multicenter European study: a report of the prevention of late

stent thrombosis by an interdisciplinary global European effort consortium. *Eur. Heart J.* **37**, 1538-1549, doi:10.1093/eurheartj/ehv419 (2016).

126 de Boer, O. J. *et al.* Neutrophils, neutrophil extracellular traps and interleukin-17 associate with the organisation of thrombi in acute myocardial infarction. *Thromb. Haemost.* **109**, 290-297, doi:10.1160/TH12-06-0425 (2013).

127 Brill, A. *et al.* Neutrophil extracellular traps promote deep vein thrombosis in mice. *J. Thromb. Haemost.* **10**, 136-144, doi:10.1111/j.1538-7836.2011.04544.x (2012).

128 Savchenko, A. S. *et al.* Neutrophil extracellular traps form predominantly during the organizing stage of human venous thromboembolism development. *J. Thromb. Haemost.* **12**, 860-870, doi:10.1111/jth.12571 (2014).

129 Diaz, J. A. *et al.* Plasma DNA is Elevated in Patients with Deep Vein Thrombosis. *J Vasc Surg Venous Lymphat Disord* **1**, doi:10.1016/j.jvsv.2012.12.002 (2013).

130 van Montfoort, M. L. *et al.* Circulating nucleosomes and neutrophil activation as risk factors for deep vein thrombosis. *Arterioscler. Thromb. Vasc. Biol.* **33**, 147-151, doi:10.1161/ATVBAHA.112.300498 (2013).

131 Henke, P. K. *et al.* Toll-like receptor 9 signaling is critical for early experimental deep vein thrombosis resolution. *Arterioscler. Thromb. Vasc. Biol.* **31**, 43-49, doi:10.1161/ATVBAHA.110.216317 (2011).

132 Heestermans, M. *et al.* Role of platelets, neutrophils, and factor XII in spontaneous venous thrombosis in mice. *Blood* **127**, 2630-2637, doi:10.1182/blood-2015-10-672766 (2016).

133 El-Sayed, O. M. *et al.* Intact Toll-like receptor 9 signaling in neutrophils modulates normal thrombogenesis in mice. *J. Vasc. Surg.* **64**, 1450-1458 e1451, doi:10.1016/j.jvs.2015.08.070 (2016).

134 Shantsila, E. & Lip, G. Y. The role of monocytes in thrombotic disorders. Insights from tissue factor, monocyte-platelet aggregates and novel mechanisms. *Thromb. Haemost.* **102**, 916-924, doi:10.1160/TH09-01-0023 (2009).

135 Ito, T. *et al.* High-mobility group box 1 protein promotes development of microvascular thrombosis in rats. *J. Thromb. Haemost.* **5**, 109-116, doi:10.1111/j.1538-7836.2006.02255.x (2007).

136 Toltl, L. J., Beaudin, S., Liaw, P. C. & Canadian Critical Care Translational Biology, G. Activated protein C up-regulates IL-10 and inhibits tissue factor in blood monocytes. *J. Immunol.* **181**, 2165-2173 (2008).

137 Swystun, L. L. & Liaw, P. C. The role of leukocytes in thrombosis. *Blood* **128**, 753-762, doi:10.1182/blood-2016-05-718114 (2016).

138 Ponomaryov, T., Payne, H., Fabritz, L., Wagner, D. D. & Brill, A. Mast Cells Granular Contents Are Crucial for Deep Vein Thrombosis in Mice. *Circ. Res.*, doi:10.1161/CIRCRESAHA.117.311185 (2017).

139 Pil, P. M., Chow, C. S. & Lippard, S. J. High-mobility-group 1 protein mediates DNA bending as determined by ring closures. *Proc. Natl. Acad. Sci. U. S. A.* **90**, 9465-9469 (1993).

140 Bianchi, M. E. & Beltrame, M. Upwardly mobile proteins. Workshop: the role of HMG proteins in chromatin structure, gene expression and neoplasia. *EMBO Rep* **1**, 109-114, doi:10.1093/embo-reports/kvd030 (2000).

141 Chan, J. K. *et al.* Alarmins: awaiting a clinical response. *J. Clin. Invest.* **122**, 2711-2719, doi:10.1172/JCI62423 (2012).

142 Scaffidi, P., Misteli, T. & Bianchi, M. E. Release of chromatin protein HMGB1 by necrotic cells triggers inflammation. *Nature* **418**, 191-195, doi:10.1038/nature00858 (2002).

143 Andersson, U., Yang, H. & Harris, H. High-mobility group box 1 protein (HMGB1) operates as an alarmin outside as well as inside cells. *Semin. Immunol.*, doi:10.1016/j.smim.2018.02.011 (2018).

144 Yang, H. *et al.* Reversing established sepsis with antagonists of endogenous high-mobility group box 1. *Proc. Natl. Acad. Sci. U. S. A.* **101**, 296-301, doi:10.1073/pnas.2434651100 (2004).

145 Kokkola, R. *et al.* Successful treatment of collagen-induced arthritis in mice and rats by targeting extracellular high mobility group box chromosomal protein 1 activity. *Arthritis Rheum.* **48**, 2052-2058, doi:10.1002/art.11161 (2003).

146 Yang, H. *et al.* A critical cysteine is required for HMGB1 binding to Toll-like receptor 4 and activation of macrophage cytokine release. *Proc. Natl. Acad. Sci. U. S. A.* **107**, 11942-11947, doi:10.1073/pnas.1003893107 (2010).

147 Yang, H., Wang, H., Chavan, S. S. & Andersson, U. High Mobility Group Box Protein 1 (HMGB1): The Prototypical Endogenous Danger Molecule. *Mol. Med.* **21 Suppl 1**, S6-S12, doi:10.2119/molmed.2015.00087 (2015).

148 Schiraldi, M. *et al.* HMGB1 promotes recruitment of inflammatory cells to damaged tissues by forming a complex with CXCL12 and signaling via CXCR4. *J. Exp. Med.* **209**, 551-563, doi:10.1084/jem.20111739 (2012).

149 Venereau, E. *et al.* Mutually exclusive redox forms of HMGB1 promote cell recruitment or proinflammatory cytokine release. *J. Exp. Med.* **209**, 1519-1528, doi:10.1084/jem.20120189 (2012).

150 Hoppe, G., Talcott, K. E., Bhattacharya, S. K., Crabb, J. W. & Sears, J. E. Molecular basis for the redox control of nuclear transport of the structural chromatin protein Hmgb1. *Exp. Cell Res.* **312**, 3526-3538, doi:10.1016/j.yexcr.2006.07.020 (2006).

151 Yang, H. *et al.* Redox modification of cysteine residues regulates the cytokine activity of high mobility group box-1 (HMGB1). *Mol. Med.* **18**, 250-259, doi:10.2119/molmed.2011.00389 (2012).

152 Yang, H. *et al.* MD-2 is required for disulfide HMGB1-dependent TLR4 signaling. *J. Exp. Med.* **212**, 5-14, doi:10.1084/jem.20141318 (2015).

153 Kazama, H. *et al.* Induction of immunological tolerance by apoptotic cells requires caspase-dependent oxidation of high-mobility group box-1 protein. *Immunity* **29**, 21-32, doi:10.1016/j.immuni.2008.05.013 (2008).

154 Lu, B. *et al.* JAK/STAT1 signaling promotes HMGB1 hyperacetylation and nuclear translocation. *Proc. Natl. Acad. Sci. U. S. A.* **111**, 3068-3073, doi:10.1073/pnas.1316925111 (2014).

155 Bianchi, M. E. & Manfredi, A. A. How macrophages ring the inflammation alarm. *Proc. Natl. Acad. Sci. U. S. A.* **111**, 2866-2867, doi:10.1073/pnas.1324285111 (2014).

156 Bonaldi, T. *et al.* Monocytic cells hyperacetylate chromatin protein HMGB1 to redirect it towards secretion. *EMBO J.* **22**, 5551-5560, doi:10.1093/emboj/cdg516 (2003).

157 Gardella, S. *et al.* The nuclear protein HMGB1 is secreted by monocytes via a non-classical, vesicle-mediated secretory pathway. *EMBO Rep* **3**, 995-1001, doi:10.1093/embo-reports/kvf198 (2002).

158 Lu, B. *et al.* Novel role of PKR in inflammasome activation and HMGB1 release. *Nature* **488**, 670-674, doi:10.1038/nature11290 (2012).

159 Hori, O. *et al.* The receptor for advanced glycation end products (RAGE) is a cellular binding site for amphoterin. Mediation of neurite outgrowth and co-expression of rage and amphoterin in the developing nervous system. *J. Biol. Chem.* **270**, 25752-25761 (1995).

160 Meng, X. *et al.* The differentiation of mesenchymal stem cells to vascular cells regulated by the HMGB1/RAGE axis: its application in cell therapy for transplant arteriosclerosis. *Stem Cell. Res. Ther.* **9**, 85, doi:10.1186/s13287-018-0827-z (2018).

161 Yang, D. *et al.* High mobility group box-1 protein induces the migration and activation of human dendritic cells and acts as an alarmin. *J. Leukoc. Biol.* **81**, 59-66, doi:10.1189/jlb.0306180 (2007).

162 Dumitriu, I. E., Bianchi, M. E., Bacci, M., Manfredi, A. A. & Rovere-Querini, P. The secretion of HMGB1 is required for the migration of maturing dendritic cells. *J. Leukoc. Biol.* **81**, 84-91, doi:10.1189/jlb.0306171 (2007).

163 Dumitriu, I. E. *et al.* Release of high mobility group box 1 by dendritic cells controls T cell activation via the receptor for advanced glycation end products. *J. Immunol.* **174**, 7506-7515 (2005).

164 Xu, J. *et al.* Macrophage endocytosis of high-mobility group box 1 triggers pyroptosis. *Cell Death Differ.* **21**, 1229-1239, doi:10.1038/cdd.2014.40 (2014).

165 Park, J. S. *et al.* Involvement of toll-like receptors 2 and 4 in cellular activation by high mobility group box 1 protein. *J. Biol. Chem.* **279**, 7370-7377, doi:10.1074/jbc.M306793200 (2004).

166 Wang, H. *et al.* HMG-1 as a late mediator of endotoxin lethality in mice. *Science* **285**, 248-251 (1999).

167 Andersson, U. *et al.* High mobility group 1 protein (HMG-1) stimulates proinflammatory cytokine synthesis in human monocytes. *J. Exp. Med.* **192**, 565-570 (2000).

168 Fan, J. *et al.* Hemorrhagic shock induces NAD(P)H oxidase activation in neutrophils: role of HMGB1-TLR4 signaling. *J. Immunol.* **178**, 6573-6580 (2007).

169 Tadie, J. M. *et al.* HMGB1 promotes neutrophil extracellular trap formation through interactions with Toll-like receptor 4. *Am. J. Physiol. Lung Cell Mol. Physiol.* **304**, L342-349, doi:10.1152/ajplung.00151.2012 (2013).

170 Apetoh, L. *et al.* Toll-like receptor 4-dependent contribution of the immune system to anticancer chemotherapy and radiotherapy. *Nat. Med.* **13**, 1050-1059, doi:10.1038/nm1622 (2007).

171 Chen, G. Y., Tang, J., Zheng, P. & Liu, Y. CD24 and Siglec-10 selectively repress tissue damage-induced immune responses. *Science* **323**, 1722-1725, doi:10.1126/science.1168988 (2009).

172 Tian, J. *et al.* Toll-like receptor 9-dependent activation by DNA-containing immune complexes is mediated by HMGB1 and RAGE. *Nat. Immunol.* **8**, 487-496, doi:10.1038/ni1457 (2007).

173 Ivanov, S. *et al.* A novel role for HMGB1 in TLR9-mediated inflammatory responses to CpG-DNA. *Blood* **110**, 1970-1981, doi:10.1182/blood-2006-09-044776 (2007).

174 Yanai, H. *et al.* HMGB proteins function as universal sentinels for nucleic-acid-mediated innate immune responses. *Nature* **462**, 99-103, doi:10.1038/nature08512 (2009).

175 Bianchi, M. E. & Celona, B. Ancient news: HMGBs are universal sentinels. *J. Mol. Cell. Biol.* **2**, 116-117, doi:10.1093/jmcb/mjp051 (2010).

176 Popovic, P. J. *et al.* High mobility group B1 protein suppresses the human plasmacytoid dendritic cell response to TLR9 agonists. *J. Immunol.* **177**, 8701-8707 (2006).

177 Kalinina, N. *et al.* Increased expression of the DNA-binding cytokine HMGB1 in human atherosclerotic lesions: role of activated macrophages and cytokines.

Arterioscler. Thromb. Vasc. Biol. **24**, 2320-2325, doi:10.1161/01.ATV.0000145573.36113.8a (2004).

178 Hu, X. *et al.* Increased serum HMGB1 is related to the severity of coronary artery stenosis. *Clin. Chim. Acta* **406**, 139-142, doi:10.1016/j.cca.2009.06.016 (2009).

179 Kanellakis, P. *et al.* High-mobility group box protein 1 neutralization reduces development of diet-induced atherosclerosis in apolipoprotein e-deficient mice. *Arterioscler. Thromb. Vasc. Biol.* **31**, 313-319, doi:10.1161/ATVBAHA.110.218669 (2011).

180 Goldstein, R. S. *et al.* Elevated high-mobility group box 1 levels in patients with cerebral and myocardial ischemia. *Shock* **25**, 571-574, doi:10.1097/01.shk.0000209540.99176.72 (2006).

181 Giallauria, F. *et al.* Autonomic dysfunction is associated with high mobility group box-1 levels in patients after acute myocardial infarction. *Atherosclerosis* **208**, 280-284, doi:10.1016/j.atherosclerosis.2009.07.025 (2010).

182 Andrassy, M. *et al.* HMGB1 as a predictor of infarct transmurality and functional recovery in patients with myocardial infarction. *J. Intern. Med.* **270**, 245-253, doi:10.1111/j.1365-2796.2011.02369.x (2011).

183 Cirillo, P. *et al.* Increased high mobility group box-1 protein levels are associated with impaired cardiopulmonary and echocardiographic findings after acute myocardial infarction. *J. Card. Fail.* **15**, 362-367, doi:10.1016/j.cardfail.2008.11.010 (2009).

184 Sorensen, M. V., Pedersen, S., Mogelvang, R., Skov-Jensen, J. & Flyvbjerg, A. Plasma high-mobility group box 1 levels predict mortality after ST-segment elevation myocardial infarction. *JACC Cardiovasc. Interv.* **4**, 281-286, doi:10.1016/j.jcin.2010.10.015 (2011).

185 Hashimoto, T. *et al.* Circulating high-mobility group box 1 and cardiovascular mortality in unstable angina and non-ST-segment elevation myocardial infarction. *Atherosclerosis* **221**, 490-495, doi:10.1016/j.atherosclerosis.2012.01.040 (2012).

186 Andrassy, M. *et al.* High-mobility group box-1 in ischemia-reperfusion injury of the heart. *Circulation* **117**, 3216-3226, doi:10.1161/CIRCULATIONAHA.108.769331 (2008).

187 Oozawa, S. *et al.* Effects of HMGB1 on ischemia-reperfusion injury in the rat heart. *Circ. J.* **72**, 1178-1184 (2008).

188 Kitahara, T. *et al.* High-mobility group box 1 restores cardiac function after myocardial infarction in transgenic mice. *Cardiovasc. Res.* **80**, 40-46, doi:10.1093/cvr/cvn163 (2008).

189 Kohno, T. *et al.* Role of high-mobility group box 1 protein in post-infarction healing process and left ventricular remodelling. *Cardiovasc. Res.* **81**, 565-573, doi:10.1093/cvr/cvn291 (2009).

190 Limana, F. *et al.* Exogenous high-mobility group box 1 protein induces myocardial regeneration after infarction via enhanced cardiac C-kit+ cell proliferation and differentiation. *Circ. Res.* **97**, e73-83, doi:10.1161/01.RES.0000186276.06104.04 (2005).

191 Ahrens, I. *et al.* HMGB1 binds to activated platelets via the receptor for advanced glycation end products and is present in platelet rich human coronary artery thrombi. *Thromb. Haemost.* **114**, doi:10.1160/TH14-12-1073 (2015).

192 Maugeri, N. *et al.* Activated platelets present high mobility group box 1 to neutrophils, inducing autophagy and promoting the extrusion of neutrophil extracellular traps. *J. Thromb. Haemost.* **12**, 2074-2088, doi:10.1111/jth.12710 (2014).

193 Rouhiainen, A. *et al.* Regulation of monocyte migration by amphoterin (HMGB1). *Blood* **104**, 1174-1182, doi:10.1182/blood-2003-10-3536 (2004).

194 Hatada, T. *et al.* Plasma concentrations and importance of High Mobility Group Box protein in the prognosis of organ failure in patients with disseminated intravascular coagulation. *Thromb. Haemost.* **94**, 975-979, doi:10.1160/TH05-05-0316 (2005).

195 Vogel, S. *et al.* Platelet-derived HMGB1 is a critical mediator of thrombosis. *J. Clin. Invest.* **125**, 4638-4654, doi:10.1172/JCI81660 (2015).

196 Stark, K. *et al.* Disulfide HMGB1 derived from platelets coordinates venous thrombosis in mice. *Blood* **128**, 2435-2449, doi:10.1182/blood-2016-04-710632 (2016).

197 Rouhiainen, A., Imai, S., Rauvala, H. & Parkkinen, J. Occurrence of amphoterin (HMG1) as an endogenous protein of human platelets that is exported to the cell surface upon platelet activation. *Thromb. Haemost.* **84**, 1087-1094 (2000).

198 Abeyama, K. *et al.* The N-terminal domain of thrombomodulin sequesters high-mobility group-B1 protein, a novel antiinflammatory mechanism. *J. Clin. Invest.* **115**, 1267-1274, doi:10.1172/JCI22782 (2005).

199 Ito, T. *et al.* Proteolytic cleavage of high mobility group box 1 protein by thrombin-thrombomodulin complexes. *Arterioscler. Thromb. Vasc. Biol.* **28**, 1825-1830, doi:10.1161/ATVBAHA.107.150631 (2008).

200 Huebener, P. *et al.* The HMGB1/RAGE axis triggers neutrophil-mediated injury amplification following necrosis. *J. Clin. Invest.* **125**, 539-550, doi:10.1172/JCI76887 (2015).

201 Andersson, U., Yang, H. & Harris, H. Extracellular HMGB1 as a therapeutic target in inflammatory diseases. *Expert Opin. Ther. Targets* **22**, 263-277, doi:10.1080/14728222.2018.1439924 (2018).

202 Liu, K. *et al.* Anti-high mobility group box 1 monoclonal antibody ameliorates brain infarction induced by transient ischemia in rats. *FASEB J.* **21**, 3904-3916, doi:10.1096/fj.07-8770com (2007).

203 Lundback, P. *et al.* A novel high mobility group box 1 neutralizing chimeric antibody attenuates drug-induced liver injury and postinjury inflammation in mice. *Hepatology* **64**, 1699-1710, doi:10.1002/hep.28736 (2016).

204 Chin, L., Hsu, SC, Wang, KC. Method for producing human monoclonal antibodies that binds to at least one part of HMGB1, US patent application US20180066047A1 . USA patent (2018).

205 Nagato, M., Okamoto, K., Abe, Y., Higure, A. & Yamaguchi, K. Recombinant human soluble thrombomodulin decreases the plasma high-mobility group box-1 protein levels, whereas improving the acute liver injury and survival rates in experimental endotoxemia. *Crit. Care Med.* **37**, 2181-2186, doi:10.1097/CCM.0b013e3181a55184 (2009).

206 Lutterloh, E. C. *et al.* Inhibition of the RAGE products increases survival in experimental models of severe sepsis and systemic infection. *Crit. Care* **11**, R122, doi:10.1186/cc6184 (2007).

207 Yamada, S., Yakabe, K., Ishii, J., Imaizumi, H. & Maruyama, I. New high mobility group box 1 assay system. *Clin. Chim. Acta* **372**, 173-178, doi:10.1016/j.cca.2006.04.016 (2006).

208 Zhang, J. *et al.* Anti-high mobility group box-1 monoclonal antibody protects the blood-brain barrier from ischemia-induced disruption in rats. *Stroke* **42**, 1420-1428, doi:10.1161/STROKEAHA.110.598334 (2011).

209 Yang, H. *et al.* Deleterious role of anti-high mobility group box 1 monoclonal antibody in retinal ischemia-reperfusion injury. *Curr. Eye Res.* **36**, 1037-1046, doi:10.3109/02713683.2011.594201 (2011).

210 Diaz, J. A., Farris, D. M., Wrobleski, S. K., Myers, D. D. & Wakefield, T. W. Inferior vena cava branch variations in C57BL/6 mice have an impact on thrombus size in an IVC ligation (stasis) model. *J. Thromb. Haemost.* **13**, 660-664, doi:10.1111/jth.12866 (2015).

211 Carr, K. D. *et al.* Specific depletion reveals a novel role for neutrophil-mediated protection in the liver during Listeria monocytogenes infection. *Eur. J. Immunol.* **41**, 2666-2676, doi:10.1002/eji.201041363 (2011).

212 Sunderkotter, C. *et al.* Subpopulations of mouse blood monocytes differ in maturation stage and inflammatory response. *J. Immunol.* **172**, 4410-4417 (2004).

213 Swamydas, M., Luo, Y., Dorf, M. E. & Lionakis, M. S. Isolation of Mouse Neutrophils. *Curr. Protoc. Immunol.* **110**, 3 20 21-23 20 15, doi:10.1002/0471142735.im0320s110 (2015).

214 Vong, L., Sherman, P. M. & Glogauer, M. Quantification and visualization of neutrophil extracellular traps (NETs) from murine bone marrow-derived neutrophils. *Methods Mol. Biol.* **1031**, 41-50, doi:10.1007/978-1-62703-481-4_5 (2013).

215 Waters, A. M., Trinh, L., Chau, T., Bourchier, M. & Moon, L. Latest statistics on cardiovascular disease in Australia. *Clin. Exp. Pharmacol. Physiol.* **40**, 347-356, doi:10.1111/1440-1681.12079 (2013).

216 Statistics, A. B. o. *3303.0 - Causes of Death, Australia, 2016* <http://www.abs.gov.au/ausstats/abs@.nsf/0/47E19CA15036B04BCA257757001466 8B?Opendocument> (2017, September 27).

217 Antithrombotic Trialists, C. *et al.* Aspirin in the primary and secondary prevention of vascular disease: collaborative meta-analysis of individual participant data from randomised trials. *Lancet* **373**, 1849-1860, doi:10.1016/S0140-6736(09)60503-1 (2009).

218 Li, L., Geraghty, O. C., Mehta, Z., Rothwell, P. M. & Oxford Vascular, S. Age-specific risks, severity, time course, and outcome of bleeding on long-term antiplatelet treatment after vascular events: a population-based cohort study. *Lancet* **390**, 490-499, doi:10.1016/S0140-6736(17)30770-5 (2017).

219 Fuchs, T. A. *et al.* Extracellular DNA traps promote thrombosis. *Proc. Natl. Acad. Sci. U. S. A.* **107**, 15880-15885, doi:10.1073/pnas.1005743107 (2010).

220 Engelmann, B. & Massberg, S. Thrombosis as an intravascular effector of innate immunity. *Nat. Rev. Immunol.* **13**, 34-45, doi:10.1038/nri3345 (2013).

221 Daley, J. M., Thomay, A. A., Connolly, M. D., Reichner, J. S. & Albina, J. E. Use of Ly6G-specific monoclonal antibody to deplete neutrophils in mice. *J. Leukoc. Biol.* **83**, 64-70, doi:10.1189/jlb.0407247 (2008).

222 Henke, P. K. *et al.* Deep vein thrombosis resolution is modulated by monocyte CXCR2-mediated activity in a mouse model. *Arterioscler. Thromb. Vasc. Biol.* **24**, 1130-1137, doi:10.1161/01.ATV.0000129537.72553.73 (2004).

223 Lv, B. *et al.* High-mobility group box 1 protein induces tissue factor expression in vascular endothelial cells via activation of NF-kappaB and Egr-1. *Thromb. Haemost.* **102**, 352-359, doi:10.1160/TH08-11-0759 (2009).

224 Qian, Q., Jutila, M. A., Van Rooijen, N. & Cutler, J. E. Elimination of mouse splenic macrophages correlates with increased susceptibility to experimental disseminated candidiasis. *J. Immunol.* **152**, 5000-5008 (1994).

225 Wiviott, S. D. *et al.* Prasugrel versus clopidogrel in patients with acute coronary syndromes. *N. Engl. J. Med.* **357**, 2001-2015, doi:10.1056/NEJMoa0706482 (2007).

226 Dyer, M. R. *et al.* Deep vein thrombosis in mice is regulated by platelet HMGB1 through release of neutrophil-extracellular traps and DNA. *Sci. Rep.* **8**, 2068, doi:10.1038/s41598-018-20479-x (2018).

227 Ito, I. *et al.* Physiological concentration of estradiol inhibits polymorphonuclear leukocyte chemotaxis via a receptor mediated system. *Life Sci.* **56**, 2247-2253 (1995).

228 Lockyer, S. & Kambayashi, J. Demonstration of flow and platelet dependency in a ferric chloride-induced model of thrombosis. *J. Cardiovasc. Pharmacol.* **33**, 718-725 (1999).

229 Steinberg, D. In celebration of the 100th anniversary of the lipid hypothesis of atherosclerosis. *J. Lipid Res.* **54**, 2946-2949, doi:10.1194/jlr.R043414 (2013).

230 Kannel, W. B., Castelli, W. P. & Gordon, T. Cholesterol in the prediction of atherosclerotic disease. New perspectives based on the Framingham study. *Ann. Intern. Med.* **90**, 85-91 (1979).

231 Emerging Risk Factors, C. *et al.* Lipid-related markers and cardiovascular disease prediction. *JAMA* **307**, 2499-2506, doi:10.1001/jama.2012.6571 (2012).

232 Lewington, S. *et al.* Seasonal variation in blood pressure and its relationship with outdoor temperature in 10 diverse regions of China: the China Kadoorie Biobank. *J. Hypertens.* **30**, 1383-1391, doi:10.1097/HJH.0b013e32835465b5 (2012).

233 Stone, N. J. *et al.* 2013 ACC/AHA guideline on the treatment of blood cholesterol to reduce atherosclerotic cardiovascular risk in adults: a report of the American College of Cardiology/American Heart Association Task Force on Practice Guidelines. *Circulation* **129**, S1-45, doi:10.1161/01.cir.0000437738.63853.7a (2014).

234 Bilheimer, D. W., Grundy, S. M., Brown, M. S. & Goldstein, J. L. Mevinolin and colestipol stimulate receptor-mediated clearance of low density lipoprotein from plasma in familial hypercholesterolemia heterozygotes. *Proc. Natl. Acad. Sci. U. S. A.* **80**, 4124-4128 (1983).

235 Nissen, S. E. *et al.* Effect of very high-intensity statin therapy on regression of coronary atherosclerosis: the ASTEROID trial. *JAMA* **295**, 1556-1565, doi:10.1001/jama.295.13.jpc60002 (2006).

236 Crisby, M. *et al.* Pravastatin treatment increases collagen content and decreases lipid content, inflammation, metalloproteinases, and cell death in human carotid plaques: implications for plaque stabilization. *Circulation* **103**, 926-933 (2001).

237 Schartl, M. *et al.* Use of intravascular ultrasound to compare effects of different strategies of lipid-lowering therapy on plaque volume and composition in patients with coronary artery disease. *Circulation* **104**, 387-392 (2001).

238 Bea, F. *et al.* Simvastatin promotes atherosclerotic plaque stability in apoE-deficient mice independently of lipid lowering. *Arterioscler. Thromb. Vasc. Biol.* **22**, 1832-1837 (2002).

239 Maxwell, K. N. & Breslow, J. L. Proprotein convertase subtilisin kexin 9: the third locus implicated in autosomal dominant hypercholesterolemia. *Curr. Opin. Lipidol.* **16**, 167-172 (2005).

240 Nicholls, S. J. *et al.* Effect of Evolocumab on Progression of Coronary Disease in Statin-Treated Patients: The GLAGOV Randomized Clinical Trial. *JAMA* **316**, 2373-2384, doi:10.1001/jama.2016.16951 (2016).

241 Tang, Z. H. *et al.* New role of PCSK9 in atherosclerotic inflammation promotion involving the TLR4/NF-kappaB pathway. *Atherosclerosis* **262**, 113-122, doi:10.1016/j.atherosclerosis.2017.04.023 (2017).

242 Slager, C. J. *et al.* The role of shear stress in the destabilization of vulnerable plaques and related therapeutic implications. *Nat. Clin. Pract. Cardiovasc. Med.* **2**, 456-464, doi:10.1038/ncpcardio0298 (2005).

243 Chatzizisis, Y. S. *et al.* Role of endothelial shear stress in the natural history of coronary atherosclerosis and vascular remodeling: molecular, cellular, and vascular behavior. *J. Am. Coll. Cardiol.* **49**, 2379-2393 (2007).

244 Asai, K., Kuzuya, M., Naito, M., Funaki, C. & Kuzuya, F. Effects of splenectomy on serum lipids and experimental atherosclerosis. *Angiology* **39**, 497-504, doi:10.1177/000331978803900602 (1988).

245 Yla-Herttuala, S. *et al.* Stabilisation of atherosclerotic plaques. Position paper of the European Society of Cardiology (ESC) Working Group on atherosclerosis and vascular biology. *Thromb. Haemost.* **106**, 1-19, doi:10.1160/TH10-12-0784 (2011).

246 Swirski, F. K. *et al.* Ly-6Chi monocytes dominate hypercholesterolemia-associated monocytosis and give rise to macrophages in atheromata. *J. Clin. Invest.* **117**, 195-205, doi:10.1172/JCI29950 (2007).

247 Ketelhuth, D. F. & Hansson, G. K. Adaptive Response of T and B Cells in Atherosclerosis. *Circ. Res.* **118**, 668-678, doi:10.1161/CIRCRESAHA.115.306427 (2016).

248 Navarese, E. P. *et al.* Association of PCSK9 with platelet reactivity in patients with acute coronary syndrome treated with prasugrel or ticagrelor: The PCSK9-REACT study. *Int. J. Cardiol.* **227**, 644-649, doi:10.1016/j.ijcard.2016.10.084 (2017).

249 Ridker, P. M. *et al.* Cardiovascular Efficacy and Safety of Bococizumab in High-Risk Patients. *N. Engl. J. Med.* **376**, 1527-1539, doi:10.1056/NEJMoa1701488 (2017).

250 Getz, G. S. & Reardon, C. A. ApoE knockout and knockin mice: the history of their contribution to the understanding of atherogenesis. *J. Lipid Res.* **57**, 758-766, doi:10.1194/jlr.R067249 (2016).

251 Bjorklund, M. M. *et al.* Induction of atherosclerosis in mice and hamsters without germline genetic engineering. *Circ. Res.* **114**, 1684-1689, doi:10.1161/CIRCRESAHA.114.302937 (2014).

252 Roche-Molina, M. *et al.* Induction of sustained hypercholesterolemia by single adeno-associated virus-mediated gene transfer of mutant hPCSK9. *Arterioscler. Thromb. Vasc. Biol.* **35**, 50-59, doi:10.1161/ATVBAHA.114.303617 (2015).

253 Pecoraro, V., Moja, L., Dall'Olmo, L., Cappellini, G. & Garattini, S. Most appropriate animal models to study the efficacy of statins: a systematic review. *Eur. J. Clin. Invest.* **44**, 848-871, doi:10.1111/eci.12304 (2014).

254 Kubo, T. *et al.* Assessment of culprit lesion morphology in acute myocardial infarction: ability of optical coherence tomography compared with intravascular ultrasound and coronary angioscopy. *J. Am. Coll. Cardiol.* **50**, 933-939, doi:10.1016/j.jacc.2007.04.082 (2007).

255 Cullen, P. *et al.* Rupture of the atherosclerotic plaque: does a good animal model exist? *Arterioscler. Thromb. Vasc. Biol.* **23**, 535-542, doi:10.1161/01.ATV.0000060200.73623.F8 01.ATV.0000060200.73623.F8 [pii] (2003).

256 Rosenfeld, M. E. *et al.* Advanced atherosclerotic lesions in the innominate artery of the ApoE knockout mouse. *Arterioscler. Thromb. Vasc. Biol.* **20**, 2587-2592 (2000).

257 Falk, E., Schwartz, S. M., Galis, Z. S. & Rosenfeld, M. E. Neointimal cracks (plaque rupture?) and thrombosis in wrapped arteries without flow. *Arterioscler. Thromb. Vasc. Biol.* **27**, 248-249; author reply 250-242, doi:27/1/248 [pii]

10.1161/01.ATV.0000249644.86759.81 (2007).

258 Sasaki, T. *et al.* A simple method of plaque rupture induction in apolipoprotein E-deficient mice. *Arterioscler. Thromb. Vasc. Biol.* **26**, 1304-1309, doi:10.1161/01.ATV.0000219687.71607.f7 (2006).

259 Getz, G. S. & Reardon, C. A. Apoprotein E as a lipid transport and signaling protein in the blood, liver, and artery wall. *J. Lipid Res.* **50 Suppl**, S156-161, doi:10.1194/jlr.R800058-JLR200 (2009).

260 Thorngate, F. E., Rudel, L. L., Walzem, R. L. & Williams, D. L. Low levels of extrahepatic nonmacrophage ApoE inhibit atherosclerosis without correcting hypercholesterolemia in ApoE-deficient mice. *Arterioscler. Thromb. Vasc. Biol.* **20**, 1939-1945 (2000).

261 Barter, P. J. & Rye, K. A. Cholesteryl Ester Transfer Protein Inhibition Is Not Yet Dead--Pro. *Arterioscler. Thromb. Vasc. Biol.* **36**, 439-441, doi:10.1161/ATVBAHA.115.306879 (2016).

262 Daugherty, A. *et al.* Recommendation on Design, Execution, and Reporting of Animal Atherosclerosis Studies: A Scientific Statement From the American Heart Association. *Arterioscler. Thromb. Vasc. Biol.* **37**, e131-e157, doi:10.1161/ATV.0000000000000062 (2017).

263 Finn, A. V., Nakano, M., Narula, J., Kolodgie, F. D. & Virmani, R. Concept of vulnerable/unstable plaque. *Arterioscler. Thromb. Vasc. Biol.* **30**, 1282-1292, doi:10.1161/ATVBAHA.108.179739 (2010).

264 Bennett, M. R. Breaking the plaque: evidence for plaque rupture in animal models of atherosclerosis. *Arterioscler. Thromb. Vasc. Biol.* **22**, 713-714 (2002).

265 Naghavi, M. *et al.* From vulnerable plaque to vulnerable patient: a call for new definitions and risk assessment strategies: Part I. *Circulation* **108**, 1664-1672, doi:10.1161/01.CIR.0000087480.94275.97 (2003).

266 Ishida, B. Y., Blanche, P. J., Nichols, A. V., Yashar, M. & Paigen, B. Effects of atherogenic diet consumption on lipoproteins in mouse strains C57BL/6 and C3H. *J. Lipid Res.* **32**, 559-568 (1991).

267 Nishina, P. M., Verstuyft, J. & Paigen, B. Synthetic low and high fat diets for the study of atherosclerosis in the mouse. *J. Lipid Res.* **31**, 859-869 (1990).

268 Ando, H. *et al.* Regulation of cholesterol 7alpha-hydroxylase mRNA expression in C57BL/6 mice fed an atherogenic diet. *Atherosclerosis* **178**, 265-269, doi:10.1016/j.atherosclerosis.2004.09.016 (2005).

269 Lambert, G. *et al.* The farnesoid X-receptor is an essential regulator of cholesterol homeostasis. *J. Biol. Chem.* **278**, 2563-2570, doi:10.1074/jbc.M209525200 (2003).

270 Vergnes, L., Phan, J., Strauss, M., Tafuri, S. & Reue, K. Cholesterol and cholate components of an atherogenic diet induce distinct stages of hepatic inflammatory gene expression. *J. Biol. Chem.* **278**, 42774-42784, doi:10.1074/jbc.M306022200 (2003).

271 Paalvast, Y. *et al.* Male apoE*3-Leiden.CETP mice on high-fat high-cholesterol diet exhibit a biphasic dyslipidemic response, mimicking the changes in plasma lipids observed through life in men. *Physiol Rep* **5**, doi:10.14814/phy2.13376 (2017).

272 Slager, C. J. *et al.* The role of shear stress in the generation of rupture-prone vulnerable plaques. *Nat. Clin. Pract. Cardiovasc. Med.* **2**, 401-407 (2005).

273 Kumar, A. & Lindner, V. Remodeling with neointima formation in the mouse carotid artery after cessation of blood flow. *Arterioscler. Thromb. Vasc. Biol.* **17**, 2238-2244 (1997).

274 Moroi, M. *et al.* Interaction of genetic deficiency of endothelial nitric oxide, gender, and pregnancy in vascular response to injury in mice. *J. Clin. Invest.* **101**, 1225-1232, doi:10.1172/JCI1293 (1998).

275 Ference, B. A., Majeed, F., Penumetcha, R., Flack, J. M. & Brook, R. D. Effect of naturally random allocation to lower low-density lipoprotein cholesterol on the risk of coronary heart disease mediated by polymorphisms in NPC1L1, HMGCR, or both: a 2 x 2 factorial Mendelian randomization study. *J. Am. Coll. Cardiol.* **65**, 1552-1561, doi:10.1016/j.jacc.2015.02.020 (2015).

276 Collins, R. *et al.* Interpretation of the evidence for the efficacy and safety of statin therapy. *Lancet* **388**, 2532-2561, doi:10.1016/S0140-6736(16)31357-5 (2016).

277 Skalen, K. *et al.* Subendothelial retention of atherogenic lipoproteins in early atherosclerosis. *Nature* **417**, 750-754, doi:10.1038/nature00804 (2002).

278 Libby, P. Inflammation in atherosclerosis. *Nature* **420**, 868-874, doi:10.1038/nature01323 (2002).

279 Rekhter, M. D. *et al.* Hypercholesterolemia causes mechanical weakening of rabbit atheroma : local collagen loss as a prerequisite of plaque rupture. *Circ. Res.* **86**, 101-108 (2000).

280 Jovinge, S., Crisby, M., Thyberg, J. & Nilsson, J. DNA fragmentation and ultrastructural changes of degenerating cells in atherosclerotic lesions and smooth muscle cells exposed to oxidized LDL in vitro. *Arterioscler. Thromb. Vasc. Biol.* **17**, 2225-2231 (1997).

281 Wang, N. & Tall, A. R. Cholesterol in platelet biogenesis and activation. *Blood* **127**, 1949-1953, doi:10.1182/blood-2016-01-631259 (2016).

282 Kwon, H. J., Lagace, T. A., McNutt, M. C., Horton, J. D. & Deisenhofer, J. Molecular basis for LDL receptor recognition by PCSK9. *Proc. Natl. Acad. Sci. U. S. A.* **105**, 1820-1825, doi:10.1073/pnas.0712064105 (2008).

283 Yla-Herttuala, S. *et al.* Stabilization of atherosclerotic plaques: an update. *Eur. Heart J.* **34**, 3251-3258, doi:10.1093/eurheartj/eht301 (2013).

284 Narula, J. *et al.* Histopathologic characteristics of atherosclerotic coronary disease and implications of the findings for the invasive and noninvasive detection of vulnerable plaques. *J. Am. Coll. Cardiol.* **61**, 1041-1051, doi:10.1016/j.jacc.2012.10.054 (2013).

285 Baker, M. Reproducibility crisis: Blame it on the antibodies. *Nature* **521**, 274-276, doi:10.1038/521274a (2015).

286 Baker, M. Antibody anarchy: A call to order. *Nature* **527**, 545-551, doi:10.1038/527545a (2015).

287 Polakiewicz, R. D. Antibodies: The solution is validation. *Nature* **518**, 483, doi:10.1038/518483b (2015).

288 Lin, J., Kakkar, V. & Lu, X. Impact of MCP-1 in atherosclerosis. *Curr. Pharm. Des.* **20**, 4580-4588 (2014).

289 Kolbus, D. *et al.* CD8+ T cell activation predominate early immune responses to hypercholesterolemia in Apoe(-)(/)(-) mice. *BMC Immunol.* **11**, 58, doi:10.1186/1471-2172-11-58 (2010).

290 Gurbel, P. A., Navarese, E. P. & Tantry, U. S. Exploration of PCSK9 as a Cardiovascular Risk Factor: Is There a Link to the Platelet? *J. Am. Coll. Cardiol.* **70**, 1463-1466, doi:10.1016/j.jacc.2017.07.779 (2017).

291 Stoneman, V. *et al.* Monocyte/macrophage suppression in CD11b diphtheria toxin receptor transgenic mice differentially affects atherogenesis and established plaques. *Circ. Res.* **100**, 884-893, doi:10.1161/01.RES.0000260802.75766.00 (2007).

292 Warnatsch, A., Ioannou, M., Wang, Q. & Papayannopoulos, V. Inflammation. Neutrophil extracellular traps license macrophages for cytokine production in atherosclerosis. *Science* **349**, 316-320, doi:10.1126/science.aaa8064 (2015).

293 Bennett, M. R., Sinha, S. & Owens, G. K. Vascular Smooth Muscle Cells in Atherosclerosis. *Circ. Res.* **118**, 692-702, doi:10.1161/CIRCRESAHA.115.306361 (2016).

294 Nus, M. *et al.* Marginal zone B cells control the response of follicular helper T cells to a high-cholesterol diet. *Nat. Med.* **23**, 601-610, doi:10.1038/nm.4315 (2017).

295 Daugherty, A. & Whitman, S. C. Quantification of atherosclerosis in mice. *Methods Mol. Biol.* **209**, 293-309 (2003).

296 Nabel, E. G. & Braunwald, E. A tale of coronary artery disease and myocardial infarction. *N. Engl. J. Med.* **366**, 54-63, doi:10.1056/NEJMra1112570 (2012).

297 Chen, Y. C., Huang, A. L., Kyaw, T. S., Bobik, A. & Peter, K. Atherosclerotic Plaque Rupture: Identifying the Straw That Breaks the Camel's Back. *Arterioscler. Thromb. Vasc. Biol.* **36**, e63-72, doi:10.1161/ATVBAHA.116.307993 (2016).

298 Jin, S. X. *et al.* Endogenous renovascular hypertension combined with low shear stress induces plaque rupture in apolipoprotein E-deficient mice. *Arterioscler. Thromb. Vasc. Biol.* **32**, 2372-2379, doi:10.1161/ATVBAHA.111.236158 (2012).

299 Raedler, L. A. Praluent (Alirocumab): First PCSK9 Inhibitor Approved by the FDA for Hypercholesterolemia. *Am Health Drug Benefits* **9**, 123-126 (2016).

300 Busygina, K., Waldmann, E. & Parhofer, K. THE EFFECT OF PCSK9 INHIBITION IN FAMILIAL DYSBETALIPOPROTEINEMIA (TYPE III HYPERLIPOPROTEINEMIA): 4 CASES. *J. Am. Coll. Cardiol.* **71**, A1759, doi:10.1016/s0735-1097(18)32300-3 (2018).

301 Giunzioni, I. *et al.* Local effects of human PCSK9 on the atherosclerotic lesion. *J. Pathol.* **238**, 52-62, doi:10.1002/path.4630 (2016).

302 Ricci, C. *et al.* PCSK9 induces a pro-inflammatory response in macrophages. *Sci. Rep.* **8**, 2267, doi:10.1038/s41598-018-20425-x (2018).

303 Shatylo, V. B. *et al.* [Efficacy of treatment-and-prophylactic diets including soya-based food in elderly patients with atherogenic dislipidemia and glucose intolerance]. *Lik. Sprava*, 89-97 (2007).

304 Ferri, N. *et al.* Proprotein convertase subtilisin kexin type 9 (PCSK9) secreted by cultured smooth muscle cells reduces macrophages LDLR levels. *Atherosclerosis* **220**, 381-386, doi:10.1016/j.atherosclerosis.2011.11.026 (2012).

305 Ridker, P. M., Mora, S., Rose, L. & Group, J. T. S. Percent reduction in LDL cholesterol following high-intensity statin therapy: potential implications for guidelines and for the prescription of emerging lipid-lowering agents. *Eur. Heart J.* **37**, 1373-1379, doi:10.1093/eurheartj/ehw046 (2016).

306 Zhu, Y. M. *et al.* Association of Proprotein Convertase Subtilisin/Kexin Type 9 (PCSK9) With Cardiovascular Risk in Primary Prevention. *Arterioscler. Thromb. Vasc. Biol.* **35**, 2254-2259, doi:10.1161/ATVBAHA.115.306172 (2015).

307 Pradhan, A. D., Aday, A. W., Rose, L. M. & Ridker, P. M. Residual Inflammatory Risk on Treatment With PCSK9 Inhibition and Statin Therapy. *Circulation* **138**, 141-149, doi:10.1161/CIRCULATIONAHA.118.034645 (2018).

308 Whitman, S. C. A practical approach to using mice in atherosclerosis research. *Clin. Biochem. Rev.* **25**, 81-93 (2004).

309 Cholesterol Treatment Trialists, C. *et al.* The effects of lowering LDL cholesterol with statin therapy in people at low risk of vascular disease: meta-analysis of

individual data from 27 randomised trials. *Lancet* **380**, 581-590, doi:10.1016/S0140-6736(12)60367-5 (2012).

310 Kashef, M. A. & Giugliano, G. Legacy effect of statins: 20-year follow up of the West of Scotland Coronary Prevention Study (WOSCOPS). *Glob Cardiol Sci Pract* **2016**, e201635, doi:10.21542/gcsp.2016.35 (2016).

311 Robinson, J. G. & Gidding, S. S. Curing atherosclerosis should be the next major cardiovascular prevention goal. *J. Am. Coll. Cardiol.* **63**, 2779-2785, doi:10.1016/j.jacc.2014.04.009 (2014).

312 Ganda, O. P. Statin-induced diabetes: incidence, mechanisms, and implications. *F1000Res* **5**, doi:10.12688/f1000research.8629.1 (2016).

313 Sorensen, R. *et al.* Risk of bleeding in patients with acute myocardial infarction treated with different combinations of aspirin, clopidogrel, and vitamin K antagonists in Denmark: a retrospective analysis of nationwide registry data. *Lancet* **374**, 1967-1974, doi:10.1016/S0140-6736(09)61751-7 (2009).

314 Schulz, C., Engelmann, B. & Massberg, S. Crossroads of coagulation and innate immunity: the case of deep vein thrombosis. *J. Thromb. Haemost.* **11 Suppl 1**, 233-241, doi:10.1111/jth.12261 (2013).

315 Clark, S. R. *et al.* Platelet TLR4 activates neutrophil extracellular traps to ensnare bacteria in septic blood. *Nat. Med.* **13**, 463-469, doi:10.1038/nm1565 (2007).

316 Wang, X. *et al.* Towards effective and safe thrombolysis and thromboprophylaxis: preclinical testing of a novel antibody-targeted recombinant plasminogen activator directed against activated platelets. *Circ. Res.* **114**, 1083-1093, doi:10.1161/CIRCRESAHA.114.302514 (2014).

317 Shirey, K. A. *et al.* The TLR4 antagonist Eritoran protects mice from lethal influenza infection. *Nature* **497**, 498-502, doi:10.1038/nature12118 (2013).

318 Chung, S. C. *et al.* Acute myocardial infarction: a comparison of short-term survival in national outcome registries in Sweden and the UK. *Lancet* **383**, 1305-1312, doi:10.1016/S0140-6736(13)62070-X (2014).